

**Fakultät Wissenschaftszentrum Weihenstephan für Ernährung, Landnutzung und Umwelt
Helmholtz Zentrum München, Institut für Entwicklungsgenetik**

Function of Dj-1 in the pathoetiology of Parkinson's disease

Artem Romanov

Vollständiger Abdruck der von der Fakultät Wissenschaftszentrum Weihenstephan für Ernährung, Landnutzung und Umwelt der Technischen Universität München zur Erlangung des akademischen Grades eines

Doktors der Naturwissenschaften

genehmigten Dissertation.

Vorsitzende:

Prof. Dr. Angelika Schnieke

Prüfer der Dissertation:

- 1. Prof. Dr. Wolfgang Wurst**
- 2. Prof. Dr. Aphrodite Kapurniotu**

Die Dissertation wurde am 11.09.2018 bei der Technischen Universität München eingereicht und durch die Fakultät Wissenschaftszentrum Weihenstephan für Ernährung, Landnutzung und Umwelt am 5.02.2019 angenommen.

Index

	Page
1 Abstract	9
2 Zusammenfassung	11
3 Introduction	13
3.1 Parkinson's disease	13
3.1.1 Motor symptoms of Parkinson's disease	13
3.1.1.1 Classic motor symptoms	13
3.1.1.2 Secondary motor symptoms	15
3.1.2 Non-motor symptoms	15
3.1.3 Pathology of Parkinson's disease	17
3.1.3.1 Basal ganglia system	17
3.1.3.2 Stages of neurodegeneration and their correlation with symptoms	19
3.1.3.3 Synucleinopathy	21
3.1.4 Etiology of Parkinson's disease	21
3.1.4.1 Environmental factors	21
3.1.4.2 Genetic factors	21
3.2 Dj-1 and Parkinson's disease	24
3.2.1 History of Dj-1	24
3.2.2 Structure of Dj-1	24
3.2.3 Functions of Dj-1	24
3.2.3.1 Function of Dj-1 in oxidative stress	24
3.2.3.2 Dj-1 and mitochondrial homeostasis	25
3.2.3.3 Regulation of genes expression and cellular pathways	27
3.2.3.3.1 Nuclear factor (erythroid-derived 2)-like 2 (Nrf2) pathway	27
3.2.3.3.2 Regulation of dopamine related genes	28
3.2.3.3.3 The extracellular signal regulated kinase (ERK) pathway	29

3.2.3.3.4 The apoptosis signal-regulating kinase 1 (ASK1) pathway	30
3.2.3.3.5 The Tumor protein p53 (p53) pathway	30
3.2.3.3.6 The phosphoinositide 3-kinase/protein kinase B (PI3K/AKT) pathway	31
3.2.3.3.7 Other pathways	31
3.2.3.4 Chaperone function of Dj-1	32
3.2.3.5 Enzymatic activities of Dj-1	33
3.3 Neuroinflammation and Parkinson's disease	34
3.3.1 Neuroinflammation in Parkinson's disease patients	34
3.3.2 Microglia polarization stages	35
3.3.3 Parkinson's disease animal models and neuroinflammation	37
4 Aim of the thesis	40
5 Results	41
5.1 Isolation of primary microglia and determination of their purity	41
5.2 Morphological analysis of wildtype and Dj-1 knockout primary microglia during LPS treatment	42
5.3 Validation of MTHFR dysregulation in primary wildtype and Dj-1 knockout microglia ..	44
5.3.1 Validation by quantitative PCR	44
5.3.2 Validation by Western Blot	47
5.4 Analysis of metabolites linked to the one-carbon cycle	48
5.4.1 Detection of S-Adenosylmethionine (SAM), S-Adenosylhomocysteine (SAH), homocysteine, and methylated DNA in primary wildtype and Dj-1 knockout microglia	48
5.4.2 Metabolome analysis of the ventral midbrain in wildtype and Dj-1 knockout mice .	50
5.5 Investigation of the mechanisms and molecular pathways by which Dj-1 regulates the expression of <i>Mthfr</i>	51
5.5.1 LPS upregulates the <i>Mthfr</i> expression via the NFkB pathway	51
5.5.2 Search of possible interactors of Dj-1 within transcription factors' families	52
5.5.2.1 <i>In silico</i> promoter analysis of <i>Mthfr</i> transcripts	52

5.5.2.2 Transcriptional analysis of the <i>Mthfr</i> promoters with Nurr1 and Dj-1 overexpression in HEK293 cells using Luciferase assay	53
5.5.2.3 Nurr1 overexpression in primary microglia does not affect <i>Mthfr</i> expression	55
5.5.3 Identification of the Dj-1 interactome in primary microglia by mass spectrometry .	56
5.6 SIM A9 – a new murine microglial cell line	59
5.6.1 Expression of pro-inflammatory genes in the SIM A9 cell line under different concentrations of LPS treatment	59
5.6.2 Establishment of a Dj-1 knockout SIM A9 cell line using the CRISPR/CAS 9 technique	60
5.6.2.1 Design and cloning of the guide RNAs against Dj-1	60
5.6.2.2 Validation of the selected guide RNAs in the Neuro2a (N2a) cell line	60
5.6.2.3 Introduction of a Dj-1 knockout in the Sim A9 cell line	61
5.6.3 Cell type specificity and comparison of the SIM A9 cell line with primary microglia and immortalized MEFs from Dj-1 knockout mouse	64
5.6.3.1 Comparison of NFκB, ERK and the P38 pathways between wildtype and Dj-1 knockout SIM A9 cells upon LPS treatment	64
5.6.3.2 Comparison of <i>Mthfr</i> expression between wildtype and Dj-1 knockout SIM A9 cells	67
5.6.4 Optimization of Dj-1 Immunoprecipitation (IP) in SIM A9 cells and subsequent mass spectrometry experiments	69
5.6.4.1 Optimization of Dj-1 immunoprecipitation (IP) in the SIM A9 cell line	69
5.6.4.2 Identification of Dj-1 interaction partners by mass spectrometry in SIM A9 cells	71
5.6.4.3 Validation of identified candidates	72
5.6.4.4 Further results of mass spectrometry data	74
5.6.5 Metabolic activity analysis in wildtype and Dj-1 knockout SIM A9 cells	77
5.6.5.1 Respiratory assessment of wildtype and Dj-1 knockout SIM A9 cells	77
5.6.5.2 Lactate measurement in SIM A9 wildtype and Dj-1 knockout cells	85
5.6.5.3 Quantification of the amount of mitochondrial complexes in wildtype and Dj-1 knockout SIM A9 cells	86

6 Discussion	88
6.1 A possible role of Dj-1 in central one-carbon metabolism	88
6.1.1 Dj-1 deficiency induces changes in MTHFR	88
6.1.2 Dj-1 does not regulate <i>Mthfr</i> expression via general modulation of the NFkB signaling pathway	89
6.1.3 Dj-1 does not regulate <i>Mthfr</i> expression via interaction with the TF Nurr1	90
6.1.4 Dj-1 interactors in primary microglia are not readily identifiable	91
6.1.5 Dj-1 deficiency induces changes in homocysteine levels	91
6.1.6 Dj-1 deficiency induces changes in polyamine levels	92
6.2 Cell type specificity of Dj-1 function	96
6.3 Mass spectrometry	99
6.4 Energy metabolism in Dj-1 deficient SIM A9 cells is affected	101
6.4.1 Under non-treatment conditions Dj-1 deficient cells highly likely exhibit higher cellular ATP-demand.....	101
6.4.2 Under LPS-treatment conditions Dj-1 deficient cells have problems with performance of metabolic switch	104
7. Conclusions and future perspectives	107
8. Materials and methods	109
8.1 Material	109
8.1.1 Equipment	109
8.1.2 Chemicals	110
8.1.3 General consumables	112
8.1.4 Cell culture consumables	113
8.1.5 Commercial kits	115
8.1.6 Solutions and buffers	116
8.1.7 Antibodies	118
8.1.7.1 Primary antibodies	118
8.1.7.2 Secondary antibodies	120

8.1.8 Enzymes	121
8.1.9 Primers	121
8.1.10 DNA vectors	122
8.1.11 Taqman probes	123
8.1.12 Cell lines	123
8.1.13 Bacterial strains	124
8.1.14 Mouse strains	124
8.2 Methods	125
8.2.1 Cell culture	125
8.2.1.1 Storage and thawing of the cell lines	125
8.2.1.2 Culture conditions	125
8.2.1.3 Counting of cells	125
8.2.1.4 Coating culture plates and flasks	125
8.2.1.5 Isolation and culture of primary microglia cells	126
8.2.1.6 Culture of SIM A9 microglia cell line	127
8.2.1.7 Culture of HEK293, N2A, and primary MEFs	127
8.2.1.8 Lipofection	127
8.2.1.8.1 Lipofection of HEK293 cells for luciferase assay	127
8.2.1.8.2 Lipofection of N2A cells for T7 assay	128
8.2.1.8.3 Lipofection of SIM A9 cells for Dj-1 knockout generation	128
8.2.1.9 Transduction of primary microglia with Lentiviruses	128
8.2.1.10 Clonal selection of SIM A9 cells	129
8.2.1.11 LPS treatment experiments	129
8.2.2 Nucleic acid isolation procedure	130
8.2.2.1 RNA isolation	130
8.2.2.2 DNA isolation	130
8.2.3 Complementary DNA (cDNA) synthesis	130

8.2.4 Agarose gel electrophoresis	131
8.2.5 Molecular cloning	131
8.2.5.1 Cloning of <i>Mthfr</i> promoters under the luciferase gene reporter system	131
8.2.5.2 Cloning of Dj-1 guide RNAs	131
8.2.5.3 Transformation of competent bacteria, plasmid multiplication and purification	132
8.2.6 Luciferase assay	132
8.2.7 T7 assay	133
8.2.8 Homocysteine ELISA	133
8.2.9 S-Adenosylmethionine (SAM) and S-Adenosylhomocysteine (SAH) ELISA	134
8.2.10 Methylated DNA determination	134
8.2.11 Cellular DNA content quantification	134
8.2.12 L-lactate measurement	134
8.2.13 Immunocytochemistry and microscopy	135
8.2.14 Quantitative real-time polymerase chain reaction (qRT-PCR)	135
8.2.15 Western Blot	136
8.2.16 Dj-1 Co-IP in primary microglia for mass spectrometry analysis	137
8.2.17 Dj-1 Co-IP optimization in SIM A9 cells for mass spectrometry analysis	137
8.2.18 Dj-1 Co-IP in SIM A9 cells for mass spectrometry analysis	138
8.2.19 Respiratory analysis (Seahorse)	138
8.2.20 Statistical analysis	139
9 Appendix	140
9.1 Supplementary materials	140
9.2 List of figures	164
9.3 List of tables	166
9.4 List of abbreviations	168
10 Bibliography	172
11 Eidesstattliche Erklärung	202

12 Acknowledgements 203

1 Abstract

Parkinson's disease is one of the most common age related neurodegenerative disorders affecting human population all around the world. Within the last decades, significant advances in biomedical science and healthcare related disciplines have been made which have greatly increased the life expectancy. However, generally speaking, aging of the human population has caused a dramatic increase in the incidence of age-related disorders. Despite many years of intensive biomedical research, the molecular mechanisms underlying the development of Parkinson's disease are still not completely understood, and therefore, no effective causative treatment exists. To this day, Parkinson's disease research was mainly concentrated on the investigation of the pathophysiological processes in dopaminergic neurons of the substantia nigra, degeneration of which is known to be the major pathological hallmark of the disorder. However, recent findings and deeper understanding of glia cell physiology prompted the scientific society to accelerate research on glia cell metabolism in the context of Parkinson's disease. A pivotal role within this thesis is attributed to microglia, which are the immune cells of the brain, participating in a wide range of processes associated with brain homeostasis.

In our laboratory it was recently demonstrated that during the inflammatory activation associated with the polarization of microglia towards the M1 pro-inflammatory stage, Dj-1-deficient mice (a gene strongly associated with autosomal-recessive early-onset Parkinson's disease) have a dysregulated expression of MTHFR (one of the major enzymes in the one-carbon metabolism) in the substantia nigra. The underlying hypothesis of this thesis is that the onset of Parkinson's disease, linked with loss-of-function mutations in Dj-1, can be associated with metabolic dysregulation during the polarization of microglia towards the M1 pro-inflammatory stage. Respectively, the main focus of the thesis is to analyze the metabolic pathways linked to the one-carbon metabolism and the energy metabolism in Dj-1-deficient microglia, in the non-activated state and during their polarization towards M1 pro-inflammatory stage.

Results obtained within this thesis demonstrate significant dysregulation of *Mthfr* expression in primary Dj-1 knockout microglia during their polarization towards the M1 stage. Moreover, this effect could be attributed to cell-type-specific functions of Dj-1. It was shown that other metabolic pathways connected to the one-carbon metabolism, such as the methionine cycle or the polyamine pathway are also dysregulated in Dj-1 knockout animals. Comparison of the obtained results with published meta-analyses data from idiopathic Parkinson's disease patients revealed a significant correlation within certain parameters, which hints towards a common root of the pathoetiological pathways involved in the development of the Dj-1 related and idiopathic forms of Parkinson's disease. In addition, assessment of the energy metabolism of microglial cells revealed an important role of Dj-1 in the regulation of energy homeostasis. Cells lacking Dj-1 were found to have an increased rate of oxidative phosphorylation in the non-activated stage, supposedly caused by their higher energy demand. Moreover, Dj-1 deficient microglial cells were found to be unable to properly perform a metabolic switch during the polarization towards the

M1 pro-inflammatory stage, which hints towards an important role of this gene in the modulation of the microglial response. To my knowledge, this is the first description of Dj-1 being involved in the energy metabolism in microglial cells.

In summary, the results provided within this thesis demonstrate an important role of Dj-1 in the metabolism and bioenergetics of microglial cells and open new doors for a better understanding of the pathoetiological mechanisms underlying Parkinson's disease development.

2 Zusammenfassung

Morbus Parkinson ist eine der häufigsten altersbedingten neurodegenerativen Erkrankungen, und ist in der gesamten Weltbevölkerung verbreitet. In den letzten Jahrzehnten wurden signifikante Fortschritte auf dem Gebiet der biomedizinischen Forschung und in anderen Disziplinen aus dem Sektor Healthcare gemacht, welche die allgemeine Lebenserwartung bedeutend erhöht haben. Allerdings führt das "Altern der Gesellschaft" zu einem dramatischen Anstieg der Häufigkeit altersbedingter Erkrankungen. Trotz vieler Jahre intensiver biomedizinischer Forschung, sind die molekularen Mechanismen, die der Entwicklung von Morbus Parkinson zu Grunde liegen, immer noch nicht vollständig geklärt, und folglich existiert noch keine ursächliche Therapie. Bis zum heutigen Zeitpunkt fokussierte sich die Parkinson-Forschung hauptsächlich auf die Untersuchung pathophysiologischer Prozesse in dopaminergen Neuronen der Substantia nigra, deren Degeneration eines der Hauptkennzeichen der Parkinson-Krankheit ist. Im Kontext dieser Promotionschrift nehmen jedoch Mikroglia eine zentrale Rolle ein – die Immunzellen des Gehirns, welche in einem weiten Spektrum verschiedener homöostatischer Prozesse im Gehirn involviert sind.

In unserer Arbeitsgruppe wurde unlängst gezeigt, dass in der Maus während der inflammatorischen Aktivierung von Mikroglia, die mit deren Polarisierung zur M1 pro-inflammatorischen Phase assoziiert ist, der Verlust von Dj-1 (ein Gen, das kausal mit autosomal-rezessivem early-onset Parkinson verbunden ist) zur Dysregulation der Expression von *Mthfr* (eines der wichtigsten Enzyme im Einkohlenstoff-Zyklus (C1-Stoffwechsel)) in der Substantia nigra führt. Hieraus leitet sich die grundlegende Hypothese dieser Promotionschrift ab: nämlich, dass die Manifestierung der Parkinson-Erkrankung – in Verbindung mit loss-of-function-Mutationen des Dj-1 Proteins – mit metabolischer Dysregulation während der mikroglialen Polarisierung hin zur M1 pro-inflammatorischen Phase verknüpft werden kann. Daher liegt der Hauptschwerpunkt dieser Arbeit auf der Analyse von Pathways, die mit den C1- und Energiestoffwechselwegen in Dj-1-defizienten Mikroglia verbunden sind, und zwar in deren nicht-aktiviertem (naivem) Zustand wie auch während der Polarisierung zum M1 pro-inflammatorischen Phänotyp.

Die in dieser Arbeit erlangten Erkenntnisse demonstrieren eine signifikante Dysregulation der *Mthfr*-Expression in primären Dj-1-KO Mikroglia während deren Polarisierung zum M1-Zustand. Desweiteren konnte dieser Effekt mit zelltyp-spezifischen Funktionen von Dj-1 in Verbindung gebracht werden. Es konnte auch gezeigt werden, dass diverse Stoffwechselwege, die mit dem C1-Stoffwechsel zusammenhängen (wie der Methionin-Zyklus oder Polyamin-Pathway), in Dj-1-defizienten Tieren dysreguliert sind. Vergleich der hier generierten Resultate mit publizierten Meta-Analysen idiopathischer Parkinson-Fälle ergab eine starke Korrelation diverser Parameter, die auf gemeinsame pathophysiologische Prozesse in der Ätiologie idiopathischer und Dj-1-assoziiierter Parkinson-Fälle hinweisen könnte. Zusätzlich zeigte die Untersuchung des mikroglialen Energiehaushaltes eine wichtige Rolle von Dj-1 bei dessen Regulation. Es konnte gezeigt werden, dass Dj-1-defiziente Zellen eine erhöhte Aktivität der oxidativen

Phosphorylierung im nicht-aktivierten Zustand besitzen, was möglicherweise durch deren erhöhten Energiebedarf bedingt ist. Zusätzlich wurde gezeigt, dass Dj-1-KO Mikroglia keinen vollständigen Metabolic Switch während deren Polarisierung zum pro-inflammatorischen M1-Phänotypen durchführen können, was ein weiterer Hinweis auf die Wichtigkeit dieses Gens bei der Modulierung mikroglialer Antworten ist. Meines Wissens ist diese Arbeit die erste Beschreibung der Implikation von Dj-1 im mikroglialen Energiemetabolismus.

Zusammenfassend lässt sich sagen, dass die in dieser Promotionschrift dargelegten Ergebnisse, eine wichtige Rolle von Dj-1 für den Metabolismus und die Bioenergetik von Mikroglia zeigen, und neue Türen für ein besseres Verständnis der patho-äthiologischen Mechanismen bei der Entwicklung von Morbus Parkinson öffnen.

3 Introduction

3.1 Parkinson's disease

Parkinson's disease (PD) is one of the most common neurodegenerative disorders affecting the worldwide human population. Onset of PD is quite rare before the age of 50 and dramatically increases during aging. A meta-analysis study performed by Pringsheim and colleagues comparing 47 studies conducted between 1985 and 2010 showed that the prevalence of PD increases during aging from 41 cases per 100.000 at the age of 40 to 49 years, to 1903 cases per 100.000 in the group of individuals older than 80 years (Pringsheim et al., 2014). Likewise, the worldwide number of the people affected by PD is expected to double from 2005 to 2030 (Dorsey et al., 2007).

Europe and Northern America (von Campenhausen et al., 2005; Pringsheim et al., 2014) have a higher prevalence of PD than, for example, African and Arabian populations (Benamer et al., 2008; Okubadejo et al., 2006). There could be many explanations for this: geography itself, i.e. environmental and nutritional factors, quality of life or ethnicity. Ethnicity in particular is known to be a risk factor for PD onset: in USA the highest abundance of PD occurs within the Hispanic population (16.6, 95% CI: 12.0, 21.3), followed by the non-Hispanic Whites (13.6, 95% CI: 11.5, 15.7), the Asians (11.3, 95% CI: 7.2, 15.3), and the African-American population (10.2, 95% CI: 6.4, 14.0) per 100 000 (Van Den Eeden et al., 2003). Furthermore, also gender is a known contributor to PD pathogenesis as males are more prone to develop PD than females (Dluzen and McDermott, 2000; Van Den Eeden et al., 2003).

Originally, PD, which was at that time not defined according to nosological criteria, was characterized by James Parkinson in his "An essay on shaking palsy" in 1817, where he described his observations in six patients. Later on, this disease was named Parkinson's disease in honor of the person who first described it in detail (Lees, 2007).

3.1.1 Motor symptoms of Parkinson's disease

3.1.1.1 Classic motor symptoms

PD is characterized by a classic triad of motor symptoms: bradykinesia (akinesia), rigidity, and rest tremor. Bradykinesia (slowness of the movement) and akinesia (difficulties with initiation of movement) are considered as a primary motor phenotypes upon the diagnosis of PD. Several types of bradykinesia are described: proximal, distal and axial. Although in clinics generally only the distal type is diagnosed, since it is not so easy to determine the other two. Bradykinesia accounts as a central restrictive symptom in the development of PD, as clumsiness and inability to properly perform voluntary and spontaneous movements significantly decrease the patients' quality of life (Garcia Ruiz et al., 2005; Lees et al., 2009; Martínez-Martín et al., 1994; Salarian et al., 2009).

Another classic motor symptom of PD is tremor. Approximately 70% of patients experience the development of tremor during PD, which can affect both, the upper and lower limbs (Helmich et al., 2012). The most common type of tremor in the course of the disease is a resting tremor (tremor which takes place during rest phases) with a frequency diapason of 3-6 Hz, although postural and action tremor also could be detected during PD. Yet again, these two types of tremor are not so easily distinguishable from the essential tremor (Bhidayasiri, 2005; Thenganatt and Louis, 2012) . In general, resting tremor is not the most compromising symptom of Parkinson's disease, however in some cases it is the most distressing one (Gironell et al., 2007). In contrast to bradykinesia symptoms, the tremor can decrease during the time of disease progression (Helmich et al., 2012). Sometimes patients complain about an initial tremor (the so called subjective tremor) which cannot be observed or registered by modern techniques - and very often this tremor precedes the objective one by months or even years (de Lau et al., 2006).

The last characteristic motor feature of PD is rigidity, which is characterized by muscle resistance and stiffness. Clinically, this symptom is often explained as a cogwheel, as the patient is not able to perform smooth and flowing motor actions anymore (Jankovic, 2008). Like the tremor symptoms, rigidity can be distal (affecting wrists and ankles) and proximal (affecting shoulders and neck) (Broussolle et al., 2007). Rigidity also can explain the high abundance of muscular pain in the PD patients (Jankovic, 2008). It was shown that in early, untreated PD patients within the period of 1 year the rigidity progression was the fastest in comparison to the other motor symptoms (Schüpbach et al., 2010).

It is important to note that not all of the patients develop all classic motor symptoms during the onset of the disease. In general, the disease progression phenotype can be attributed to three major subtypes: akinetic-rigid, tremor-dominant and mixture phenotype. The progression of PD in the akinesia rigidity subtype is considered to be faster than the rate of progression in tremor-dominant subtype (Hallett, 2003; Rajput et al., 2008). Clinical observations indicate that the amount of loss of dopaminergic neurons in the substantia nigra pars compacta (SNpc) correlates with the phenotypic subgroups of the PD patients. Thus, patients from the fast developing akinetic-rigid subgroup have a more severe degeneration of the neurons in SNpc in comparison with the mild, tremor-dominant phenotype (Jellinger, 1999). Moreover, single-photon emission computed tomography (SPECT) data suggests that the density of the dopamine transporter (DAT) in PD patients from different subgroups also shows strong correlation to the PD subtypes: the akinetic-rigid subgroup has a lower density of DAT in comparison to the tremor-dominant subgroup. Furthermore, the striatal density of DAT strongly correlates with the severity of the bradykinesia and rigidity phenotype progression, but not with the tremor score (Benamer et al., 2000; Brooks et al., 1992; Otsuka et al., 1996; Rossi et al., 2010; Schillaci et al., 2011; Tissingh et al., 1998). Patients from the tremor-dominant subgroup were found to survive longer in comparison with non-tremor patients (Lo et al., 2009). Variations between and within the major subgroups in the prevalence of the symptoms, the progression of the disease, the degeneration of nigral neurons and the density of DAT indicate the complexity of the pathoetiology of this disorder and the existence of the various pathophysiological patterns within the different groups.

3.1.1.2 Secondary motor symptoms

Besides the classic motor symptoms, secondary motor features can be diagnosed in the progression of PD. Postural instability is one of the common symptoms of PD. In general, it is diagnosed later on, after the major clinical symptoms' appearance and worsens during disease progression. It is also recognized as one of the most disabling symptoms in the late stages of the disease. It is linked with the inability to balance the body and, as consequence, increased incidences of falls of the patients (Grimbergen et al., 2009; Kim et al., 2013c). Another typical motor symptom is the impairment of the gait, which is almost universal in patients at the late stages of PD, although slight gait changes can precede the appearance of the major phenotype. Problems with lifting the legs and controlling the steps, sudden freezing, shrinking of step distance and sometimes uncontrollable acceleration of the gait are the main characteristics of gait impairment. Together with postural instability, gait impairment is the most common reason for traumas which are caused by falls of the sufferers (Lewis and Barker, 2009; Morris et al., 2001; Rudzińska et al., 2013). Another common secondary symptom of PD is micrographia. Early studies showed, that a big part of PD patients in the late stages have problems with handwriting, termed micrographia. This feature could be separated from the other motor symptoms and, therefore, is defined as separate unit (McLennan et al., 1972). The specific patterns of changes in handwriting can be used as an instrument for an early diagnosis of PD (Rosenblum et al., 2013). Along this line, speech changes, including difficulties with speech initiation are also quite common in the course of the disease (Ho et al., 1998). Speech of PD patients is usually soft, rapid and monotonic (Jankovic, 2008). It is interesting to mention, that speech changes are mostly observed in patients with strong freezing of the gait symptoms (Park et al., 2014). Other motor symptoms such as changes in the precision of grip (Gordon et al., 1997), mask-like expression (Livingstone et al., 2016), bulbar dysfunction, and dystonia (Shahed and Jankovic, 2007) can also occur during the progression of PD, and this is not even the whole list of motor disturbances which can appear within the course of the disease.

3.1.2 Non-motor symptoms

Even though PD is a well-known motor disorder, many patients experience non-motor symptoms in different stages of the disease. In many cases these non-motor complications can be very disabling for the patients and together with the motor symptoms dramatically decrease the quality of the patients' life. The most typical non-motor symptoms include neuropsychiatric dysfunction (cognitive dysfunction, depression, anxiety), olfaction deficit, sleep disturbances, and gastrointestinal symptoms (Chaudhuri and Naidu, 2008; Chaudhuri et al., 2006).

Among the non-motor symptoms during disease progression, especially neuropsychiatric dysfunction affects many patients in one way or another. Cognitive dysfunction and dementia affect from 20 to 40 percent of the PD patients according to different sources (Aarsland et al., 2005; Emre, 2003; Rippon and Marder, 2005). In general, disturbances in cognitive function

appear in the later stages of the disease, although cases of early appearance of these symptoms are also reported (Lees and Smith, 1983). Cognitive slowing, visuospatial and executive deficits and difficulties with recall memories (this is the major difference from memory impairment in Alzheimer's disease where recognition memory is affected) are the main characteristics of cognitive dysfunction of PD patients, united in the so called dysexecutive syndrome (Aarsland et al., 2004; Dubois and Pillon, 1997). Depression is another non-motor symptom found in big proportion (up to 50%) in PD patients (Burn, 2002; Shulman et al., 2001). Decreased motivation, lack of interest, self-incrimination, mood swings, and self-destructive thoughts make the life of the patients even more distressing. Depression is found to correlate with the progression of motor symptoms (Schrag et al., 2001), and it is more prevalent in the patients with the akinetic-rigid type of PD (Starkstein et al., 1998). Anxiety is also known as a common feature of PD and occurs with a frequency of up to 40% (Pontone et al., 2011; Richard et al., 1996), very often paralleled by a depression phenotype (Menza et al., 1993). The study of Weisskopf suggests that an anxiety phenotype can precede the onset of motor phenotype during the development of Parkinson's disease (Weisskopf et al., 2003).

Rapid eye movement (REM) behavior is the major aspect in the sleep disturbance phenotypes of PD and it frequently occurs during disease progression (Schenck et al., 1996). Within the REM stage PD patients don't have a normal skeletal muscle atonia, which leads to a physically active dreaming with a lot of discomfort (Gagnon et al., 2002). Often REM sleep abnormalities can precede the appearance of motor symptoms of the disease, as about a half of the patients with REM disorder develop PD, and therefore, this symptom may be used in the early diagnostics of the PD (Olson et al., 2000; Postuma et al., 2006).

Constipation is also reported to be a common non-motor feature of Parkinson's disease. According to the different studies it occurs up to 7 times more often in PD patients in comparison to age control group (Kaye et al., 2006; Singer et al., 1992). Disturbances of anorectal sphincter and pelvic floor function were revealed as a common cause of constipation phenotype in PD patients. Constipation as many of the other non-motor phenotypes of PD could precede years or decades the onset of the motor symptoms (Byrne et al., 1994). Abbot and colleagues examined 6790 men between 51 and 75 years old in long-term study - 97 of them developed Parkinson's disease in average of 12 years. It was also shown that people with less than 1 bowel movement (BM) per day are 2.7 times more prone to have PD in comparison with 1 BM per day men, 4.1 times in comparison with 2 BM per day men, and 4.5 times in comparison to people with more than 2 BM per day (Abbott et al., 2001).

Olfaction deficit (hyposmia) is one of the common sensory non-motor symptoms of PD, which is observed in up to 90% of the patients (Bohnen et al., 2008; Doty, 2012; Hawkes et al., 1997). In many cases hyposmia is reported to precede the motor symptoms of Parkinson's disease, and even was suggested to be used as a marker for preclinical diagnostics of this disorder (Ponsen et al., 2004). It is important to mention that the study which was published by our group

demonstrates that *Pink1* knockout mice have an olfaction deficit in comparison to control animals (Glasl et al., 2012).

Olfaction deficit, constipation, REM sleep disorder and depression are considered as strong evidence markers in the diagnostics of the prodromal phase of PD (Chaudhuri et al., 2006). This idea fits with a potential time line described by Schapira and colleagues, which represents the appearance of non-motor phenotypes in the progression of PD. They proposed that PD starts with the prodromal stage (duration 2-5 years), characterized by appearance of hyposmia, REM sleep disturbances, depression and constipation, followed by an early motor stage (3-6 years) characterized by fatigue, pain and diplopia, an early – mid stage (4-12 years) with anxiety, dysphagia, hypophonia, and sleep disturbances, and concluded by a late stage (8 years) which is characterized by cognitive dysfunction, dementia, hallucinations, incontinence, sexual dysfunction and orthostatic hypotension (Schapira et al., 2017).

Within the last decades, the attention to non-motor symptoms of PD has dramatically increased. Studying these features revealed the huge impact they have on the quality of life of the patients, presenting themselves sometimes even more severe than the motor symptoms (Schrag et al., 2000). In addition, it was indicated that in many cases non-motor symptoms precede the onset of motor phenotype by years or even decades. Thus, understanding these non-motor symptoms as well as the development of more sophisticated techniques for their detection will be a priority in the enhancement in PD diagnostics (Chaudhuri et al., 2006).

3.1.3 Pathology of Parkinson's disease

The pathology of PD has been studied well and generally recognized as degeneration of dopaminergic neurons in the SNpc (Fearnley and Lees, 1991; Hornykiewicz, 2008). It was shown that the loss of dopaminergic neurons mainly in this region is responsible for the appearance of motor symptoms during PD progression and that, by the time when motor symptoms are diagnosed, from 30 to 70% of these neurons are already degenerated (Dickson et al., 2009; Jacobson and Marcus, 2011; Kordower et al., 2013).

3.1.3.1 Basal ganglia system

SNpc is a part of the basal ganglia (BG) system – a group of subcortical nuclei which are involved in control of motor function. Originally, these nuclei were proposed to control and correct the movement programs, since large outputs from the BG are linked with the motor areas of the cortex. However, in addition to motor control and motor learning, this system is involved in non-motor functions such as motivation, memory, emotional control and saccadic eye movement. According to nuclei position in processing of information, the BG system can be divided into three groups: input nuclei, intrinsic nuclei, and output nuclei. Nuclei of the striatum – putamen, caudate nucleus and nucleus accumbens are considered as input nuclei getting the signal from

the cortex, thalamus and other structures. Intrinsic nuclei include the globus pallidus external (GPe), subthallamic nucleus (STN), and SNpc. They are thought to create additional controlling loops and signals for a more sophisticated processing of information. Finally, the output nuclei, which mainly send the information to thalamus, consist of the globus pallidus internal (GPi) and substantia nigra pars reticulata (SNpr) (Lanciego et al., 2012; 2008, 2009).

The commonly accepted idea of the BG system function is the sophisticated processing of information. The signal comes from the cortex to the BG, and within this system the modulation and fine tuning of the signal is performed by the different loops and interconnections and then sent back to the cortex (fig 1a). The glutamatergic neurons of the cortex activate the striatal medium spiny gamma-aminobutyric acid (GABAergic) neurons. There are two major groups of these GABAergic neurons in the striatum: one expressing the dopamine receptor D1 (DRD1), dynorphyn and substance P; the second group are neurons expressing dopamine receptor D2 (DRD2) and enkephalin. These two types of the striatal neurons are the origin for the direct and indirect pathways of the BG, with DRD1 GABAergic neurons being mostly involved in the direct pathway. After DRD1 GABAergic neurons activation from the cortex, the inhibition of the activity of GABAergic neurons of SNpr and GPi occurs. Therefore, SNpr and GPi decrease their inhibitory modulation of the thalamic nuclei, which subsequently leads to a higher activity of thalamic nuclei and increase in the release of glutamate to the cortex regions. This chain of events results in the activation of the cortex and movement potentiation.

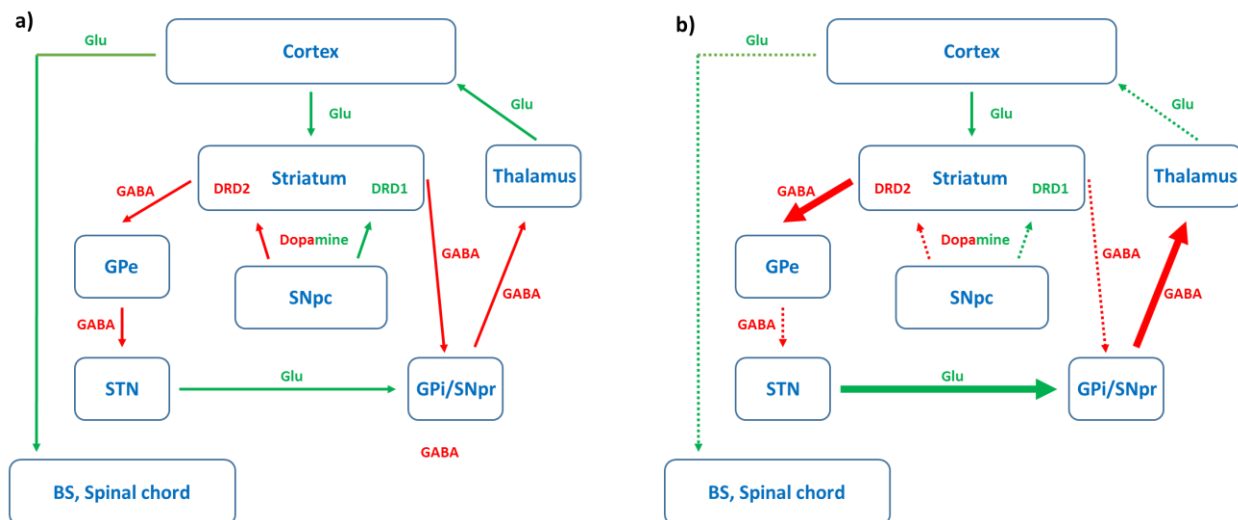


Figure 1: Simplified scheme of basal ganglia system, (a) under normal conditions and (b) with Parkinson's disease. Inhibitory stimuli are indicated with red arrows, activation stimuli with green arrows. Dotted arrows represent decreased signal, fat arrows - increased signal. Abbreviations: Glu – glutamine, GABA - gamma-Aminobutyric acid, SNpc – substantia nigra pars compacta, SNpr – substantia nigra pars reticulata, GPe – globus pallidus external, GPi – globus pallidus internal, STN – subthallamic nucleus, BS – brain stem, DRD1 and 2 – dopamine receptor D1 and D2.

From the other side, the activation signal from cortical neurons to the DRD2 enkepalin GABAergic neurons gives rise to the indirect pathway. Release of GABA from this type of neurons inhibits

the GABAergic neurons of the GPe, which subsequently attenuate their inhibitory effect on the STN. Finally, these conditions result in a stimulatory effect on the neurons of the SNpr and the GPe, which results in the following inhibition of the thalamic nuclei and finally the cortex. Therefore, the activation of the indirect pathway leads to movement potential inhibition (Calabresi et al., 2014; Gerfen et al., 1990; Lanciego et al., 2012). A study of Tai and colleagues with implementation of modern optogenetic techniques demonstrated, that stimulation of DRD1 striatal GABAergic neurons in rodent brains in one hemisphere leads to activation of goal directed behavioral, whereas the stimulation of DRD2 striatal neurons caused the opposite effect (Tai et al., 2012). Similar results were obtained by Kravitz (Kravitz et al., 2010). Together these findings argue for the classic model of the BG system functioning.

The SNpc is an intrinsic nucleus in BG system. It regulates the processing of information within this system by release of dopamine to the striatum. Dopamine facilitates the activity of the direct pathway via activation of DRD1 and inhibits the indirect pathway via activation of DRD2. This results in inhibition of the GPi and the SNpr nuclei. Therefore, the SNpc leads to an attenuation of the thalamic nuclei suppression by release of dopamine via direct and indirect pathway with a following movement potentiation. Degeneration of the SNpc dopaminergic neurons in PD progression leads to a decrease in dopamine release with a subsequent imbalance in the BG system. This provokes the inability to regulate the relationship between the direct and indirect pathway, resulting in the induction of hyper inhibition of the thalamic nuclei (fig. 1b), and as consequence the previously described motor symptoms of PD (Jacobson and Marcus, 2011; Obeso et al., 2000). Therefore, it is understandable why the deep brain stimulation (DBS) of the STN and the GPi (these nuclei are highly active as a consequence of decreasing modulatory activity of SNpc) leads to significant improvement of motor symptoms in PD patients (Odekerken et al., 2016).

There is a common opinion that SNpc is a very susceptible region because of the high rate of dopamine metabolism. During the metabolism of dopamine and its autoxidation (it is a highly reactive and unstable molecule in the neutral pH) different toxic and reactive molecules, such as 3,4-dihydroxyphenyl-acetaldehyde (DOPAL), semi-quinones, and quinones are produced, in addition to free radicals and reactive oxygen species (ROS). Therefore, disturbances of the equilibrium of this system, which are able to destroy the homeostasis, could serve as triggers in initiation of pathological cascades and dopaminergic neurons neurodegeneration (Marchitti et al., 2007; Muñoz et al., 2012; Napolitano et al., 2011; Segura-Aguilar et al., 2014).

It should be noted that the BG system is a complex multicomponent system: everything is interconnected within this system to achieve a high level of integration and sophisticated regulation of the circuits. However, one thing is absolutely clear – the SNpc is one of the major components of this system, and degenerative processes linked to this region lead to imbalance in motor circuits processing, with subsequent PD pathogenesis.

3.1.3.2 Stages of neurodegeneration and their correlation with symptoms

Although, historically PD has been linked to degeneration of the SNpc, it is known that the degenerative events during the progression of this disorder are not limited to degenerative processes in SNpc. Braak and colleagues described the regions affected during the progression of idiopathic PD (table 1, modified from (Braak et al., 2003; Kalia and Lang, 2015; Mørkeberg Nilsson, 2012; Postuma et al., 2010)). As visible, the SNpc region appears only to be affected from the third stage on, and this event is linked with the onset of the motor symptoms. The first stage is characterized by an accumulation of α -synuclein and degenerative processes in the peripheral nerve system, olfactory bulbs and dorsomotor nuclei of vagal and glossopharyngeal nerves. This could be underlying reason why an olfaction deficit and some autonomic dysfunctions precede the onset of the motor symptoms. Subsequently, the pathological processes penetrate deeper into the brain affecting the raphe nuclei and the ceruleus and subceruleus complex, which could explain the emergence of depressions and the REM sleep disorders. During the third stage, more and more midbrain regions are getting damaged, including the SNpc, which is linked with an onset of motor phenotype as already mentioned above. In the following stages, the neuropathological pattern spreads across the multiple cortex region with appearance of cognitive and emotional symptoms. Thus, taken together, PD is not a disorder of one particular brain region but affects multiple regions during disease progression. An interesting observation found during the analysis of the pathological pattern distribution is that it seems that PD enters the brain from outside (olfactory bulb and medulla oblongata) with following penetration into the deep brain regions with appearance of specific symptoms.

Stage	Affected regions	Phase	Symptoms
1	Dorsal motor nuclei of X and IX nerves, Olfactory bulb and anterior olfactory nucleus	Prodromal phase	Olfactory deficit, autonomic dysfunction (e.g. constipation)
2	Locus ceruleus, gigantocellular reticular nucleus, posterior raphe nucleus		REM sleep disorders, depression
3	Substantia nigra pars compacta, pedunculopontine nucleus, central subnucleus of amygdala, magnocellular nuclei of basal forebrain	Motor phase	Motor symptoms
4	Accessory cortical and basolateral nuclei of amygdala, intestinal nucleus of stria terminalis, ventral claustrum, intralaminar nuclei of thalamus, temporal mesocortex (transentorhinal region) and allocortex (CA2-plexus)		Cognition and emotion symptoms
5	Sensory association areas of the neocortex and prefrontal neocortex		
6	First order sensory association areas of the neocortex and premotor areas, occasionally mild changes in primary sensory areas and the primary motor field		

Table 1: Braak stages of idiopathic Parkinson’s disease. Affected regions of each stage include the areas indicated in the previous stages. Modified from (Braak et al., 2003; Kalia and Lang, 2015; Mørkeberg Nilsson, 2012; Postuma et al., 2010)).

3.1.3.3 Synucleinopathy

Another important hallmark of PD pathology is the presence of Lewy bodies in the different neuronal populations. Lewy bodies mainly consist of misfolded α -synuclein protein which aggregates in the cytoplasm of affected neurons (Spillantini et al., 1997). α -synuclein is presumably a neuronal protein and under normal conditions it is mainly presented in the neuronal terminals where it is believed to play a role in synaptic transmission (Burré et al., 2010; George, 2002).

During the pathological processes, α -synuclein aggregates into different oligomers types, which are mainly still soluble forms of α -synuclein. During the continuing aggregation process these protofibrils become insoluble and merge to form the high molecular weight structures known as fibrils (they are the main components of Lewy bodies). α -synuclein aggregates have been proposed to play an important role in neuronal death and the progression of PD (Melki, 2015; Schulz-Schaeffer, 2010). Age related decline of the activity of the systems which utilize or repair

misfolded α -synuclein is proposed to be one of the major factors, contributing to synucleinopathy linked with an idiopathic PD onset in elderly people (Xilouri et al., 2013).

The majority of PD cases is characterized by the presence of Lewy bodies, however there are cases when the pathological characteristics of PD do not include accumulation of α -synuclein. These are mainly incidents of autosomal recessive juvenile Parkinsonism and in some cases linked with mutations in the leucine rich repeat kinase 2 (*LRRK2*). Although Lewy body pathology is the most common hallmark of idiopathic PD, it could also be observed in other neuropathological disorders such as dementia with Lewy bodies and multiple system atrophy (Dickson et al., 2009).

3.1.4 Etiology of Parkinson's disease

3.1.4.1 Environmental factors

PD is a multifactorial disorder caused by many environmental and genetic factors. Originally it was believed to be of non-genetic origin and that synergetic action of adverse environmental factors leads to the onset of the disease. Until today, there have been many environmental factors discovered which have a positive or negative correlation with the disease onset. Examples of the harmful risk factors include pesticide exposure, prior head injury, rural living, beta-blockers use and agricultural occupation. Factors which decrease the risk of PD development include smocking, coffee drinking, nonsteroidal anti-inflammatory drugs use, calcium channel blocker use and alcohol consumption (Kalia and Lang, 2015; Noyce et al., 2012).

3.1.4.2 Genetic factors

With the development and advances in sequencing technologies many genetic factors associated with development of PD were unraveled. The first gene which was found to be associated with PD when mutated was α -synuclein (*SNCA*) (Polymeropoulos et al., 1997). Although, most of the PD cases are still sporadic, since the discovery of *SNCA* as a genetic risk factor, disease etiology has started to acknowledge also a genetic origin (approximately up to 10% of PD cases are considered to have genetic origin (Trinh and Farrer, 2013)). Mutations in many genes were found to be associated with PD development. Several of them are involved in monogenic forms of PD (table 2, modified from (Ferreira and Massano, 2017; Verstraeten et al., 2015)). Mutations in the genes which are inherited in autosomal dominant manner (e.g. *Lrrk2* or vacuolar protein sorting-associated protein 35 (*VPS35*)) are usually linked with a late onset of PD, while autosomal recessive inheritance (*Parkin*, PTEN-induced putative kinase 1 (*PINK-1*), *Dj-1*) causes early onset PD.

According to GWAS (Genome-Wide Association Studies), there are also genes, mutations in which lead to increased or decreased risk of PD development (Nalls et al., 2014). Furthermore, besides the genes involved in monogenic forms of Parkinson's disease, there were other genes identified like F-box only protein 7 (*FBX07*), probable cation-transporting ATPase 13A2 (*ATP13A2*), pantothenate kinase 2, mitochondrial (*PANK2*), calcium-independent phospholipase A2 (*PLA2G6*), dynactin subunit 1 (*DCTN1*), sodium/potassium-transporting ATPase subunit alpha-3

(*ATP1A3*), ataxin-2 (*ATXN2*), ataxin-3 (*ATXN3*), fragile X mental retardation 1 (*FMR1*) and the DNA polymerase subunit gamma (*POLG1*), mutations in which are strongly associated with non-PD monogenic disorders with Parkinsonism as main clinical feature (Ferreira and Massano, 2017).

Gene	Gene location (human)	Inheritance	Gene function	Clinical phenotype	Neuropathology
<i>SNCA</i>	4q22-1	AD	α -synuclein protein is abundant in neurons, especially presynaptic terminals. It is believed to control vesicular neurotransmission. Some data also point to the role of human α -synuclein in regulating dopamine neurotransmission	Early onset - late onset	Degeneration of SN and LC neurons. LB pathology
<i>LRRK2</i>	12q12	AD	The <i>LRRK2</i> gene encodes a protein of largely unknown function. It belongs to the Roco protein family, with a Roc GTPase domain, a COR dimerization region, and a protein kinase domain. <i>LRRK2</i> also contains four predicted repeat structures: the N-terminal ankyrin, armadillo, the leucine-rich repeat regions, and a C-terminal WD40 domain, all of which have been associated with protein interactions. Recent results also demonstrate a role of <i>LRRK2</i> in cytoskeletal dynamics, vesicular transport, and autophagy	Late onset	Heterogeneous: LB in the brainstem and loss of neurons in the SN; Some cases: neurofibrillary tangle pathology and neuronal nigral loss without LB pathology
<i>VPS35</i>	16q11.2	AD	The <i>VPS35</i> gene encodes a component of the retromer cargo-recognition complex critical for the endosome-trans-Golgi trafficking and the recycling of membrane-associated proteins	Late onset	Unknown
<i>EIF4G1</i>	3q27.1	AD	The product of the <i>EIF4G1</i> gene is the eukaryotic translation initiation factor 4G1, which is ubiquitous and abundantly expressed in different tissues. It operates as a scaffold protein that interacts with many initiation factors, including PABP, eIF3, and two eIF4F components (eIF4E and RNA helicase eIF4A), and then with the 40S ribosome	Late onset	LB pathology
<i>CHCHD2</i>	7p11.2	AD	<i>CHCHD2</i> gene encodes the CHCHD2 protein, a transcription factor that binds to and activates a conserved oxygen response element in the <i>COX4I2</i> gene, a nuclear gene that encodes two isoforms of subunit IV of the cytochrome c oxidase, the terminal enzyme of the mitochondrial respiratory chain	Late onset	Unknown
<i>Parkin</i>	6q25.2-q27	AR	Parkin is a RING domain-containing E3 ubiquitin ligase involved in proteasome-dependent degradation of proteins, destroying unneeded proteins by tagging damaged and excess proteins with ubiquitin	Early onset	Absence of LB, loss of dopaminergic neurons from the SN, and neurofibrillary tangles in the cerebral cortex and brainstem
<i>DJ-1</i>	1p36.23	AR	Encodes the DJ-1 protein, which is found in many organs and tissues, including the brain. Known to protect cells from oxidative stress. Also serves as chaperone. Recently Dj-1 was found to have glyoxalase (1) and deglycase (2) enzymatic activities	Early onset	Severe degeneration of SN and LC neurons, with diffuse LB pathology (3)
<i>PINK1</i>	1p36.12	AR	The <i>PINK1</i> gene encodes a protein called PTEN-induced putative kinase 1. This protein is found in cells throughout the body. Within cells, the protein is located in the mitochondria. Although the function of PTEN-induced putative kinase is not yet fully acknowledged, it appears to help protect the mitochondria from deteriorating during episodes of cellular stress	Early onset	Neuronal loss in the SNpc. LB pathology in the reticular nuclei of the brainstem, SNpc and nucleus basalis of Meynert
<i>RAB39B</i>	Xq28	X-linked	RAB proteins, such as <i>RAB39B</i> , are small GTPases involved in the regulation of vesicular trafficking between membrane compartments	Early onset	Extensive dopaminergic neuronal loss in the SN and classic LB pathology
<i>DNAJC6</i>	1p31.3	AR	The <i>DNAJC6</i> gene encodes auxilin, a neuronal protein that participates specifically in the pathway of clathrin-mediated endocytosis	Early onset	Unknown

Table 2: Genes involved in monogenic forms of Parkinson's disease. Abbreviations: AD – autosomal dominant, AR – autosomal recessive, LB – Lewy bodies, SN – substantia nigra, LC – locus ceruleus, *SNCA* – α -synuclein, *LRRK2* - leucine-rich repeat kinase 2, *VPS35* - Vacuolar protein sorting-associated protein 35, *EIF4G1* - Eukaryotic translation initiation factor 4 gamma, *CHCHD2* - Coiled-coil-helix-coiled-coil-helix domain containing 2, *PINK1* - PTEN-induced putative kinase 1, *RAB39B* - Ras-related protein Rab-39B, *DNAJC6* - Putative tyrosine-protein phosphatase auxilin. 1 - (Lee et al., 2012), 2 - (Richarme et al., 2015), 3 - (Taipa et al., 2016). Modified from (Ferreira and Massano, 2017; Verstraeten et al., 2015).

3.2 Dj-1 and Parkinson's disease

Mutations in *Dj-1* cause an early onset PD. They are very rare, and found in only 1-2% of early onset PD cases (Abou-Sleiman et al., 2003; Singleton et al., 2013). The phenotype of PD patients with mutations in *Dj-1* is similar to *Parkin* and *Pink-1* PD carriers and represent early (from 20 to 40 years) age onset, a slow progression and usually a good response to levodopa treatment (Abou-Sleiman et al., 2003; Bonifati, 2012; Schulte and Gasser, 2011). Until recently, neuropathology of Dj-1 PD cases was not known, however, Taipa and colleagues published neuropathological features from a patient with a novel *Dj-1* mutation L172Q (in vitro experiments revealed significant decrease of L172Q Dj-1 content due to unstable and fast degrading properties of the protein). The L172Q mutation in *Dj-1* was associated with a severe degeneration of SN and LC neurons, and widespread α -synucleinopathy (Taipa et al., 2016). It is worthwhile to mention here, that up to 2012, there were no Dj-1 knockout mouse models, which demonstrated severe neurodegenerative processes in SNpc, with an exception of one publication (Rousseaux et al., 2012).

3.2.1 History of Dj-1

Originally Dj-1 was described by Nagakubo and colleagues as novel oncogene with a cDNA sequence which did not have significant homology with any sequences reported by that time. The authors reported that Dj-1 is widely expressed in human tissues and that this protein together with the rat sarcoma protein (RAS) transformed mouse NIH3T3 cells more effectively, in comparison to a RAS/Myc combination (Nagakubo et al., 1997). Later a function of Dj-1 was discovered in sperm cells, where it is highly expressed and seemingly plays an important role in male fertility. (Klinefelter et al., 1997; Wagenfeld et al., 1998). Afterwards, Takahashi and coauthors reported the ability of Dj-1 to positively regulate androgen receptor expression via binding to the protein inhibitor of activated STAT α (PIAS α) (the androgen receptor expression inhibitor) (Takahashi et al., 2001). In 2003 Bonifati and co-workers discovered the first time a connection of Dj-1 with Parkinson's disease. They described a deletion (in Dutch family) and a missense point mutation L166P (in an Italian family) in Dj-1 as a cause for onset of a familiar recessive form of PD (Bonifati, 2003). Since then huge attempts were made to understand the functions of Dj-1 and unravel pathological mechanisms, which lead to the onset of the PD.

3.2.2 Structure of Dj-1

Dj-1 consists of 189 amino acids with 9 α -helices and 7 β -sheets. The protein implements its biological functions as a dimer. Methionine at position 17 (M17) and phenylalanine at position 162 (F162) are the most important residues for dimer formation. Structurally, Dj-1 is similar to the protease I from *Pyrococcus horikoshii*. A detailed review is given in the publication of Honbou and colleagues (Honbou et al., 2003).

3.2.3 Functions of Dj-1

3.2.3.1 Function of Dj-1 in oxidative stress

Dj-1 has three cysteine residues – C46, C53, and C106 which have been proposed to play an important role in the function of Dj-1 as an oxidative sensor. Among these residues C106 is the most conserved in mammals and the most sensitive for oxidation. Indeed, mutations of this amino acid lead to loss of function of the protein, which was demonstrated in different cell lines, rodents and drosophila models (Aleyasin et al., 2007; Canet-Avilés et al., 2004; Kinumi et al., 2004; Lucas and Marín, 2007; Meulener et al., 2006), although the oxidation of C46 and C53 was also proposed to play a role in the functional activity of Dj-1 (Waak et al., 2009). C106 can be oxidized to cysteine-sulfenic (SOH), cysteine-sulfinic (SO₂H), and cysteine-sulfonic (SO₃H) acids, with Dj-1 with sulfenic and sulfinic modification of C106 being more active than Dj-1 with non-oxidized C106 (Ariga et al., 2013; Wilson, 2011). In contrast sulfonic C106 appears to inactivate the functions of Dj-1 (Zhou et al., 2006). Cysteine residues of Dj-1 can be modified by S-nitrosylation. Recently Choi and co-workers found, via a crystallography assay and site-directed mutagenesis, that the C106 residue can be nitrosylated with a following trans-nitrosylation of phosphatase and tensin homologue (PTEN) by Dj-1. Therefore, a mechanism of PTEN phosphatase activity inhibition and promotion of cell survival by Dj-1 was proposed, with additional knowledge about the mechanism of nitric oxide (NO) detoxification by Dj-1 (Choi et al., 2014). Other results were published earlier by Ito and colleagues, where they described that C106 cannot be nitrosylated, whereas nitrosylation of C43 and C53 leads to inability of Dj-1 to form dimers with a subsequent loss of protein function (Ito et al., 2006). In summary, it is doubtless that the cysteine residues of Dj-1 play an important role in the regulation of its activity and are critical for the function of this protein. Lack of Dj-1 leads to cell death caused by oxidative stress, induced by H₂O₂, paraquat, 1-methyl-4-phenylpyridinium (MPP⁺), or 6-hydroxy dopamine (6-OHDA). Overexpression of Dj-1 was able to decrease cell death caused by these compounds, indicating a protective role of Dj-1 against oxidative stress (Taira et al., 2004; Yokota et al., 2003). Interestingly, the mutant L166P (which Bonifati and colleagues originally described in the Italian family) is not able to counteract oxidative stress, which was proven by several studies (Miller et al., 2003a; Taira et al., 2004; Takahashi-Niki et al., 2004).

In addition to in vitro studies, in vivo experiments could also prove the importance of Dj-1 in oxidative stress response. Billia and colleagues showed that Dj-1 counteracts oxidative stress development in the murine heart, and that the mechanism of this protection is independent from other known antioxidant systems (Billia et al., 2013). Dj-1 also showed a neuroprotective effect against the neurodegenerative processes caused by ischemia/reperfusion injury in rats. Injections of Dj-1 into the brain led to a decrease of lesion size and lower nitrotyrosine production, with a significant rescue of behavioral phenotype (Yanagisawa et al., 2008). It was also shown, that Dj-1 knockout mice are more susceptible to ischemia-induced damage and that overexpression of Dj-1 in these mice lead to the reduction of oxidative stress markers (Aleyasin et al., 2007). Overexpression of Dj-1 in the brain of 1-methyl-4-phenyl-1,2,3,6-tetrahydropyridin (MPTP) mouse models of parkinsonism ameliorated the signs of oxidative damage and decreased the neurodegeneration of dopaminergic neurons of SN (Kim et al., 2005a; Paterna et al., 2007).

The protective effect of Dj-1 was also observed in 6-OHDA mouse and rat models (Batelli et al., 2015; Sun et al., 2012).

3.2.3.2 Dj-1 and mitochondrial homeostasis

During the last decade studies of bioenergetics and other mitochondrial functions became a hot topic in biomedical science, which promoted many researchers to investigate the role of mitochondria within the context of Parkinson's disease. Mitochondrial dysfunction, elevated levels of free radicals and impaired respiration, linked to a decrease in mitochondrial complex I activity with reduced mitochondria membrane potential were found in PD patients (Hu and Wang, 2016; Moon and Paek, 2015; Orth and Schapira, 2002; Schapira et al., 1990).

Mitochondria are known to be one of the main source of free radicals in the cells (Murphy, 2009), whereas Dj-1 represents an oxidative sensor which participates in the processes of oxidative stress resistance (discussed above). Therefore, many attempts were made to find out the link between Dj-1 and mitochondrial homeostasis.

Under basal conditions Dj-1 mainly localized in the cytoplasm and the nucleus (Canet-Avilés et al., 2004; Taira et al., 2004), although a fraction is present in mitochondria, and even was found to interact with mitochondrial complex I to maintain its activity, which was supported by Dj-1 knockdown experiments in NIH3T3 and HEK293 cells (Hayashi et al., 2009). The maintenance of complex I activity by Dj-1 during oxidative stress, induced by bisphenol A, was demonstrated by work of Ooe and colleagues in Neuro2a and GC1 cells (Ooe et al., 2005). During oxidative stress conditions Dj-1 is translocated to the outer mitochondrial membrane (OMM) where it stabilizes mitochondria and supports mitochondrial function (Kahle et al., 2009; Zhang et al., 2005). Under oxidative conditions C106 of Dj-1 is oxidized to cysteine-sulfinic acid, which is an important event for the transport of Dj-1 to mitochondria and its dimerization. Furthermore, it was reported that the N-terminal part of the protein is needed for efficient Dj-1 translocation to the OMM. Interestingly, it was shown that the cysteine mutants C46S and C53A and some other pathological Dj-1 mutants observed in PD patients (M26I and L166P) were not able to organize an active dimeric form of Dj-1, despite that fact that it was still possible for them to be transported to the mitochondria (Canet-Avilés et al., 2004; Maita et al., 2013). Li and co-workers demonstrated that Dj-1 does not have its own mitochondrial translocation sequence, therefore, special transporter protein is needed to translocate it into the mitochondria. It was shown that Dj-1 interacts with different chaperons such as heat shock protein, 70kDa (Hsp70), C-terminus of HSC70-interacting protein (CHIP) and mortalin (mtHsp70/Grp75), which translocate Dj-1 to the mitochondria. Moreover interaction of Dj-1 with the chaperon HSP70 is increased under the oxidative stress conditions (Li et al., 2005).

Dj-1 function was also studied in the process of mitochondrial autophagy, termed mitophagy. Mitophagy is an important process to utilize damaged or non-functional mitochondria in the cells, which helps to maintain proper cellular homeostasis. This process is also necessary for the general mitochondrial turnover (Zhang, 2013). Krebiehl and colleagues demonstrated that mouse embryonic fibroblasts (MEF) isolated from Dj-1 knockout mice had reduced levels of autophagy and accumulated impaired mitochondria. In addition, the authors showed that in fibroblasts from

the Dj-1 E64D patients the level of mitochondrial co-localization with lysosomes was significantly reduced in comparison to matched controls, which supports the idea of a Dj-1 participation in the mitophagy process (Krebiehl et al., 2010). In the study of Irrcher and co-workers on cell lines (Irrcher et al., 2010), mouse cortical neurons, in vivo, and lymphoblasts from PD patients (Dj-1 C106P or Del) was demonstrated that deficiency of Dj-1 is associated with changes in mitochondrial morphology. Overexpression of Dj-1 in cortical neurons was shown to rescue the mitochondrial morphology phenotype, whereas overexpression of the C106A Dj-1 mutant did not have a positive effect. It was also found that lack of Dj-1 can be associated with disturbances in the autophagy process. Interestingly, the mitochondria phenotype also could be rescued by overexpression of Parkin and PINK-1 in primary cortical neurons and SH-5Y5Y cells (Irrcher et al., 2010). It is known that the Parkin/Pink-1 pathway plays an important role in mitophagy, however, Dj-1 mediated mitophagy seems to be independent from the Parkin/Pink-1 pathway (Thomas et al., 2011). So far, the molecular mechanisms by which Dj-1 regulates autophagy are still unknown, therefore, further experiments are needed to provide more detailed information about Dj-1 function in these processes.

Although, the pathway by which Dj-1 regulates mitophagy seems to be independent from the Parkin/Pink-1 pathway (Thomas et al., 2011), it was shown that Dj-1 interacts with Pink-1 (Tang et al., 2006) and with Parkin under oxidative stress conditions (Moore et al., 2005). Moreover, Xiong and co-workers demonstrated on human brain lysates and in mammalian cell lines that Dj-1, Pink-1 and Parkin interact with each other by formation of a complex. The authors named this complex PPD (Parkin - Pink-1 - Dj-1). The PPD complex has a presumably cytoplasmic localization and serves as E3 ligase for Parkin substrates, promoting the degradation of misfolded proteins (Xiong et al., 2009). As already mentioned above, Dj-1 interacts with mortalin, the protein, which acts as a molecular chaperone transporting nuclear encoded proteins inside mitochondria. Moreover, association of Dj-1 with mortalin and its transport to mitochondria was increased under oxidative stress conditions, fortifying the function of mortalin in the translocation of Dj-1 into mitochondria. Interestingly, Parkin and Pink-1 are also known to interact with mortalin (Davison et al., 2009; Rakovic et al., 2011) and mutations in the mortalin gene itself are known to be a contributive risk factor for development of Parkinson's disease (Mena et al., 2009). Taken all together, Dj-1 seems to be tightly associated with Parkin/Pink-1 pathway, and this association could have an important role in mitochondrial homeostasis.

3.2.3.3 Regulation of genes expression and cellular pathways

Even though it is known that Dj-1 does not have its own DNA binding motif (Yamaguchi et al., 2012), there are many studies confirming the role of Dj-1 as a gene expression regulator. This function is executed via different mechanisms, for example direct regulation of the transcription factors' activity, regulation of the pathways, which are involved in gene expression control and regulation of the gene expression on the promoter level via various adapter proteins.

3.2.3.3.1 Nuclear factor (erythroid-derived 2)-like 2 (Nrf2) pathway

Taking into account tremendous role of Dj-1 in oxidative stress response, many affords were made to figure out the relationship of Dj-1 with Nrf2, the master transcription factor for the oxidative stress response. Nrf2 controls many genes involved in the antioxidant defense system under basal and pathological conditions (Ma, 2013). Under normal conditions, Nrf2 is generally localized in cytoplasm and exists in a complex with kelch-like ECH-associated protein 1 (Keap1). Keap1, with some adaptor proteins, activates poly-ubiquitination of Nrf2 and its degradation by the proteasome. Therefore, under basal conditions, Nrf2 is a fast degrading protein and its level is low in many cell types (Kobayashi et al., 2004; Wakabayashi et al., 2003). However, under oxidative stress conditions Dj-1 promotes dissociation of Nrf2 from Keap1, and thereby, its translocation into the nucleus with a following activation of many genes controlled by Nrf2 in response to oxidative stress (Clements et al., 2006). Yan and co-workers showed that overexpression of Dj-1 in H9c2 cells, under hypoxia/re-oxygenation induced oxidative stress, led to significant upregulation of the antioxidant system enzymes such as manganese superoxide dismutase (SOD2), catalase and glutathione peroxidase; in contrast, knockdown of Dj-1 in this cell line had an opposite effect (Yan et al., 2015). Im and colleagues demonstrated in their study that in Dj-1 knockout mice and SH-SY5Y Dj-1 knockdown cells the expression of thioredoxin 1 (Trx1 - a disulfide oxidoreductase playing an important role in cytoprotection) was significantly decreased and that for the activation of Trx1 by Dj-1, via Nrf2, adenylate-uridylate-rich elements (ARE) on the promoter of the Trx1 gene play a crucial role. Interestingly, L166P and M26I Dj-1 mutants were not able to activate Trx1 gene expression (Im et al., 2012).

3.2.3.3.2 Regulation of dopamine related genes

Dj-1 was also found to regulate the expression of several genes involved in dopamine synthesis and metabolism, which is highly relevant in the context of PD, where metabolism of dopamine in the SNpc and its high turnover are considered to be one of the main factors encompassed in the progressive loss of dopaminergic neurons. Dj-1 positively regulates human tyrosine hydroxylase (TH) gene by direct interaction, inhibiting the pyrimidine tract-binding protein-associated splicing factor (PSF) which serves as a repressor of *TH* expression. Dj-1 prevents sumoilation of PSF, and thus, non-sumoilated PSF is unable to recruit histone deacetylase 1 onto the *TH* promoter region which leads to suppression of inhibition of *TH* expression (Xu et al., 2005; Zhong et al., 2006). An interesting observation was made by Ishikawa and colleagues, where they described that murine *TH* expression is not regulated by Dj-1. Basically, the same mechanism cannot be implemented in rodents, as the murine *Th* promoter lacks the PSF recognition sequence, which presents in the human *TH* promoter. This observation could be a possible answer for the question of why Dj-1 deficient mice show no change in *Th* gene expression in comparison to wildtype littermates (Ishikawa et al., 2010). Further intriguing results were obtained by the same group, when they showed that Dj-1 in SH-SY5Y cells can directly interact with TH and the 4-dihydroxy-l-phenylalanine decarboxylase (DDC), stimulating their activity. They could also demonstrate that in this activation the C106 residue plays a critical role. Only Dj-1 with reduced (SH) and cysteine-sulfenic (SOH) forms of C106 was capable of activating TH and DDC, whereas cysteine-sulfinic (SO₂H) and cysteine-sulfonic (SO₃H) C106 of Dj-1 were not able to do so. Moreover, for the TH

and DDC activity promotion by Dj-1, the amount of SH and SOH forms of Cy106 has to be more than 50% of the total amount of Dj-1 protein. In addition, it was demonstrated that M26I, L166P and some other Dj-1 mutants are not able to up-regulate the activity of TH and DDC to the same level as wild type Dj-1 does (Ishikawa et al., 2009).

Dj-1 is also known to regulate vesicular monoamine transporter 2 (*VMAT2*) expression and activity via direct protein-protein interaction. *VMAT2* is a unique transporter, which pumps the dopamine into storage vesicles. A low pH inside these vesicles stabilizes the dopamine and prevents it from self-oxidation. Therefore, *VMAT2* is important protein which prevents cells from the aggressive and toxic dopamine intermediates produced during its oxidation; promotion of *VMAT2* activity and expression mediated by Dj-1 activity attenuates these deleterious effects of dopamine (Ishikawa et al., 2012).

Another connection of Dj-1 to the dopamine metabolism was made, when it was shown that Dj-1 can coexist with the dopamine transporter (*DAT*) in a complex, partially through direct interactions. Co-expression of these proteins in HEK293 and Luhmes cells led to an increase of *DAT* activity and dopamine uptake, although Dj-1 did not upregulate the expression of *DAT*. Thus, this data showed a possible role of Dj-1 in the regulation of *DAT* activity (Luk et al., 2015).

In regards to the regulation of dopamine genes, it worth to mention the nuclear receptor related 1 protein (*Nurr1*) transcription factor. It was shown to regulate the expression of *TH*, *DDC* and *VMAT2* (Hermanson et al., 2003; Iwawaki et al., 2000). *In vitro* and *in vivo* experiments could demonstrate that overexpression of Dj-1 led to an increase of *Nurr1* expression, promoted its translocation into the nucleus and upregulated the expression of *Nurr1* target proteins. Overexpression of the C106P mutant of Dj-1 was not able to do so, thereby suggesting that the C106 of Dj-1 is necessary for implementing this function. Furthermore, the effect of Dj-1 overexpression on *Nurr1* was mediated via the extracellular signal regulated kinase (ERK) pathway (Lu et al., 2012, 2016).

3.2.3.3.3 The extracellular signal regulated kinase (ERK) pathway

As already mentioned above, Dj-1 promotes the function of *Nurr1* via activation of the ERK pathway. The ERK pathway (also known as MAPK/ERK pathway or Ras-Raf-MEK-ERK pathway) is a cellular pathway involved in the regulation of various functions such as cell survival, proliferation, differentiation and many others (McCubrey et al., 2007). Currently, there is some data available, supporting the role of Dj-1 in ERK pathway regulation. Overexpression of Dj-1 in many cellular models and *in vivo* was shown to increase the phosphorylation of ERK with subsequent downstream effects (Gu et al., 2009; Lu et al., 2012, 2016). Although, *Nrf2* is the main transcription factor via which Dj-1 executes its antioxidative function, it was also demonstrated that the ERK pathway, at least partially, is responsible for the protective function of Dj-1 under oxidative stress conditions. Wang and colleagues revealed that during oxidative stress conditions Dj-1 promotes the translocation of ERK into the nucleus with subsequent activation of the ETS-domain containing protein (Elk) transcription factor; in turn, Elk activates expression of *SOD1*. Moreover, they could show that Dj-1 directly interacts with ERK1/2, and that this interaction is

necessary for the nuclear translocation of ERK (Wang et al., 2011). The positive effects of Dj-1 overexpression during oxidative stress conditions, shown by several studies, were found to be abolished upon the use of ERK pathways inhibitors (Gao et al., 2012; Gu et al., 2009). From the other side, experiments with Dj-1 knockdown revealed a decrease in ERK1/2 phosphorylation (Zhang et al., 2016), and reduction in the ERK1/2 and the pElk1 nuclear fraction (Gu et al., 2009).

Dj-1 was also found to control, via modulation of the ERK pathway, eye and wing development in drosophila. It was also shown in the same study that mouse double mutants (knockout of a receptor which is a neuronal survival factor (receptor tyrosine kinase (Ret)) and Dj-1 knockout) had a significantly higher rate of degeneration of dopaminergic neurons in the SNpc in comparison with Ret single knockout animals. Since Ret acts upstream of the ERK pathway, the authors suggested that Dj-1 could promote cell survival via the ERK pathway (Aron et al., 2010). Takahashi-Niki and co-workers revealed in their study that Dj-1 interacts with c-Raf (an upstream regulator of the ERK pathway) and promotes phosphorylation of c-Raf S338 with subsequent activation of the ERK pathway (Takahashi-Niki et al., 2015). Therefore, an additional level of complexity was added to the mechanisms of ERK regulation by Dj-1.

3.2.3.3.4 The apoptosis signal-regulating kinase 1 (ASK1) and P38 pathway

The Ask1 pathway is an important pathway which regulates cell response against various stress signals and promotes apoptosis (Liu et al., 2013). This pathway regulates the activity of specific mitogen-activated protein kinase kinases (MAPKKs) with following activation of c-Jun N-terminal kinase (JNK) and p38 mitogen-activated protein kinase (p38) pathways (Keshet and Seger, 2010; Tobiume et al., 2001). Dj-1 was suggested to modulate the ASK1 pathway by several mechanisms: it was found to physically interact with the Death domain-associated protein 6 (DAXX) in the nucleus, preventing its release to cytoplasm under stress conditions and, therefore, its interaction with ASK1 with subsequent apoptosis pathway activation. Interestingly, the C166P Dj-1 mutant was not able to interfere with DAXX translocation to cytoplasm under stress conditions (Junn et al., 2005). Tang and coauthors demonstrated that p38 regulated/activated kinase (PRAK) is responsible for nuclear translocation of Dj-1 (Tang et al., 2014) and it seems like this could be one of the negative feedback loops for ASK1 pathway inhibition.

From the other side, Dj-1 was also found to interact with ASK1 itself, and the C106 residue of Dj-1 is proposed to play an important role for the initiation of this interaction. With this interaction Dj-1 prevents activation of ASK1 by DAXX, and therefore, inhibits the downstream apoptotic pathways (Mo et al., 2010; Waak et al., 2009).

An additional mechanism of ASK1 pathway inhibition, promoted by Dj-1, was proposed by Im and coworkers. Under basal conditions, ASK1 is bound by Trx and this inhibitory complex exist to limit the activity of ASK1. Under stress conditions, Trx dissociates from ASK1, thereby promoting the activation of apoptotic pathways. However, upon oxidative stress exposure, Dj-1 prevents the dissociation of the ASK1-Trx complex, thus, preventing ASK1 interaction with DAXX, and therefore reducing the activation of apoptotic pathways. The C106 Dj-1 mutant was not able to suppress the dissociation of ASK1-Trx complex (Im et al., 2010; Saitoh et al., 1998). Furthermore,

as already mentioned in the section of the Nrf2 pathway, Dj-1 upregulates Trx expression, and therefore, more Trx protein is available for ASK1 inhibition (Im et al., 2012).

Cao and colleagues showed that *in vitro* and *in vivo*, under mild oxidative stress conditions, Dj-1 inhibits the ASK1 pathway, however, excessive oxidative stress causes dissociation of Dj-1 from ASK1 with a following activation of the P38 pathway and cell death (Cao et al., 2014).

3.2.3.3.5 The Tumor protein p53 (p53) pathway

Tumor protein p53 is a transcription factor which is activated in response to different stress stimuli with following initiation of cell cycle arrest, autophagy, cellular senescence and apoptosis, and it is also known as one of the major proteins with tumor suppression function (Levine and Harris, 2005; Menendez et al., 2009). Kato and colleagues demonstrated that under oxidative stress conditions Dj-1 binds to the DNA binding motif of p53, and thereby, blocks the transcriptional activity of p53, which was confirmed by the decreased expression of dual-specificity phosphate 1 (DUSP1), one of the genes, regulated by p53. In addition, they could show that the C106 residue of Dj-1 was essential for this interaction, since a C106S mutant was not able to interact with p53 (Kato et al., 2013). Interestingly, the additional level of complexity in regulation of the ERK pathway by Dj-1 can be found here; since DUSP1 is a negative regulator of ERK (Jeffrey et al., 2007), and therefore, Dj-1 via binding to p53 decreases DUSP1 expression and positively regulates the ERK pathway. Negative regulation of p53 by Dj-1 was also demonstrated by Fan and co-workers, who showed that Dj-1 downregulates p53-mediated expression of Bcl-2-associated X protein (BAX), thus, decreasing the activity of the p53-BAX-caspase pathway and promoting the cytoprotection (Fan et al., 2008). It was also described that Dj-1 interacts with Sirtuin-1 (SIRT1) and activates SIRT-1 deacetylase activity, thereby facilitating sequential inhibition of p53 transcriptional activity by SIRT1 (Takahashi-Niki et al., 2016). In addition, it worthwhile to mention that Dj-1 could be phosphorylated in a p53-dependent manner, although the functional role of this modification is still unknown (Rahman-Roblick et al., 2008).

3.2.3.3.6 The phosphoinositide 3-kinase/protein kinase B (PI3K/AKT) pathway

Another pathway, which was shown to be regulated by Dj-1 is the PI3K/AKT pathway. This pathway is one of the major cellular mechanisms controlling cell growth and preventing cell death. Under growth stimuli, such as epidermal growth factor (EGF) exposure, PI3K activates AKT by phosphorylation, which subsequently leads to stimulation of downstream effectors of AKT, with following promotion of cell growth; PTEN is known as a negative regulator of this pathway (Martini et al., 2014; Salmena et al., 2008). Originally, Dj-1 was found as a suppressor of PTEN function in drosophila and mammalian cells (Kim et al., 2005b). Later on it was demonstrated that Dj-1 can directly bind to PTEN and inhibit its enzymatic activity. Interestingly, under oxidative stress conditions, this interaction was increased which led to hyper activation of the PI3K/AKT pathway and promoted cell survival. Moreover, the C106 residue of Dj-1 was found to be important for this mediatory function (Kim et al., 2009). Brain lysates from Dj-1 knockout mice and rats were found to have an increased level of PTEN and decreased levels of phosphorylated

AKT, which again supports the role of DJ-1 in PI3K/AKT pathway regulation (Hauser et al., 2017). Aleyasin and colleagues showed that in mice, under MPTP treatment, Dj-1 promotes the survival of dopaminergic neurons via AKT mediated pathways. Inhibition of AKT, or Dj-1 deficiency, led to more drastic neuronal damage. *In vitro* experiments performed by authors revealed the similar results (Aleyasin et al., 2010). Recently, Wu and co-workers published that Dj-1 plays a role in glucose homeostasis and maintenance of the energy balance via regulation of brown adipose tissue activity. The authors revealed a molecular mechanism, according to which Dj-1, together with mind bomb-2 (Mib2), inhibits PTEN activity, which is associated with a subsequent AKT pathway activation and inhibition of uncoupling protein-1 (UCP1) expression. Therefore, on a high fat diet, Dj-1 knockout mice had higher UCP1 expression and as consequence increased energy expenditure and lower fat mass; in contrast, Dj-1 transgene animals had a lower UCP1 expression, higher fat mass and developed glucose intolerance (Wu et al., 2017). In addition, mice with a knockout of Dj-1 are also found to have lower UCP4 and UCP5 (known as major uncoupling proteins of the brain) expression and increased oxidation of matrix proteins, especially in the SNpc (Guzman et al., 2010).

3.2.3.3.7 Other pathways

Dj-1 was found to activate cholecystokinin (CCK) gene expression via interaction with the Ras-responsive element binding protein 1 (RREBP1) on the promoter region of *CCK*. Interestingly, CCK is known to be expressed in dopaminergic neurons of the SNpc and regulates dopamine release. Therefore, Dj-1 could possibly play a role in mediating dopamine turnover (Yamane et al., 2013).

It was reported that Dj-1 participates in the regulation of fatty acids metabolism via mediating the expression of low-density lipoprotein receptor (LDLR) gene. Dj-1 via interaction with sterol regulatory element binding protein (SREBP) binds to the sterol regulatory element (SRE) of *LDLR* gene promoter, with following activation of *LDLR* expression (Yamaguchi et al., 2012).

Another mediating role of Dj-1 was demonstrated in the nuclear factor kappa-light-chain-enhancer of activated B-cells (NFkB) pathway. Dj-1 was found to interact with Cezanne, a negative regulator of the NFkB pathway. This interaction led to a decrease of de-ubiquitination activity of Cezanne which promoted the transcriptional activity of NFkB (McNally et al., 2011). Furthermore, Dj-1 was found to interact with the N-lysine methyltransferase SET-domain containing 6 protein (SETD6) at chromatin level under basal conditions (Chen et al., 2016). SETD6 is known to down-regulate activity of NFkB by direct methylation of L310 of the NFkB Rel A subunit (Levy et al., 2011). Therefore, it is possible that Dj-1 mediates NFkB via interaction with SETD6. Interestingly, SETD6 activates the Wnt/ β -catenin pathway via direct interaction and methylation of p21-activated kinase 4 (PAK4). This pathway is well known to play an important role in the development and homeostasis of midbrain dopaminergic neurons (Joksimovic and Awatramani, 2014; L'Episcopo et al., 2014). Therefore, unraveling the potential functional consequences of DJ-1 and SETD6 interaction could be a perspective direction in pathoetiological studies of Dj-1 associated PD.

3.2.3.4 Chaperone function of Dj-1

Shendelman and colleagues found that *in vitro* and *in vivo* Dj-1 has a redox-sensitive molecular chaperone activity, and under oxidative stress conditions could inhibit α -synuclein aggregation (Shendelman et al., 2004). It was also shown that Dj-1 directly interacts with α -synuclein mono- and oligomers, and overexpression of Dj-1 leads to a decrease of α -synuclein dimerization (Zondler et al., 2014). Similar results were obtained by Zhou and co-workers, as they also showed that the reduced form of Dj-1 does not interact and not inhibit the aggregation of α -synuclein, and that mild oxidation of the C106 residue is important for implementation of this function (Zhou et al., 2006). However, an additional, Dj-1 dependent mechanism of α -synuclein aggregate degradation was revealed by Xu and co-authors, when they demonstrated that Dj-1 knockdown in SH-SY5Y cells and Dj-1 knockout in mice led to a decrease in the levels of lysosomal 70 kDa heat-shock cognate protein (HSC70) and lysosome-associated membrane protein 2a (LAMP2A) in lysosomes, which was linked with disturbances in chaperone-mediated autophagy and, as consequence, increased α -synuclein aggregation was observed (Xu et al., 2017).

As mentioned above, Dj-1 can activate SOD1 expression via the ERK pathway (Wang et al., 2011). Furthermore, Dj-1 was found to modulate the activity of SOD1 in a copper dependent manner, and possibly represents a copper chaperone for SOD1, although the exact mechanism is still unknown (Giroto et al., 2014; Xu et al., 2010). Interestingly, copper(II)-diacetyl-di(N4-methylthiosemicarbazone) (Cu(II)ATSM) treatment increased intracellular Cu(II) levels, the association of Dj-1 and SOD1 and activity of SOD1 in human vascular smooth muscle cells and cardiomyocytes (Srivastava et al., 2016).

3.2.3.5 Enzymatic activities of Dj-1

Dj-1 structure is similar to protease I from *Pyrococcus horikoshii*, although, its catalytic site is blocked by the 9th α -helix (Honbou et al., 2003). Apparently, Dj-1 is a zymogen with a low-intrinsic proteolytic activity. Under moderate oxidative stress, in the SH-SY5Y cells, C-terminal amino acid residues of Dj-1 are cleaved and it becomes an active protease. It was also shown that the C-terminally cleaved Dj-1 with activated protease activity possesses a higher protective function against oxidative stress (Chen et al., 2010). Mitsugi and co-authors described in their studies that the C-terminal α -helix cleaved Dj-1 has a higher protease activity in comparison with wildtype Dj-1. They also clarified the most sensitive sequence for Dj-1 protease activity – VKVA, and could demonstrate that cleaved α -helix Dj-1 was able to cleave the c-abl oncogene 1 product (ABL1) and kinesin family member 1B (KIF1B) containing VKVA motifs (Mitsugi et al., 2013).

Dj-1 was reported to have a peroxidase activity. Andres-Mateos and colleagues described Dj-1 as an atypical peroxiredoxin-like peroxidase. They also showed that isolated mitochondria from young and old Dj-1 knockout mice have a 2-fold increase in H₂O₂ content, and that Dj-1 implements its peroxidase activity by scavenging H₂O₂ via oxidation of C106 residue (Andres-Mateos et al., 2007).

Glycative stress, caused by highly reactive bicarbonyls and carbonyls reactions with proteins and other substrates (products of these reactions are called advance glycated end products (AGEs)),

is associated with many pathological conditions, including neurodegeneration (Rabbani and Thornalley, 2015). Interestingly, concerning the link of AGEs and PD, Uchiki and co-workers demonstrated that in mice fed with high glycemic index diet, the region mostly affected by AGEs was SN, which points towards a higher susceptibility of this region (Uchiki et al., 2012). Dj-1 was found to counteract the production of AGEs by two types of enzymatic activities. From one side, Lee and colleagues described Dj-1 as a novel glutathione independent glyoxalase, which can directly convert highly reactive 2-oxoaldehydes, such as methylglyoxal (MG) and glyoxal (GO) to D-lactate and glycolate (Lee et al., 2012). Intriguing data were produced by Toyoda and co-authors who could demonstrate that supplementation of Dj-1 knockdown HeLa cells with D-lactate or glycolate is able to rescue altered mitochondrial potential, which was promoted by the knockdown of Dj-1 in these cells. Moreover, they revealed that supplementation of D-lactate or glycolate increased the survival rate of mesencephalic dopaminergic neurons *in vitro* during paraquat treatment (Toyoda et al., 2014). Thus, Dj-1 with its glyoxalase activity prevents production of AGEs and in addition promotes mitochondrial homeostasis by generation of D-lactate and glycolate.

From the other side, Dj-1 was described as a novel deglycase, preventing Schiff bases formation by MG and GO with cysteine, arginine, and lysine residues of the proteins. It was demonstrated that it could recover serum albumin, glyceraldehyde-3-phosphate dehydrogenase, aldolase, and aspartate aminotransferase, thereby reducing Schiff bases formation and proteins damage. C106 residue plays an important role in deglycase activity of Dj-1 (Richarme et al., 2015). The same group displayed the ability of Dj-1 to repair glycated guanine (Richarme et al., 2017). Thus, Dj-1 with its deglycase activity can potentially directly counteract the processes of protein and DNA damage.

Recently, additional enzymatic activity of Dj-1 was characterized by Vázquez-Mayorga and collaborators. They demonstrated that Dj-1 has an esterase activity against 4-nitrophenyl acetate (pNPA). This enzymatic activity was increased during oxidative stress exposure, and the residue C106 is essential for this functional activity. Furthermore, the PD associated mutant of Dj-1 - M26I, was inefficient to hydrolase pNPA compound (Vázquez-Mayorga et al., 2016).

Taken all together, it is unquestionable that Dj-1 is a multifunctional, ubiquitously expressed protein, which plays an important role in the regulation of various cellular and physiological processes. Being an oxidative stress sensor with a various enzymatic activities and abilities to regulate many cellular pathways, Dj-1, with no doubt, appears to be a crucial protein participating in cellular protection mechanisms. Homozygote mutations in Dj-1 are known to be a pathological factor for early onset PD, which is undoubtedly due to disturbances in many crucial functions of this protein.

3.3 Neuroinflammation and Parkinson's disease

3.3.1 Neuroinflammation in Parkinson's disease patients

Neuroinflammatory processes have been known to be associated with the development and progression of PD for a long time. One of the first, who described the presence of reactive

microglia in the SN of PD patients' postmortem brains was McGeer and colleagues in the late 80s of the last century (McGeer et al., 1988). Later on, Boka and co-workers detected a high content of tumor necrosis factor- α (TNF- α) reactive glial cells in the SN of PD patients, which was not observed in the control group. In addition they found receptors for TNF- α in almost all the SN dopaminergic neurons of the patients and control group, which led them to propose the idea that TNF- α driven inflammation could be involved in pathogenesis of PD (Boka et al., 1994). It was also reported that the amount of major histocompatibility complex (MHC) class II-positive microglia was increased in the SN of PD patients, together with cytokines such as TNF- α and interleukin-6 (IL-6). This observation further hints towards increased inflammatory and neuropathological processes within the SN region of PD patients (Imamura et al., 2003). Since the time of McGeer's publication, much research was done on this topic, most of which indicated the presence of highly reactive glial cells and an increased amount of pro-inflammatory cytokines in the SN region of PD patients' brains (Blandini, 2013; Hirsch and Hunot, 2009; Hirsch et al., 2012; Khandelwal et al., 2011; Tufekci et al., 2012). Furthermore, observations made by positron emission tomography (PET) revealed the presence of activated glial cells and inflammatory processes in various regions, including the SN, of PD patients' brains. It was also demonstrated that the inflammatory processes had a positive correlation with the motor symptoms of PD and a negative correlation with dopaminergic terminal density (Gerhard et al., 2006; Ouchi et al., 2005). Interestingly, signs of neuroinflammation were also found in the cerebrospinal fluid (CSF) of patients, although, it is still quite difficult to find universe biological markers for an early diagnosis of PD; these complications could be explained by the multifactorial pathoetiology of this complex disorder (Andersen et al., 2017; Kim et al., 2014; Parnetti et al., 2013).

Although, neuroinflammatory processes were extensively studied in the context of PD development, there is no common opinion whether the inflammation is cause or consequence of neurodegenerative events. From one side, it is possible that prior infections or systemic inflammation could propagate into the brain and activate inflammatory events there, which in the end will lead to neurodegenerative processes. From the other side, it is also possible that the outbreak can happen inside the brain, when stressed neurons activate glial cells with following upregulation of neuroinflammatory processes with subsequent neurodegeneration as result. It is worthwhile to mention, that the dopaminergic neurons of the SN are highly sensitive to inflammatory stimuli, such as cytokines. Interestingly, the density of microglial cells is very high in the region of the SN (Kim et al., 2000; Tansey and Goldberg, 2010; Vivekanantham et al., 2015). Therefore, activated inflammatory processes during the development of PD could have more detrimental effects on the neurons of the SN, degeneration of which usually is linked with an onset of the motor phenotypes of this disorder.

3.3.2 Microglia polarization stages

Microglia are the main immune cells in the central nervous system (CNS), providing the immune defense through innate and adaptive immune responses. Although they represent only up to 20% of the brain's cells, their functions are crucial. Under physiological conditions they scan the brain, remove debris and dead cells via phagocytosis and support the homeostasis of CNS (Nimmerjahn et al., 2005; Streit, 2002). Microglia express a variety of different receptors, which are important

for the recognition of pathogen associated molecular patterns (PAMPs) or endogenous signals (Kielian, 2006; Saijo et al., 2013). Interestingly, there are several reports which indicate that microglia expresses specific receptors for the chemokines and immunomodulators produced by neurons, indicating an importance of microglia-neuronal interaction in the context of CNS homeostasis (Chang et al., 2000a, 2000b; Mott et al., 2004; Sheridan and Murphy, 2013). In addition, microglia express high amounts of P2Y receptors, for which ATP molecules are ligands. Damaged neuronal and glial cells in the inflamed region release high amounts of ATP, serving as an attractant for microglia, which come to the injured area and, via further activation of P2Y receptors, release pro-inflammatory cytokines such as TNF- α and IL-1 β (Davalos et al., 2005; George et al., 2015).

Microglia exist in two major phenotypes: pro-inflammatory stage (M1) and anti-inflammatory stage (M2). Microglia can polarize towards different phenotypes according the stimulus, which the cells receive from the surrounding area. Classical ligands, driving microglia towards the pro-inflammatory stage are interferon gamma (IFN- γ) and lipopolysaccharide (LPS) (Colton and Wilcock, 2010; Martinez and Gordon, 2014; Wilcock, 2012). These compounds are recognized via different receptors (interferon gamma receptors 1 and 2 for IFN- γ and toll-like receptor 4 (TLR4) in case of LPS) and activate the expression of similar gene combinations, typically expressed in the pro-inflammatory stages (Hu and Ivashkiv, 2009). Polarized towards the M1 stage microglia produce and release pro-inflammatory cytokines such as TNF- α , IL-1 β , IL-6, IL-12, IL-23 as well as some chemokines (C-X-C motif chemokine 10 (CXCL10) and CC-motif ligand 2 (CCL2)). Furthermore, expression of several redox enzymes (nicotinamide adenine dinucleotide phosphate (NADPH) oxidase and nitric oxide synthases (iNOS)) and free radical production were found to be up-regulated by microglia during this stage, as well as surface exposure of MHCII (Block et al., 2007; Boche et al., 2013; Colton and Wilcock, 2010; Ransohoff and Perry, 2009).

In contrast to the M1 pro-inflammatory and pro-killing state, the M2 phenotype is known to be associated with healing processes. This stage consist of three subclasses: M2a, M2b and M2c. These three subclasses are subdivided according several parameters. First of all, they are characterized by a different set of molecules and factors expressed during the activation state. Second, the polarization of microglia towards the different subclasses of the M2 stage is driven by different ligands. The M2a stage is activated by IL-4/IL-13, the M2b stage by immune complexes and the M2c stage by IL-10 (Wilcock, 2012). Despite the fact that during the different M2 subtype activation various combinations of molecules need to be produced, most of them belong to the inflammation suppression molecules and such molecules that activate healing and tissue reparation processes. Thus, IL-4 or IL-13 lead to expression activation of arginase 1 (which is most probably linked with an increased production of polyamines). Furthermore, many anti-inflammatory cytokines and mediator molecules such as IL-4, IL-6, IL-10, IL-13, IL-1RA, YM1, peroxisome proliferator-activated receptor gamma (PPAR γ) and FIZZ1 are released during this stage. Activation of M2 polarization by IL-10 causes the upregulation of expression and release of TGF- β , IL-10, FIZZ1 and PPAR γ (Lu et al., 2013; Orihuela et al., 2016). From the three M2 subclasses, M2b polarization, mediated by the immune complexes, is not so well understood. Experiments with macrophage polarization could demonstrate that during the M2b stage cells have similar cytokine profiles (IL-12 low, IL-10 high) with other M2 subclasses, although the other typical markers of the M2 stage such as arginase 1, FIZZ1 and YM1 were missing, which in turn

resembles the profile of M1 stage (Mosser and Edwards, 2008; Orihuela et al., 2016). In addition, during the M2b stage, cells had a high expression of MHCII and cluster of differentiation 86 (CD86) (like at M1 stage), which speaks for an ability to activate T cells. Interestingly, M2b macrophages were able to activate T cells towards the Th2 lineage differentiation, which could probably mean that cells in the M2b stage could be possible initiators of the M2 stage (Edwards et al., 2006).

Although, the stages of microglia/macrophage polarization are quite well characterized in regards of pro- and anti-inflammatory responses, recent publications shed more light on this topic, which makes it more complicated. Several collectives described that during multiple sclerosis or traumatic brain injury the profiles of many microglia and macrophage cells could not be completely attributed to one of the polarization stages (Martinez and Gordon, 2014; Morganti et al., 2016; Vogel et al., 2013). It looks like the immune cells could co-exist in different stages simultaneously. These results were supported by Kim and colleagues, who could demonstrate, using the modern single cell RNA-sequencing method, that during the traumatic brain injury macrophages simultaneously expressed high levels of different polarization stage markers (Kim et al., 2016). These results revealed that the picture of microglia/macrophage polarization is probably much more complex, than the classical explanation. It might be, that the cells exist within an equilibrium of different stages, which can be moved by different internal and external stimuli. Moreover, when the stimuli are specific, strong or persist during a particular period of time, this equilibrium could be destroyed in some cell populations, and the phenotype of these cells will be moved towards aggressive pro-inflammatory stage, with a following progression of inflammatory events, or towards the anti-inflammatory stages, and therefore, healing and tissue repair events. As already mentioned above, different types of analysis of PD patients revealed the presence of neuroinflammatory processes, attributed, according the markers, to the M1 stage of microglia polarization. Therefore, during PD progression, the M1 stage microglia are getting predominant and inflammatory events, linked with neurodegenerative processes, are taking place.

3.3.3 Parkinson's disease animal models and neuroinflammation

Since the time of McGeer's publication about possible involvement of neuroinflammation in the neurodegenerative processes and development of PD, a lot of research was done to investigate the link between inflammation and neurodegeneration in animal models of PD. Several commonly accepted pharmacological models of PD were described to show significant upregulation of neuroinflammatory processes subsequent to administration of chemical agents. It was demonstrated in 6-OHDA mouse models that the degeneration of dopaminergic neurons of SN was accompanied by a pronounced microglia activation (Marinova-Mutafchieva et al., 2009) and TNF- α release (Mogi et al., 2000). Degeneration of dopaminergic neurons in SN of mice during the course of paraquat treatment was also found to be associated with the presence of reactive microglia, and increased content of IL-1 β and NO in this region (Purisai et al., 2007; Yadav et al., 2012). Furthermore, microglia activation in the SN of rats was also observed in a rotenone PD model, and was preceding the anatomical indication of dopaminergic neurons loss (Sherer et al., 2003). Neuronal loss in SN of MPTP treated rodents was found to be associated with microglia

activation and the production of cytokines (IL-1 β , TNF- α) and mediatory molecules (IFN- γ , NO) associated with the M1 microglia polarization state (Członkowska et al., 1996; Lofrumento et al., 2011; Luchtman et al., 2009). Interestingly, some of the markers of the anti-inflammatory microglia stage M2 (TGF- β , CD206) were found to be reduced during MPTP exposure (Pisanu et al., 2014). Intriguingly, the use of minocycline (a selective inhibitor of the M1 stage of microglia polarization (Kobayashi et al., 2013)) was found to protect dopaminergic neurons from degeneration due to paraquat (Purisai et al., 2007), 6-OHDA (He et al., 2001), and MPTP (Du et al., 2001; Wu et al., 2002) exposure in rodents models, indicating the involvement of M1 polarized microglia in neurodegenerative processes within these models of PD.

Neuroinflammatory processes were also routinely analyzed in the different genetic animal models of PD. As it was already mentioned above, α -synuclein was the first gene identified to be involved in the dominantly inherited form of PD (Polymeropoulos et al., 1997). It was demonstrated that activated microglia show a high correlation with the deposition of α -synuclein in the SN of PD patients' brains. Different α -synuclein animal models were also found to have inflammatory hallmarks in the SN. Thus, mice overexpressing human α -synuclein under the Thy1-promoter were found to have activated microglia in the SN, which was accompanied with high levels of TNF- α (Watson et al., 2012). Similar results were demonstrated in mice overexpressing human α -synuclein under the TH-promoter (Su et al., 2008). In an alternative model, where α -synuclein was overexpressed just in the SN of mice by the use of recombinant adeno-associated virus (rAAV), activation of microglia and increased expression of the M1 polarization stage markers were observed in this region, whereas M2 markers were unchanged (Theodore et al., 2008). Intriguing results were demonstrated by Barkholt and co-authors, who showed that overexpression of the α -synuclein mutant A53T in monkeys' midbrain led to degeneration of dopaminergic neurons, although wildtype α -synuclein did not have such an effect. Furthermore, the neurodegeneration was accompanied with an increase in microglia with macrophage morphology, whereas, in a wildtype α -synuclein treated animals, there were different types of microglia morphology present. Therefore, already a point mutation in α -synuclein is able to change the properties of the protein in a way to cause a more harmful inflammatory response (Barkholt et al., 2012).

Lrrk2 is another gene, mutations in which are known to be associated with dominant inherited forms of PD. Several rodent models with *Lrrk2* pathological mutations or knockout/knockdown of *Lrrk2* were able to demonstrate the involvement of this protein in inflammatory processes, mostly via regulation of the M1 polarization stage of microglia (Daher et al., 2014; Kim et al., 2012; Moehle et al., 2012).

Genes, involved in recessive inherited forms of PD, were also reported to be involved in neuroinflammatory processes. Thus, mice, lacking *Parkin*, were found to have an aberrant activation of microglia in the midbrain (Rodríguez-Navarro et al., 2007). Additional LPS treatment of *Parkin* knockout mice led to an increased inflammatory response in comparison with wildtype animals (Frank-Cannon et al., 2008; Tran et al., 2011). Increased levels of inflammation were demonstrated in PINK-1 knockout models under basal and LPS treated conditions (Akundi et al., 2011; Kim et al., 2013a).

There is not so much known about neuroinflammatory processes in animals lacking Dj-1. Chien and colleagues reported that Dj-1 knockout mice have a higher level of IFN- γ and interferon-inducible T-cell alpha chemoattractant (I-TAC) in the SN. Moreover, this increase was accelerated by intra-nigral injections of LPS, accompanied by the increased degeneration of dopaminergic neurons in Dj-1 knockout animals (Chien et al., 2016). It was demonstrated by Kim and co-workers that microglia from Dj-1 null mice expressed higher amounts of neuroinflammatory genes in response to IFN- γ treatment. Furthermore, they unraveled the mechanism by which Dj-1 attenuated the inflammation. During IFN- γ exposure Dj-1 facilitated the interaction between signal transducer and activator of transcription 1 (STAT1) and Src-homology region 2 domain-containing phosphatase-1 (SHP-1), which downregulated the inflammatory processes (Kim et al., 2013b). Therefore, probably loss of function mutations of Dj-1 could be associated with a greater neuroinflammatory potential and neurodegenerative processes.

As discussed above, Dj-1 is a multifunctional protein, homozygote mutations in which lead to the onset of PD. From the other side, neuroinflammatory processes are known to be associated with the development of this disorder. Unfortunately, too little is known about the function of Dj-1 in cells responsible for the neuroinflammatory processes, and therefore, unraveling the role of Dj-1 in microglia cells is a high priority task.

4 Aim of the thesis

Parkinson's disease is one of the most abundant neurodegenerative diseases affecting human population around the world. Currently there is no efficient treatment, since pathoetiological mechanisms of this disorder are not completely understood. Nowadays more and more attention of scientific society is given to understand the function of glial cells, which are known to play a crucial role in the processes of brain tissues homeostasis. Amongst these cells an important place is attributed to microglia cells – immune guardians of the brain. Up to date a huge amount of studies was performed, which demonstrated the involvement of microglia cells in the process of PD development. Most of this research is concentrated on the function of microglia cells at M1 polarization stage, since overrepresentation of cells within this stage can lead to intensification of inflammatory processes with consequent neurodegeneration events.

Recently in our laboratory it was demonstrated that during the inflammatory activation, associated with polarization of microglia towards M1 stage, expression of MTHFR - one of the major enzyme of one-carbon metabolism is dysregulated in Dj-1 deficient microglia. Thus, the main hypothesis behind this thesis is that the Parkinson's disease associated processes linked with loss-of-function mutations in Dj-1, could be attributed to the malfunction of metabolic processes or changes in their dynamics during the transformation of microglia towards M1 polarization stage.

Therefore, the aim of this thesis is to assess the metabolic pathways linked to the one-carbon metabolism and the energy metabolism in Dj-1 deficient microglia, in the non-activated state and during their polarization towards M1 pro-inflammatory stage.

5 Results

Previously results in our laboratory, obtained from microarray analyses, showed that under LPS exposure, expression of several genes in primary microglia and the SNpc of Dj-1 knockout mice was changed (unpublished). Amongst these genes was *Mthfr*, which is one of the main enzymes in the one-carbon cycle. This cycle is an important cellular hub, with which many other biochemical pathways are linked (e.g. nucleotides synthesis, methylation pathways and glutathione production via the transsulfuration pathway) and dysregulation of only one enzyme could theoretically lead to an imbalance in many branches of the cellular metabolism. Therefore, as stated above, one of the main objective of this thesis was to investigate the consequences of *Mthfr* dysregulation in Dj-1 knockout microglial cells as well as defining the molecular mechanism by which Dj-1 might regulate *Mthfr* expression.

5.1 Isolation of primary microglia and determination of their purity

To investigate the role of Dj-1 in primary microglia I first had to establish a protocol of isolation of primary microglia resulting in a microglia culture of high purity and a reasonable amount of cells. The former is necessary in order not to unequivocally attribute the obtained results to microglia when they might be obtained due to contamination with other cell types, specifically astrocytes. The latter is vital for having enough material for population based analysis such as qPCR and western blotting. Thus, to this end I applied a protocol which was formerly set up in our laboratory (see 8.2.1.5) and assessed the purity by immunohistochemical stainings for ionized calcium-binding adapter molecule 1 (IBA-1) as a microglial marker and glial fibrillary acidic protein (GFAP) as an astrocytic marker (fig. 2). As a positive control for the GFAP stain, which was never detected in the primary microglial cultures using the above protocol, I performed an “incomplete” astrocytic layer isolation (a step necessary in this protocol) resulting in detection of GFAP positive astrocytes in these cultures (fig. 2c).

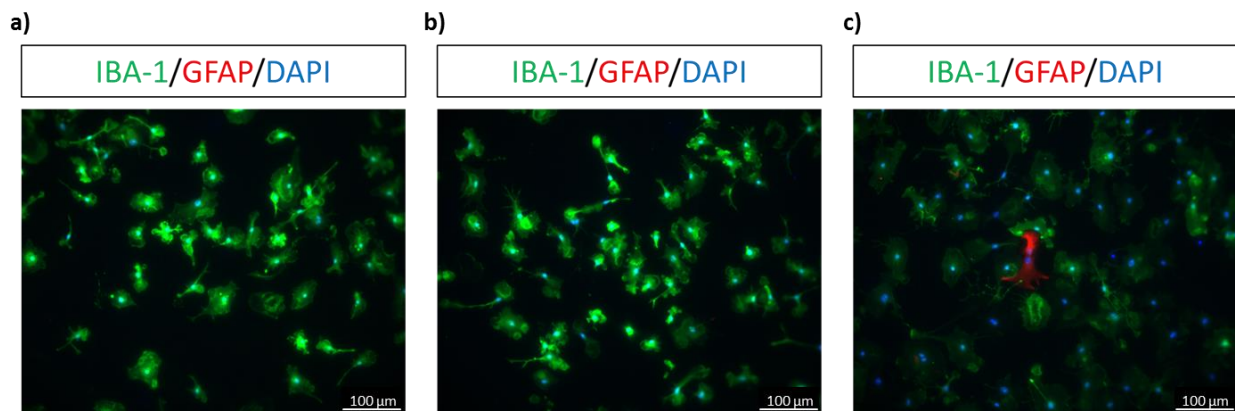


Figure 2: ICC of primary microglial culture isolated from 2-4 days old wildtype (a) and Dj-1 knockout (b) littermates using the microglial marker ionized calcium-binding adapter molecule 1 (IBA-1). (c) Shows a primary microglial culture with astrocytic (marked by glial fibrillary acidic protein (GFAP) expression) contamination.

5.2 Morphological analysis of wildtype and Dj-1 knockout primary microglia during LPS treatment

To investigate whether the lack of Dj-1 protein affects the cell morphology of primary microglia the immunocytochemical stainings of wildtype and Dj-1 knockout cells were performed 6, 12, 24 and 48 hours after LPS treatment (fig. 3).

After LPS treatment both wildtype and Dj-1 knockout primary microglia underwent an activation stage which was characterized by morphological changes from ramified like cells towards amoeboid like phenotype. Qualitatively, there was no obvious difference detected between the genotypes upon LPS treatment.

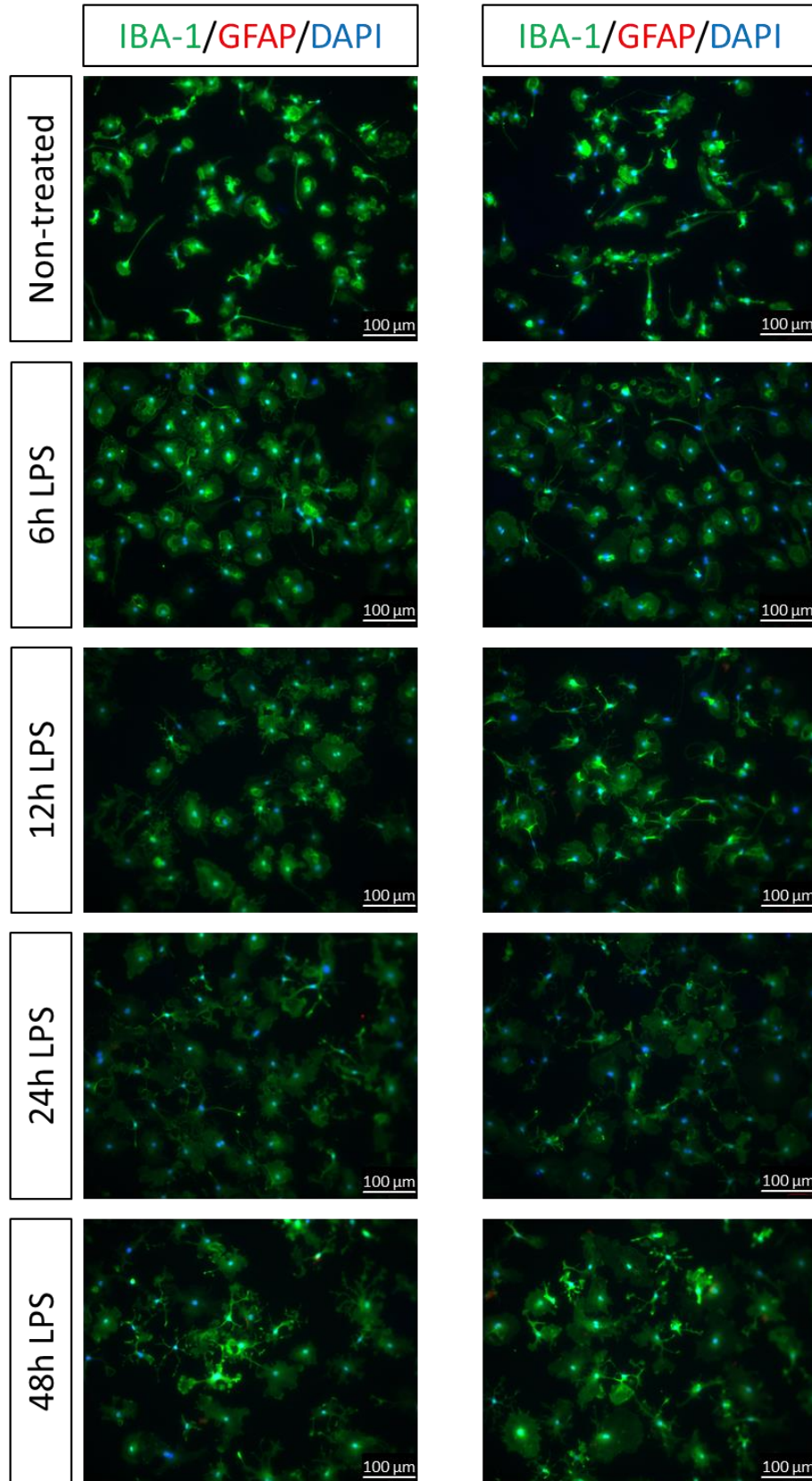


Figure 3: ICC of primary microglia during the course of LPS treatment.

5.3 Validation of MTHFR dysregulation in primary wildtype and Dj-1 knockout microglia

5.3.1 Validation by quantitative PCR

To validate the dysregulation of *Mthfr* detected in the former microarray assays I performed a quantitative polymerase chain reaction (qPCR) with cDNA samples obtained from wildtype and Dj-1 knockout primary microglia. Under basal condition the level of *Mthfr* expression was found to be significantly downregulated in Dj-1 deficient microglia cells (wildtype 0.00072 ± 0.00018 and Dj-1 knockout 0.00047 ± 0.00009 , $p=0.0089$) (fig. 4).

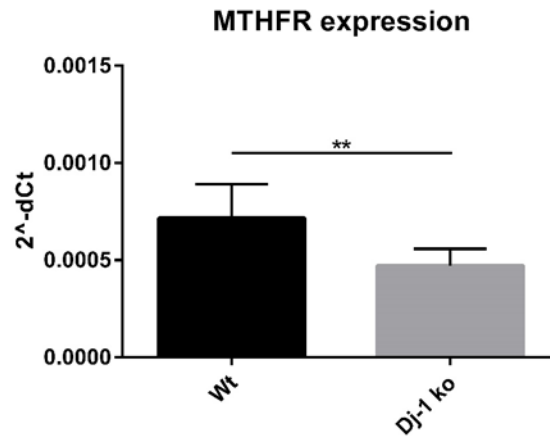


Figure 4: mRNA expression analysis of *Mthfr* in wildtype and Dj-1 knockout primary microglia. Samples were measured with sufficient biological replicates (wt n=8, ko n=6) and in technical triplicates. Bars represent mean \pm sd. Quantification was done via unpaired t-Test: * $p \leq 0.05$, ** $p \leq 0.01$.

To investigate the expression of *Mthfr* during the inflammatory response, analysis of cDNA samples obtained from wildtype and Dj-1 knockout primary microglia was performed under basal and 8 hours after LPS treatment conditions (fig. 5).

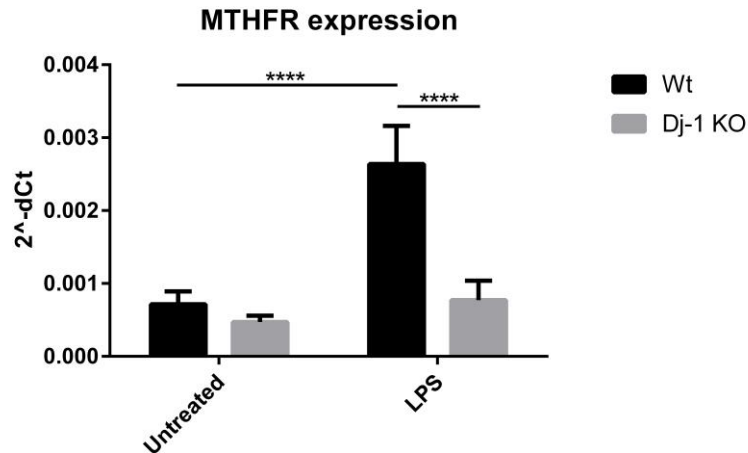


Figure 5: mRNA expression analysis of *Mthfr* in wildtype and Dj-1 knockout primary microglia. Samples were measured with sufficient biological replicates (wt n=8, ko n=6) and in technical triplicates. Bars represent mean \pm sd. Quantification was done using two-way ANOVA analysis and Tukey's multiple comparison test. * $p \leq 0.05$; ** $p \leq 0.01$; * $p \leq 0.001$; **** $p \leq 0.0001$.**

Two-way ANOVA analysis revealed a significant effect of genotype ($F=72.72$, **** $p < 0.0001$), treatment ($F=80.43$, **** $p < 0.0001$) and interaction of genotype and treatment ($F=42.99$, **** $p < 0.0001$). Post-hoc results from qPCR analysis demonstrate that there is a significant difference in *Mthfr* expression between the two genotypes under LPS treatment condition (wildtype 0.002639 ± 0.000524 and knockout 0.00077 ± 0.000267 , $p < 0.0001$), which is caused by an increased elevation of *Mthfr* expression in wildtype microglia (untreated wildtype 0.000715 ± 0.000175 and LPS wildtype 0.002639 ± 0.000524 , $p < 0.0001$) compared to Dj-1 knockout microglia (untreated Dj-1 knockout 0.000471 ± 0.000086 and LPS Dj-1 knockout 0.00077 ± 0.000267 , $p=0.4$).

According to the ensemble database mouse *Mthfr* gene has two major protein coding transcripts (fig. 6a). Therefore, the qPCR with specific primers against these transcripts was performed to understand their relative contribution to the above observed expression analysis, which detected both isoforms (fig. 6b, c).

Two-way ANOVA analysis revealed a significant effect of genotype in (b) ($F=67.68$, **** $p < 0.0001$) and (c) ($F=4.835$, * $p=0.0378$), treatment in (b) ($F=155.8$, **** $p < 0.0001$) and (c) ($F=66.47$, **** $p < 0.0001$), and interaction of genotype and treatment in (b) ($F=44.95$, **** $p < 0.0001$) and (c) ($F=6.819$, * $p=0.0153$). Results from Post hoc test revealed that the *Mthfr*-001 transcript is much higher expressed in primary microglial cells, compared to the *Mthfr*-003 transcript, and that it is responsible for the differences in *Mthfr* expression under LPS condition between wildtype and Dj-1 knockout cells. *Mthfr*-001 transcript has a similar pattern with general *Mthfr* expression profile represented in fig. 5. Thus, there is a significant difference found between the genotypes in *Mthfr*-001 transcript under LPS treatment (wildtype 0.003987 ± 0.000666 and knockout 0.001522 ± 0.000429 , $p < 0.0001$), which is as in case of general *Mthfr* expression is

attributed to a stronger activation under LPS treatment in wildtype microglia (untreated 0.000819 ± 0.000188 and LPS 0.003987 ± 0.000666 , $p < 0.0001$) in comparison to Dj-1 knockout microglia cells (untreated 0.000568 ± 0.000206 and LPS 0.001522 ± 0.000429 , $p = 0.0043$).

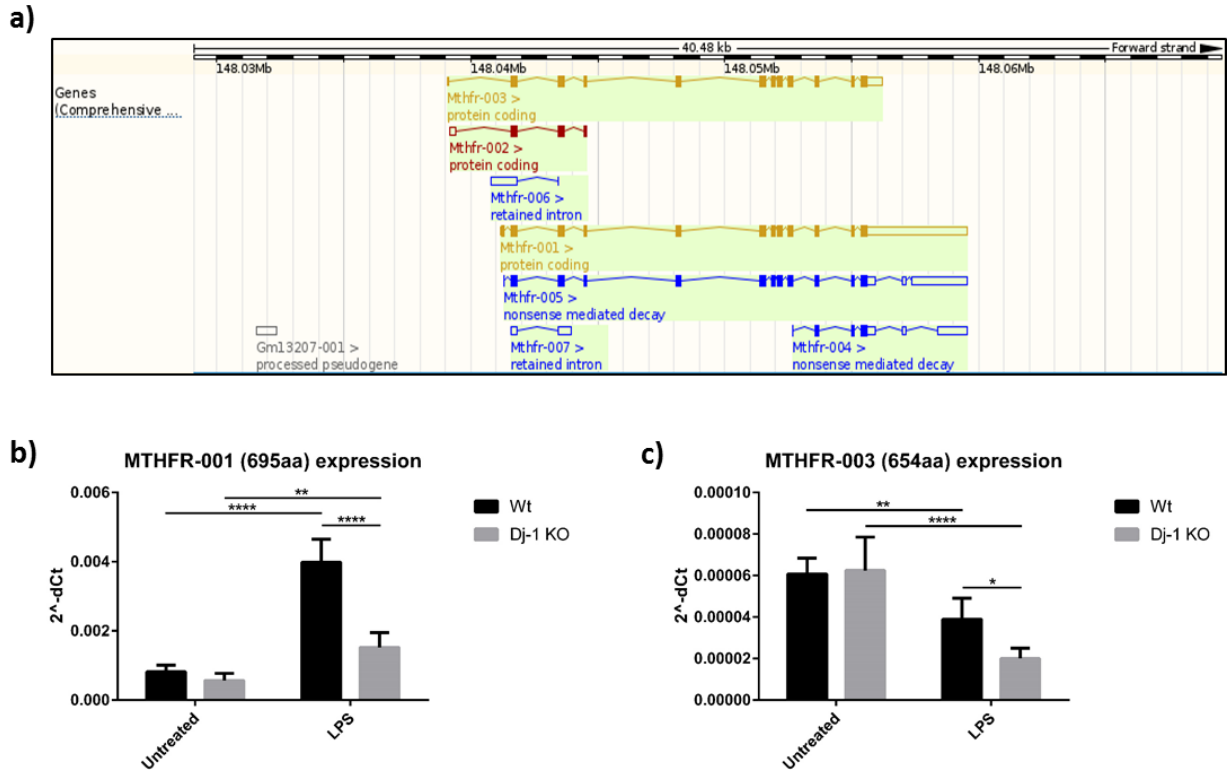


Figure 6: Shown are the different transcripts of *Mthfr*. (a) Displays the *Mthfr* transcript map from ensemble.org; (b) and (c) show qPCR analysis of the protein coding *Mthfr* transcripts, (b) the *Mthfr*-001 transcript and (c) the *Mthfr*-003 transcript under basal and LPS treatment conditions in wildtype and Dj-1 knockout primary microglia. All samples were analyzed with a sufficient biological n (wt n=8, ko n=6) and in technical triplicates. Bars represent mean \pm sd. Quantification was done using two-way ANOVA analysis and Tukey's multiple comparison test. * $p < 0.05$; ** $p < 0.01$; *** $p < 0.001$; **** $p < 0.0001$.

5.3.2 Validation by Western Blot

The next step was to check for differences in *Mthfr* expression on the protein level. Protein samples were isolated from primary wildtype and Dj-1 knockout microglia under basal conditions and after 24 hours of LPS treatment with subsequent western blot analysis (fig. 7).

Two-way ANOVA analysis revealed a significant effect of genotype ($F=18.97$, $***p=0.0003$), treatment ($F=58.98$, $****p<0.0001$) and interaction of genotype and treatment ($F=11.87$, $**p=0.0023$). Post hoc test revealed significant differences in MTHFR protein content under LPS treatment condition between the genotypes (wildtype 4.059 ± 1.333 and Dj-1 knockout 1.914 ± 0.436 , $p<0.0001$). As in case of *Mthfr* expression this effect was attributed to more robust upregulation of MTHFR in response to LPS in wildtype cells (untreated 1.000 ± 0.313 and LPS 4.059 ± 1.333 , $p<0.0001$), than in Dj-1 knockout microglia (untreated 0.750 ± 0.194 and LPS 1.914 ± 0.436 , $p=0.024$). Thus, the pattern of MTHFR upregulation on protein level after LPS treatment mirrored the results obtained from the mRNA expression analysis. Taken together, these results support the data obtained by the microarray assays and suggest that Dj-1 knockout in primary microglia results in the inability to upregulate *Mthfr* expression in response to LPS treatment as efficiently as in wildtype cells.

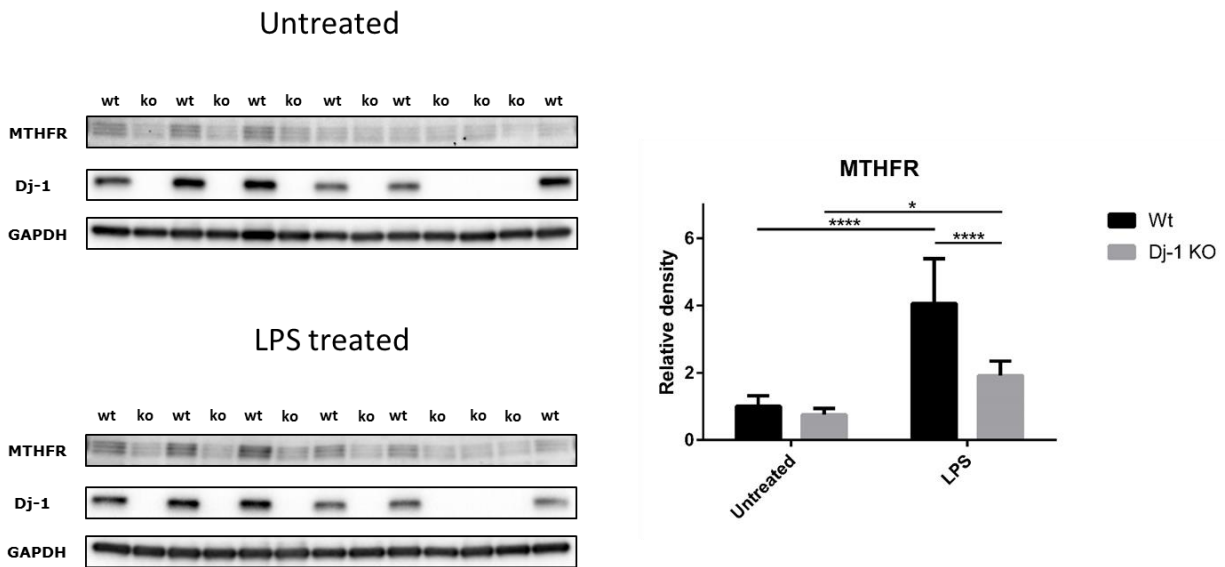


Figure 7: Detection of MTHFR in wildtype and Dj-1 knockout primary microglia under basal conditions and after LPS treatment (24hours) using Western blot. All samples were analyzed with a sufficient biological n (wt n=6, ko n=7). Bars represent mean \pm sd. Quantification was done via two-way ANOVA analysis and Tukey's multiple comparison test. * $p\leq 0.05$; ** $p\leq 0.01$; * $p\leq 0.001$; **** $p\leq 0.0001$.**

5.4 Analysis of metabolites linked to the one-carbon cycle

5.4.1 Detection of S-Adenosylmethionine (SAM), S-Adenosylhomocysteine (SAH), homocysteine, and methylated DNA in primary wildtype and Dj-1 knockout microglia

mRNA and protein expression analysis disclosed that Dj-1 knockout in primary microglia cells causes a dysregulation of *Mthfr* expression. As it was mentioned above, MTHFR is a key enzyme in the one-carbon metabolism, which is connected with several other metabolic cycles (fig. 8). In my analysis I focused on the methionine cycle. Therefore, it was decided to check some components of this one-carbon-linked cycle specifically SAM, SAH and homocysteine. Four wildtypes and Dj-1 knockout microglia cell cultures were either not treated or treated with LPS and analyzed 24 hours later.

Afterwards cells were lysed and enzyme-linked immunosorbent assay (ELISA) performed to detect SAM, SAH or homocysteine. However, ELISA analyses revealed that the levels of all metabolites to be measured in these cell lysates were below the detection level of the ELISAs, highly likely due to the low amount of starting material. Therefore, it is not possible to make any conclusions according the content of these metabolites in wildtype and Dj-1 knockout microglia cells. More sophisticated techniques, such as High-Performance Liquid Chromatography with Electrochemical Detection (HPLC-ED), will have to be used to detect these components in such a low amount of material.

A dysregulated methionine cycle could also lead to changes in the methylation of DNA. Therefore, in addition cell lysate samples were used for DNA isolation with a following methylated DNA detection with ELISA kit. However, I could not detect any significant differences between the genotypes under basal or LPS treatment conditions (fig. 9).

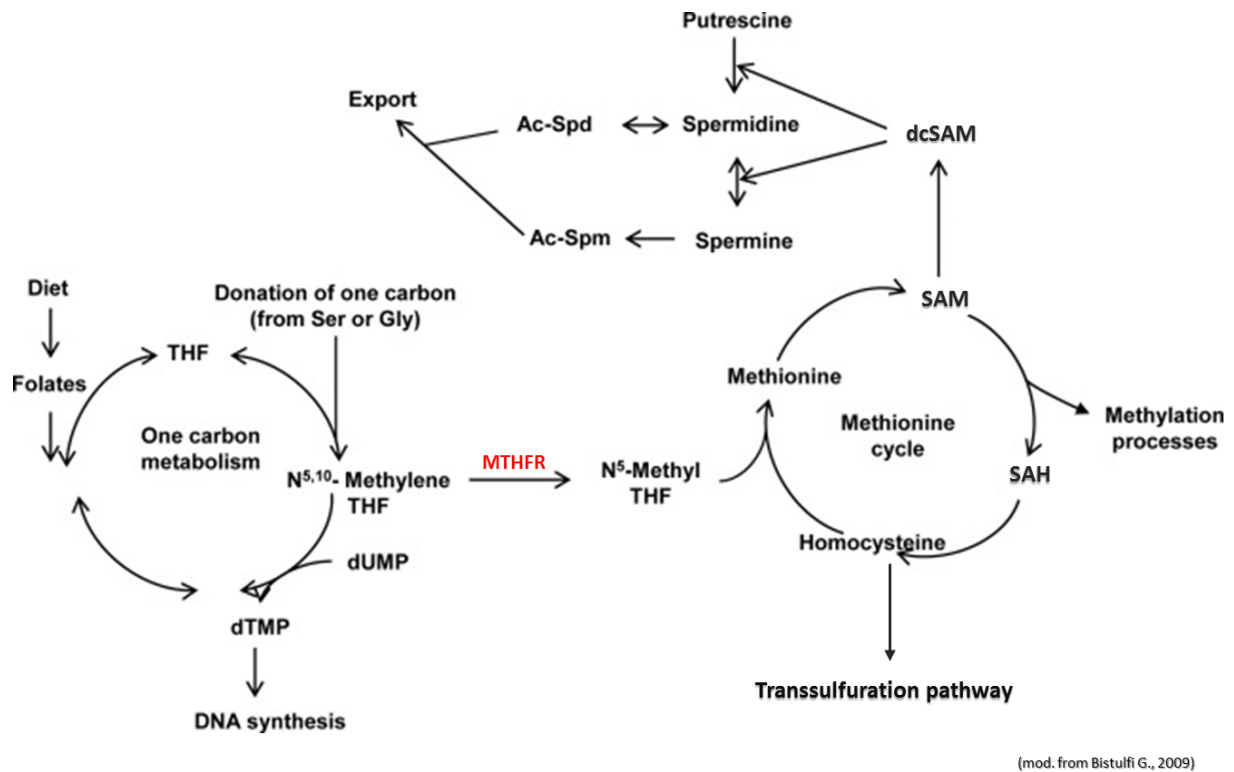


Figure 8: Metabolic map of several cycles with connection to MTHFR. Modified from Bistulfi (Bistulfi et al., 2009).

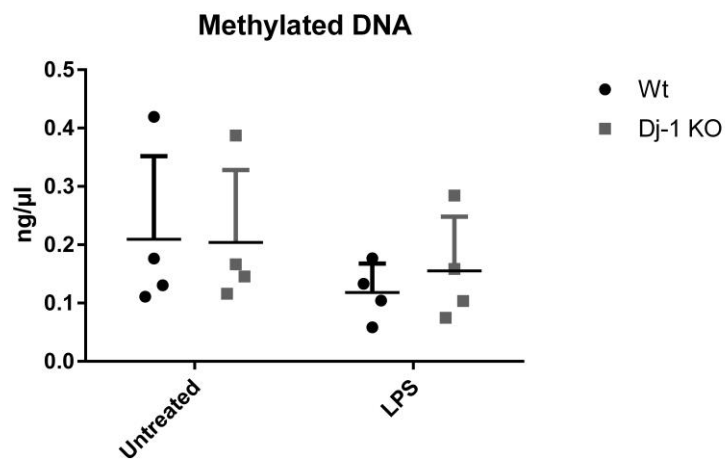


Figure 9: ELISA for methylated DNA in wildtype and Dj-1 knockout primary microglia. All samples were analyzed with a sufficient biological n (wt n=4, ko n=4) and in technical duplicates. Bars represent mean \pm sd. Quantification was done via two-way ANOVA analysis and Tukey's multiple comparison test. * $p \leq 0.05$; ** $p \leq 0.01$; *** $p \leq 0.001$; **** $p \leq 0.0001$.

5.4.2 Metabolome analysis of the ventral midbrain in wildtype and Dj-1 knockout mice

Even though, mainly due to technical issues, I was not able to detect changes in the methionine cycle which might be imposed by the dysregulation of MTHFR in primary microglia, results from the Dj-1 knockout mice (generated in our laboratory) support the idea of metabolic consequences of the dysregulated *Mthfr* expression. On one hand the analysis of homocysteine in the ventral midbrain revealed a significant increase of this metabolite in Dj-1 knockouts (not published data, U. Hafen), on the other hand targeted metabolomics performed in ventral midbrain tissue revealed several metabolites, which were significantly different between the wildtype and Dj-1 knockout animals (table 3). Importantly, two polyamines (putrescine and spermine) were found to be increased in the ventral midbrain of knockout animals. This is an intriguing observation because the synthesis of polyamines is tightly bound with one-carbon metabolism, where MTHFR, which is dysregulated in Dj-1 knockouts plays an important role. Thus, a dysregulation of one-carbon cycle and conjugated with it pathways is highly likely in Dj-1 knockout animals.

Metabolite	p-value	FDR	Ratio (Dj-1 KO vs WT)
Putrescine	0.0000160	0.0028508	1.30
Spermine	0.0000483	0.0043006	1.21
Glutamate	0.0000753	0.0044660	1.19
Hexose	0.0007828	0.0348326	1.32
Asparagine	0.0047371	0.1686393	1.23
Serotonin	0.0062848	0.1864487	1.18
PC.aa.C42.2	0.0150688	0.3084735	0.82
Spermidine	0.0150688	0.3084735	1.12
C14	0.0163559	0.3084735	1.09
PC.aa.C42.6	0.0177360	0.3084735	0.95
Aspartic acid	0.0192142	0.3084735	1.15
PC.aa.C42.1	0.0207960	0.3084735	0.78
PC.ae.C44.6	0.0242929	0.3326265	0.92
SM.C24.1	0.0352626	0.4483386	0.84
C16.1	0.0436317	0.5177633	1.05

Table 3: Metabolites differences in the ventral midbrain of wildtype and Dj-1 knockout mice discovered by targeted metabolomic analysis. Samples from 19 wildtypes (10 males and 9 females) and 20 Dj-1 knockout animals (9 males and 11 females) were analyzed. To assess the statistical significance the Mann-Whitney test was used (column p-value) with subsequent false discovery rate (column FDR) analysis, according to the method of Benjamini and Hochberg (Benjamini and Hochberg, 1995) to correct the p-value for multiple testing (statistical analysis was performed by Dietrich Truembach).

5.5 Investigation of the mechanisms and molecular pathways by which Dj-1 regulates the expression of *Mthfr*

5.5.1 LPS upregulates the *Mthfr* expression via the NFκB pathway

Signal transduction after the activation of the Toll-like receptor 4 (TLR4) by LPS occurs by different molecular pathways including NFκB, ERK, P38, JNK and interferon regulatory factor 3 (IRF3). Of particular interest was the identification of the pathway involved in the upregulation of *Mthfr* expression after LPS exposure. Pickell and colleagues demonstrated that, in the macrophage cell line RAW264.7, upregulation of *Mthfr* expression occurs under control of NFκB (Pickell et al., 2005). It was a good hint for us since macrophages and microglia are relatively closely related in terms of cellular lineage and are likely to share some common regulatory pathways, which may play a role under certain conditions. Therefore, the hypothesis that the NFκB pathway is involved in upregulation of the *Mthfr* expression after LPS exposure in primary microglia cells was checked first. To do so, the inhibitor of NFκB, ammonium pyrrolidinedithiocarbamate (PDTC), was applied for 1 hour before LPS stimulation. *iNos* was chosen as reference gene to check for the efficiency of NFκB inhibition as it well known that expression of this pro-inflammatory gene is tightly regulated by the NFκB pathway.

Two-way ANOVA analysis revealed in (fig. 10a) a significant effect of treatment ($F=23.36$, **** $p<0.0001$), genotype ($F=19.05$, *** $p=0.0003$) and interaction ($F=15.95$, **** $p<0.0001$); in (fig. 10b) only a significant effect of treatment ($F=242.5$, **** $p<0.0001$). Post hoc test of mRNA expression analysis disclosed two important points: 1) upregulation of *Mthfr* expression under LPS condition is NFκB dependent (fig. 10a) (untreated wildtype 0.0009 ± 0.0002 and LPS wildtype 0.0031 ± 0.0008 , $p<0.0001$; LPS wildtype 0.0031 ± 0.0008 and PDTC+LPS wildtype 0.0007 ± 0.0001 , $p<0.0001$) and 2) there is no general problem in the NFκB pathway activation between genotypes as there is no difference in *iNos* expression under LPS treatment (fig. 10b). Taken together, this data suggests that *Mthfr* upregulation under LPS treatment is executed via NFκB pathway and that, most probably, Dj-1 plays a role in this upregulation somewhere downstream of NFκB, potentially in the promoter region of *Mthfr* as otherwise differences between the genotypes in *iNos* expression after LPS exposure would have been observed.

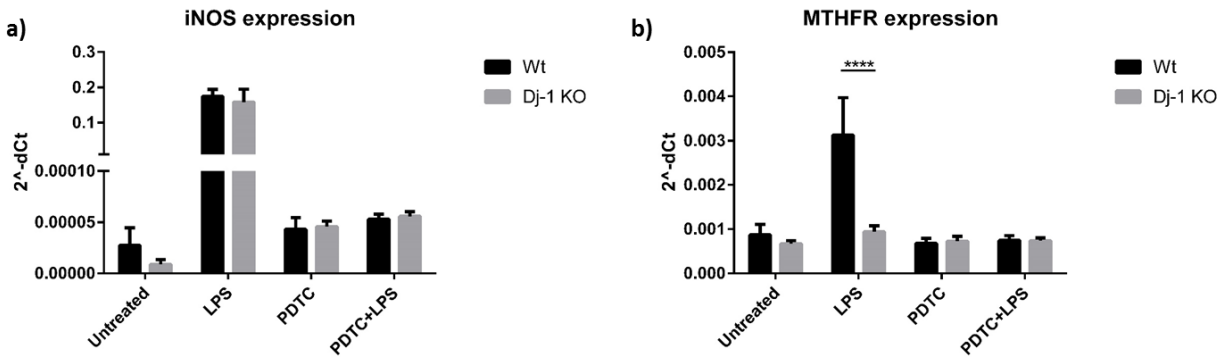


Figure 10: mRNA expression analysis of *Mthfr* (a) and *iNos* (b) in wildtype and Dj-1 knockout primary microglia under different conditions (LPS – activator of TLR4, PDTC – inhibitor of the NF-κB pathway). All samples were measured with an appropriate biological n (wt n=4, ko n = 3) and in technical triplicates. Bars represent mean ± sd. Quantification was done via Two-way ANOVA analysis and Tukey's multiple comparison test. *p≤0.05; **p≤0.01; *p≤0.001; ****p≤0.0001.**

5.5.2 Search of possible interactors of Dj-1 within transcription factors' families

5.5.2.1 *In silico* promoter analysis of *Mthfr* transcripts

Since Dj-1 does not have its own DNA binding motif I assumed that it could regulate *Mthfr* expression in primary microglia cells by interacting with a transcription factor. Therefore, an *in silico* promoter analysis of the *Mthfr* transcripts was performed (*in silico* work done by Dietrich Truembach). Firstly, literature research was done to find information about any transcription factors (TFs) interacting with Dj-1. Additionally, all TFs found to participate in common pathways with Dj-1 were also taken in account. Thus, a list of TFs which could have a close relationships with Dj-1 was established (table 4).

Subsequently, an *in silico* promoter analysis of *Mthfr* transcripts with the purpose of identification of possible binding sites for the chosen TFs was performed.

Among the identified TF binding sites three were possible binding sites for Nr4a2 (Nurr1). This TF is of particular interest because of three reasons: 1) Nurr1 is known to play an important role in the development of dopaminergic neurons (Luo, 2012; Perlmann and Wallén-Mackenzie, 2004), 2) Dj-1 is known to regulate the expression of TH via Nurr1 transcription factor activity (Lu et al., 2012) and 3) Nurr1 inhibits the expression of inflammatory genes on the promoter level via the REST corepressor 1 (COREST) complex by direct binding to NF-κB subunits (Saijo et al., 2009).

Based on these facts, Nurr1 was chosen for validation as the main candidate via which Dj-1 may execute regulation of *Mthfr* expression in primary microglia.

Transcription factor (TF)	Source	Transcription factor family	(most important) Function
Jun	Literature	V\$AP1F	DNA methylation
Nfe2i2	Literature	V\$AP1R	Endoplasmic reticulum unfolded protein response
Lin54	DiGtoP	V\$CHRF	Cell cycle gene homology region (CDE/CHR tandem elements regulate cell cycle dependent repression)
Jun	Literature	V\$CREB	cAMP-mediated signaling, Endoplasmic reticulum unfolded protein response
Ar	Literature	V\$GREF	Glucocorticoid mediated signaling pathway
Nr4a2 (Nurr1)	Literature	V\$NBRE	Dopaminergic neuron differentiation
Tp53	Literature	V\$P53F	DNA damage response, signal transduction by p53 class mediator
Znf281	DiGtoP	V\$ZF02	Cellular defense response, lipid metabolic process, negative regulation of gene expression

Table 4: Transcription factors known to interact with Dj-1 or to regulate common pathways.

5.5.2.2 Transcriptional analysis of the *Mthfr* promoters with Nurr1 and Dj-1 overexpression in HEK293 cells using Luciferase assay

As mentioned above, *in silico* promoter analysis revealed three potential Nurr1 binding sites in the *Mthfr* promoter region (fig. 11a, green bars). Therefore, to investigate the possible role of Dj-1 and Nurr1 in the regulation of *Mthfr* expression, three different promoters, cloned under a luciferase reporter gene, were co-transfected with Nurr1 and Dj-1 overexpression vectors (fig. 11a, c, d, and e) into HEK293 cells.

Results from Kruskal-Wallis tests for (c) and (d) did not reveal significance, however one-way ANOVA analysis for (e) was found significant ($F=27.12$, **** $p<0.0001$). Post hoc test of luciferase activity showed that there was no influence of Nurr1 or Dj-1 on the promoters from the protein coding transcripts (fig. 11c, d), although there was a slight effect of Nurr1 (independent on Dj-1 overexpression) on the promoter region of the *Mthfr*-004 transcript (control 0.2638 ± 0.0819 and Nurr1 overexpression 0.9503 ± 0.2848 , $p<0.0001$; control 0.2638 ± 0.0819 and Dj-1 overexpression 0.2974 ± 0.0954 , $p=0.9886$; Nurr1 overexpression 0.9503 ± 0.2848 and Nurr1 plus Dj-1 overexpression 0.9547 ± 0.412 , $p=0.9999$) (fig. 11e). As was already shown in this thesis, the differences in *Mthfr* expression between wildtype and Dj-1 knockout microglia are due to the differences in the protein coding transcript *Mthfr*-001. Nevertheless, an additional experiment,

to assess whether Nurr1 may modulate the expression of the luciferase gene via interaction with its binding site in the promoter of *Mthfr*-004 transcript, was performed.

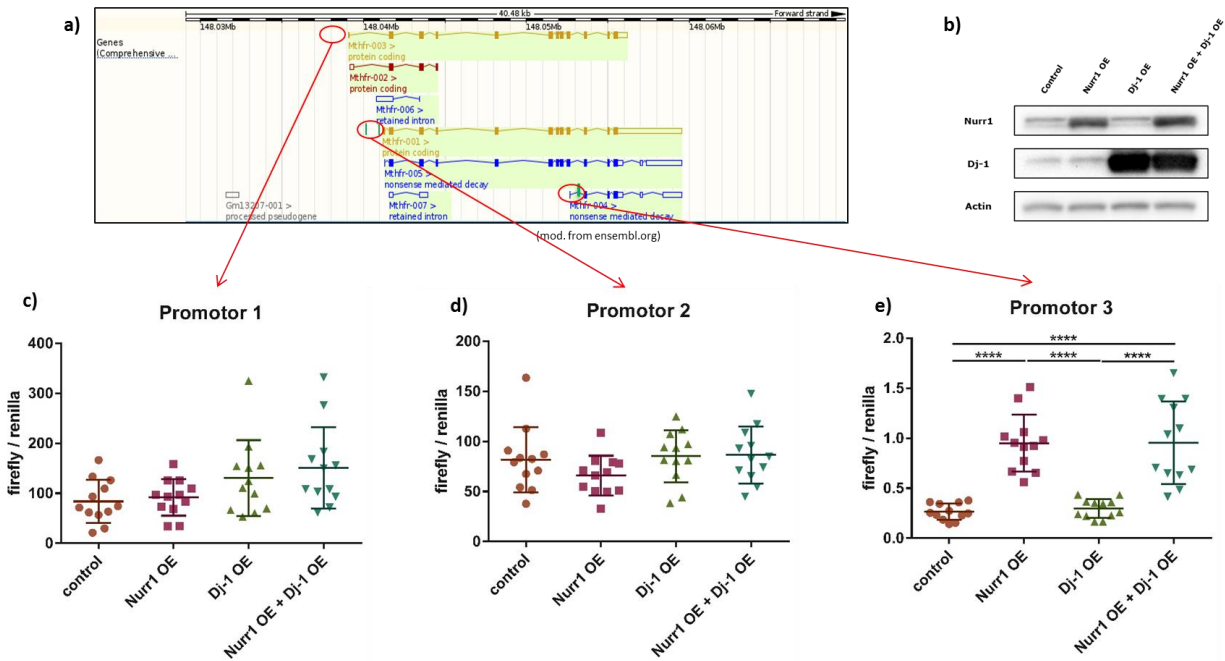


Figure 11: (a) *Mthfr* transcripts map, green bars indicate predicted Nurr1 binding sites; (b) Validation of Nurr1 and Dj-1 overexpression constructs in HEK293 cells by Western Blot; (c), (d), (e) Luciferase activity assay with different *Mthfr* promoters cloned under luciferase gene. All samples were measured with an appropriate biological n=12 and in technical triplicates. Bars represent mean \pm sd. Quantification was done in (c) and (d) in Graphpad Prism6 using Kruskal-Wallis test and Dunn’s multiple comparison test, in (e) using ordinary one-way ANOVA analysis and Tukey’s multiple comparison test: * $p \leq 0.05$; ** $p \leq 0.01$; * $p \leq 0.001$; **** $p \leq 0.0001$.**

To do so, two mutated variants of the Nurr1 binding site in the promoter region of the *Mthfr*-004 transcript were created (fig. 12). One-way ANOVA analysis was significant for all three promoters: for (b) $F=27.06$, **** $p < 0.0001$; for (c) $F=93.63$, **** $p < 0.0001$ and for (d) $F=70.57$, **** $p < 0.0001$. Subsequent post hoc test for luciferase activity assay revealed the similar pattern in mutated promoters in comparison with “wildtype” promoter (fig. 12 b, c, d).

Obtained results from the transcriptional analysis indicate that Nurr1 and Dj-1 do not regulate promoters of protein coding transcripts in HEK293 cells. Although Nurr1 shows slight regulation of promoter activity from *Mthfr*-004 transcript, this effect cannot be attributed to the Nurr1 binding site, since constructs with mutated core sequences of the former one show similar results as the original sequence.

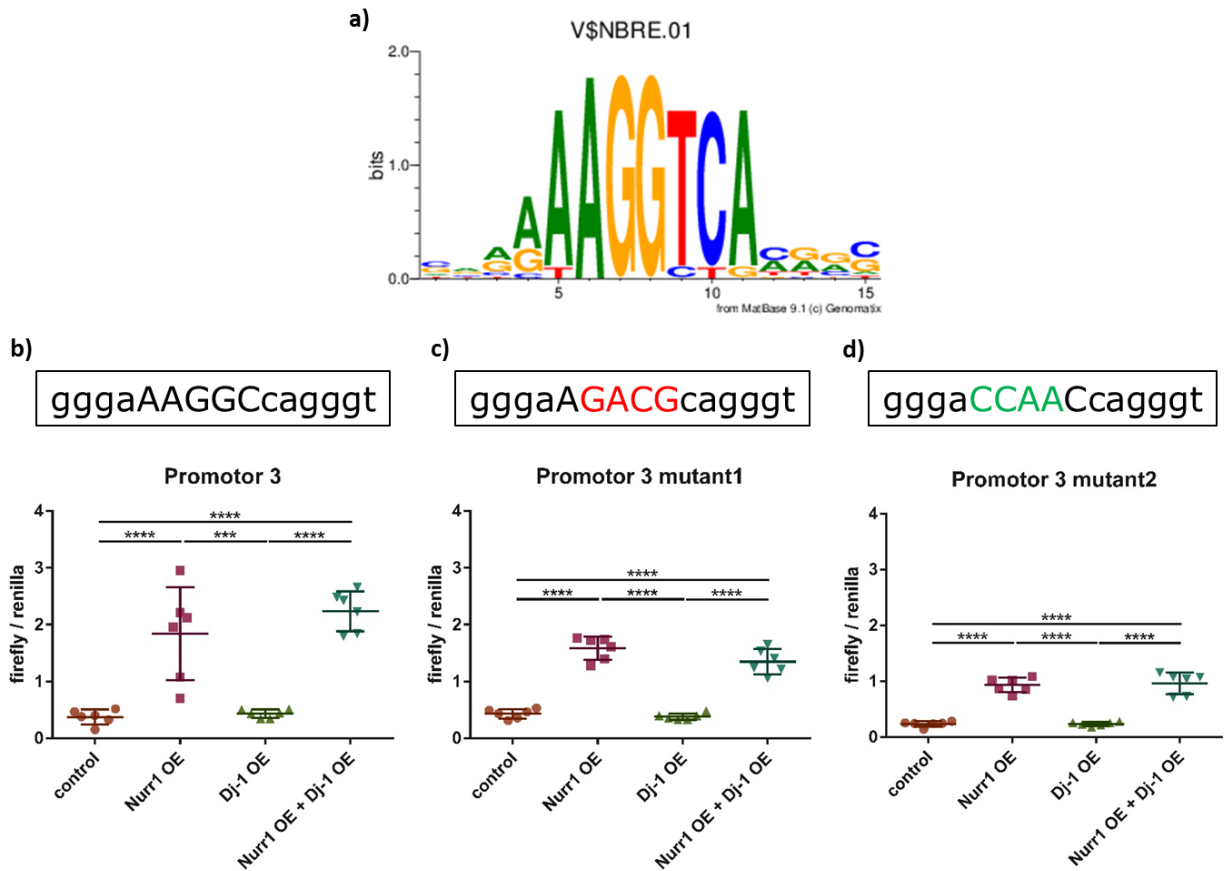


Figure 12: (a) Core of the Nurr1 binding sequence in the promoter of the *Mthfr-004* transcript (from MatBase 9.1(c) Genomatix); Luciferase activity assay with (b) wildtype promoter *Mthfr-004* and (c) the mutated sequence: AGGC substituted by GACG, (d) mutated sequence: AGGC substituted by CCAA. All samples were measured with an appropriate biological n=12 and in technical triplicates. Bars represent mean \pm sd. Quantification was done via ordinary one-way ANOVA analysis and Tukey's multiple comparison test: * $p \leq 0.05$; ** $p \leq 0.01$; *** $p \leq 0.001$; **** $p \leq 0.0001$.

5.5.2.3 Nurr1 overexpression in primary microglia does not affect *Mthfr* expression

According to Saijo and colleagues, knock down of Nurr1 in primary microglia leads to an increased expression of pro-inflammatory genes during LPS stimulation (Saijo et al., 2009). The authors suggested that Nurr1 executes its inhibitory function by direct interaction with an NF κ B subunit on the promoter region of those inflammatory genes. As shown above, *Mthfr* upregulation in primary microglia upon LPS stimulation is NF κ B dependent process. Therefore, overexpression of Nurr1 was done by lentiviruses in primary microglia and *Mthfr* expression under basal conditions and after LPS treatment checked, with *iNos* as reference gene for NF κ B pathway activation (fig. 13).

Nurr1 overexpression led to a decrease in activation of *iNos* upon LPS treatment (control virus 0.02868 ± 0.00311 and Nurr1 overexpression virus 0.00817 ± 0.00098 , $p = 0.0004$) (fig. 13c), which

supports data of Saijo and colleagues. However, Nurr1 overexpression did not affect the level of *Mthfr* expression upon LPS stimulation (control virus 0.00227 ± 0.00009 and Nurr1 overexpression virus 0.00239 ± 0.00015 , $p=0.2976$) (fig. 13b).

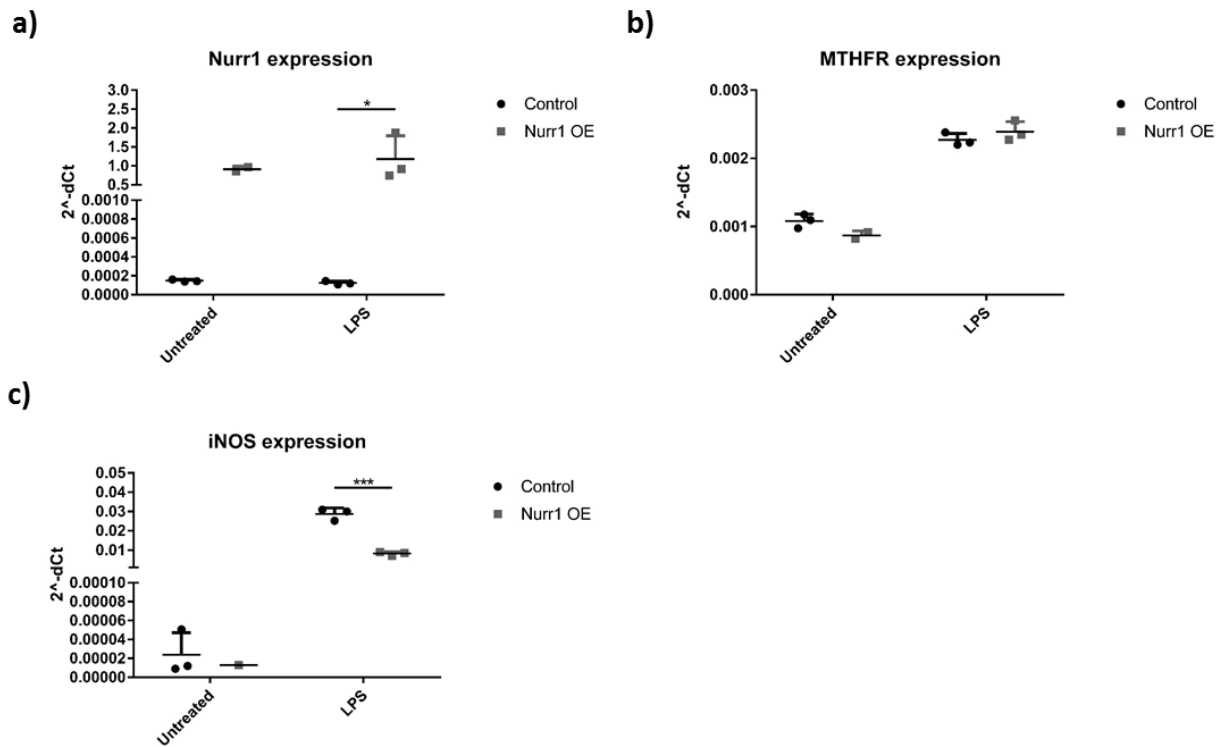


Figure 13: mRNA expression analysis in primary microglia (a) *Nurr1*, (b) *Mthfr* and (c) *iNos*. Nurr1 overexpression under basal condition samples had n=2 (for all the other samples n=3), therefore quantification was done only in LPS treated microglia using unpaired t-Test: * $p \leq 0.05$; ** $p \leq 0.01$; * $p \leq 0.001$; **** $p \leq 0.0001$. Bars represent mean \pm sd.**

Taken together, these results combined with results from the transcriptional analyses (luciferase assay) lead to the conclusion that Nurr1 does not participate in regulation of *Mthfr* expression in primary microglia cells. Thus, future studies will have to concentrate on other possible interaction partners.

5.5.3 Identification of the Dj-1 interactome in primary microglia by mass spectrometry

To further investigate possible mechanisms by which Dj-1 regulates *Mthfr* expression, Dj-1 immunoprecipitation with subsequent mass spectrometry analysis was performed in order to identify proteins which interact with Dj-1 upon LPS treatment. In the beginning, a test experiment was performed to make sure that the experimental conditions of the immunoprecipitation are suitable and efficient enough for a subsequent mass spectrometry analysis. Due to limitations in the amount of cellular material, the test experiment was performed with one sample of the wildtype and Dj-1 knockout microglia for the control condition and two samples of the wildtype

and Dj-1 knockout microglia for the LPS treatment (4 hours). After Dj-1 pull down and purification of possible interactors proteins, the samples were send to our collaborators performing mass spectrometry analysis (Dr. Stefanie Hauck from the proteomics core facility of Helmholtz Zentrum München). The results of the test mass spectrometry run (table 5) revealed that the amount of proteins in the samples was too small to obtain a solid and biologically significant data set. Still, two possible interaction candidates of Dj-1 upon LPS treatment were found: annexin A1 (enrichment 20.7, $p=0.073$) and the mediator of RNA polymerase II transcription subunit 7 (MED7) (enrichment 2.9, $p=0.043$). However, to get more reliable results, the protein content in the samples should be significantly higher. As discussed above, the main limitation is the amount of cells obtained during isolation and purification of primary microglia, which was too small to perform solid mass spectrometry experiments. Therefore, a suitable microglial cell line was found, a Dj-1 knockout established and the mass spectrometry experiments repeated with a higher amount of material (see following section).

ratio wt/ko	ratio wt/ko LPS	t-Test wt/ko	gene Symbol	description
infinity	38.2	0.182	Park7	Protein deglycase DJ-1 OS=Mus musculus GN=Park7 PE=1 SV=1
infinity	20.7	0.073	Anxa1	Annexin A1 OS=Mus musculus GN=Anxa1 PE=1 SV=2
1.4	2.9	0.043	Med7	Mediator of RNA polymerase II transcription subunit 7 OS=Mus musculus GN=Med7 PE=1 SV=2
1.5	1.7	0.379	Krt13	Keratin, type I cytoskeletal 13 OS=Mus musculus GN=Krt13 PE=1 SV=2
1.1	1.6	0.656	Blmh	Bleomycin hydrolase OS=Mus musculus GN=Blmh PE=1 SV=1
0.0	1.4	0.652	Hspa5	78 kDa glucose-regulated protein OS=Mus musculus GN=Hspa5 PE=1 SV=3
infinity	1.4	0.761	Atp5a1	ATP synthase subunit alpha, mitochondrial OS=Mus musculus GN=Atp5a1 PE=1 SV=1
32.0	1.4	0.645	Prdx2	Peroxiredoxin-2 OS=Mus musculus GN=Prdx2 PE=1 SV=3
102.0	1.2	0.770	Myh9	Myosin-9 OS=Mus musculus GN=Myh9 PE=1 SV=4
0.5	1.1	0.579	Krt79	Keratin, type II cytoskeletal 79 OS=Mus musculus GN=Krt79 PE=1 SV=2
1.0	1.1	0.944	1 SV	Ig lambda-1 chain V region OS=Mus musculus PE=1 SV=2
1.5	1.1	0.937	Arg1	Arginase-1 OS=Mus musculus GN=Arg1 PE=1 SV=1
6.9	1.0	0.966	Hist1h1c	Histone H1.2 OS=Mus musculus GN=Hist1h1c PE=1 SV=2
1.7	1.0	0.996	Krt75	Keratin, type II cytoskeletal 75 OS=Mus musculus GN=Krt75 PE=1 SV=1
infinity	1.0	1.000	Aldoa	Fructose-bisphosphate aldolase A OS=Mus musculus GN=Aldoa PE=1 SV=2
0.9	1.0	0.995	Krt12	Keratin, type I cytoskeletal 12 OS=Mus musculus GN=Krt12 PE=1 SV=2
4.8	1.0	0.987	Dsg1b	Desmoglein-1-beta OS=Mus musculus GN=Dsg1b PE=1 SV=1
infinity	1.0	0.990	Krt35	Keratin, type I cuticular Ha5 OS=Mus musculus GN=Krt35 PE=1 SV=1
2.3	1.0	0.975	Tgm1	Protein-glutamine gamma-glutamyltransferase K OS=Mus musculus GN=Tgm1 PE=1 SV=2
1.1	1.0	0.930	Krt6a	Keratin, type II cytoskeletal 6A OS=Mus musculus GN=Krt6a PE=1 SV=3
1.3	0.9	0.900	Gapdh	Glyceraldehyde-3-phosphate dehydrogenase OS=Mus musculus GN=Gapdh PE=1 SV=2
2.0	0.9	0.807	Mdh2	Malate dehydrogenase, mitochondrial OS=Mus musculus GN=Mdh2 PE=1 SV=3
4.9	0.9	0.934	Nccrp1	F-box only protein 50 OS=Mus musculus GN=Nccrp1 PE=1 SV=2
14.0	0.9	0.941	Krt83	Keratin, type II cuticular Hb3 OS=Mus musculus GN=Krt83 PE=2 SV=2
infinity	0.9	0.899	Asic3	Acid-sensing ion channel 3 OS=Mus musculus GN=Asic3 PE=1 SV=2
0.6	0.8	0.683	Gsdma3	Gasdermin-A3 OS=Mus musculus GN=Gsdma3 PE=1 SV=1
0.4	0.8	0.690	Krt14	Keratin, type I cytoskeletal 14 OS=Mus musculus GN=Krt14 PE=1 SV=2
1.3	0.8	0.679	Krt42	Keratin, type I cytoskeletal 42 OS=Mus musculus GN=Krt42 PE=1 SV=1
0.3	0.8	0.182	Ankrd17	Ankyrin repeat domain-containing protein 17 OS=Mus musculus GN=Ankrd17 PE=1 SV=2
1.9	0.8	0.489	Dsp	Desmoplakin OS=Mus musculus GN=Dsp PE=1 SV=1
7.2	0.7	0.396	Slc25a4	ADP/ATP translocase 1 OS=Mus musculus GN=Slc25a4 PE=1 SV=4
2.2	0.7	0.531	Cdsn	Corneodesmosin OS=Mus musculus GN=Cdsn PE=2 SV=2
5.6	0.7	0.630	Tuba1b	Tubulin alpha-1B chain OS=Mus musculus GN=Tuba1b PE=1 SV=2
2.1	0.7	0.300	Ubb	Polyubiquitin-B OS=Mus musculus GN=Ubb PE=2 SV=1
infinity	0.7	0.447	Cat	Catalase OS=Mus musculus GN=Cat PE=1 SV=4
2.7	0.7	0.665	Krt80	Keratin, type II cytoskeletal 80 OS=Mus musculus GN=Krt80 PE=1 SV=1
1.9	0.7	0.233	Jup	Junction plakoglobin OS=Mus musculus GN=Jup PE=1 SV=3
4.1	0.7	0.481	Vim	Vimentin OS=Mus musculus GN=Vim PE=1 SV=3
0.2	0.7	0.478	Zfp292	Zinc finger protein 292 OS=Mus musculus GN=Zfp292 PE=1 SV=2
1.5	0.7	0.500	Anxa2	Annexin A2 OS=Mus musculus GN=Anxa2 PE=1 SV=2
infinity	0.6	0.094	Krt19	Keratin, type I cytoskeletal 19 OS=Mus musculus GN=Krt19 PE=1 SV=1
79.3	0.6	0.046	Vcan	Versican core protein OS=Mus musculus GN=Vcan PE=1 SV=2
1.6	0.6	0.191	Krt1	Keratin, type II cytoskeletal 1 OS=Mus musculus GN=Krt1 PE=1 SV=4
1.5	0.6	0.306	Krt16	Keratin, type I cytoskeletal 16 OS=Mus musculus GN=Krt16 PE=1 SV=3
2.0	0.6	0.122	Hist1h2bc	Histone H2B type 1-C/E/G OS=Mus musculus GN=Hist1h2bc PE=1 SV=3
1.7	0.6	0.280	Krt5	Keratin, type II cytoskeletal 5 OS=Mus musculus GN=Krt5 PE=1 SV=1
2.2	0.6	0.347	Actb	Actin, cytoplasmic 1 OS=Mus musculus GN=Actb PE=1 SV=1
1.9	0.6	0.163	Hist1h4a	Histone H4 OS=Mus musculus GN=Hist1h4a PE=1 SV=2
7.3	0.6	0.309	Hspa8	Heat shock cognate 71 kDa protein OS=Mus musculus GN=Hspa8 PE=1 SV=1
infinity	0.6	0.156	S100a14	Protein S100-A14 OS=Mus musculus GN=S100a14 PE=1 SV=1
0.9	0.6	0.058	Specc1	Cytospin-B OS=Mus musculus GN=Specc1 PE=1 SV=2
1.5	0.5	0.508	Krt10	Keratin, type I cytoskeletal 10 OS=Mus musculus GN=Krt10 PE=1 SV=3
1.4	0.5	0.373	Krt2	Keratin, type II cytoskeletal 2 epidermal OS=Mus musculus GN=Krt2 PE=1 SV=1
1.1	0.5	0.107	Lyz1	Lysozyme C-1 OS=Mus musculus GN=Lyz1 PE=1 SV=1
4.2	0.5	0.096	Plec	Plectin OS=Mus musculus GN=Plec PE=1 SV=3
2.2	0.5	0.393	Txn	Thioredoxin OS=Mus musculus GN=Txn PE=1 SV=3
1.1	0.5	0.228	Krt77	Keratin, type II cytoskeletal 1b OS=Mus musculus GN=Krt77 PE=1 SV=1
infinity	0.5	0.115	Eno1	Alpha-enolase OS=Mus musculus GN=Eno1 PE=1 SV=3
1.9	0.4	0.037	Krt17	Keratin, type I cytoskeletal 17 OS=Mus musculus GN=Krt17 PE=1 SV=3
0.9	0.4	0.104	Tgm3	Protein-glutamine gamma-glutamyltransferase E OS=Mus musculus GN=Tgm3 PE=1 SV=2
0.7	0.4	0.141	Krt76	Keratin, type II cytoskeletal 2 oral OS=Mus musculus GN=Krt76 PE=1 SV=1
1.3	0.4	0.405	Krt31	Keratin, type I cuticular Ha1 OS=Mus musculus GN=Krt31 PE=1 SV=2
2.2	0.3	0.053	Spr2b	Small proline-rich protein 2B OS=Mus musculus GN=Spr2b PE=2 SV=1
1.4	0.3	0.023	Flg2	Filaggrin-2 OS=Mus musculus GN=Flg2 PE=1 SV=2
0.1	0.2	0.508	1 SV	Ig kappa chain V-II region 26-10 OS=Mus musculus PE=1 SV=1
0.0	0.2	0.329	Mettl3	N6-adenosine-methyltransferase subunit METTL3 OS=Mus musculus GN=Mettl3 PE=1 SV=2
infinity	0.0	#DIV/0!	Krt73	Keratin, type II cytoskeletal 73 OS=Mus musculus GN=Krt73 PE=1 SV=1
0.0	0.0	0.423	Pkp1	Plakophilin-1 OS=Mus musculus GN=Pkp1 PE=1 SV=1

Table 5: Table represents the results obtained by a first test mass spectrometry experiment with n=1 of wildtype and Dj-1 knockout primary microglia under control conditions and n=2 of wildtype and Dj-1 knockout primary microglia after LPS treatment (4 hours).

5.6 SIM A9 – a new murine microglial cell line

Nagamoto-Combs with colleagues isolated, established and described a clonal population of spontaneously immortalized cells stemming from a primary murine microglia culture (Nagamoto-Combs et al., 2014). They characterized this clone for microglial properties and made the conclusion that “SIM-A9 cells exhibit key characteristics of cultured primary microglia and may serve as a valuable model system for the investigation of microglial behavior in vitro” (Nagamoto-Combs et al., 2014). In addition, the way of primary microglia cells isolation as well as the source of the cells (cerebral cortices) used in their experimental procedure was similar to the one used in this thesis, therefore, this cell line was used as model for primary microglia cells here.

5.6.1 Expression of pro-inflammatory genes in the SIM A9 cell line under different concentrations of LPS treatment

First, it was validated whether this cell line is able to activate the expression of pro-inflammatory genes upon LPS treatment. Therefore, different concentrations of LPS were applied for 8 hours with subsequent RNA isolation and expression analysis (fig. 14).

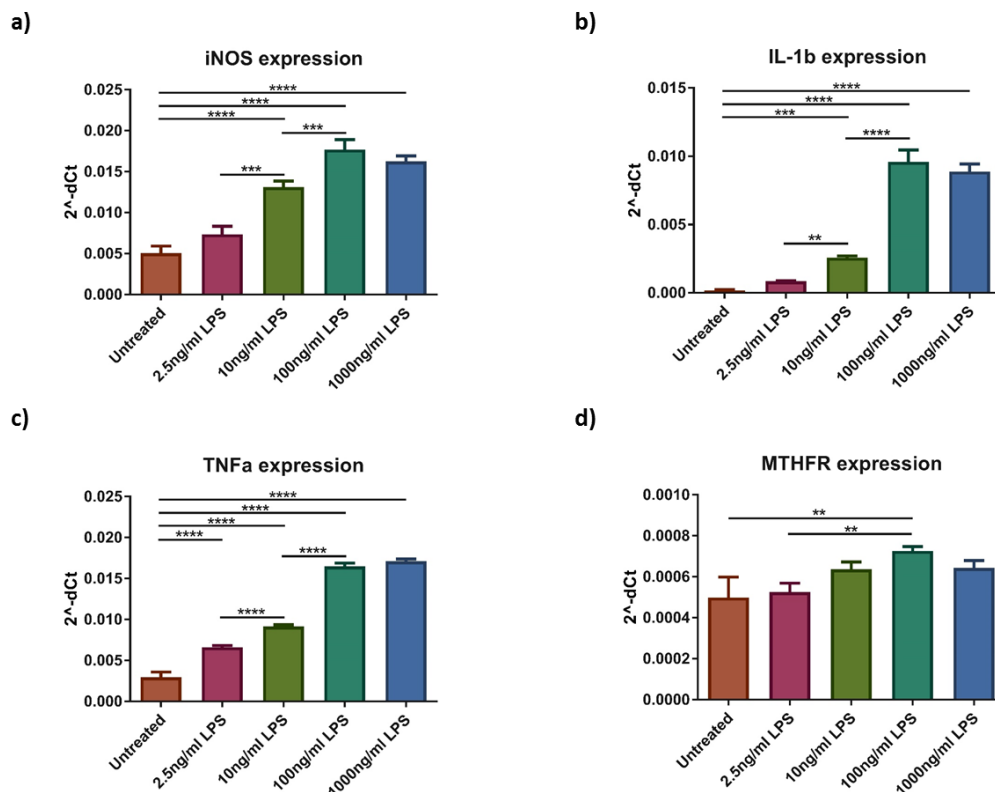


Figure 14: mRNA expression analysis of selected inflammatory genes in the SIM A9 cell line upon LPS treatment. (a) *iNos*; (b) *Il-1β*; (c) *Tnfα*; (d) *Mthfr*. All samples were measured with a biological n=3 and in technical triplicates. Bars represent mean ± sd. Quantification was done via ordinary one-way ANOVA analysis and Tukey’s multiple comparison test: *p≤0.05; **p≤0.01; *p≤0.001; ****p≤0.0001.**

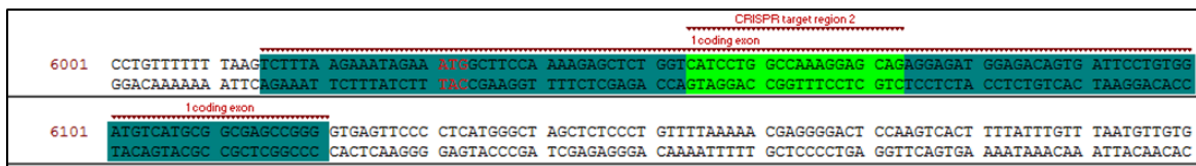
One-way ANOVA analysis was found to be significant for all four genes: for (a) $F=109.9$, $****p<0.0001$; for (b) $F=285.3$, $****p<0.0001$; for (c) $F=818.6$, $****p<0.0001$ and for (d) $F=8.7$, $**p=0.0027$. The post hoc test of mRNA expression analysis shows a dose dependent activation of pro-inflammatory genes (*iNos*, *Il-1 β* , *Tnfa*) upon LPS treatment, with the maximum effect at the 100ng/ml LPS concentration. In addition, 100ng/ml LPS treatment resulted in a significant upregulation of *Mthfr* expression after 8 hours (untreated 0.0004985 ± 0.0001003 and LPS 100ng/ml 0.0007262 ± 0.000021 , $p=0.0033$), the same effect as observed in primary wildtype microglia. Hence, it was decided to continue experiments with this cell line as a model of primary microglia cells.

5.6.2 Establishment of a Dj-1 knockout SIM A9 cell line using the CRISPR/CAS 9 technique

5.6.2.1 Design and cloning of the guide RNAs against Dj-1

The design of the guide RNAs against the murine Dj-1 gene was performed using the freely available internet platform benchling.com. Two guide RNAs were chosen for testing and were cloned in the pMasterblaster Cas9 expressing vector designed by Jeffery Truong (IDG). One guide RNA was directed against a part of coding region of exon 2 (first coding exon) of Dj-1, the other against exon 3 (second coding exon) of Dj-1 (fig. 15).

a)



b)

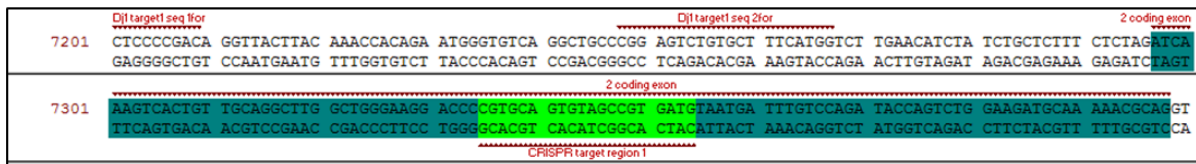


Figure 15: Fragments of Dj-1 murine genomic sequences represent in blue, (a) first coding exon of Dj-1 and (b) second coding exon of Dj-1; green marks represent the part of the exons complementary to guides RNA, (a) guide RNA N2 and (b) guide RNA N1.

5.6.2.2 Validation of the selected guide RNAs in the Neuro2a (N2a) cell line

Since design and cloning of the guide RNAs against Dj-1 was performed before the Sim A9 cell line was delivered, it was decided to test the guide RNAs in the murine Neuro2a cell line. Neuro2a cells were lipofected with different concentrations of DNA (vector with guide RNAs) and, after

two days, genomic DNA from lipofected cells was isolated with subsequent amplification of DNA target regions by PCR and performance of a T7 assay to assess gRNA efficiency (fig. 16).

The results obtained revealed that already the lowest concentration of lipofectamine 2000 guide RNA 2 against the first coding exon of Dj-1 worked (indicated by a ≈ 420 bp DNA fragments, marked by the arrow on figure 16). Guide RNA 1 did not work efficiently in Neuro2a cells as no DNA fragments of 200bp and 150bp could be seen on the gel.

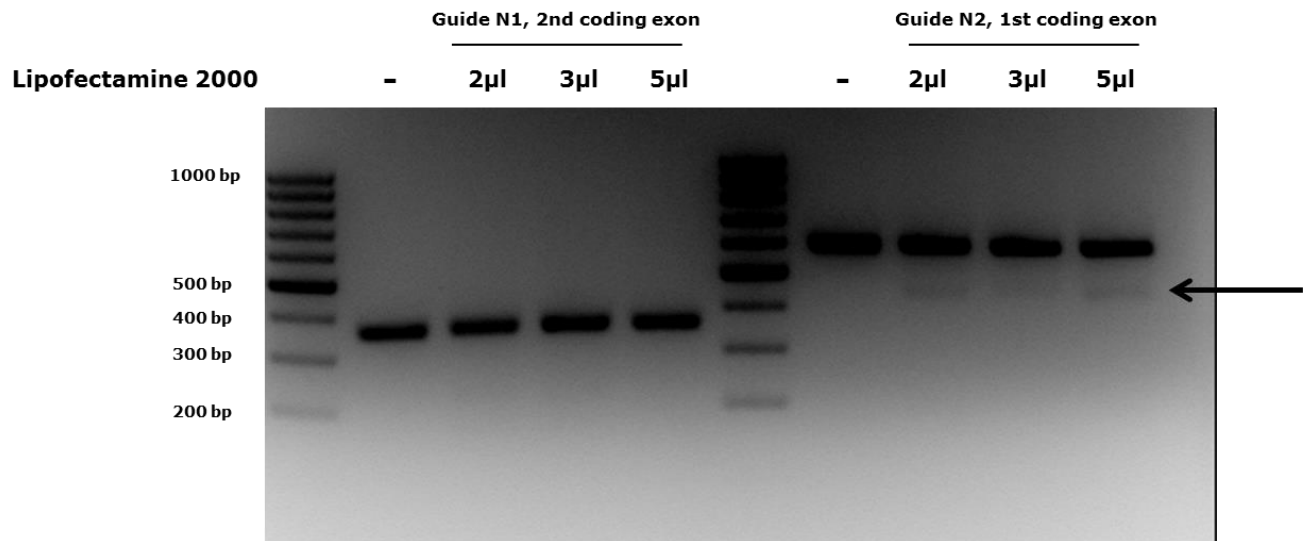


Figure 16: Visualization of the performed T7 assay on an agarose gel. The arrow marks a 420bp DNA fragment which indicates that guide RNA N2 against Dj-1 worked.

5.6.2.3 Introduction of a Dj-1 knockout in the Sim A9 cell line

The next step was the establishment of a Dj-1 knockout SIM A9 cell line. Cells were lipofected with the plasmid expressing the guide RNA 2 under the same conditions as previously optimized in Neuro2a cells. Subsequently, clonal selection by dilution was performed and positive clones termed N1, N10 and N47 were established (fig. 17).

During the analysis of the sequences from clones N1, N10 and N47, it was observed frequently that each clone had more than two nucleotide signals in one position appearing in the histogram. This feature could have two main explanations: 1) during the clonal selection, in one well, there were more than one clone conjugated together or, cut by Cas9 after cell division, 2) the SIM A9 cell line could be polyploid, i.e. have more than 2 alleles. To exclude the first possibility, one more round of clonal selection was performed with clones N1, 10 and 47 and additional three wildtype clones N38, 41 and 48 (to have a proper, clonal control cell line in the end). After the second round of clonal selection, several subclones were sequenced again for the CRISPR/CAS9 target region in Dj-1 gene. The sequencing results of all subclones from clone N1, 10, and 47 again showed more than two nucleotides in many single positions (data not shown). Therefore, the most likely scenario is that the SIM A9 cell line is a polyploid cell line. To test this hypothesis, PCR

products of the Dj-1 CRISPR/CAS9 target region from subclone N2 from clone N10 (10-2) were cloned into a vector with sequential transformation to bacteria. 17 colonies were taken for the sequencing of the CAS9 target region (fig. 18).



Figure 17: Alignments of clone sequences with the genomic target region of Dj-1 (from Benchling.com). (a) sequence of murine wildtype genomic region of Dj-1, (b) sequence of the CRISPR/CAS9 target region of clone N1, (c) clone N10, (d) clone N47 and (e) wildtype clone N38. The arrow in the top indicates the theoretical CAS9 cutting site.

According to the sequencing results from subclone 10-2, there can be more than two alleles of the Dj-1 CAS9 target region identified. Therefore, it could be postulated that SIM A9 is a polyploid cell line. One could suspect that spontaneous immortalization of primary microglia was a consequence of the polyploidization process, which randomly occurred in the original primary microglia cells.

Another interesting point of the subclone 10-2 sequencing experiment was that among all sequences the wildtype Dj-1 allele could not be identified, which indicates that this subclone has a full Dj-1 knockout. To validate this result, western blot analysis was performed with several sub clones from clone N1, N10 and N47 and with the wildtype subclones from clone 38, 41 and 48 (fig. 19).



Figure 18: Alignments of sub clone N2 clone N10 sequences with a genomic target region of Dj-1. (a), (b), (c), (d) and e) represent the obtained sequences during analysis of 17 colonies. Deletions of nucleotides marked in pink.

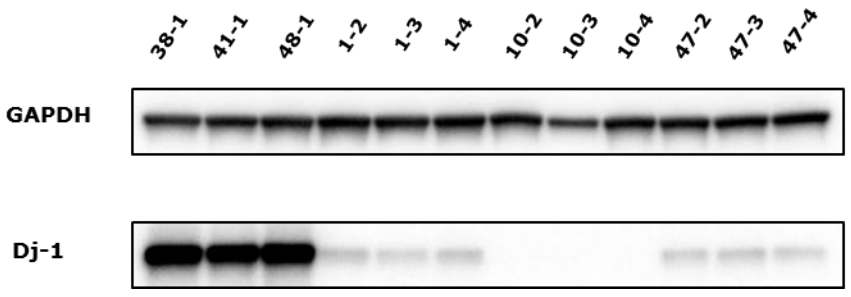


Figure 19: Protein expression analysis for Dj-1 in Dj-1 knockout candidates sub clones and wildtype sub clones. Sub clones 38-1, 41-1, and 48-1 represent wildtype cells; sub clones from 1-2 to 47-4 represent Dj-1 knockout candidate cells.

Western blot analysis confirmed the assumption that no Dj-1 is present in subclone 10-2. Moreover, other subclones from clone 10 are also knockouts. Therefore, a second round of clonal selection was not necessary as the original clone N10 was also Dj-1 knockout.

Taken together, a Dj-1 knockout SIM A9 cell line was established with matched wildtype controls. In addition, it could be demonstrated that SIM A9 cells have similar biological properties as

primary microglia cells (including intracellular pathways similarities (will be discussed later)) and still appeared to be of the best model of primary microglia cells.

5.6.3 Cell type specificity and comparison of the SIM A9 cell line with primary microglia and immortalized MEFs from Dj-1 knockout mouse

5.6.3.1 Comparison of NF κ B, ERK and the P38 pathways between wildtype and Dj-1 knockout SIM A9 cells upon LPS treatment

In order to characterize the function of Dj-1 in the microglial cell line SIM A9 in comparison with primary microglia, some of the molecular pathways, which were previously looked at in primary microglia, were again assessed and compared to primary microglia as well as immortalized mouse embryonic fibroblasts (MEFs). A former student in our laboratory (Ulrich Hafen) showed that there is a significant difference in between the molecular pathways in the different genotypes in primary microglia and immortalized MEFs during the course of LPS treatment. In particular, in MEFs there was a significantly weaker activation of the NF κ B and P38 pathways in Dj-1 knockouts in comparison to wildtype during LPS treatment. This difference becomes especially interesting, as there were no differences found between genotypes in these pathways in primary microglia cells. Since SIM A9 cells are of microglial origin, but immortalized, they are an ideal model to interrogate whether the differences between Dj-1 deficient MEFs and Dj-1 deficient primary microglia derived from the same mouse model in intracellular signal transduction upon LPS stimulation is due to immortalization of the MEFs or indeed due to cell type specific effects of Dj-1. Therefore, pathway analysis was performed in SIM A9 cells during the course of LPS treatment. To do so, three independent experiments were performed with LPS treatment of the wildtype clone 38-1 and the Dj-1 knockout clone 10-2 and three molecular pathways were analyzed: NF- κ B (fig. 20), ERK (fig. 21) and P38 (fig. 22).

Pathway comparison analysis revealed that, in SIM A9 cells, there are no significant differences between the genotypes in the NF κ B, ERK and P38 pathway activation during LPS treatment, since there were no differences found in the levels of phosphorylated nuclear factor of kappa light polypeptide gene enhancer in B-cells inhibitor, alpha (pI κ B), pERK and pP38, which protein content is typically used to assess the mentioned pathways activity. It is worth to mention, that pathway activities in SIM A9 cells under LPS treatment was validated in the independent wildtype and Dj-1 knockout clones within the bachelor work of Irina Petcu, whom I supervised. Thus, it can be concluded that the SIM A9 cell line is more similar to primary microglia cells and both differ from the immortalized MEFs.

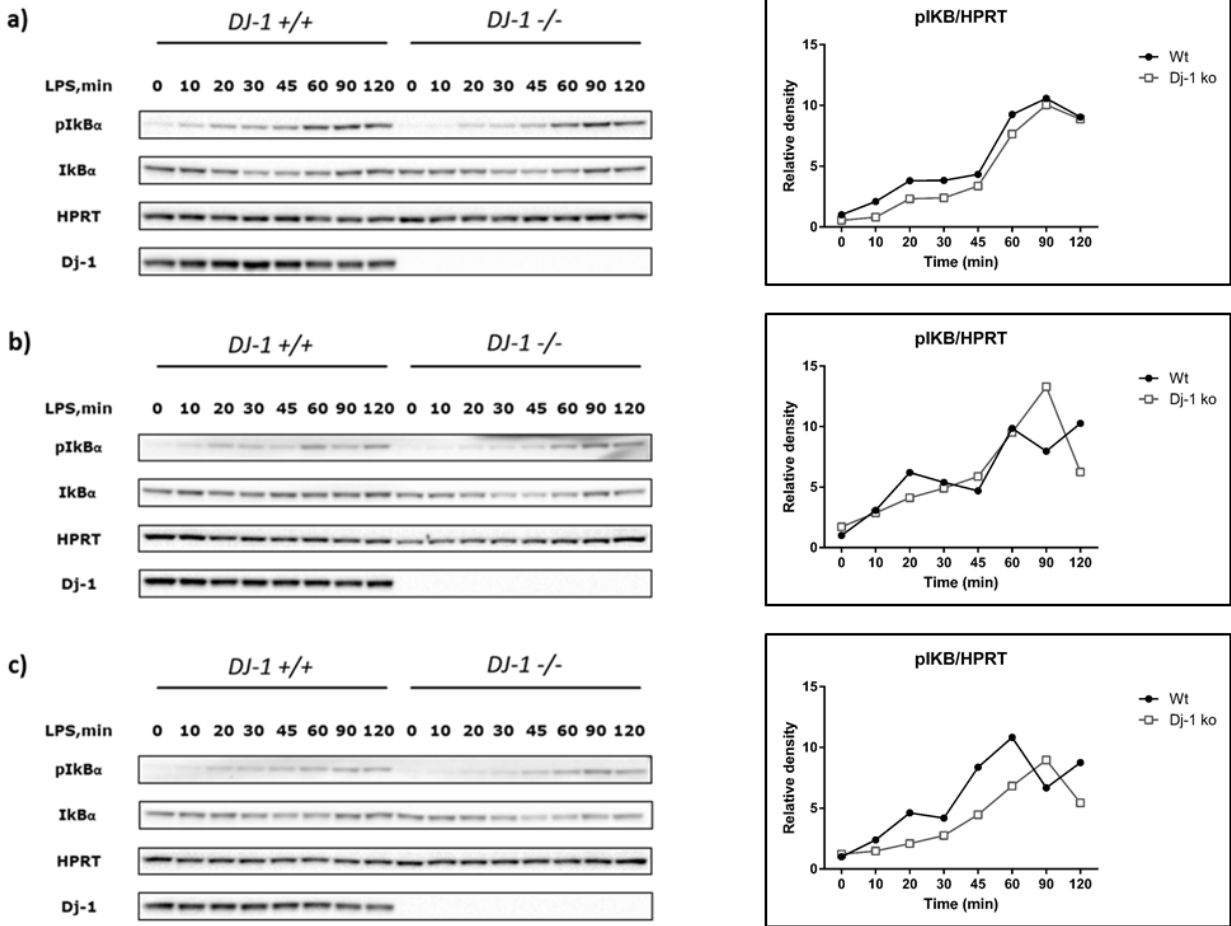


Figure 20: Western blot for NF κ B pathway activation during course of LPS treatment in SIM A9 wildtype and Dj-1 knockout cells. (a), (b), (c) represent three independent experiments. Abbreviations: HPRT - Hypoxanthine-guanine phosphoribosyltransferase (used as a protein loading control); IkB α - nuclear factor of kappa light polypeptide gene enhancer in B-cells inhibitor, alpha; pIkB α - phosphorylated nuclear factor of kappa light polypeptide gene enhancer in B-cells inhibitor, alpha.

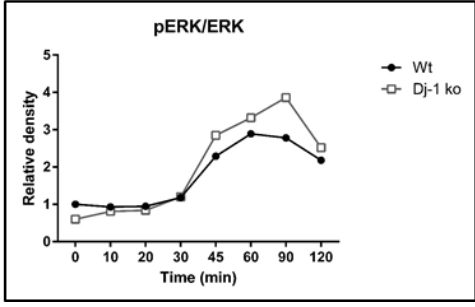
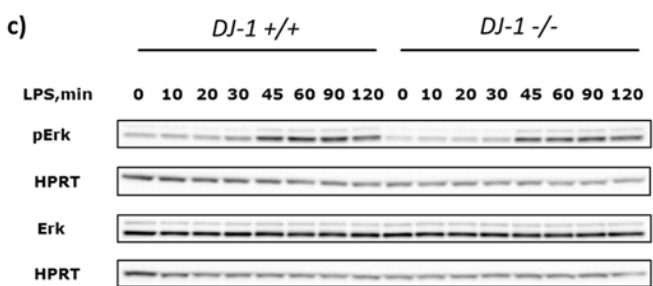
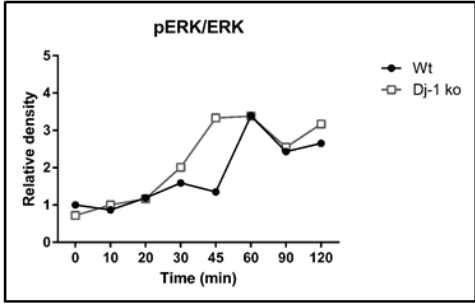
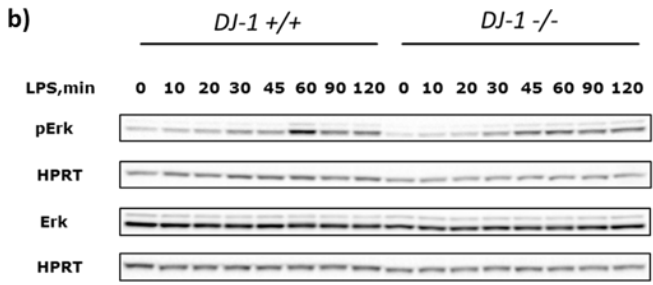
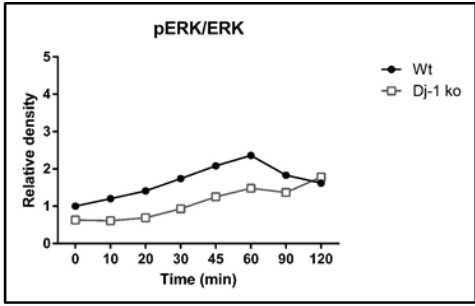
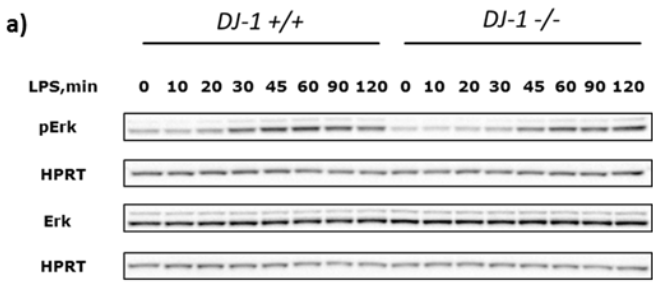


Figure 21: Western blot for ERK pathway activation during course of LPS treatment in SIM A9 wildtype and Dj-1 knockout cells. (a), (b), (c) represent three independent experiments. Abbreviations: HPRT - Hypoxanthine-guanine phosphoribosyltransferase (used as a protein loading control); ERK - Extracellular signal-regulated kinases; pERK – phosphorylated Extracellular signal-regulated kinases.

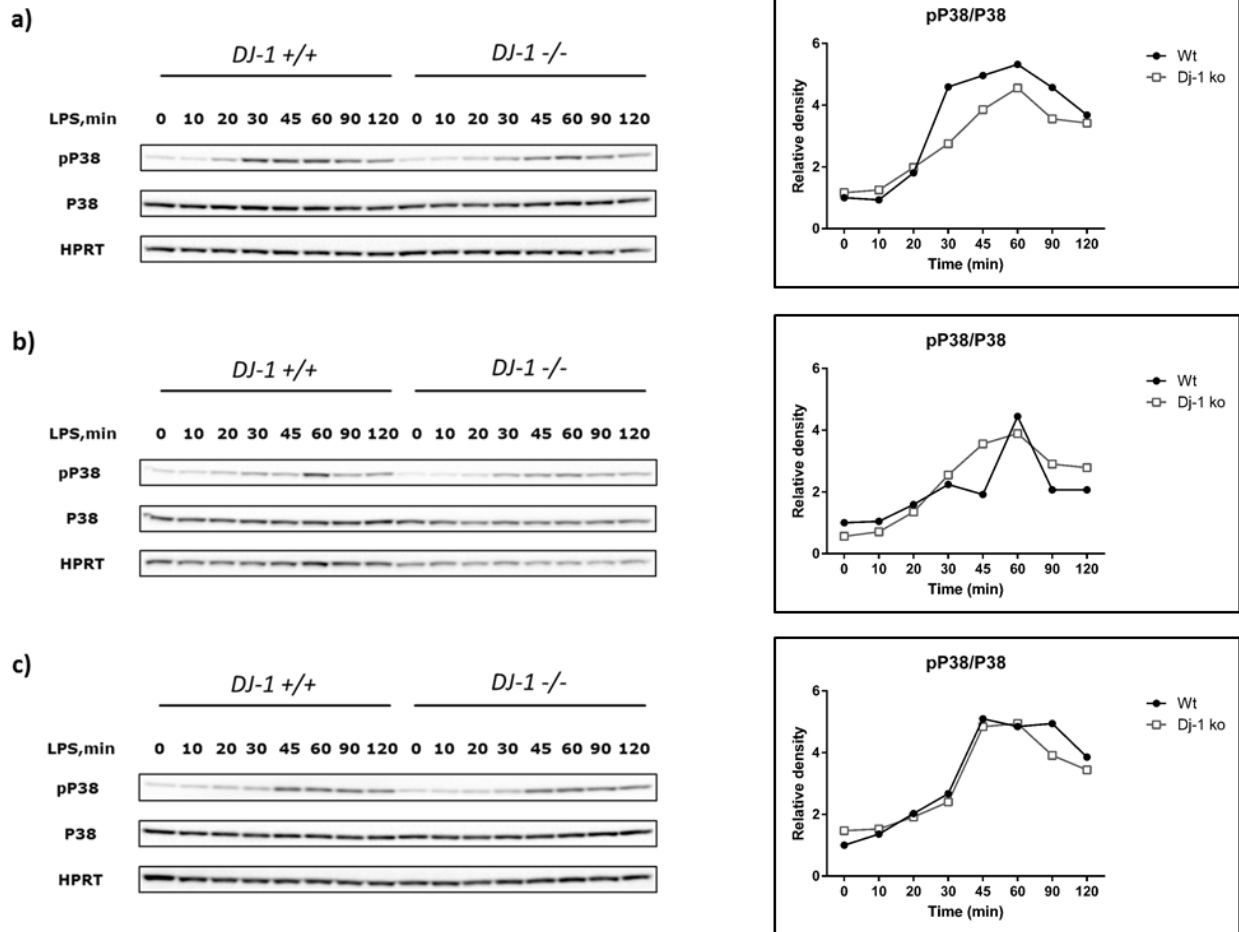


Figure 22: Western blot for P38 pathway activation during course of LPS treatment in SIM A9 wildtype and Dj-1 knockout cells. (a), (b), (c) represent three independent experiments. Abbreviations: HPRT - Hypoxanthine-guanine phosphoribosyltransferase (used as a protein loading control); P38 - P38 mitogen-activated protein kinase; pP38 – phosphorylated P38 mitogen-activated protein kinase.

5.6.3.2 Comparison of *Mthfr* expression between wildtype and Dj-1 knockout SIM A9 cells

As shown before, Dj-1 does not affect the activation of the NFκB, ERK and P38 pathways in SIM A9 cells in response to LPS as was also observed in primary microglia cells. Therefore, I checked whether the lack of Dj-1 has a similar effect on *Mthfr* expression during LPS treatment, as it was observed in primary microglia. To do so, experiment with the wildtype clone 38-1 and the Dj-1 knockout clone 10-2 was performed with subsequent mRNA expression analysis for *Mthfr* and *iNos* as a reference gene for NFκB pathway activation.

According to the results obtained in this experiment (fig. 23), I was not able to observe a similar effect of Dj-1 on *Mthfr* expression in SIM A9 cell line as in primary microglia. Two-way ANOVA analysis revealed: in *Mthfr* expression a significant effect of treatment ($F=4.839$, $*p=0.0035$); in

iNos expression a significant effect of genotype ($F=35.11$, **** $p<0.0001$), treatment ($F=647$, **** $p<0.0001$) and interaction of genotype and treatment ($F=31.38$, **** $p<0.0001$).

Wildtype and knockout cells were not able to significantly upregulate *Mthfr* expression in response to LPS (fig. 23a). The small, but significant, upregulation of *Mthfr* expression which was detected in the preliminary experiments (fig. 14d) disappeared upon clonal selection and passaging of the cells. Interestingly, Nagamoto-Combs and colleagues described similar effect on arginase1 (ARG1) during the characterization of this cell line. In addition, they also demonstrated that during the passaging SIM A9 cells significantly reduced TNF α release in response to LPS (Nagamoto-Combs et al., 2014).

However, there was a significant downregulation of *iNos* expression found in Dj-1 knockout SIM A9 cells in response to LPS treatment - Post hoc test - LPS wildtype 0.01227 ± 0.00173 and LPS Dj-1 knockout 0.00780 ± 0.00155 , $p<0.0001$. It was an interesting observation, especially since no significant differences in the NF κ B pathway activation by Western blot in these cells between the genotypes could be found (fig. 20).

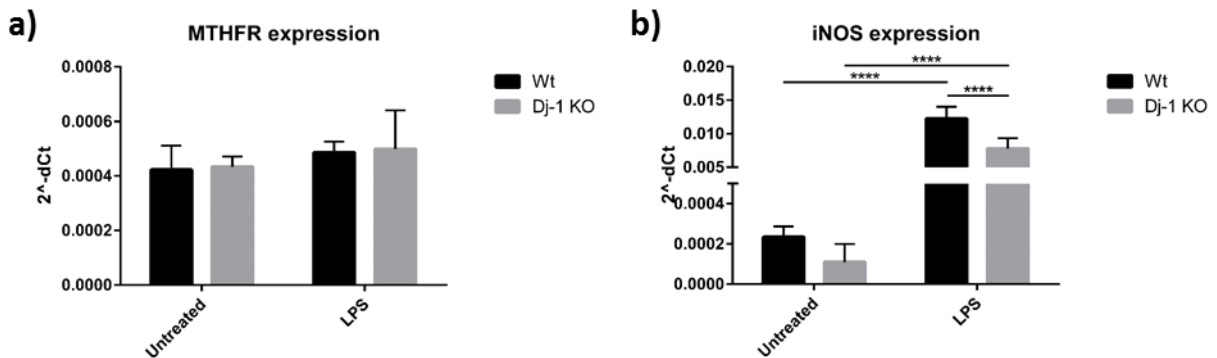


Figure 23: mRNA expression analysis for (a) *Mthfr* and (b) *iNos* in SIM A9 cells under basal conditions and after LPS treatment (8 hours). All samples were analyzed with a biological n=9 and in technical triplicates. Bars represent mean \pm sd. Quantification was done via two-way ANOVA analysis and Tukey's multiple comparison test. * $p\leq 0.05$; ** $p\leq 0.01$; *** $p\leq 0.001$; **** $p\leq 0.0001$.

Additionally, to test the hypothesis that *Mthfr* dysregulation in Dj-1 knockout primary microglia is cell type specific, *Mthfr* expression in liver tissue from 2-4 days old pups and in primary MEFs, isolated from wildtype and Dj-1 knockout embryos, was assessed (fig. 24). Results revealed that only in primary microglia cells *Mthfr* expression is affected by the lack of Dj-1 (wildtype 0.00072 ± 0.00018 and Dj-1 knockout 0.00047 ± 0.00009 , $p=0.0089$).

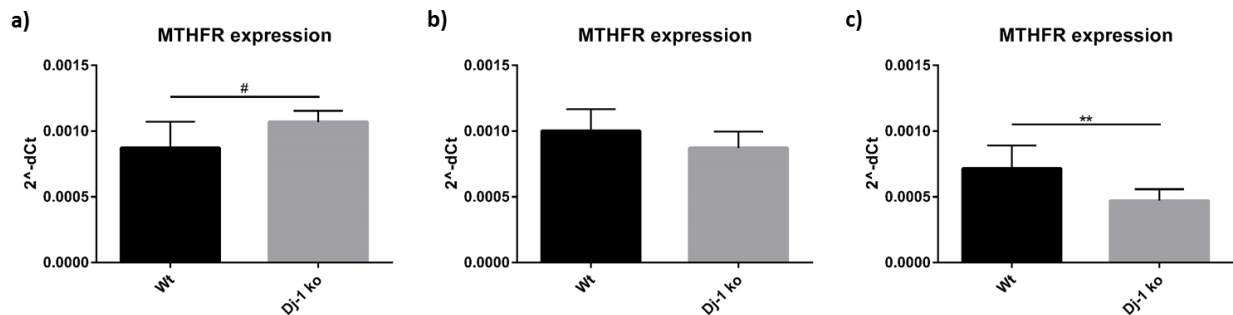


Figure 24: mRNA expression analysis for *Mthfr* in (a) MEFs from wildtype and Dj-1 knockout embryos, (b) liver lysates from 2-4 days old pups and (c) primary microglia from 2-4 days old pups. All samples were analyzed with a sufficient biological n ((a) wt n=6, ko n=6; (b) wt n=4, ko n=4; (c) wt n=8, ko n=6) and in technical triplicates. Bars represent mean \pm sd. Quantification was done via unpaired t-Test: #p \leq 0.1, *p \leq 0.05, **p \leq 0.01.

Taken together, these results indicate several main points. First, according to the pathway activation upon the LPS treatment, wildtype and Dj-1 knockout SIM A9 cells behave in a similar way as primary microglia do, showing no differences between the genotypes, which is different from MEFs (there was found a significantly weaker activation of the NF κ B and P38 pathways in Dj-1 knockouts in comparison with wildtypes during LPS treatment). Second, dysregulation of the *Mthfr* expression in Dj-1 knockouts seems to be cell type dependent and attributable to primary microglia cells. Third, weaker activation of *iNos* expression in Dj-1 knockout SIM A9 cells indicates that there could still be some dysregulations in the NF- κ B pathway even though there were no differences in plkB levels observed by western blotting upon LPS treatment in this thesis.

5.6.4 Optimization of Dj-1 Immunoprecipitation (IP) in SIM A9 cells and subsequent mass spectrometry experiments

As discussed above, mass spectrometry experiments in primary microglia disclosed the problem of lack of sufficient amount of protein for effective mass spectrometry experiments. Therefore, the Dj-1 wildtype and knockout microglial cell line SIM A9 was used to perform these experiments with acceptable amount of cell material.

5.6.4.1 Optimization of Dj-1 immunoprecipitation (IP) in the SIM A9 cell line

Efficient identification of Dj-1 interaction proteins needs to meet several requirements. One of them is the amount of material, and a second one is an efficient procedure of precipitation of Dj-1. Since the first one was solved by the usage of a microglial cell line, the second parameter had to be optimized.

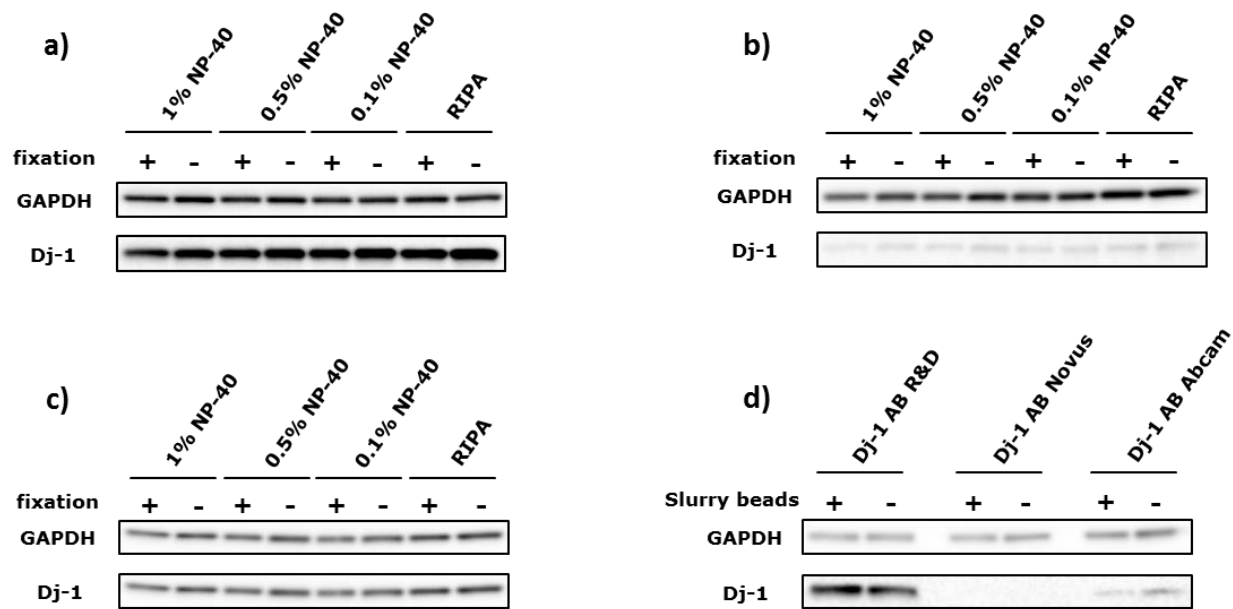


Figure 25: Western blot for testing the conditions in Dj-1 Co-IP. (a)-(c) test of the effect of variable concentrations of NP-40 buffer and fixation on the lysis efficiency in comparison with RIPA buffer, and testing efficiency of different anti-Dj-1 antibodies (AB)- (a) R&D AB, (b) Novus AB, (c) Abcam AB. (d) Different anti-Dj-1 AB testing together with or without slurry beads (slurry beads are generally used in the Co-IP experiments to decrease a background), 0.5% NP-40 buffer was used.

It was decided to start with checking the efficiency of the several parameters: 1) testing different anti-Dj-1 antibodies; 2) testing the lysis efficiency of different concentrations of the most common IP lysis buffer NP-40 in comparison to RIPA buffer; 3) testing whether fixation of the cells with formaldehyde affects the lysis efficiency; 4) testing whether the preclearance of the sample with slurry beads affects the presence of Dj-1 in the final protein solution.

The first optimization experiment answered several questions (fig. 25). The best antibody to detect Dj-1 by western blot is the anti-Dj-1 antibody from R&D. The lowest concentration (0.1%) of NP-40 was sufficient to lyse the cells and there was no significant difference in protein content between fixed and non-fixed cells. The slurry beads, which are an important component of the Co-IP protocol, do not affect the presence of Dj-1 in the final protein solution.

Subsequently, there were many optimization experiments performed to find out the best Dj-1 precipitation condition (table 6 and supplementary figure 1). Different lysis buffers (NP-40, Triton X100, CHAPS and Digitonin) were tested with different concentrations of detergents and salts, diverse antibody mixtures, different concentrations of protein solutions and antibodies, time of precipitation and many others. During the analysis of the series of optimization experiments, it was decided to use the following conditions: 25mM Tris HCl, 1% CHAPS, 1mM EDTA with 150mM NaCl, 1% formaldehyde for crosslinking the cells, 10µg of Dj-1 antibody from R&D plus 10µg of Dj-1 antibody from Abcam for overnight antigen precipitation.

Number	Buffer					Formaldehyde fixation	mg of protein for precipitation	Antibodies			Glycerol in elution buffer	1st AB time	IP efficiency in %
	Tris HCl	detergent	NaCl	EDTA	glycerol			R&D	Abcam	Novus			
1a	25mM	NP-40 0.1%	167mM	1mM		1% 10 min	1	10µg				overnight	23
1b	25mM	NP-40 0.1%	167mM	1mM		1% 10 min	1					overnight	0
1c	25mM	NP-40 0.1%	167mM	1mM		1% 10 min	1		10µg			overnight	27
2a	25mM	NP-40 0.1%	167mM	1mM		1% 10 min	1	10µg		10µg		overnight	14
2b	25mM	NP-40 0.1%	167mM	1mM		1% 10 min	1		10µg			overnight	16
2c	25mM	NP-40 0.1%	167mM	1mM		1% 10 min	0.5	10µg				overnight	15
2d	25mM	NP-40 0.1%	167mM	1mM		1% 10 min	0.5		10µg			overnight	6
3a	25mM	NP-40 0.1%	50mM	1mM		1% 10 min	1	10µg				overnight	9
3b	25mM	NP-40 0.1%	50mM	1mM		1% 10 min	1		10µg			overnight	5
3c	25mM	NP-40 0.1%	167mM	1mM		1% 10 min	1	10µg				48 hours	14
3d	25mM	NP-40 0.1%	167mM	1mM		1% 10 min	1		10µg			48 hours	16
4a	25mM	NP-40 0.1%	150mM	1mM		1% 10 min	1	10µg				overnight	25
4b	25mM	NP-40 0.1%	150mM	1mM		1% 10 min	1		10µg			overnight	18
4c	25mM	NP-40 0.1%	150mM	1mM		1% 10 min	1	10µg	10µg			overnight	34
4d	25mM	NP-40 0.1%	150mM	1mM	10%	1% 10 min	1	10µg				overnight	20
4e	25mM	NP-40 0.1%	150mM	1mM	10%	1% 10 min	1		10µg			overnight	14
5a	25mM	NP-40 0.1%	150mM	1mM		1% 10 min	1	10µg	10µg			overnight	33
5b	25mM	NP-40 0.1%	150mM	1mM		1% 10 min	1	5µg	5µg			overnight	23
5c	25mM	Tritonx100 0.1%	150mM	1mM		1% 10 min	1	10µg	10µg			overnight	6
5d	25mM	CHAPS 0.5%	150mM	1mM		1% 10 min	1	10µg	10µg			overnight	31
5e	25mM	Digitonin 0.5%	150mM	1mM		1% 10 min	1	10µg	10µg			overnight	6
6a	25mM	CHAPS 0.5%	150mM	1mM		1% 10 min	1	10µg	10µg			overnight	18
6b	25mM	CHAPS 0.5%	150mM	1mM		2% 10 min	1	10µg	10µg			overnight	21
6c	25mM	CHAPS 0.5%	150mM	1mM		1% 10 min	0	10µg	10µg			overnight	0
6d	25mM	CHAPS 1%	150mM	1mM		1% 10 min	1	10µg	10µg			overnight	43
6e	25mM	CHAPS 0.1%	150mM	1mM		1% 10 min	1	10µg	10µg			overnight	17
7a	25mM	CHAPS 0.5%	50mM	1mM		1% 10 min	1	10µg	10µg			overnight	17
7b	25mM	CHAPS 1%	50mM	1mM		1% 10 min	1	10µg	10µg			overnight	4
7c	25mM	CHAPS 0.5%	150mM	1mM		1% 10 min	1	10µg	10µg			overnight	22
7d	25mM	CHAPS 1%	150mM	1mM		1% 10 min	1	10µg	10µg			overnight	21
7e	25mM	CHAPS 0.5%	300mM	1mM		1% 10 min	1	10µg	10µg			overnight	15
7f	25mM	CHAPS 1%	300mM	1mM		1% 10 min	1	10µg	10µg			overnight	27
8a	Dynabeads kit 14321D buffer + 100mM NaCl					1% 10 min	1	10µg	10µg			overnight	18
8b	Dynabeads kit 14321D buffer + 100mM NaCl, 2mM MgCl2, 1mM DTT					1% 10 min	1	10µg	10µg			overnight	9
8c	Dynabeads, Tris HCl 25mM, CHAPS 1%, 100mM NaCl, 1mM EDTA					1% 10 min	1	10µg	10µg			overnight	16
9a	25mM	NP-40 0.1%	50mM	1mM		1% 10 min	1	10µg	10µg			overnight	36
9b	25mM	CHAPS 1%	50mM	1mM		1% 10 min	1	10µg	10µg			overnight	48
9c	25mM	NP-40 0.1%	300mM	1mM		1% 10 min	1	10µg	10µg			overnight	27
9d	25mM	CHAPS 1%	300mM	1mM		1% 10 min	1	10µg	10µg			overnight	46
10a	25mM	NP-40 0.1%	150mM	1mM		1% 10 min	1	10 + 10	10 + 10			2xovernight	22 + 21
10b	25mM	CHAPS 1%	150mM	1mM		1% 10 min	1	10 + 10	10 + 10			2xovernight	36 + 17
11a	25mM	NP-40 0.1%	150mM	1mM		1% 10 min	1	10µg	10µg	26,3%		overnight	19
11b	25mM	NP-40 0.1%	150mM	1mM		1% 10 min	1	10µg	10µg			overnight	25
11c	25mM	CHAPS 1%	150mM	1mM		1% 10 min	1	10µg	10µg	26,3%		overnight	23
11d	25mM	CHAPS 1%	150mM	1mM		1% 10 min	1	10µg	10µg			overnight	31

Table 6: Table represents IP conditions which were used during Dj-1 IP optimization procedure. Western blots for each condition can be found in supplementary materials (supplementary fig. 1), calculations of the IP efficiencies represented in supplementary table 1.

5.6.4.2 Identification of Dj-1 interaction partners by mass spectrometry in SIM A9 cells

After the optimization experiments were finished and the best condition for the Dj-1 IP was chosen, three independent experiments for sample collection were performed. SIM A9 wildtype clone 38-1 and Dj-1 knockout clone 10-2 were used in these experiments. Cells were treated with 100ng/ml LPS for 1 hour and control cells were treated with only medium. After one hour, all the cells were fixed with 1% formaldehyde for 10 minutes at 37°C and the procedure of Dj-1 Co-IP was performed with subsequent purification of the Co-IPed proteins. After three experiments were finished, 12 samples collected during the experiment were sent to Dr. Stefanie Hauck in core proteomics facility.

Mass spectrometry experiment worked, since Dj-1 was found to be significantly enriched (marked in blue in table 7). Data analysis revealed only a few proteins which were enriched in wildtype SIM A9 cells as compared to Dj-1 knockout cells (table 7). That means that only a few possible Dj-1 interaction proteins were disclosed. The most significant candidates were the mitochondrial phosphate carrier (Slc25a3), the phospholipid scramblase 4 (Plscr4) and the sodium/potassium-transporting ATPase subunit alpha-3 (ATP1a3). Full data set from mass spectrometry analysis available in supplementary materials (supplementary table 2).

ratio wt/ko	T-test wt/ko	ratio LPS wt/ko	T-test LPS wt/ko	gene symbol	protein
2.1	0.0002	2.1	0.0198	Slc25a3	Phosphate carrier protein, mitochondrial
0.6	0.0066	0.6	0.0897	Hadha	Trifunctional enzyme subunit alpha, mitochondrial
0.2	0.0071	0.0	0.0266	Cct3	T-complex protein 1 subunit gamma
0.1	0.0084	0.1	0.1124	Ide	Insulin-degrading enzyme
0.5	0.0115	0.9	0.6981	Phb2	Prohibitin-2
0.5	0.0136	0.5	0.1329	Bcap29	B-cell receptor-associated protein 29
0.5	0.0174	0.5	0.1351	Adsl	Adenylosuccinate lyase
0.2	0.0174	0.3	0.0409	Cat	Catalase
0.5	0.0217	1.0	0.9295	Phb	Prohibitin
0.1	0.0222	0.1	0.1200	Clcc1	Chloride channel CLIC-like protein 1
0.3	0.0224	0.4	0.3073	Rpl3	60S ribosomal protein L3
58.2	0.0252	63.8	0.0224	Park7	Protein deglycase DJ-1
0.5	0.0288	0.5	0.1432	Lrrfp1	Leucine-rich repeat flightless-interacting protein 1
0.9	0.0331	0.9	0.5846	Slc25a4	ADP/ATP translocase 1
2.3	0.0385	0.6	0.4809	Atp1a3	Sodium/potassium-transporting ATPase subunit alpha-3
0.7	0.0391	0.6	0.2719	Srm	Spermidine synthase
2.5	0.0495	1.7	0.1345	Plscr4	Phospholipid scramblase 4
0.3	0.1332	0.2	0.0057	Pabpc1	Polyadenylate-binding protein 1
0.6	0.2182	0.4	0.0174	Fabp5	Fatty acid-binding protein, epidermal
0.9	0.7429	1.6	0.0324	Tuba1c	Tubulin alpha-1C chain
0.6	0.1077	0.7	0.0426	Usmg5	Up-regulated during skeletal muscle growth protein 5

Table 7: Table represents part of mass spectrometry results of Dj-1 interactome in SIM A9 cells. In red indicated best candidates to be validated. In yellow P≤0.05.

5.6.4.3 Validation of identified candidates

To validate the candidates found by mass spectrometry experiment the same procedure of Dj-1 Co-IP was performed and the samples were validated by western blot (fig. 26).

Western blot results from validation revealed several severe problems. First, all the antibodies against the candidate proteins (Slc25a3, ATP1a3, Plscr4) did not perform well. Second, detection of Slc25a3 and Plscr4 in IP samples could be problematic because of the high background probably caused by contamination of A/G proteins during elution procedure. A/G recombinant proteins with IgG binding motifs are usually conjugated with beads and used for antibody precipitation experiments.

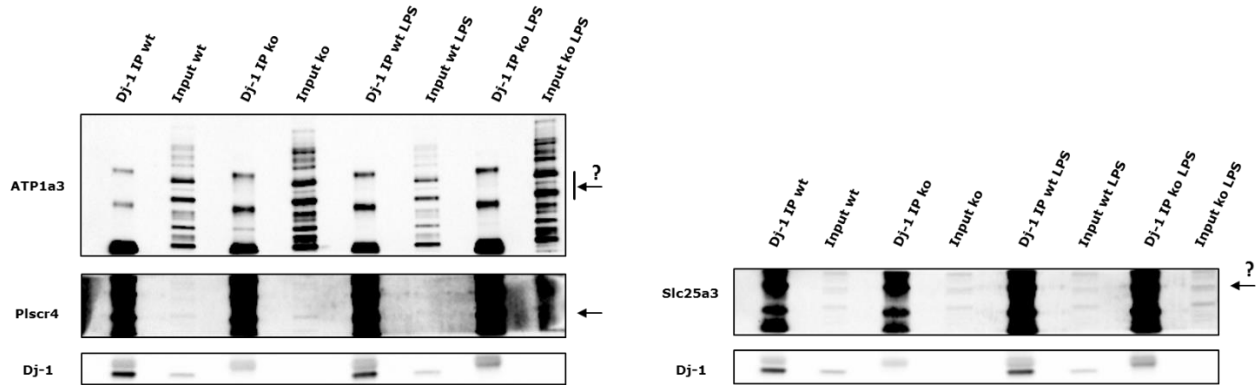


Figure 26: Western blots of validation of Dj-1 possible interaction with Scl25a3, ATP1a3 and Plscr4 under basal and LPS treatment conditions. Arrows represent possible position of indicated proteins. All the IP samples (Dj-1 IP wt, Dj-1 IP ko, Dj-1 IP wt LPS, Dj-1 IP ko LPS) have the similar patterns on western blot in all possible Dj-1 interaction proteins tested, which most probably caused by the contamination with A/G proteins during the elution step. Poor antibodies efficiency together with high background did not allow to determine the chosen Dj-1 interaction proteins.

The next step was to repeat the validation procedure with conditions which could help to solve the problems indicated above. First of all, new AB against ATP1a3 and Slc25a3 were tested. Unfortunately, ATP1a3 AB were still very unspecific, but performed a bit better than the old ones. The new Slc25a3 AB did not work at all. Therefore, it was decided to use the new anti-ATP1a3 antibody in all following experiments. The second problem, probably caused by A/G protein contamination, likely happening during the elution step, could be partially solved by changing the elution conditions to milder ones. Therefore, low pH elution was performed in all following experiments (fig. 27).

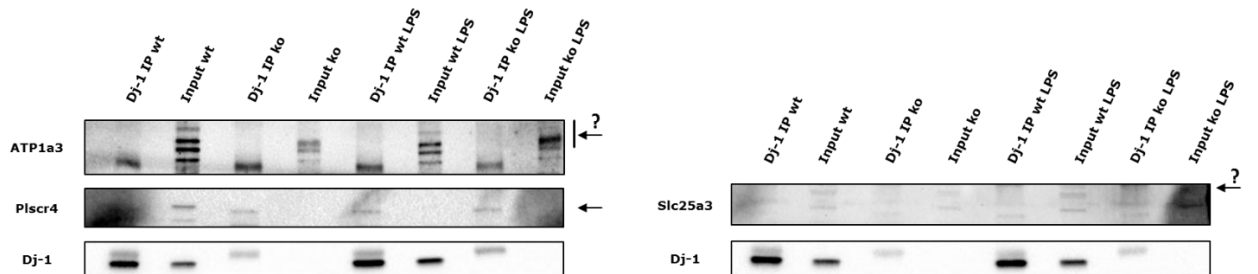


Figure 27: Western blots of validation of Dj-1 possible interaction with Scl25a3, ATP1a3 and Plscr4 under basal and LPS treatment conditions. Arrows represent possible position of indicated proteins.

The second validation experiment showed that the low pH elution worked and was efficient enough to remove the background from IP samples in the region of Slc25a3 and Plscr4 sizes. However, it still was not possible to show here that Dj-1 interacts with Slc25a3, Plscr4 or ATP1a3. The limiting point in the validation experiment was the poor efficiency of Slc25a3, Plscr4 and ATP1a3 antibodies, moreover there is seemingly limiting choice of these antibodies on the market at the moment. Taken together, it was difficult to validate and make a clear conclusion about Dj-1 interaction proteins in SIM A9 cells by western blot. More efficient and specific

antibodies against these candidates are needed to be able to perform an efficient validation experiment.

5.6.4.4 Further results of mass spectrometry data

Upon taking a look on mass spectrometry data (table 7) it becomes obvious that there are several proteins which have wildtype to knockout ratios less than 1 with a p value less than 0.05. On first glance, this does not make much sense since Dj-1 knockout cells do not have Dj-1 and no interaction proteins could be pulled down by anti-Dj-1 antibodies. It can be suspected that these proteins were pulled down by unspecific interactions with agarose beads, and if this holds true, the amount of these proteins in the Dj-1 knockout could be higher than in wildtype cells. To test this hypothesis, 3 proteins (mitochondrial trifunctional enzyme subunit alpha (Hadha) – wt/ko ratio = 0.6, $p=0.0066$; Catalase (Cat) - wt/ko ratio = 0.2, $p=0.0174$; spermidine synthase (Srm) - wt/ko ratio = 0.7, $p=0.0391$) were chosen from the list for mRNA expression analysis (fig. 28) and two of them (Cat and Srm) for western blot validation.

It should be mentioned here that during the bachelor work of Irina Petcu, whom I was supervising, we obtained three additional Dj-1 knockout clones from SIM A9 cells – N50, N78, and N79 with respective wildtype control clones – N57, N60, and N61. These clones were included for further validation too, to exclude possible clone specific differences (fig. 28b).

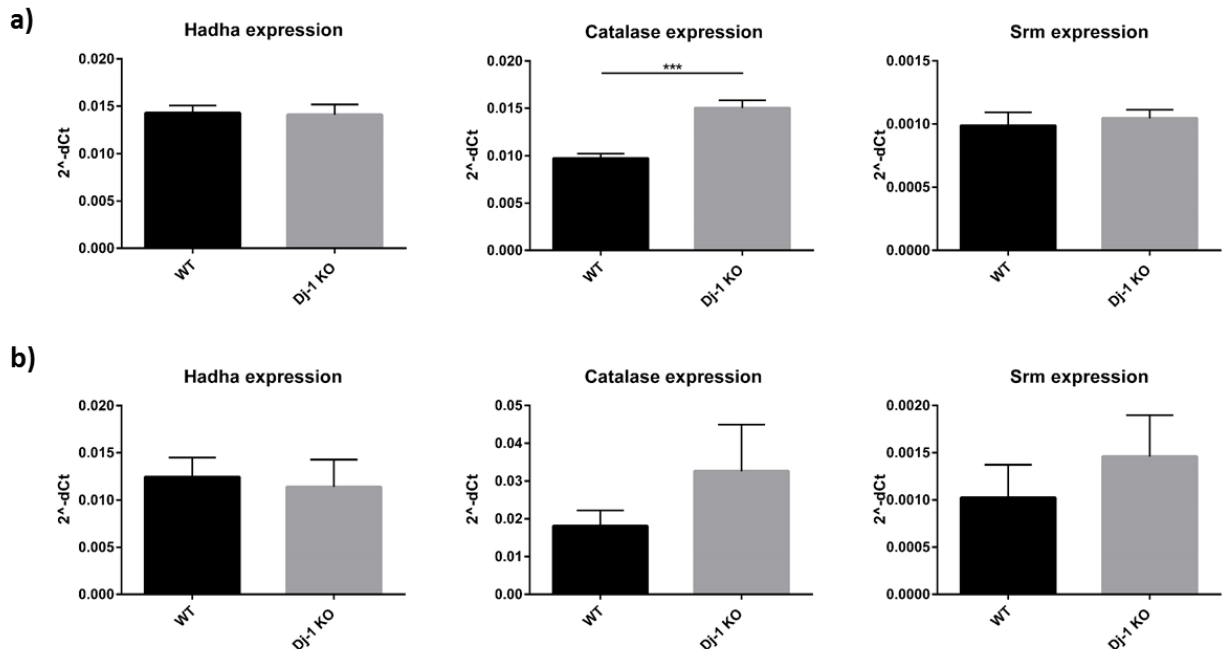


Figure 28: mRNA expression analysis for Hadha, Catalase and Srm in (a) SIM A9 wildtype clone N38-1 and Dj-1 knockout clone N10-2 and (b) SIM A9 wildtype clones N57, 60, 61 and Dj-1 knockout clones N50, 78, 79. All samples were analyzed with a biological n=3 and in technical triplicates. Bars represent mean ± sd. Quantification was done via unpaired t-Test: * $p \leq 0.05$; ** $p \leq 0.01$; *** $p \leq 0.001$.

Results obtained from the mRNA expression analysis in clones 38-1 and 10-2 revealed that there is a significant higher expression of catalase in the Dj-1 knockout clone (wildtype 0.00971 ± 0.00049 and Dj-1 knockout 0.01502 ± 0.00082 , $p=0.0006$), which perfectly fits with the results obtained by mass spectrometry. However, there were no differences found between the genotypes in expression of Hadha and Srm (fig. 28a). Moreover, analysis of the new clones (wt: 57, 60, 61; ko: 50, 78, 79) showed no differences in Hadha, Cat, and Srm mRNA expression levels, even though for catalase expression a trend was detected (wildtype 0.01809 ± 0.00412 and Dj-1 knockout 0.03260 ± 0.01232 , $p=0.1251$) (fig. 28b).

To further validate the possible differences between the genotypes western blot experiments for Cat and Srm were done (fig. 29).

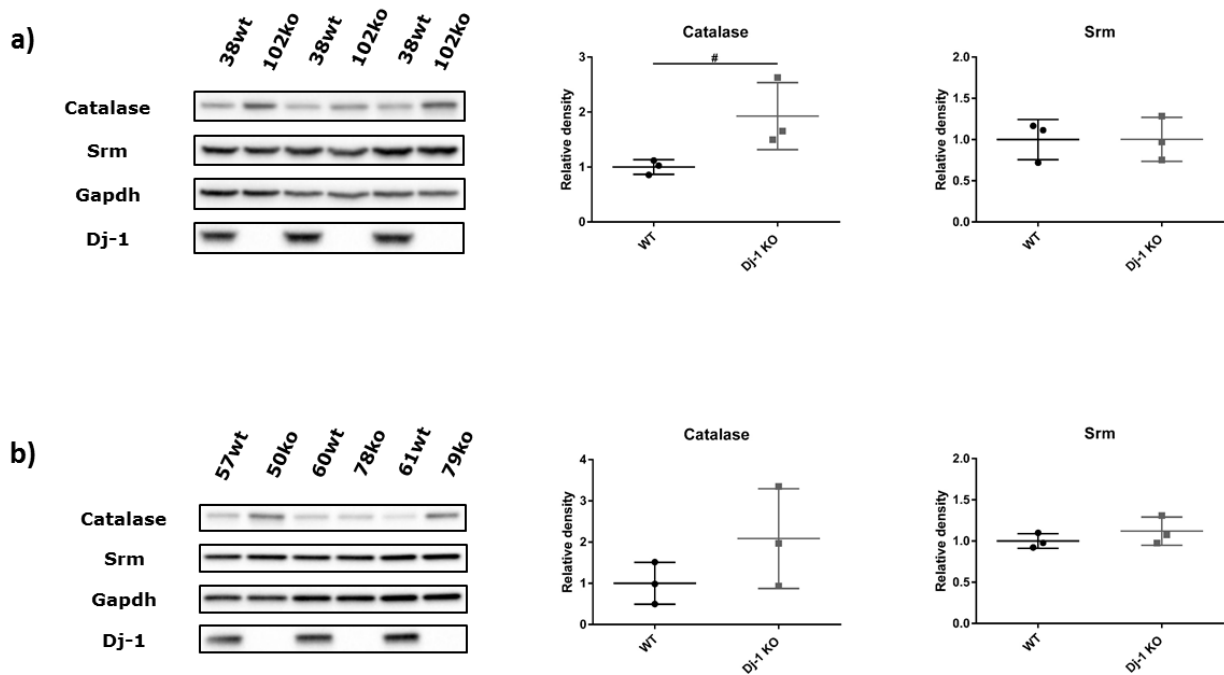


Figure 29: Western blot analysis for Catalase and Srm in (a) SIM A9 wildtype clone N38-1 and Dj-1 knockout clone N10-2, (b) SIM A9 wildtype clones N57, 60, 61 and Dj-1 knockout clones N50, 78, 79. All samples were analyzed with a biological n=3. Bars represent mean \pm sd. Quantification was done via unpaired t-Test: $0.05 \leq \#p \leq 0.1$.

Western blot results from three independent experiments with clones 38-1 and 10-2 (fig. 29a) revealed a trend in higher catalase abundance in the knockout clone 10-2 (wildtype 1 ± 0.134 and Dj-1 knockout 1.926 ± 0.611 , $p=0.0622$). Despite the fact that western blot with the other clones (wt: 57, 60, 61; ko: 50, 78, 79) did not show a significant difference in catalase abundance between the genotypes, one can clearly see that the knockout clones 50 and 79 have a higher catalase content (fig. 29b). The presence of Srm in the samples of wildtype and Dj-1 knockout clones was not different.

Since our hypothesis could be true for the wt/ko ratios less than 1, it could also be true for the ratios larger than 1 either. Therefore, it was decided to perform western blot experiments with different wildtype and Dj-1 knockout clones to detect protein levels of Slc25a3, Plscr4 and ATP1a3 (fig. 30).

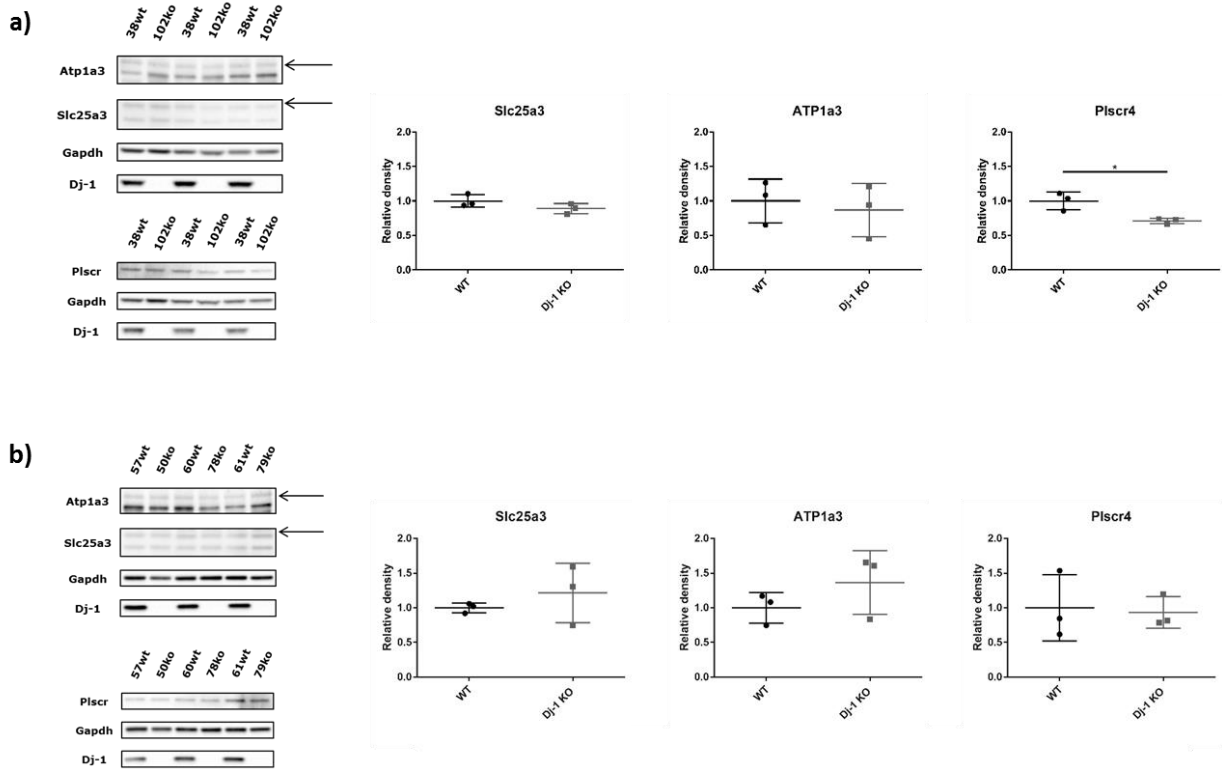


Figure 30: Western blot analysis for Slc25a3, Plscr4 and ATP1a3 in (a) SIM A9 wildtype clone N38-1 and Dj-1 knockout clone N10-2, (b) SIM A9 wildtype clones N57, 60, 61 and Dj-1 knockout clones N50, 78, 79. Arrows represent positions of the desired proteins. All samples were analyzed with a biological n=3. Bars represent mean \pm sd. Quantification was done via unpaired t-Test: $0.05 \leq p \leq 0.1$.

According to the western blot results, there is no differences between the genotypes in Slc25a3, Plscr4 and ATP1a3 levels in three independent wildtype and Dj-1 knockout clones (fig. 30b) (poor performance of Slc25a3 and ATP1a3 antibodies as indicated above could influence the results). Although the content of Plscr4 was significantly higher in wildtype clone 38-1 in comparison to Dj-1 knockout clone 10-2 (wildtype 1 ± 0.130 and Dj-1 knockout 0.712 ± 0.038 , $p=0.021$) (fig. 30a), which fits with the ratio data from mass spectrometry.

Taken together, these data show the possibility of the unspecific binding hypothesis to be true. Although it is not so easy to confirm by western blot when the ratios between wildtype and Dj-1 knockout clones are near to one. Example of catalase demonstrate that more potential distance of ratio from 1 between the genotypes in MS data – more chances to disclose this variation by mRNA expression and western blot analyses.

5.6.5 Metabolic activity analysis in wildtype and Dj-1 knockout SIM A9 cells

5.6.5.1 Respiratory assessment of wildtype and Dj-1 knockout SIM A9 cells

The oxidative phosphorylation and glycolytic activity in SIM A9 cells was assessed for changes in the Dj-1 knockout cells. This was of particular interest due to the possible interaction of Dj-1 with Slc25a3, which is the inorganic phosphate transporter important for ATP synthesis in mitochondria and with ATP1a3 - a subunit of Na/K ATPase, which is responsible for huge energy expenditure.

To do so respiratory analysis was performed on a Seahorse XF96 analyzer. This platform allows real time and parallel assessment of the oxygen consumption rate (OCR) and the extracellular acidification rate (ECAR). Addition of specific chemicals during the run allows to obtain additional layers of information, which help to characterize the properties of oxidative phosphorylation and glycolysis within the cellular systems (reviewed in detail by Divakaruni and colleagues (Divakaruni et al., 2014)).

An example of a routine OCR measurement during a Seahorse run is presented in figure 31a. The basal OCR is composed of oxygen consumption linked to ATP production, oxygen consumption due to the proton leak and non-mitochondrial oxygen consumption. Non mitochondrial respiration is determined in the last step by addition inhibitors of complex I (rotenone) and complex III (antimycin-A) and is subtracted from all other obtained values for normalization purposes. Addition of oligomycin leads to the inhibition of the F₀F₁-ATPase, but not the electron transport chain (ETC), therefore, the OCR after addition of this compound represents the oxygen consumption linked to the proton leak. By subtracting the OCR linked to the proton leak from the basal OCR, the oxygen consumption linked to ATP production is obtained. Maximal respiratory capacity is assessed by addition of the protonophore carbonyl cyanide 4-(trifluoromethoxy) phenylhydrazone (FCCP). This compound leads to breakdown of mitochondrial membrane potential, as it shuttles protons across the inner mitochondrial membrane into the mitochondrial matrix. The mitochondria, on the other hand, try to re-establish the membrane potential by activating the ETC, which leads to the measurement of the maximal respiratory capacity.

As mentioned above, in parallel to the OCR measurements, the ECAR is obtained. This is possible as the medium used in these experiments is unbuffered and allows to register the extracellular acidification as parameter. The ECAR is mainly attributed to glycolytic activity, although it is noteworthy that other cellular processes including production of CO₂ within the TCA could partially be responsible for media acidification. An example of a routine ECAR measurement during a run is presented in figure 31b. Addition of oligomycin leads to an increase of ECAR in comparison with the basal ECAR (i.e. basal glycolytic activity) and is called maximal glycolytic capacity as after a blockade of the ATP synthase, the system needs to fulfill its ATP demand which is done by upregulation of glycolysis. FCCP can slightly increase ECAR because of the increase production of CO₂ within the TCA due to increase oxidative activity. In the end, 2-deoxyglucose

(2-DG) is added. This compound inhibits glycolysis by allosteric inhibition of the hexokinase, and therefore, the ECAR values obtained after 2-DG are used for normalization.

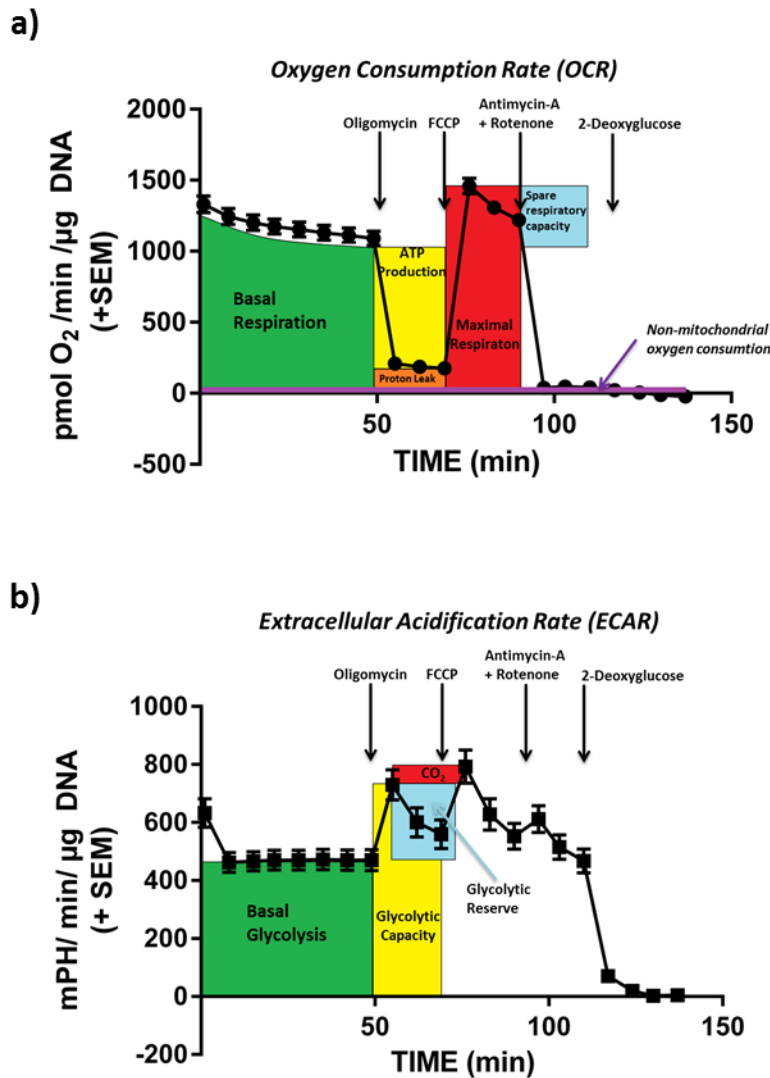


Figure 31: Examples of (a) the oxygen consumption rate (OCR) and (b) the extracellular acidification rate (ECAR) in a routine run on a Seahorse XF96 analyzer. Oligomycin – inhibitor of the ATP synthase; carbonyl cyanide 4-(trifluoromethoxy) phenylhydrazone (FCCP) – protonophore breaking down the membrane potential; rotenone – inhibitor of mitochondrial complex I; antimycin A - inhibitor of mitochondrial complex III; 2-deoxyglucose – inhibitor of hexokinase (inhibition of glycolysis). Figures are made and provided by C. Stautner, 2018

To do this experiment three wildtype (N57, 60, 61) and Dj-1 knockout (N50, 78, 79) clones were plated with sufficient replicates on one seahorse XF96-well plate. Metabolic rates of these cells with four different conditions were checked: 1) only glucose supplemented, 2) only glucose supplemented and LPS treatment 1 hour in advance, 3) only pyruvate supplemented and 4) only pyruvate supplemented and LPS treatment 1 hour in advance. Pyruvate as a supplement was used for more precise assessment of oxidative phosphorylation processes.

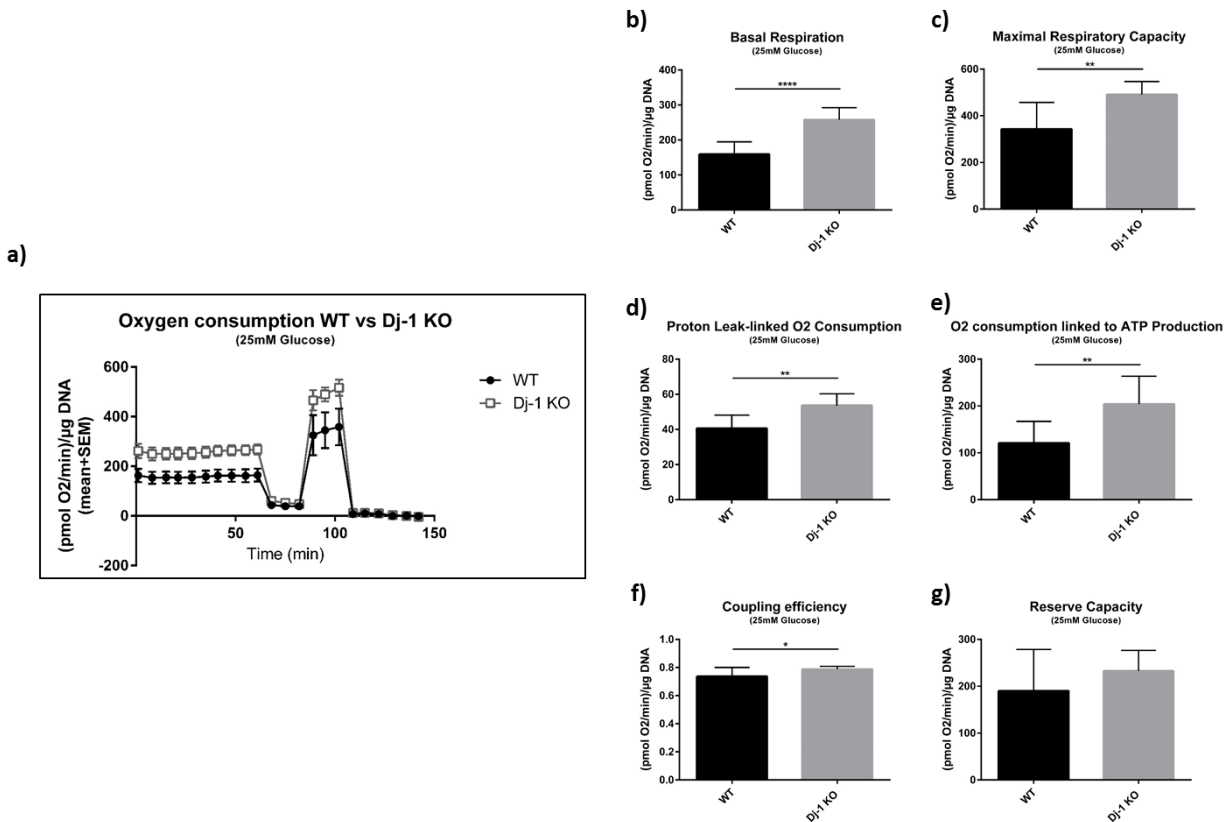


Figure 32: Respiratory analysis using a Seahorse XF96 analyzer with three wildtype and three Dj-1 knockout SIM A9 clones with 25mM glucose only during the time frame of the experiment. (a) Represents oxygen consumption; (b) basal respiration; (c) maximal respiratory capacity; (d) proton leak linked to oxygen consumption; (e) oxygen consumption linked to ATP production; (f) coupling efficiency and (g) reserve capacity. Bars represent mean \pm sd for (b-g) and mean \pm sem for (a). Statistical analysis was done using Mann-Whitney test for (b) and (e) and unpaired student's t-Test for (c, d, f, g). * $p \leq 0.05$, ** $p \leq 0.01$, * $p \leq 0.001$, **** $p \leq 0.0001$.**

Respiratory measurements with only glucose supplement disclosed significant differences in oxygen consumption between the genotypes (fig. 32). Dj-1 knockout SIM A9 cells have significantly higher rates of basal respiration (wildtype 159.1 ± 35.8 and Dj-1 knockout 258 ± 34.1 , $p < 0.0001$) and maximal respiratory capacity (wildtype 342.7 ± 114.4 and Dj-1 knockout 490.6 ± 56.2 , $p < 0.0001$), moreover, proton leak linked oxygen consumption (wildtype 40.6 ± 7.6 and Dj-1 knockout 53.7 ± 6.6 , $p = 0.0013$), oxygen consumption linked to ATP production (wildtype 121.2 ± 46 and Dj-1 knockout 204.3 ± 59.4 , $p = 0.0013$) and coupling efficiency (wildtype 0.7358 ± 0.0646 and Dj-1 knockout 0.7877 ± 0.0213 , $p = 0.0156$) were also higher with only glucose supplemented. In general, it can be concluded that under the taken conditions, the rate of oxidative phosphorylation is greater in knockout cells in comparison to wildtype cells.

The extracellular acidification rate (ECAR) serves as framework of glycolytic activity. With only glucose supplemented (fig. 33), a trend towards higher basal glycolytic activity shows in wildtype cells (wildtype 101.7 ± 18.7 and Dj-1 knockout 93.4 ± 13.2 , $p = 0.0772$), although maximal rate of glycolysis (wildtype 157.7 ± 35.3 and Dj-1 knockout 187.3 ± 20.1 , $p = 0.0438$) and glycolytic reserve

(wildtype 56.9 ± 17.6 and Dj-1 knockout 94.4 ± 22.5 , $p=0.001$) are significantly higher in knockout cells.

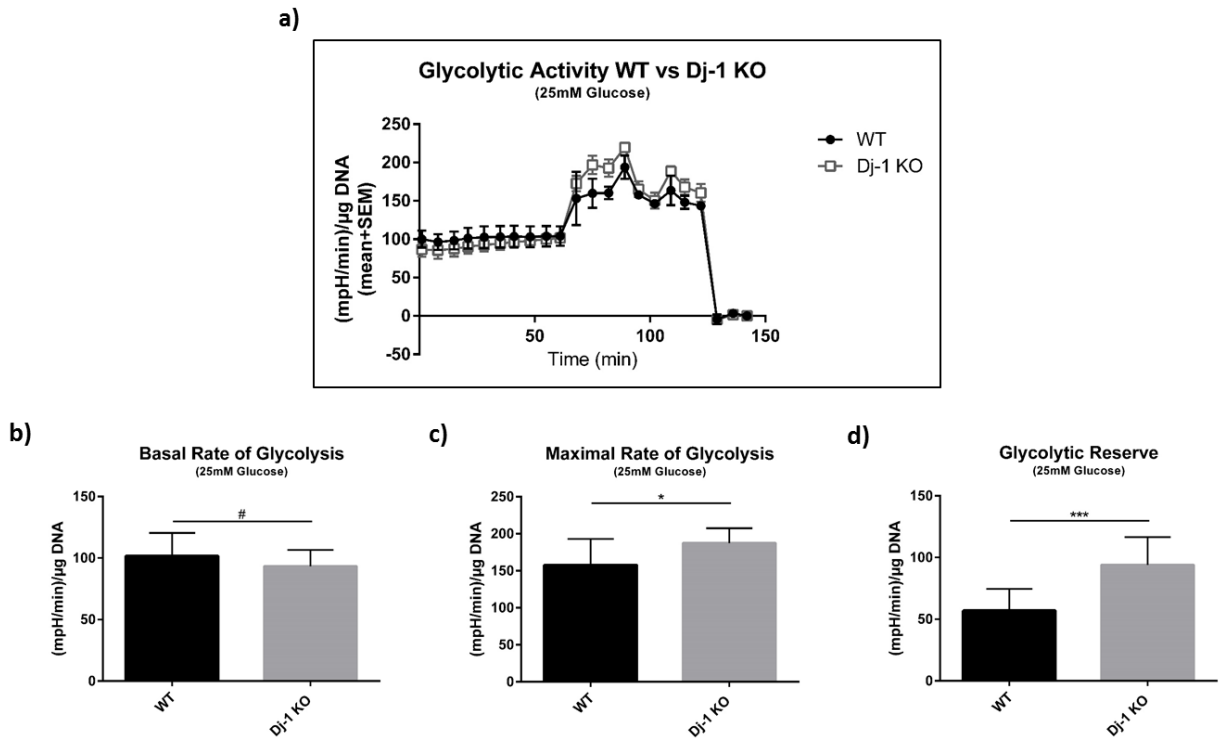


Figure 33: ECAR values from the seahorse experiment with three wildtype and three Dj-1 knockout SIM A9 clones with only 25mM glucose supplemented during the time frame of the experiment. (a) Graph represents ECAR; (b) basal rate of glycolysis; (c) maximal rate of glycolysis and (d) glycolytic reserve. Bars represent mean \pm sd for (b-d) and mean \pm sem for (a). Statistical analysis was done using Mann-Whitney test for (b) and (d) and unpaired student's t-Test for (c). $0.05 \leq \#p \leq 0.1$, $*p \leq 0.05$, $p \leq 0.01$, $***p \leq 0.001$.**

It is known that immune cells, during the activation of M1 stage (LPS treatment), change their metabolic profile. They decrease the rate of oxidative phosphorylation and upregulate the glycolytic pathway. Therefore, it was rather intriguing to see how the SIM A9 microglial cell line performs metabolic reactions under LPS condition dependent on genotype.

Results depicted in figure 34 show that there is no differences in the oxygen consumption rate (OCR) between the genotypes with glucose supplemented plus LPS treatment. Moreover, several parameters such as maximal respiratory capacity (wildtype 531.8 ± 134.1 and Dj-1 knockout 429.7 ± 112.3 , $p=0.0625$), proton leak linked to oxygen consumption (wildtype 46.5 ± 5.5 and Dj-1 knockout 39.5 ± 8.2 , $p=0.0518$) and reserve capacity (wildtype 316.2 ± 140.6 and Dj-1 knockout 230 ± 69 , $p=0.0802$), which were significantly enhanced in Dj-1 knockout cells without LPS treatment, show now a trend to be higher in wildtype cells in comparison to Dj-1 knockout cells.

Extracellular acidification rate with only glucose supplement and upon LPS treatment revealed that the wildtype cells under given conditions have significantly higher rates of basal glycolysis (wildtype 122.1 ± 10.1 and Dj-1 knockout 84.8 ± 8.1 , $p < 0.0001$) and maximal glycolytic capacity

(wildtype 216 ± 26.2 and Dj-1 knockout 174.1 ± 17.9 , $p=0.0011$) (fig. 35), which is different from the results obtained without LPS treatment.

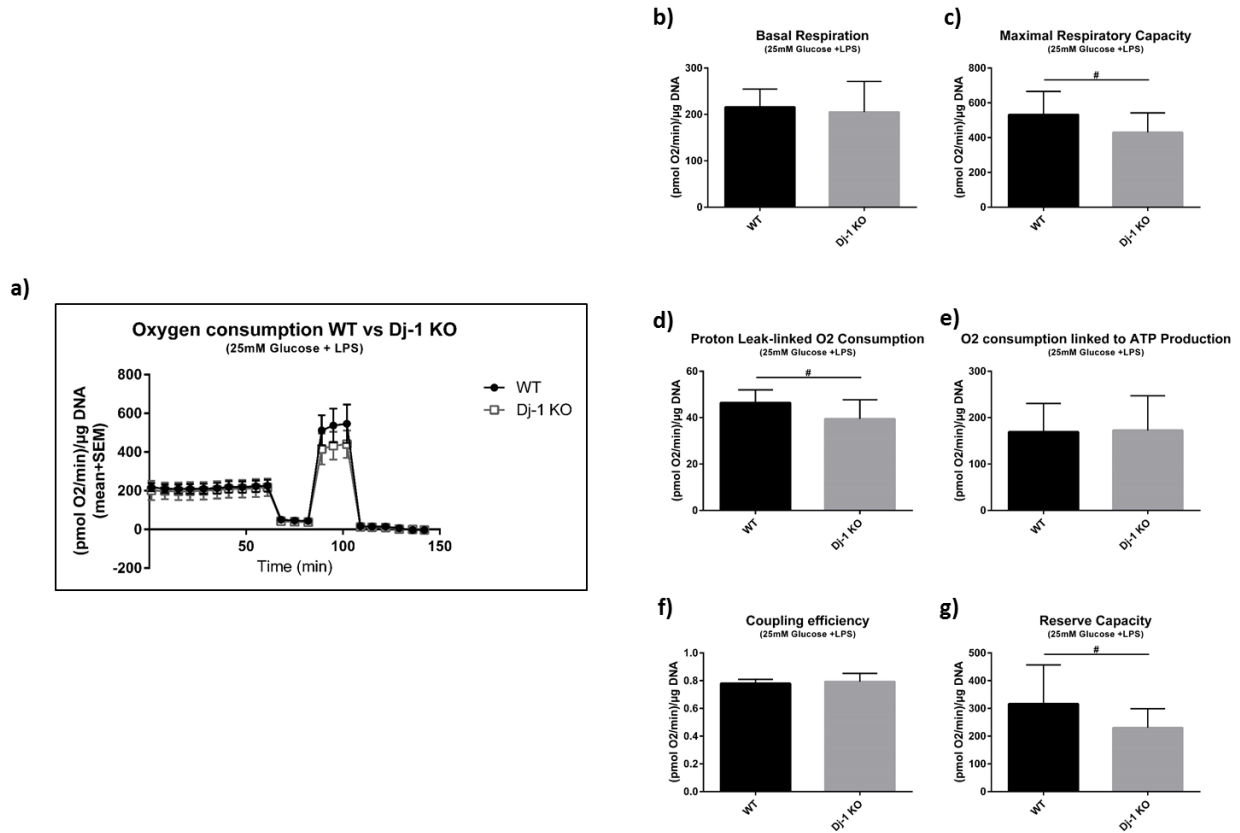


Figure 34: Respiratory analysis using a Seahorse XF96 analyzer with three wildtype and three Dj-1 knockout SIM A9 clones with only 25mM glucose supplemented plus LPS treatment during the time frame of the experiment. (a) Graph represents oxygen consumption; (b) basal respiration; (c) maximal respiratory capacity; (d) proton leak linked to oxygen consumption; (e) oxygen consumption linked to ATP production; (f) coupling efficiency; and (g) reserve capacity. Bars represent mean \pm sd for (b-g) and mean \pm sem for (a). Statistical analysis was using Mann-Whitney's test for (b) and (c); and unpaired student's t-Test for (d, e, f, g). $0.05 \leq p \leq 0.1$.

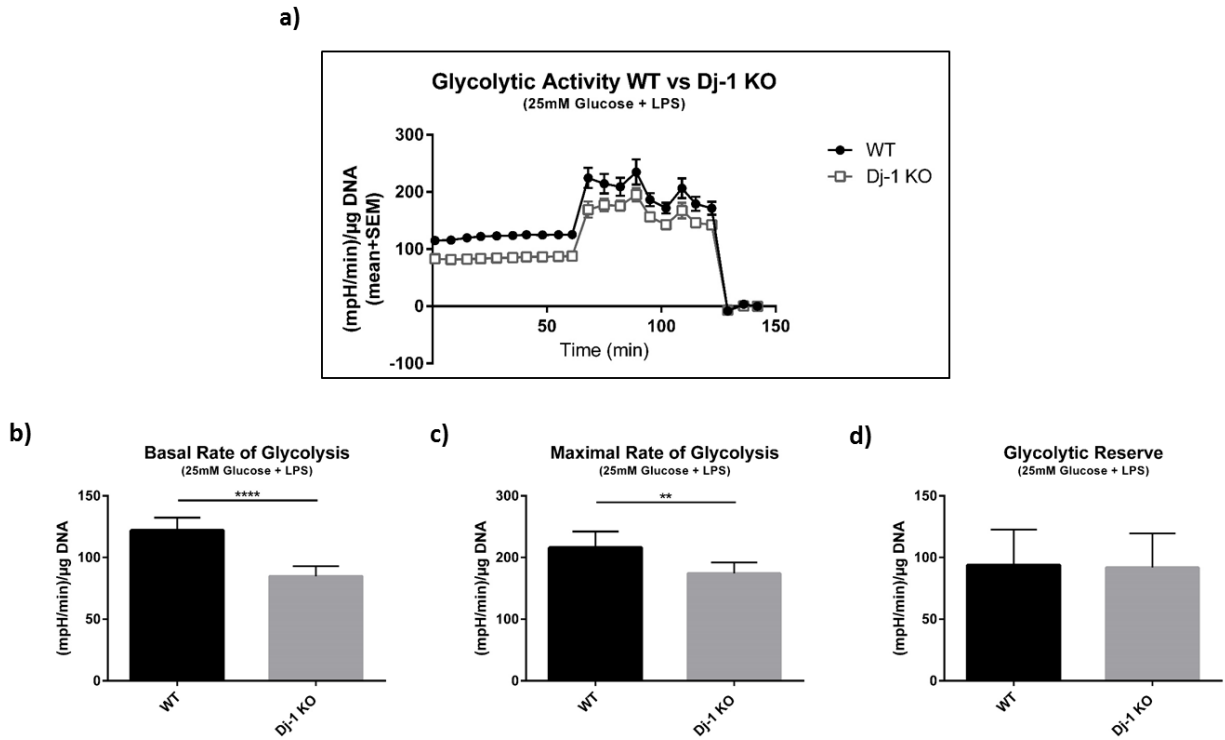


Figure 35: ECAR values from seahorse experiment with three wildtype and three Dj-1 knockout SIM A9 clones with only 25mM glucose supplemented plus LPS treatment during the time frame of the experiment. (a) Graph represents ECAR; (b) basal rate of glycolysis; (c) maximal rate of glycolysis and (d) glycolytic reserve. Bars represent mean \pm sd for (b-d) and mean \pm sem for (a). Statistical analysis was done using Mann-Whitney's test for (b) and unpaired student's t-Test for (c) and (d). * $p \leq 0.05$, ** $p \leq 0.01$, * $p \leq 0.001$, **** $p \leq 0.0001$.**

To be able to compare several important parameters of the OCR and ECAR between the genotypes and different conditions two-way Anova tests were performed (fig. 36). Statistical analysis revealed in (a) a significant effect of genotype ($F=28.21$, **** $p < 0.0001$) and interaction of genotype and treatment ($F=43.13$, **** $p < 0.0001$); in (b) a significant effect of interaction of genotype and treatment ($F=12.01$, ** $p = 0.0015$); in (c) a significant effect of interaction of genotype and treatment ($F=17.97$, *** $p = 0.0002$); in (d) a significant effect of genotype ($F=5.735$, * $p = 0.0212$) and interaction of genotype and treatment ($F=4.88$, * $p = 0.0327$); in (e) a significant effect of genotype ($F=89.66$, **** $p < 0.0001$), treatment ($F=6.068$, * $p = 0.0152$) and interaction of genotype and treatment ($F=36.12$, **** $p < 0.0001$); in (f) a significant effect of treatment ($F=6.871$, * $p = 0.0133$) and interaction of genotype and treatment ($F=17.37$, *** $p = 0.0002$).

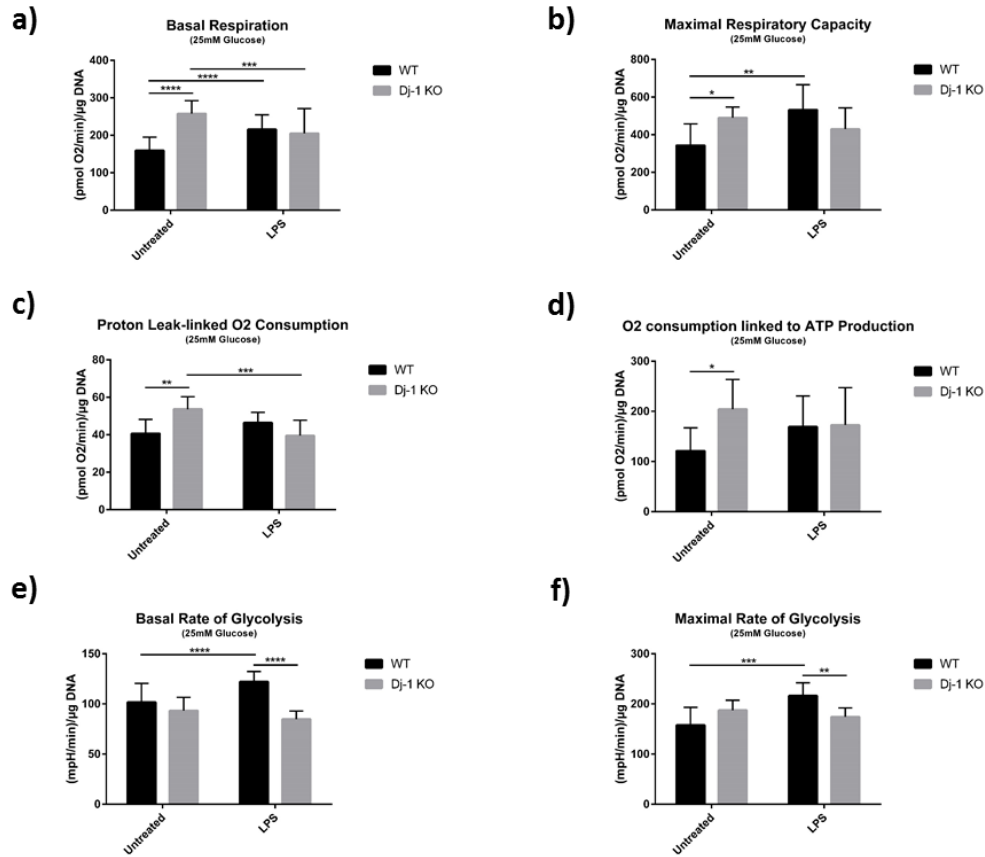


Figure 36: OCR and ECAR values from seahorse experiment with three wildtype and three Dj-1 knockout SIM A9 clones with only 25mM glucose supplemented under basal and LPS treatment conditions. (a) Basal respiration, (b) maximal respiratory capacity, (c) proton leak linked to oxygen consumption, (d) oxygen consumption linked to ATP production, (e) basal rate of glycolysis and (f) maximal rate of glycolysis. Analysis was performed with three wildtype and three Dj-1 knockout SIM A9 clones. Bars represent mean \pm sd. Statistical analysis was done using two-way ANOVA analysis and Tukey's multiple comparison test: * $p \leq 0.05$, ** $p \leq 0.01$, * $p \leq 0.001$, **** $p \leq 0.0001$.**

Post hoc statistical analysis of represented parameters revealed differences in the capability to perform metabolic switch during LPS treatment between the genotypes. Thus, Dj-1 knockout cells perform with a higher basal respiration than wildtypes with only glucose supplemented, however during LPS treatment, it could be observed that distinct patterns concerning the metabolic switch appear between the genotypes. Thus, clear upregulation of basal respiration is found in wildtype cells during LPS treatment (wildtype 159.1 ± 35.8 and wildtype LPS 215.6 ± 39 , $p < 0.0001$) and at the same time knockout cells behave the opposite by decreasing basal respiratory activity (Dj-1 knockout 258 ± 34.1 and Dj-1 knockout LPS 205.1 ± 65 , $p = 0.0001$). Concerning the other parameters of oxygen consumption (maximal respiratory capacity, proton leak linked oxygen consumption, and oxygen consumption linked to ATP production), more or less the same effect was observed. Wildtypes increase these parameters (maximal respiratory capacity (wildtype 342.7 ± 114.4 and wildtype LPS 531.8 ± 134.1 , $p = 0.0042$) or do not significantly change them (proton leak linked oxygen consumption (wildtype 40.6 ± 7.6 and wildtype LPS 46.5 ± 5.5 , $p = 0.318$), oxygen consumption linked to ATP production (wildtype 121.2 ± 46 and

wildtype LPS 169.2 ± 61.5 , $p=0.2525$), whereas knockouts decrease (proton leak linked oxygen consumption (Dj-1 knockout 53.7 ± 6.6 and Dj-1 knockout LPS 39.5 ± 8.3 , $p=0.0009$) or do not significantly change them (maximal respiratory capacity (Dj-1 knockout 490.6 ± 56.2 and Dj-1 knockout LPS 429.8 ± 112.3 , $p=0.6257$), oxygen consumption linked to ATP production (Dj-1 knockout 204.3 ± 59.4 and Dj-1 knockout LPS 172.5 ± 74.7 , $p=0.6021$)) (fig 36a-d). The differences in the metabolic switch between the genotypes can equally be observed at the level of the extracellular acidification rate. Thus, during the LPS treatment wildtype SIM A9 cells upregulate the basal (wildtype 101.7 ± 18.7 and wildtype LPS 122.1 ± 10.2 , $p < 0.0001$) and maximal rates of glycolysis (wildtype 157.7 ± 35.3 and wildtype LPS 216 ± 26.2 , $p=0.0002$) whereas knockouts do not (fig. 36e, f).

Taken together, these results indicate that there are differences between the genotypes already under basal conditions with only glucose as substrate, where Dj-1 knockout SIM A9 cells rely more on oxidative phosphorylation than wildtypes. Under LPS treatment conditions, wildtype cells do not decrease the rate of oxidative phosphorylation but increase the rate of glycolysis, whereas knockouts decrease the rate of oxidative phosphorylation and seem to have a problem with the upregulation of the glycolytic pathway.

Two-way ANOVA analysis of OCR results obtained with pyruvate as substrate, with and without LPS treatment, revealed in (37c) a significant effect of genotype ($F=115.5$, **** $p < 0.0001$) and interaction of genotype and treatment ($F=29.67$, **** $p < 0.0001$); in (37d) a significant effect of genotype ($F=15.06$ *** $p=0.0005$); in (37e) a significant effect of genotype ($F=18.8$, *** $p=0.0001$) and interaction of genotype and treatment ($F=11.07$, ** $p < 0.0022$); in (37f) a significant effect of genotype ($F=13.42$ *** $p=0.0007$). Post hoc test results, obtained under conditions with pyruvate show similar patterns like in the experiments with only glucose supplemented (fig. 37), indicating existence of differences in metabolic rates between the genotypes.

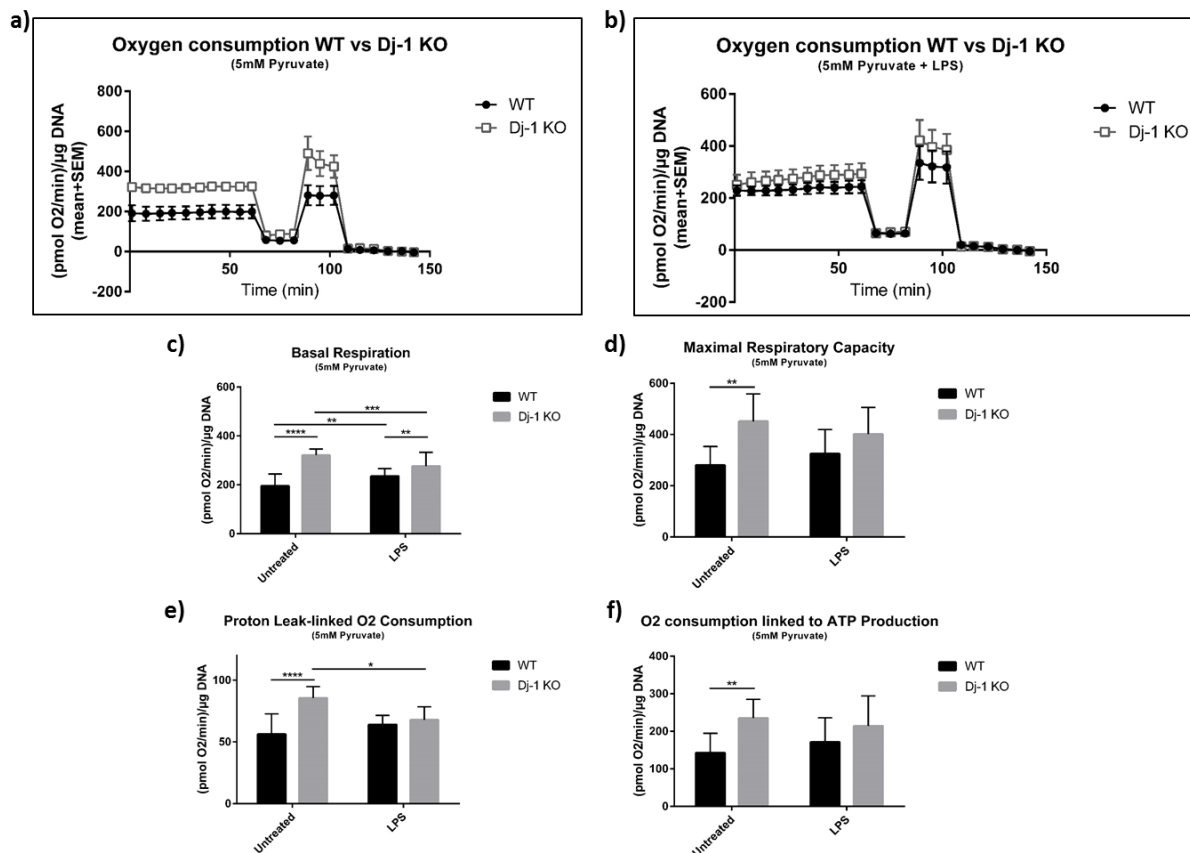


Figure 37: Respiratory analysis using a Seahorse XF96 analyzer with three wildtype and three Dj-1 knockout SIM A9 clones with only 5mM pyruvate supplemented under basal and LPS treatment conditions. (a) Graph represents oxygen consumption with only 5mM pyruvate supplemented during the time frame of the experiment, while (b) represents oxygen consumption with 5mM pyruvate supplemented plus LPS treatment during the time frame of the experiment. (c) Basal respiration, (d) maximal respiratory capacity, (e) proton leak linked to oxygen consumption and (f) oxygen consumption linked to ATP production. Analysis was performed with three wildtype and three Dj-1 knockout SIM A9 clones. Bars represent mean \pm sd for (c-f) and mean \pm sem for (a) and (b). Statistical analysis was done using two-way ANOVA analysis and Tukey's multiple comparison test: * $P \leq 0.05$, ** $P \leq 0.01$, * $P \leq 0.001$, **** $P \leq 0.0001$.**

5.6.5.2 Lactate measurement in SIM A9 wildtype and Dj-1 knockout cells

After a seahorse run was completed 50 μ l of supernatant from each sample was collected to perform a lactate assay from the supernatants from all conditions (fig. 38).

The lactate measurement data revealed no differences between the genotypes under various conditions. After analysis of ECAR seahorse data under LPS treatment with only glucose as substrate, one could expect some elevations in lactate levels of wildtypes due to increased glycolysis. Even though there is a slight increase in lactate in LPS treated wildtype cells, the level is not high enough to be significant and this event could be explained by the not efficient time frame of the experiment and chemicals usage, which bring their perturbations in metabolic

processes. Increased time of LPS treatment without any additional drugs may increase the reliability of the lactate measurement data.

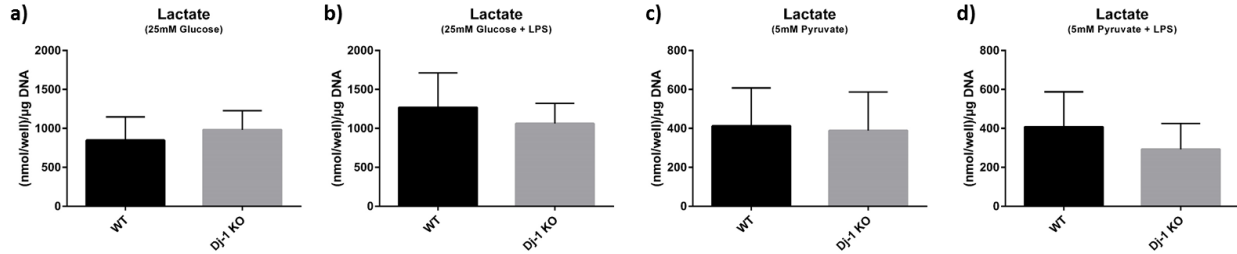


Figure 38: Lactate content normalized to μ g of DNA in SIM A9 wildtype and Dj-1 knockout cells. (a) 25mM glucose, (b) 25mM glucose plus 100ng/ml LPS, (c) 5mM pyruvate and (d) 5mM pyruvate plus 100ng/ml LPS. Samples were measured with sufficient biological replicates (wt n=9, ko n=9). Bars represent mean \pm sd. Statistical analysis was done using unpaired student's t-Test for (b-c) and Mann-Whitney test for (a).

5.6.5.3 Quantification of the amount of mitochondrial complexes in wildtype and Dj-1 knockout SIM A9 cells

According to the respiratory data, Dj-1 knockout cells have a higher basal rates of respiration under glucose and pyruvate conditions. A higher efficiency of oxidative phosphorylation performance can be attributed to many reasons, one of them is an increased amount of mitochondria and / or mitochondrial complexes, which execute the process of oxidative phosphorylation. Therefore, a quantitative analysis of mitochondrial complexes in SIM A9 wildtype (N57, 60, 61) and Dj-1 knockout clones (N50, 78, 79) (fig. 39) was done.

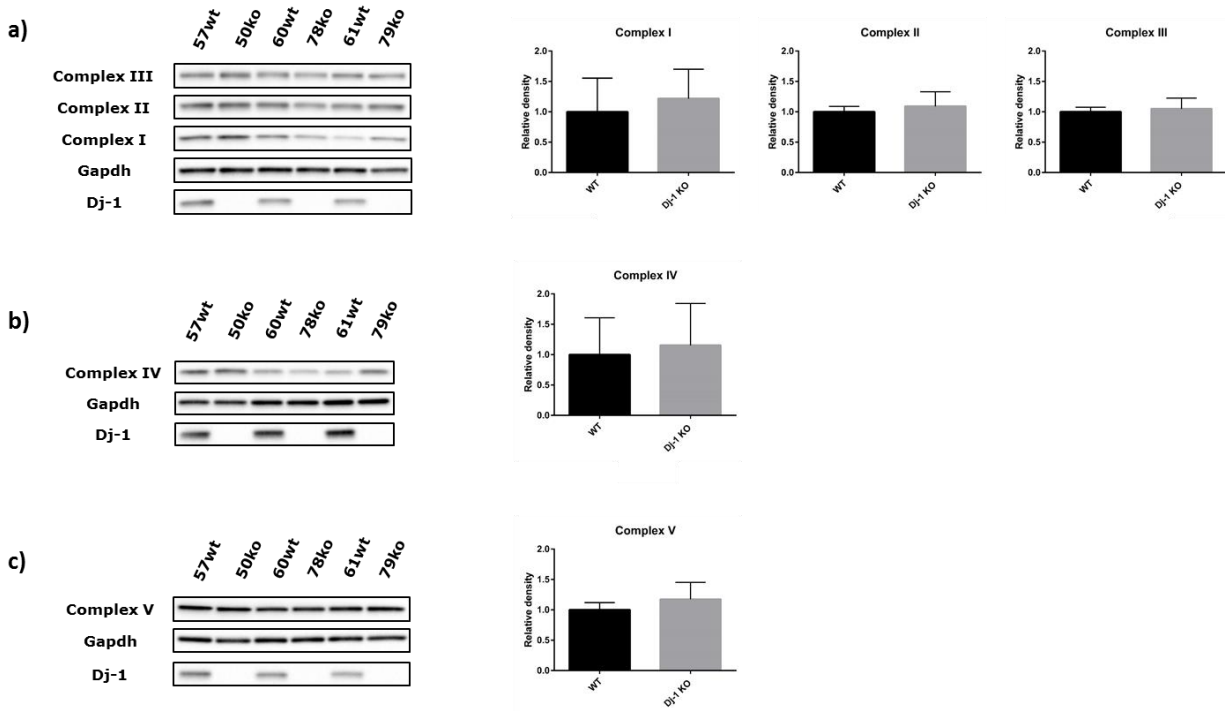


Figure 39: Western blot results represent mitochondrial complexes abundance in wildtype and Dj-1 knockout SIM A9 cells. (a) Complexes I, II, III; (b) complex IV and (c) complex V. Samples were measured with biological n=3 for both genotypes. Bars represent mean \pm sd. Statistical analysis was done using unpaired student's t-Test, * $p < 0.05$ was considered significant.

Results obtained by western blot revealed no differences in the amount of complexes between the genotypes. Therefore the differences in metabolic rates between the wildtype and Dj-1 knockout cells cannot be attributed to complexes availability and most likely also not to in- or decrease mitochondrial mass, as complex V serves as marker for such.

6 Discussion

PD is a multifactorial disease and increased neuroinflammation has been suggested to be involved in its etiology. Indeed several PD associated genes are known to influence the biology of microglia in the brain. However, the role of Dj-1 – a gene associated with early onset of PD - in this specific cell type has only been sporadically investigated (Kim et al., 2013b; Nash et al., 2017; Trudler et al., 2014), possibly due to its manifold known cellular functions such as an involvement in the oxidative stress response, mitochondrial homeostasis, and different intracellular pathways. In this thesis I added to this list an involvement of Dj-1 in metabolic regulation, mainly on the level of one-carbon metabolism, and its participation in energy metabolism processes in microglia.

6.1 A possible role of Dj-1 in central one-carbon metabolism

6.1.1 Dj-1 deficiency induces changes in MTHFR

Within this thesis I demonstrated that the expression of one of the main enzymes in the one-carbon metabolism (*Mthfr*) is decreased in microglia from Dj-1 knockout animals under basal and LPS treatment conditions (fig. 4 and 5). Moreover, the protein levels of MTHFR reflected the patterns of the respective mRNA profiles (fig. 7). Therefore, I suggest, that microglia lacking Dj-1 exhibit a general metabolic defect, since one of the major player of one-carbon metabolism is dysregulated. These data support and validate results, which were previously obtained in our laboratory (not published data, U. Hafen and T. Pham), including a slight dysregulation of *Mthfr* expression in SN of Dj-1 knockout mice after intracranial injection of LPS in that region.

Polymorphisms in *Mthfr* are found in many human disorders (Liew and Gupta, 2015). The two most common SNPs are - C677T (substitution of alanine to valine) and A1298C (substitution of glutamine to alanine). Both of these polymorphisms lead to a decrease in the enzymatic activity of MTHFR. Thus, the enzymatic activity of MTHFR with heterozygous mutation 677CT exhibits approximately 65% of wildtype enzyme activity, whereas, homozygous 677TT exhibits only around 30% of wildtype enzymatic activity (Frosst et al., 1995). Additionally it was associated with decreased expression of the enzyme itself. The A1298C SNP was also reported to result in lowered enzymatic activity (about 60% of wildtype MTHFR activity (Put et al., 1998)).

Initially human genetic studies performed on the association of these polymorphisms with PD revealed conflicting results. However, meta-analysis of these studies demonstrate a positive association, which seems to be highly dependent on ethnicity (Liu et al., 2018; Zhu et al., 2015, 2013). Specifically, evidence is provided that the *Mthfr* C677T polymorphism is associated with PD susceptibility in Caucasians but not in Asian population. Still, further studies are needed to validate these findings in larger sample sizes and excluding possible gene-environment interaction effects.

Taken together, there exists an evidence that decreased expression of *Mthfr* in combination with a lower enzymatic activity is a potential risk factor for the development of PD.

Interestingly, in Dj-1 deficient microglia *Mthfr* expression is significantly reduced – an effect which is specifically obvious when challenging the cells with LPS. Normally this challenge leads to a drastic increase in *Mthfr* expression (Pickell et al., 2005). Thus, *Mthfr* expression in microglia – specifically upon LPS treatment - is Dj-1 dependent, although, whether this is a direct effect of Dj-1 or it is a secondary effect remains to be elucidated.

It also has to be mentioned that *Mthfr* is located in the proximity to *Dj-1* (less than 3 MB) on the same chromosome. This is of importance that due to the technique used to generate this mouse line, the genetic region surrounding the mutation might still be SV129 in origin as opposed to the region surrounding the *Dj-1* wildtype locus, which is of C57Bl/6 in origin. This so called flanking genes problem, which was originally reported by Gerlai in 1996 (Gerlai, 1996) and it was well described in the manuscripts of Crusio and Sigmund (Crusio, 2004; Sigmund, 2000). Indeed the likelihood that this linkage of the mutation with SV129 genetic environment has been eliminated by cross-over events, thus breaking the co-segregation pattern of the surrounding region with the mutation, is not very high. Thus, expression difference could also arise from differences in expression levels between different mouse inbred strains. Unfortunately, the overexpression of Dj-1 in microglia to rescue the *Mthfr* expression did not reveal conclusive results in order to reject this working hypothesis (data not shown). However, currently we are working on generating an isogenic Dj-1 knockout model which – once analyzed – will give further insights into this issue. Still, the phenotypes observed in Dj-1 deficient mice concerning the central one-carbon metabolism correlate with findings in PD patients. Furthermore, decreased serine biosynthesis in independent cell line upon Dj-1 knockdown also suggested a possible involvement of Dj-1 in the regulation of one-carbon metabolic pathway (Meiser et al., 2016).

6.1.2 Dj-1 does not regulate *Mthfr* expression via general modulation of the NFkB signaling pathway

In order to get some insights in the molecular regulation of *Mthfr* expression via Dj-1 in microglia I first focused on possible modulations of the NFkB pathway, a pathway which was reported to upregulate *Mthfr* expression upon LPS stimulation (Pickell et al., 2005). Indeed, *Mthfr* expression upon LPS treatment is abolished upon inhibition of NFkB pathway as it is the expression of *iNos* (a marker of inflammatory activation) (fig. 10). However, in contrast to *Mthfr* expression the expression of *iNos* is not Dj-1 dependent. Thus, the effect of Dj-1 on the expression of *Mthfr* in primary microglia seems not to be mediated via a general modification of the NFkB pathway. This indicates, that the modulation of *Mthfr* expression via Dj-1 is either mediated additionally by another pathway and/or downstream of NFkB signaling, perhaps on the promoter level of *Mthfr*.

6.1.3 Dj-1 does not regulate *Mthfr* expression via interaction with the TF Nurr1

It is known that Dj-1 does not have a DNA-binding motif, thus the direct interaction of this protein with *Mthfr* promoter is not possible. However, Dj-1 could interact with the promoter via some adaptor proteins. This hypothesis is supported by the finding that Dj-1 is able to regulate *CCK* and *LDLR* expression via the direct interaction with adaptor proteins RREBP1 and SREBP on the promoter level of these genes (Yamaguchi et al., 2012; Yamane et al., 2013). Thus, I investigated whether transcription factors known to bind to Dj-1 might bind to the MTHFR promoter.

In silico analysis of the *Mthfr* promoter, performed by Dietrich Truembach, revealed several families of TFs, which exhibit binding sites within the *Mthfr* promoter and at the same time are known to interact or regulate molecular pathways with Dj-1 (table 4). A promising candidate was Nurr1, because of its known association with PD on several levels. It is known to play an important role in the development of DAergic neurons (Luo, 2012; Perlmann and Wallén-Mackenzie, 2004), it regulates expression of genes involved in the dopamine metabolism (TH, DDC, and VMAT2) (Hermanson et al., 2003; Iwawaki et al., 2000). Furthermore Dj-1 was found to regulate expression and activity of Nurr1 via ERK pathway (Lu et al., 2012, 2016). Most importantly, Saijo and coauthors demonstrated that Nurr1 - via the COREST complex - directly inhibits the expression of inflammatory genes in microglia cells via direct binding to NFkB (Saijo et al., 2009), and within this thesis it was shown that in primary microglia expression of *Mthfr* under LPS treatment is NFkB dependent.

Two independent approaches were used in this thesis to evaluate, whether Nurr1 is involved in the regulation of *Mthfr* expression. First I performed a luciferase assay in HEK293 cells. These experiments revealed that the major transcript of *Mthfr* is not regulated by Nurr1 (fig. 11d). However, first indications hinted towards a regulation of a specific *Mthfr* transcript (*Mthfr*-004 transcript) (fig. 11e), which, unfortunately could not be validated using mutated binding sites (fig. 12). However, this negative results might have been explained by the usage of an inappropriate cell line for this assay: HEK293 cells are human cells and they are not immune cells. Therefore, I overexpressed Nurr1 in primary microglia. Overexpression of Nurr1 in wildtype primary microglia confirmed the results of Saijo and colleagues (they demonstrated that knockdown of Nurr1 in primary microglia led to an increased expression of *iNos* under inflammatory stimulation conditions) (Saijo et al., 2009), validating the experimental approach: under LPS treatment the expression of *iNos* is significantly decreased in cells transduced with Nurr1 (fig. 13c). Unfortunately Nurr1 overexpression again has no effect on *Mthfr* expression (fig. 13b), despite the fact that *Mthfr* is also regulated by NFkB as *iNos*. These results demonstrate the complexity of organization and regulation of the inflammatory pathways within primary immune cells.

Taken together, results obtained in these experiments strongly indicate that Nurr1 (bound to Dj-1 or not) does not participate in the regulation of *Mthfr* expression, and therefore, Dj-1 executes its modulation role in *Mthfr* expression via other mechanisms, which do not involve Nurr1.

6.1.4 Dj-1 interactors in primary microglia are not readily identifiable

In order to investigate further the idea that Dj-1 can modulate expression of *Mthfr* on the promoter level via some adaptor proteins, I performed two additional experiments. The first approach – a CHIP assay – in order to prove the physical presence of Dj-1 at the *Mthfr* promoter region did not reveal conclusive results, since the negative control did not properly work (data not shown). However, further experiments are planned since the very first attempt was indicative for the physical presence of Dj-1 at the promoter region of *Mthfr* upon LPS stimulation. In a second approach I tried to identify possible Dj-1 adaptor proteins (via which it could regulate expression of *Mthfr*) by Dj-1 Co-IP experiments in primary microglia with subsequent mass spectrometry technique. However, the amount of protein possible to be harvested from primary microglia turned out to be insufficient for proper mass spectrometry analysis. Therefore, subsequently a microglial cell line with similar properties as primary microglia cells (SIM A9) was used. Even though in this case the amount of protein was sufficient, the number of Dj-1 interaction partners turns out to be very low and no transcription factor seems to interact with Dj-1 in this microglial cell line.

Taken together, even though biochemical evidence exists that Dj-1 regulates *Mthfr* expression at the transcriptional level, the presented data are due to technical limitations either inconclusive or negative (in the case of Nurr1). Still, this hypothesis is very intriguing since Dj-1 is indeed known to act as a transcriptional regulator (Yamaguchi et al., 2012; Yamane et al., 2013) and further experiments might reveal the exact molecular nature of the Dj-1 dependent *Mthfr* expression.

6.1.5 Dj-1 deficiency induces changes in homocysteine levels

MTHFR is one of the major enzyme in one-carbon metabolism which converts 5,10-methylentetrahydrofolate into 5-methyltetrahydrofolate. The last one is necessary for converting homocysteine into methionine. Therefore, MTHFR has to fulfil two major tasks in respect to cellular metabolism: 1) it supplies the system with methyl groups for further reactions of methylation and 2) it metabolizes homocysteine, which is known to be toxic when present in high concentrations (reviewed by (Boldyrev, 2009; Helane Doherty, 2013; Perła-Kaján et al., 2007)).

Interestingly, Frosst and colleagues demonstrated that carriers of 677TT polymorphism have a significantly higher homocysteine levels in plasma, confirming by this the importance of MTHFR activity in the clearance of homocysteine (Frosst et al., 1995). Also total levels of homocysteine in the CSF of AD and PD were increased (+31% for both, AD and PD as compared to age matched controls). It is worth to mention that these patients were not exposed to any treatment, and therefore, the results obtained reflect the real metabolic profile of homocysteine without any interference with drugs metabolism (Isobe et al., 2005). This is especially important, since it is known that, for example, L-Dopa treatment increases the concentration of homocysteine in the plasma and CSF of PD patients (Lamberti et al., 2005; Miller et al., 2003b), and thus data obtained

from drug treated patients cannot be used for interpretation of underlying metabolic dysfunction, in this respect.

Interestingly, results, previously obtained in our laboratory (not published data of U. Hafen) demonstrate an increased level of homocysteine in the striatum and midbrain of Dj-1 knockout mice. This data is fascinating, since it might be a direct consequence of decreased *Mthfr* expression. Possibly, the decline in *Mthfr* expression in Dj-1 knockout animals leads to inability to efficiently metabolize homocysteine, which is accumulating during the methylation processes. Unfortunately, due to technical limitations (homocysteine levels in supernatant and cellular extracts of primary microglia were below the detection level of the applied assays) it was not possible during the course of this thesis to identify the cellular source of these elevated levels. However, due to the fact that microglia are highly prominent in the SN, it is reasonable to argue, that indeed the dysregulation of MTHFR in microglia contributes to these elevated homocysteine levels. In the context of PD elevated homocysteine levels might be of special importance since besides its general toxicity effects homocysteine can be particularly involved in pathological processes within the nigrostriatal pathway. Homocysteine can act as an allosteric modulator of D2 dopamine receptors, decreasing the affinity of the D2 receptors to agonists, and therefore, interfering with the neurotransmission processes within this system (Agnati et al., 2006). It can also activate NMDA and metabotropic glutamate receptors, and thus, participate in excitotoxicity processes (Choudhury and Borah, 2015; Lazarewicz et al., 2003; Lipton et al., 1997; Poddar and Paul, 2009). Therefore, antagonists of these receptors are currently investigated in regards of antiparkinsonian therapy (reviewed by (Boldyrev, 2009; Johnson et al., 2009; Majláth and Vécsei, 2014; Olivares et al., 2012)).

Taken together, the observed increased levels of homocysteine in Dj-1 deficient mice is a second indication of dysregulated one-carbon metabolism upon Dj-1 deficiency. Furthermore, results obtained on the Dj-1 knockout mouse model mirror the data obtained in humans about the possible connection of MTHFR, homocysteine and probability of PD development.

6.1.6 Dj-1 deficiency induces changes in polyamine levels

As was already mentioned in the results part, within the common laboratory project about the characterization of metabolic profiles in several brain regions of different mouse models of PD, Dj-1 knockout animals were also analyzed. The analysis revealed increased content of several metabolites in the ventral midbrain of Dj-1 knockout animals (table 3) – putrescine, spermine, glutamine and hexose. Interestingly, these changes were observed only in the ventral midbrain and were not found in the striatum and cortex of the analyzed animals (the only exception is increased level of hexose in the striatum of Dj-1 knockout animals). The differences in metabolic profiles of the Dj-1 knockout animals specifically in the ventral midbrain region (the region predominantly affected within PD) are particularly exciting, since they could indicate disturbances in the metabolism linked to PD.

Putrescine and spermine are molecules representing the class of polyamines, characterized by containing two or more amino groups. Polyamines are known to play an important role in many physiological processes, such as transcription, translation, post-translation modifications, modulation of cellular pathways and many others (Pegg and Casero, 2011; Ramani et al., 2014). Moreover polyamines are reported to inhibit inflammatory processes (Choi and Park, 2012; Zhang et al., 2000) and decrease the level of oxidative stress (Chattopadhyay et al., 2003; Toro-Funes et al., 2013), thus, preventing damage of nucleic acids and proteins. Interestingly, in CSF of PD patients the content of polyamines is significantly increased with an exception for spermidine in comparison to age-matched controls (Paik et al., 2010). Additionally Gomes-Trolin and co-workers reported that the levels of spermidine and spermine in red blood cells are significantly higher in PD patients as compared to the control group (Gomes-Trolin et al., 2002). Although, it is not yet possible to say, whether polyamines play a harmful or protective role within the PD development, it is clear that there is a link between this disorder and increased polyamine content.

In mammals only putrescine, spermidine and spermine can be synthesized *de novo*, although, the synthetic pathway is not the only source of the polyamines in mammals. For example polyamines could be produced by the microbiome followed by an uptake via the intestinal tract. Indeed, the other polyamines, like for example agmatine (which is not produced in mammals) are supplied via the gastro-intestinal tract (Coleman et al., 2004). Another source of polyamines are dietary supplements. Some food, such as cheese, Sauerkraut, natto, corn, green pea and Mediterranean diet in general are known to have high polyamine content (Atiya Ali et al., 2011; Soda et al., 2009; Zoumas-Morse et al., 2007).

The differences in polyamines content between wildtype and Dj-1 knockout animals are highly likely caused by some changes in the *de novo* synthesis of these metabolites or changes in their influx/efflux processes in the region of ventral midbrain. This idea is supported by the following arguments: first of all, all the animals were fed with the same diet, therefore, one can exclude that the differences arise from different diets. Second, all the analyzed animals were littermates, which excludes that the differences arise from different microbiome. Although, it is still possible that Dj-1 participate in the processes of food digestion and could regulate the microbiome content, but in this case I would expect to see differences in all brain regions and not just in the ventral midbrain.

In the polyamine biosynthesis pathway ornithine plays an essential role as a precursor. It is converted to putrescine in the enzymatic reaction, which is mediated by the ornithine decarboxylase. In the next step putrescine is converted to spermidine, mediated by the spermidine synthase (SRM). In the last step spermidine is metabolized to spermine by spermine synthase (SMS). Therefore, all the three major polyamines, synthesized in mammals, are produced in a tightly regulated step wise reaction. (Madeo et al., 2018; Pegg, 2009). However, putrescine and spermine are found to be significantly increased in the ventral midbrain of Dj-1 knockout animals, the increase in spermidine levels does not pass significance after false

discovery rate analysis (FDR) (table 3). Intriguingly, metabolic analyses of CSF from PD patients, performed by Paik and colleagues, revealed even a decrease in spermidine content, whereas all the other polyamines measured in this experiment were found to be significantly increased (Paik et al., 2010). Thus, the changes in polyamine levels in the ventral midbrain of Dj-1 knockout animals are in accordance with the ones observed in the CSF of PD patients.

It is interesting to mention here, that spermidine can participate in one specific reaction, which is particularly unique for this polyamine. Thus, spermidine via two-step reaction can be covalently integrated in the eukaryotic initiation factor 5A (eIF5A) protein via interaction with a specific lysine residue of this protein. Via this reaction a non-typical amino acid hypusine (N^{ϵ} -(4-amino-2-hydroxybutyl)-lysine) is formed (Pallmann et al., 2015; Wolff and Park, 2015). Hypusine is a unique amino acid, which can be found only in the eIF5A protein. Originally, eIF-5A was associated with a translation of mRNA coding proteins enriched with prolines, although recently it was suggested that this factor has much broader effects on the processes of translation elongation and termination and therefore, it is essential for the process of cellular homeostasis (Schuller et al., 2017). Interestingly, mice which are deficient for deoxyhypusine synthase (DHS) or deoxyhypusine hydroxylase (DOHH) (two enzymes participating in the reaction of hypusine biosynthesis) are not viable, therefore, indicating the tremendously important function of spermidine in cellular homeostasis (Pallmann et al., 2015). Taken all this into account, one could hypothesize that no difference in spermidine content (when other two polyamines increased) could be explained by leakiness of spermidine into the hypusine pathway, which is necessary for stabilization of homeostasis, disturbances of which could be caused by lack of Dj-1.

Intriguingly, the process of spermidine and spermine biosynthesis could be linked with one-carbon metabolism, and therefore with MTHFR enzyme as one of its major regulator. Indeed, in the reactions of spermidine synthesis from putrescine and spermine synthesis from spermidine, decarboxylated SAM (dcSAM) serves as the donor of additional amino groups (actually the aminopropyl groups). Interestingly, dcSAM can be used specifically only in the reactions of polyamines biosynthesis, since other methyl transferases are not able to use it, therefore, availability of dcSAM can be a limiting factor in the reactions of high polyamines biosynthesis from putrescine (Pegg, 2009). dcSAM is produced in the decarboxylation reaction from SAM (Madeo et al., 2018; Pegg, 2009), which is produced from methionine within the methionine cycle (fig. 8). As it was already discussed above, MTHFR converts 5,10-methyltetrahydrofolate into 5-methyltetrahydrofolate, which is used in the reaction of homocysteine methylation into methionine. Thus, endogenous activity of this enzyme regulates the rate of methionine cycle. Decreased expression of *Mthfr* in primary microglia cells and in SN of Dj-1 knockout animals, together with observation of increased homocysteine content hints towards a possible slowdown of the methionine cycle. Therefore, in vitro assay for the estimation of SAM and SAH (two of the components of methionine cycle) was performed in primary microglia cells under basal and LPS treatment conditions, to reveal the possible disturbances within the methionine cycle. Unfortunately, the sensitivity of ELISA technique was not sufficient enough to detect these compounds in primary microglia cells (discussed in the results chapter). More sophisticated

methods (allowing to go down to femtomolar concentrations) should be applied here to further estimate the content of these metabolites in primary microglia cells.

Additionally, and in order to indirectly evaluate methylation potential, and therefore, a possible differences in SAM content, estimation of methylated DNA was performed in wildtype and Dj-1 knockout microglia under basal and LPS treatment conditions (fig. 9). This experiment revealed no differences between the genotypes, and therefore, there is no obvious dysregulation of DNA methylation processes in Dj-1 deficient microglia. Thus, the dysregulated methionine cycle, confirmed by the formation of increased homocysteine levels in Dj-1 knockouts, does not influence the general methylation processes, which is also supported by the fact that – in contrast what would be expected – polyamine content is rather increased than decreased. Several hypothesis can be put forward to explain these “contradictory” results.

First, these results could be explained by pleiotropic effects of Dj-1. Dj-1 is known to participate in many cellular processes, and therefore, the lack of it could affect independently many routes of cellular metabolism. Increased content of polyamines could be a compensatory effect caused by Dj-1 knockout and this might not be dependent on MTHFR and one-carbon metabolism, although these pathways are conjugated. In addition, it is not known, which percentage of total SAM is used for the reactions of high polyamines biosynthesis. If the proportion of SAM needed for polyamines biosynthesis is quite small, then a possible slowdown of methionine cycle should not be a limiting factor for polyamine production. In contrast, increase in polyamines content could be problematic, if the system will not find an alternative route, independent on homocysteine methylation by MTHFR product, to obtain methionine and produce SAM. The most obvious solution would be to increase the influx of exogenous methionine. In this case cells will have enough methionine for production of SAM, although, the increased SAM content theoretically could facilitate the production of homocysteine with subsequent harmful events. Therefore, the influx of methionine in this case should be tightly regulated by cellular systems, to prevent oversaturation with SAM. Interestingly, our collaborators from Luxemburg could demonstrate that in BV2 microglial cells the knockdown of Dj-1 was associated with increased content of methionine within the cells (Meiser, not published data). Thus, the idea about compensation of SAM content by intensification of exogenous methionine influx in cells lacking Dj-1 might be justifiable.

Second, the effects on MTHFR, homocysteine and increased polyamines biosynthesis could be caused by the lack of a particular Dj-1 function. Since all these metabolic pathways are interconnected, the dysregulation in one particular point could lead to a complete readjustment of interconnected cycles. In this case it can be hypothesized that the increase in polyamines biosynthesis has simply a compensatory function of decreasing homocysteine production. As it was mentioned above, downregulation of *Mthfr* expression in Dj-1 knockouts most probably directly links to an increase in homocysteine content. It is known that SAM is used in the reactions of methylation with a following production of toxic homocysteine as a side product within the methionine cycle. Therefore, reactions which use SAM with alternative chemistry mechanism,

without production of SAH and the subsequent production of homocysteine, could have a beneficial effect by lowering the otherwise increasing homocysteine levels. Indeed, within the synthesis of high polyamines, dcSAM is metabolized to 5-methylthioadenosine (MTA), which is in turn degraded by cellular 5-methylthioadenosine phosphorylases (Pegg, 2009). For that reason, increased synthesis of polyamines can have a compensatory effect on homocysteine accumulation by removing SAM from the methionine cycle.

Thus, taken together, increased polyamine content in the ventral midbrain of Dj-1 knockout animals represents the third point, besides decreased *Mthfr* expression and elevated homocysteine levels indicative for changes in the one-carbon metabolism and conjugated with it metabolic cycles. Although, it is yet not possible to distinguish whether these changes are caused by the loss of particular Dj-1 function or they reflect pleiotropic functions of Dj-1, it is clear that there is some metabolic imbalance presented in the animals and primary microglia cells from Dj-1 knockout animals. The connection between these data and meta-analysis data from PD patients is intriguing, since it could reveal a possible common dysregulation mechanisms in Dj-1 recessive form of PD and the general idiopathic PD variants. PD is known as a multifactorial disease. There are already many genes found to be linked with the development of PD, many possible risk factors are described, but it is clear that the huge variety of genes and factors are still unknown and will be discovered hopefully in the nearest future. Mutations in these genes in a combination with some factors could have a huge variety of disease initiation points, therefore, it is not so easy to nail down the molecular mechanisms underlying the development of PD. Thus, PD could be even considered as a complex of diseases which lead to common pathological hallmarks. Despite the possible complexity of the initiation stages of disease, sooner or later different pathological processes should merge in common pathway, bringing the disease on the common nosological level, which is known as PD. So far there is no data available about Dj-1 function in the regulation of one-carbon metabolism, and therefore, results obtained within this thesis could shed a light on a possible merge level between Dj-1 and idiopathic PD isoforms, which is characterized by disturbances on the level of one-carbon metabolism. However, further work is needed to distinguish the true effects of Dj-1 from the possible compensatory effects within one-carbon cycle and conjugated pathways, to be able to design causative and not symptomatic treatment.

6.2 Cell type specificity of Dj-1 function

As discussed above, the amount of protein obtained from primary microglia was not sufficient for mass spectrometry. Thus, a switch to an immortalized microglial cell line was necessary. The SIM A9 (Nagamoto-Combs et al., 2014) line was chosen based on the following arguments. This cell line exhibits a molecular profile highly reminiscent to primary microglia cells, including surface markers (CD68, Iba-1), M1 polarization stage markers (iNOS, Cox2), M2 polarization stage marker Arg1, and some other features. Moreover, the isolation protocol for primary microglia

cultures from which the spontaneously immortalized cells were derived is very similar to the one used in this thesis.

The validation of this cell line in our laboratory revealed indeed that SIM A9 cells are able to initiate M1 polarization, which was confirmed by the increased expression of *iNos*, *Il-1 β* , and *Tnf- α* (fig. 14). In addition, the expression level of *Mthfr* was found to be significantly increased under LPS treatment (fig. 14d), which goes in line with results observed in primary microglia cells (fig. 5). Although, the upregulation of *Mthfr* in SIM A9 cells was not as pronounced as in primary microglia, it was impressive, since BV2 cells (another microglial cell line) were not capable to do it (unpublished data).

The next logical step was to compare the properties of SIM A9 cell line with primary microglia cells in regards of Dj-1 function. Therefore, Dj-1 deficient SIM A9 cells using the Crispr/Cas9 technology were generated (fig. 19) and major intracellular signaling pathways known to be triggered by LPS stimulation, such as the NFkB, ERK and P38 pathways, were analyzed. Interestingly and in respect to these pathways unpublished data of U. Hafen hints towards a cell type specificity of Dj-1 function. Whereas in primary microglia cells Dj-1 deficiency does not affect the signal transduction of the NFkB, ERK and P38 pathways after LPS treatment, the activation of the NFkB and P38 pathways is severely impaired in Dj-1 deficient MEFs. By comparing the LPS induced activation of these pathways in the Dj-1 deficient SIM A9 cells with the unpublished results of U. Hafen I could answer two important questions. First, whether SIM A9 Dj-1 knockout cells behave similarly as Dj-1 deficient primary microglia upon LPS stimulation. Second, whether the difference between MEFs and primary microglia is brought about by the immortalization or whether it is rather a reflection of cell type specificity. SIM A9 cells could theoretically help to find the answer on this question, since from one side this cell line has a microglial origin, and from the other side it is an immortalized cell line.

Three independent western blot experiments revealed that there is no differences in NFkB pathway activation between the genotypes in SIM A9 cells (fig. 20). Levels of pIKB gradually increase during the time of LPS treatment in both genotypes. These results show that Dj-1 is not involved in the regulation of NFkB pathway (at least from the TLR4 receptors to IKB point of the pathway) in SIM A9 cell line, which is in line with results obtained from primary microglia cells and does not reproduce the results obtained in immortalized MEFs (U. Hafen, unpublished results). Thus, it can be concluded that SIM A9 cell line in regards of Dj-1 function within NFkB pathway behaves similar to primary microglia cells, but different from immortalized MEFs. Interestingly, McNally and coworkers report that Dj-1 knockout primary MEFs have a significant lower protein content of Intercellular Adhesion Molecule 1 (ICAM-1) after TNF- α stimulation in comparison with wildtype cells (McNally et al., 2011). They conclude that this effect is a consequence of a decreased activity of the NFkB pathway, caused by the lack of Dj-1's modulatory function. Although, the MEFs in their study were not immortalized and they used TNF- α as an inflammatory trigger, it can be hypothesized that the origin of the cells could be the most important factor determining the function of Dj-1 in regard of NFkB pathway modulation.

Concerning the activation of the ERK pathway, no differences were found between wildtype and Dj-1 knockout SIM A9 cells under LPS treatment within the given timeframe (fig. 21). These results were expected, since there are no difference in this pathway reported neither in primary microglia nor in immortalized MEFs. Thus, Dj-1 does not play a role in ERK pathway activation initiated by LPS treatment in all tested cell types. Interestingly, there are some reports about involvement of Dj-1 in activation of ERK pathway. Lu and colleagues published that overexpression of Dj-1 in MN9D cell line significantly increases the level of pERK (Lu et al., 2012). Zhang and coauthors demonstrated that knockdown of Dj-1 in T47-D and MCF-7 responsible for the lower activation of ERK signaling under neuregulin 1 (NRG-1) mediated HER3 (human epidermal growth factor receptor 3) activation (Zhang et al., 2016). Thus, the effect of Dj-1 on the regulation of the ERK pathway could be cell type specific and exists only in particular cell types (MN9D is a murine dopaminergic cell line and T47-D and MCF-7 are human cell lines derived from different types of mammary gland tumors) or this effect is highly dependent on the type of activation. Apparently, under activation with LPS in primary microglia, SIM A9 and immortalized MEFs Dj-1 does not modulate the activity of ERK pathway.

Concerning the activation of the P38 pathway in SIM A9 cells no differences between the genotypes were found after LPS stimulation (fig. 22). These data reflect the results obtained in primary microglia cells and are different from those which observed in immortalized MEFs, in which Dj-1 deficiency leads to inability to properly activate P38 pathway. Interestingly, there are many reports which demonstrate an existence of the modulatory function of Dj-1 on p38 pathway activity (Junn et al., 2005; Mo et al., 2010; Tang et al., 2014; Waak et al., 2009), however, as it was already mentioned, Dj-1 function is likely cell type specific, and thus, effects of Dj-1 observed in one cell type cannot be readily extrapolated to another cell types.

It is worth to mention, that pathways activity validation in SIM A9 cells performed within this thesis was reproduced with independent Dj-1 knockout SIM A9 clones within the bachelor work of Irina Petcu, which excludes the possibility that clonal effect influence the observed results.

Taken together, results obtained with wildtype and Dj-1 knockout SIM A9 cells with respect to intracellular pathway activation after LPS treatment lead to the following conclusions. First, SIM A9 cells with respect to Dj-1 function concerning the activation of the NFkB, ERK and P38 pathways upon LPS treatment behave in a similar manner as primary microglia cells. Second, Dj-1 functions in a highly cell type specific manner concerning its involvement in modulation of these three major intracellular signaling pathways. This specific actions is most probably predetermined by the origin of the cells and not by the immortalization effect, since immortalized SIM A9 cell line behaves similar with primary microglia cells and different from immortalized MEFs, where Dj-1 plays an important role in the regulation of NFkB and P38 pathways upon LPS treatment.

6.3 Mass spectrometry

The biochemical characterization of the SIM A9 cell line and its similarity to primary microglia cells (also upon Dj-1 deficiency) described above suggested them to be used in the mass spectrometry analysis in order to overcome the insufficient amount of protein obtained from primary microglia cultures. Thus mass spectrometry was performed in untreated and LPS treated SIM A9 cells and the results compared to Dj-1 deficient SIM A9 cells as controls. Indeed using this cell line potential interaction partners of Dj-1 in microglial cells could be identified: Slc25a3, Atp1a3 and Plscr4. These proteins were particularly enriched under basal conditions, moreover Slc25a3 was also significantly enriched after LPS treatment. Slc25a3 represents a mitochondrial protein, which serves as an inorganic phosphate carrier transporting inorganic phosphate moieties inside the mitochondria, therefore this protein plays an important role in the process of energy metabolism by providing the equivalents for ATP synthesis inside the mitochondria (Seifert et al., 2015). In humans, mutations in this gene in some cases are lethal, carriers of these mutations are characterized by cardiomyopathy symptomatic and have an increased lactate levels (Mayr et al., 2007, 2011). Thus, Slc25a3 has an important function in the process of oxidative phosphorylation. Its possible interaction with Dj-1, which was reported to play an important role in mitochondrial homeostasis (see 3.2.3.2), could be of high relevance for the bioenergetics status of the cells.

Atp1a3 is a subunit of Na/K ATPase, which is involved in the regulation of many physiological processes (Clausen et al., 2017). This protein is responsible for huge energy expenditure, especially in neuronal cells (Howarth et al., 2012). Intriguingly, mutations in Atp1a3 were found to be associated with rapid-onset dystonia parkinsonism (RDP) (Anselm et al., 2009; Brashear et al., 1993; de Carvalho Aguiar et al., 2004), therefore the potential interaction of this protein with Dj-1 could be relevant in respect to investigating molecular mechanisms underlying PD etiology.

Plscr4 is the least known protein amongst the Dj-1 interactor candidates. This protein is a member of protein scramblases family, which are involved in translocation of phospholipids between the lipid layers within the membranes (Sahu et al., 2007). It is also known that Plscr4 is localized in the plasma membrane, and that it might interact with CD4+ receptors of T lymphocytes (Py et al., 2009). Furthermore, calcium is needed to support its activity (Francis and Gummadi, 2012). Investigation of the possible interaction between Dj-1 and Plscr4 could shed more light on the functions of these proteins.

After MS experiments the procedure of validation of Dj-1 interactions with identified candidates was performed by western blot (Co-IPs). Unfortunately, these experiments were not conclusive because of the several technical issues. First of all the antibodies against the candidate proteins did not perform well (fig. 26 and 27). In case of Slc25a3 and Atp1a3 two different antibodies were tested, each of them revealing high unspecific bindings after Co-IP. Second, the expression levels of these proteins are quite low in SIM A9 cells, in some cases the detection limit by western

blotting was exceeded, which however, could again be due to the poor quality of the commercially available antibodies. Therefore, better and more specific antibodies are needed to efficiently validate the Dj-1 interaction with identified by MS candidates unambiguously.

Interestingly, after MS experiments there were several proteins found which exhibit an enrichment coefficient lower than one, being even statistically significant. In general, within the MS data analysis, proteins with an enrichment coefficient lower than one are not further considered. However, in our experiment Dj-1 knockout and not a scrambled antibody served as a negative control. Thus, these data could represent an additional layer of useful information. The proteins with enrichment coefficient lower than one indicate the enrichment of particular protein in Dj-1 knockout cells. Such an enrichment is only possible by a pull down due to an unspecific interaction with beads. Since amount of these proteins is higher in knockouts' pull down it could mean that in general the levels of these "unspecific" proteins are higher in knockout cells. To test this idea three proteins (*Hadha*, *Cat* and *Srm*) with enrichment coefficient lower than one (table 7) were chosen and their expression validated by qPCR and Western blot in SIM A9 wildtype and Dj-1 knockout cells.

Data obtained from qPCR revealed that the expression level of *Cat* is significantly increased in Dj-1 knockout SIM A9 cells (fig. 28a), however, there was no difference in expression levels of *Hadha* and *Srm* between the genotypes. Western blot results confirmed this finding, however, not fully reaching statistical significance (fig. 29a). These experiments were repeated with three independent wildtype and Dj-1 knockout clones (fig. 28b and 29b), however the differences in catalase observed in the experiments with the original clone were not so prominent here. This could be explained by interclonal differences. It is not surprising that only the catalase level was found to be significantly increased from chosen proteins, since the enrichment coefficient was the lowest in the case of *Cat* (0.2) in comparison with *Hadha* (0.6) and *Srm* (0.7); and lower the coefficient – higher the differences of the protein content.

Thus, a new concept of MS data usage was confirmed within this thesis. MS experiments in which the negative control is represented by knockouts exhibit an additional layer of data. An enrichment coefficient lower than one could indicate that in the knockout the respective proteins are overrepresented. Using this data analysis, it was found that Dj-1 knockout SIM A9 cells have a higher content of catalase. This finding could be explained by the compensatory effects in Dj-1 knockout cells, which try to counteract against possible increased free radical background caused by the lack of antioxidant Dj-1 function (see 3.2.3.1).

To test, whether the new MS data concept could be applied in the opposite direction, in proteins with enrichment coefficient higher than one, protein contents of the three possible Dj-1 interactors (*Slc25a3*, *Atp1a3* and *Plscr4*) were checked by western blot (fig. 30). According the results obtained by western blot, the level of *Plscr4* was found to be lower in the Dj-1 knockout cells which goes in line with the concept, although, that was not the case for *Slc24a3* and *Atp1a3*. Additional experiments with three newly generated SIM A9 wildtype and DJ-1 knockout clones did not reveal any differences in the content of this proteins.

Taken together, MS and the follow up experiments in wildtype and Dj-1 knockout SIM A9 cells revealed several important findings. Although, it was not possible due to technical issues to conclusively validate the interaction partners of Dj-1, it is still highly likely that these proteins interact with DJ-1, and that high quality antibodies against these possible interactors will help to resolve this issue. In addition, a new concept of MS data usage was postulated and successfully tested within this thesis, which unravel the existence of increased expression and protein content of antioxidant enzyme catalase in Dj-1 knockout SIM A9 microglial cell line.

6.4 Energy metabolism in Dj-1 deficient SIM A9 cells is affected

As was already discussed above, during the MS experiments several potential Dj-1 interaction partners were identified. Interestingly, two out of three candidates (Slc25a3 and Atp1a3) have functions particularly attributed to energy metabolism. Taking into account the possible interaction of Dj-1 with these proteins, which play an important role in energy metabolism processes, it was decided to perform energy metabolism analysis in SIM A9 wildtype and Dj-1 knockout cells. As it was described above, energy metabolism analysis was performed on a Seahorse XF platform, which allowed us to estimate the rates of OCR and ECAR under different conditions.

6.4.1 Under non-treatment conditions Dj-1 deficient cells highly likely exhibit higher cellular ATP-demand

Dj-1 deficient SIM A9 cells have in general higher oxygen consumption rates (OCR) already under basal conditions with glucose supplement as an energy substrate (fig. 32b). OCR attributed to the ATP production is also increased in Dj-1 deficient cells (fig. 32e). Differences in ATP-linked oxygen consumption could be caused by several factors (Divakaruni et al., 2014). First, an increase in cellular ATP demand could be responsible for this effect, therefore, it might be that under non-treatment conditions (non-LPS treatment condition) Dj-1 have a higher rate of mitochondrial ATP synthesis to fulfil their energy needs. Interestingly, Dj-1 potentially interacts with Atp1a3, a subunit of Na/K ATPase, which is known to use a huge amount of energy moieties within the cells. Therefore, a theoretical increase in energy demand in Dj-1 knockout cells could be caused by the lack of modulation function of Dj-1 on Na/K ATPase.

Second, changes in ATP synthesis processes could be responsible for differences in ATP-linked respiration. The efficiency of ATP machinery to transform the membrane potential into new energy moieties in general depends on three factors: activity of ATP synthase, activity of ADP translocase and activity of inorganic phosphate carriers (Divakaruni et al., 2014). Interestingly, inorganic phosphate carrier Slc25a3, as mentioned above, was identified within this thesis as a possible Dj-1 interaction partner. Thus, it might be that Dj-1 negatively regulates the activity of

this transporters, and therefore, in Dj-1 deficient cells the mitochondrial ATP synthesis is facilitated by higher abundance of inorganic phosphates inside the mitochondria.

Last but not least, differences in ATP-linked oxygen consumption could be caused by differential substrate availability and the rate of substrate transformation processes. Thus, changes in one or several cellular processes, such as transport of substrates through the plasma and mitochondrial membranes, the rate of glycolysis and Tricarboxylic acid (TCA) cycle, and efficiency of the oxidative phosphorylation processes could be responsible for the differences in OCR attributed to ATP production. To be able to exclude that metabolic glucose dependent processes upstream of the generation of pyruvate are causing the difference between the genotypes, seahorse experiments were executed with pyruvate as an energy substrate instead of glucose. Results of this experiments basically mirror the results obtained with glucose (fig. 37). Oxygen consumption linked with ATP production with pyruvate is also increased in Dj-1 deficient cells. This finding suggests, that increased ATP-linked oxygen consumption is independent of glycolysis rate and substrate transport processes upstream of pyruvate generation.

Maximal respiratory capacity was also found to be significantly higher in Dj-1 knockout cells under non-treatment condition with glucose and pyruvate as an energy supplement (fig. 32c and 37d). The differences in this parameter could be attributed to substrate availability or to the efficiency of the electron transport chain (ETC). The measured maximal respiratory capacity is highly dependent on the amount of the mitochondria, and thus, the abundance of the respiratory complexes within the cells. Therefore, western blot experiments were performed to determine mitochondrial complexes. Results of these experiments did not reveal any differences between the genotypes (fig. 39), and thus, it is also highly unlikely, that there is a differences in mitochondrial amount between the genotypes. However, it has to be kept in mind that Dj-1 deficiency might not affect the abundance of mitochondrial complexes, but rather their activity as it has been shown for Pink1 (Morais et al., 2014) – another PD associated gene.

Proton leak like basal respiration, ATP-linked respiration and maximal respiratory capacity was found to be increased in Dj-1 knockouts with glucose and with pyruvate as energy substrates (fig. 32d and 37e). This parameter is highly dependent on the membrane potential and in case of upregulation of maximal respiratory capacity (our case), differences in proton leak could not reflect the differences in membrane conductivity for protons, but simply exist because of the differences in membrane potential (Divakaruni et al., 2014). Although, it is worth to mention that Dj-1 is known to be an important player in the regulation of protonmotive forces through the inner mitochondrial membrane. Thus, Wu and colleagues could demonstrate that in brown adipose tissue Dj-1 via its interaction with PTEN and mind bomb-2 (Mib2) leads to a decrease in expression of Uncoupling protein-1 (UCP-1) via Akt-pathway. They also showed that Dj-1 knockout mice have significantly lower fat mass associated with increased energy expenditure caused by the upregulation of UCP-1 expression in brown adipose tissue, the opposite results were demonstrated with Dj-1 transgene animals (Wu et al., 2017). Hence, we cannot exclude

that increased proton leak in Dj-1 knockout SIM A9 cells could be associated with the regulatory function of Dj-1 on UCP proteins.

As was discussed above, differences in OCR between the genotypes exclude the influence of glycolysis on this observations, since the OCR obtained with pyruvate mirroring the results obtained with glucose as an energy source. Indeed, there was no significant difference found in the basal rate of glycolysis between the genotypes, only a trend towards increase in this parameter in wildtype cells (fig. 33b). Interestingly, maximal rate of glycolysis was found to be significantly increased in Dj-1 knockout cells, as well as glycolytic capacity as a function of basal and maximal rates (fig. 33c and d). However, one should keep in mind that what is called “maximal rate of glycolysis” may not necessary reflect this definition. Very often what is measured as a maximal rate of glycolysis is attributed to the energy demand of the system. In systems where energy demand is higher than the level of physical abilities of the system to upregulate the glycolysis, the “maximal glycolytic capacity” will be true, otherwise this parameter will only reflect the upregulation of glycolysis, which is enough to fulfil the energy demand of the cells. Thus, an increased maximal rate of glycolysis in Dj-1 deficient cells can possibly reflect their higher energy demand, which supports the results obtained via OCR measurements. An innovative approach was used by Mookerjee and coauthors to estimate the true maximal rate of glycolysis. The authors used monensin to increase the import of Na^+ inside the cells, by this they passively upregulated the activity of Na/K ATPase as a compensatory mechanism to support ions homeostasis, and therefore, they increased the energy expenditure. By this they could upregulate the glycolysis much higher in comparison with oligomycin treatment (Mookerjee et al., 2016). However, the usage of monensin could be a problematic issue in our model, since in this case energy expenditure will depend on the activity of Na/K ATPase, and within this thesis ATP1a3, as a subunit of Na/K ATPase, was identified as a possible Dj-1 interaction partner. Hence, we cannot exclude the regulatory function of Dj-1 on Na/K ATPase, and so, the one cannot be sure that the artificial energy expenditure caused by monensin will be not changed between the genotypes, and therefore it will be still not possible to reveal whether the differences in maximal rate of glycolysis caused by difference in energy demand or by different capacities of wildtype and knockouts to maximally upregulate glycolysis.

Taken this idea into account, increase in maximal rate of glycolysis and glycolytic capacity in Dj-1 knockout cells could be attributed to either an increase in energy demand or/and to higher capacity of Dj-1 deficient cells to upregulate glycolysis in response to ATP synthase inhibition.

To sum up the results of Seahorse experiments obtained for untreated SIM A9 cells, the following conclusions can be made. Dj-1 knockout cells in general have an increased rate of oxidative phosphorylation processes in comparison with wildtype cells. This observation is independent of the glycolysis processes, since the results obtained with pyruvate as substrate reproduced the effect found under glucose supplementation. Moreover, content of mitochondrial complexes and most probably mitochondria amount are not responsible for these differences. OCR data together with increased maximal rate of glycolysis and glycolytic capacity observed in Dj-1

knockout cells, suggest that an increased ATP demand exists in cells lacking Dj-1. Thus, potentially, under non-treatment conditions the higher ATP demand, and therefore, the higher rate of ATP turnover in Dj-1 knockout cells force the system to use energy substrates more efficiently, and thus, Dj-1 knockouts have an increased level of oxidative phosphorylation. Although, there are still many other processes which could be responsible for the observed effects (as was discussed earlier), higher energy demand in Dj-1 knockout cells seems to be the most straightforward explanation for the observed effects.

6.4.2 Under LPS-treatment conditions Dj-1 deficient cells have problems with performance of metabolic switch

Under LPS treatment and with glucose as an energy substrate the differences in OCR observed between the genotypes disappear (fig. 34). This effect is mainly caused by a generalized significant decrease of OCR in Dj-1 knockout cells and an increase of OCR in wildtype cells (fig. 36a-d). Interestingly, the basal rate of glycolysis and the maximal rate of glycolysis are found to be higher in wildtype cells (fig. 35), which is caused by significant intensification of glycolytic processes under LPS treatment in wildtype cells, but not in the Dj-1 deficient cells (fig. 36e and f). However, there were no differences found in lactate content between the genotypes (fig. 38). It is worth to mention, that the medium for the lactate analysis was immediately taken after the Seahorse experiment was performed and it was suggested (Divakaruni et al., 2014) that lactate measurements might be influenced by the chemicals used in the Seahorse experiment. Therefore, to be able to determine the true content of lactate in SIM A9 wildtype and Dj-1 knockout cells under different conditions, lactate measurements should be performed independent of Seahorse experiment.

During the polarization towards M1 stage (LPS treatment) BV2 microglial cell line and primary microglia cells were shown to perform a so called metabolic switch (Orihuela et al., 2016; Voloboueva et al., 2013): they intensify the rate of glycolysis and downregulate the oxidative phosphorylation processes. Interestingly, Orihuela and co-workers demonstrated that the upregulation of glycolytic processes happens within one hour after LPS application, while the shutdown of oxidative phosphorylation is only observable after 24 hrs. However, it is worth to mention that OCR was measured only within first 1.5 hours and then only after 24 hours, hence the downregulation of oxidative phosphorylation under LPS treatment takes place between 1.5 and 24 hours (Orihuela et al., 2016).

Wildtype SIM A9 cells, as described in this thesis, recapitulate this metabolic switch upon LPS treatment. However, Dj-1 knockout cells do not. First of all, Dj-1 deficient cells were not able to intensify glycolytic processes in response to LPS treatment (fig. 36e and f). And second, these cells significantly downregulate the oxidative phosphorylation processes already within the first hour (fig. 36a-d). This observation is very exciting, since to my knowledge, this is the first time

that Dj-1 was shown to be associated with the processes of metabolic switch during M1 polarization of microglial cells.

Interestingly, Orihuela and colleagues demonstrated that decrease in oxidative phosphorylation in microglial cells during the metabolic switch is highly dependent on NO, since inhibition of NO-synthase partially prevented the decrease in oxidative phosphorylation processes. Within this thesis it was shown that under LPS treatment SIM A9 Dj-1 knockout cells have significantly lower expression of *iNos* (fig. 23). It could be a compensatory effect, caused by an increased production of NO in knockout cells in response to LPS, and if it is true, rapid decrease of oxidative phosphorylation could be partially dependent on the differences in NO content between the genotypes. Therefore, the experiments for NO content validation in SIM A9 wildtype and Dj-1 knockout cells could shed more light on the mechanisms of rapid drop of oxidative phosphorylation in Dj-1 deficient cells under LPS treatment conditions. Another interesting observation was presented by Voloboueva and colleagues, where they showed that the metabolic switch in BV2 cells is highly dependent on mortalin, since mortalin overexpression attenuated glycolysis upregulation and oxidative phosphorylation downregulation upon LPS treatment (Voloboueva et al., 2013). Intriguingly, Dj-1 is known to interact with mortalin (Li et al., 2005), and therefore, there is a possibility that these proteins represent the players of a common pathway, responsible for the metabolic switch in microglial cells.

In addition, it should be noted, that intensification of the glycolysis, registered with Seahorse, reflects only an increase in glycolytic ATP production, since acidification of the medium during seahorse experiment is generally attributed to hydrolysis of ATP molecules (Divakaruni et al., 2014). Hence, the status of non-energy metabolism, conjugated with glycolytic processes, is still unknown. It is highly likely that the differences observed in glycolysis rate between the genotype under metabolic switch are at least partially influenced by non-energy metabolism. Thus, possible differences in the usage of glycolysis intermediates between the genotypes theoretically would affect the ECAR values obtained by seahorse platforms. Within this thesis it was demonstrated that Dj-1 regulates the expression of *Mthfr*, and thus Dj-1 could play an important role in the regulation of one-carbon metabolism. Methyl moieties within one-carbon metabolism are provided by serine, which partially can be synthesized from 3-phosphoglycerate (glycolytic intermediate metabolite), and therefore, differences in 3-phosphoglycerate transformation to serine between the genotypes (Meiser et al., 2016) could exist and influence the ECAR results of seahorse. The rate of MG formation from glyceraldehyde-3-phosphate could also be different between the genotypes, since Dj-1 is known to be involved in MG metabolism by implementing its glyoxalase (Lee et al., 2012) and deglycase (Richarme et al., 2015) activities. During the activation of microglial cells towards M1 pro-inflammatory stage in parallel with intensification of glycolysis, activation of pentose phosphate pathway (PPP) was found to be upregulated in BV2 microglial cells (Gimeno-Bayón et al., 2014). PPP is an important source of NADPH, which is used for recovery of glutathione system, and therefore promotes resistance against oxidative stress. Dj-1 is known to play an important role in the processes of free radical elimination, and thus, theoretically the rate of PPP in wildtype and Dj-1 knockout cells could also be different.

Interestingly, NO was reported to play a crucial role in the regulation of PPP, which again rise the question about importance of NO content estimation in SIMA A9 wildtype and Dj-1 deficient cells (Bolaños et al., 2008; Gimeno-Bayón et al., 2014). Taking in consideration the involvement of Dj-1 in many metabolic processes, it would be desirable to perform the metabolic flux analysis in SIM A9 wildtype and Dj-1 knockout cells to be able to estimate the rates of mentioned above processes and their influence on ECAR values under LPS treatment conditions.

Taking all together, seahorse analysis of SIM A9 wildtype and Dj-1 knockout cells under basal and LPS treatment conditions revealed several important findings. 1) Under basal conditions Dj-1 knockouts have a higher oxidative phosphorylation rate than the wildtypes, which is not due to changes in glycolysis or amount of mitochondrial complexes. It is highly likely that the observed effect is caused by a higher energy demand in Dj-1 knockout cells. 2) Under LPS treatment Dj-1 deficient cells are not able to perform the metabolic switch observed in wildtype cells. First of all, knockouts are not able to upregulate the rate of glycolysis. And second, cells which lack Dj-1 almost immediately decrease the level of oxidative phosphorylation in response to LPS. To my knowledge, this is the first time when Dj-1 was shown to play an important role in energy metabolism processes in microglial cells and in the regulation of their metabolic switch during activation.

7 Conclusions and future perspectives

Within this thesis a crucial role of Dj-1 in the regulation of the one-carbon metabolism and associated with it metabolic cycles was demonstrated *in vivo* and *in vitro*. Dj-1 knockout in primary microglia was found to result in the inability to upregulate expression of *Mthfr*, one of the main enzymes of the one-carbon metabolism, during the polarization of microglial cells towards the M1 pro-inflammatory stage. Furthermore, it was shown that upregulation of *Mthfr* is highly dependent on the activation of the NFkB signaling pathway, however, general NFkB pathway analysis did not reveal any significant differences between genotypes. This gave rise to the idea about a modulatory role of Dj-1 on *Mthfr* downstream of NFkB or in a parallel co-activation pathway. In addition, it was shown that the general NFkB pathway inhibitory feedback loop, in which Nurr1 plays an important role, does not apply for the regulation of *Mthfr* expression.

Intriguingly, metabolic analysis of Dj-1 knockout mice revealed increased content of polyamines particularly in the ventral midbrain. This observation demonstrates the dysregulation of the polyamine metabolic pathway which is highly conjugated with one-carbon metabolism and together with a dysregulated methionine cycle (increased homocysteine levels in substantia nigra of Dj-1 knockout animals) clearly points towards a general metabolic disturbance within the one-carbon metabolism and conjugated pathways in Dj-1 knockout mice. Data obtained within this thesis strongly correlate with meta-analyses data from idiopathic Parkinson's disease patients. This could indicate a possible similarity in the pathoetiological roots between recessive and idiopathic forms of PD. However, it still remains unknown what are the exact molecular mechanisms and where the trigger point(s) of these dysregulations lie. Therefore, further research is necessary to unravel the particular molecular mechanisms responsible for the dysregulation of the one-carbon pathway and conjugated with it cycles in Dj-1 knockout models.

In addition to the discovery of Dj-1 function in the regulation of metabolic processes, it was also demonstrated that Dj-1 appears to be an important player in the processes of cellular energy metabolism. It was shown that Dj-1 knockout microglial SIM A9 cells under basal conditions mainly rely on oxidative phosphorylation, which most probably is caused by a higher energy demand of the knockout cells. Moreover, during the polarization of the microglia towards the M1 pro-inflammatory stage, Dj-1 knockout cells were not able to perform the necessary metabolic switch which is an important property of microglia during activation caused by inflammatory stimuli. To my knowledge, this is the first time that Dj-1 was found to be involved in the regulation of the process of the metabolic switch in microglia.

Taken together, results obtained within this thesis demonstrate an important role of Dj-1 in the regulation of the one-carbon pathway and associated metabolic cycles, as well as a crucial role of Dj-1 in the modulation of the cellular energy metabolism in microglia. This data opens new doors towards a deeper understanding of the role of Dj-1 in pathoetiology of Parkinson's disease

and discloses new possibilities and chances for further in-depth investigations of the molecular mechanisms underlying Dj-1 function and neuroinflammation in Parkinson's disease.

8 Materials and methods

8.1 Materials

8.1.1 Equipment

Instrument	Supplier
ABI Prism 7900 HT Real-Time PCR System	Applied Biosystems, USA
AxioCam HRc camera	Zeiss, Germany
Axioplan 2 microscope	Zeiss, Germany
Biological safety cabinet, Golden Line	Kojair, Finland
Centrifuge 4K15	Sigma-Aldrich, Germany
Centrifuge 5424 and 5424R	Eppendorf, Germany
Centrifuge 5702 (cell culture)	Eppendorf, Germany
Centro LB 960 luminometer	Berthold Technologies, Germany
ChemiDoc MP imaging system	BioRad, Germany
Criterion™ Blotter	BioRad, Germany
Criterion™ Vertical Electrophoresis Cell	BioRad, Germany
Gel-Documentation system E.A.S.Y Win32	Herolab, Germany
Milli-Q® Integral Water Purification System	Merck Millipore, Germany
NanoDrop® Spectrophotometer ND-1000	Peqlab, Germany
Orbital shaker	Starlab, UK
PCR Gelelectrophoresis chambers	Peqlab, Germany
Roller mixer SRT6D	Stuart, UK
Seahorse XFe96 analyser	Agilent Technologies, USA
SpectraMax M5 Microplate Reader	Molecular Devices, Germany
Thermo cycler Mastercycler pro	Eppendorf, Germany
Thermomixer comfort	Eppendorf, Germany

Transilluminator	Herolab, Germany
Ultrasonic bath RK100	Bandelin Sonorex, Germany
T 25 basic ULTRA-TURRAX	IKA, USA

Table 8: Equipment

8.1.2 Chemicals

Chemical	Catalogue N	Supplier
2-deoxy-D-Glucose, Grade II	D8375	Sigma-Aldrich, Germany
2-Mercaptoethanol	M7522	Sigma-Aldrich, Germany
Agarose	870055	Biozym, Germany
Ampicilline	11593-027	Thermo Fisher Scientific, Germany
Antimycin A from Streptomyces sp.	A8674	Sigma-Aldrich, Germany
Bottled Water for Molecular Biology H20MB1001		Merck Millipore, Germany
Bovine serum albumin	A3059	Sigma-Aldrich, Germany
Carbonyl cyanide 4-(trifluoro-methoxy)phenylhydrazone	C2920	Sigma-Aldrich, Germany
CHAPS hydrate	C3023	Sigma-Aldrich, Germany
Chloroform	1.02445.2500	Merck KGaA, Germany
Digitonin	D141	Sigma-Aldrich, Germany
Dithiothreitol (DTT)	10197777001	Sigma-Aldrich, Germany
Ethanol	1.00983.2500	Merck Millipore, Germany
Ethidiumbromide	2218.2	Carl Roth GmbH, Germany
Ethylenediaminetetraacetic acid (EDTA)	E5134	Sigma-Aldrich, Germany
Formalin, 10%	F5554	Sigma-Aldrich, Germany

Glucose Solution	A2494001	Thermo Fisher Scientific, Germany
Isopropanol	109634	Merck KGaA, Germany
Lithium chloride	L4408	Sigma-Aldrich, Germany
Methanol	1.06009.2500	Merck Millipore, Germany
Milk powder	170-6404	Biorad, Germany
Nonidet® P-40 Substitute	786-511	G-Biosciences, USA
Oligomycin A	75351	Sigma-Aldrich, Germany
Rotenone	R8875	Sigma-Aldrich, Germany
Sodium Chloride	106404	Merck KGaA, Germany
Sodium deoxycholate (SDC)	D6750	Sigma-Aldrich, Germany
Sodium dodecyl sulfate (SDS)	L3771	Sigma-Aldrich, Germany
Sodium pyruvate solution	11360070	Thermo Fisher Scientific, Germany
Triton X 100	T9284	Sigma-Aldrich, Germany
Trizma cell culture grade	T2319	Sigma-Aldrich, Germany
TRIzol™ Reagent	15596018	Thermo Fisher Scientific, Germany
Tween 20	P1379	Sigma-Aldrich, Germany

Table 9: Chemicals

8.1.3 General consumables

Consumable	Catalogue N	Supplier
Immobilon-P PVDF Membrane	IPVH00010	Merck Millipore, Germany
10x Tris/Glycine transfer buffer	1610771	BioRad, Germany
4–12% Criterion™ XT Bis-Tris Protein Gel, 18 well, 30 µl	3450124	BioRad, Germany
Adhesive Seal Sheets	AB-1170	Thermo Fisher Scientific, Germany
AquaPolyMount	18606	Polysciences, USA
Clarity Western ECL Substrate	1705061	BioRad, Germany
cOmplete™, Mini Protease Inhibitor Cocktail	4693124001	Sigma-Aldrich, Germany
Framestar 384	4ti-0384/C	4titude, UK
GeneRuler 100 bp DNA Ladder	SM0243	Thermo Fisher Scientific, Germany
GeneRuler 1kb DNA Ladder	SM0311	Thermo Fisher Scientific, Germany
Halt™ Protease and Phosphatase Inhibitor Cocktail (100X)	78442	Thermo Fisher Scientific, Germany
Laemmli sample buffer 2x	161-0737	BioRad, Germany
Laemmli sample buffer 4x	161-0747	BioRad, Germany
Nuclei lysis solution	A7943	Promega, USA
NuPAGE® LDS Sample Buffer (4x)	NP0007	Thermo Fisher Scientific, Germany
Protein Marker VI	A8889	AppliChem, Germany
Protein precipitation solution	A7953	Promega, USA
Restore™ PLUS Western Blot Stripping Buffer	46430	Thermo Fisher Scientific, Germany

Salmon Sperm DNA, sheared	AM9680	Thermo Fisher Scientific, Germany
Seahorse XFe96 FluxPak	102416100	Agilent Technologies, Germany
Thick Blot Filter Paper, Precut, 9.5 x 15.2 cm	1704085	BioRad, Germany
XT MOPS running buffer	1610788	BioRad, Germany

Table 10: General consumables

8.1.4 Cell culture consumables

Consumable	Catalogue N	Supplier
12 Well Clear Flat Bottom TC-Treated Multiwell Cell Culture Plate	353043	Neolab, Germany
50 ml syringe	300865	BD Plastipak, USA
C-Chip Neubauer Improved	PK361	Carl Roth GmbH, Germany
Cell scraper 25CM	83.183	Sarstedt, Germany
Cover slips	1001/14	Karl Hecht, Germany
Dimethyl sulfoxide	D5879	Sigma-Aldrich, Germany
DMEM	21969	Thermo Fisher Scientific, Germany
DMEM/F12 GlutaMAX	10565018	Thermo Fisher Scientific, Germany
Doxycycline	44577	Sigma-Aldrich, Germany
DPBS	14190	Sigma-Aldrich, Germany
EasYFlask 75 cm ²	156499	Thermo Fisher Scientific, Germany

Falcon® 24 Well Polystyrene Clear Flat Bottom Not Treated Cell Culture Plate	351147	Neolab, Germany
Falcon® 48 Well Clear Flat Bottom TC-Treated Cell Culture Plate	353078	Neolab, Germany
Fetal Bovine Serum	A2153	Thermo Fisher Scientific, Germany
Hanks balanced salt solution, Mg2+/Ca2+ free	14175-053	Thermo Fisher Scientific, Germany
Horse Serum	16050-122	Thermo Fisher Scientific, Germany
Lipofectamine 2000	11668-019	Thermo Fisher Scientific, Germany
Lipopolysaccharide (LPS)	L4391	Sigma-Aldrich, Germany
Nunclon 6-Well plate	140685	Thermo Fisher Scientific, Germany
Nunc™ MicroWell™ 96-Well Microplates	167008	Thermo Fisher Scientific, Germany
Opti-MEM I	31985-047	Thermo Fisher Scientific, Germany
Penicillin/Streptomycin	15070063	Thermo Fisher Scientific, Germany
Poly-D-lysine	A-003-E	Merck Millipore, Germany
RNase-Free DNase Set	79254	Qiagen, Germany
Seahorse XF Assay Medium	102365100	Agilent Technologies, Germany
Seahorse XF Calibrant Solution	100840000	Agilent Technologies, Germany
Syringe 0.22 µm PES filter	SLGP033RS	Merck Millipore, Germany
Trypsin-EDTA Solution (0.05%)	25300054	Thermo Fisher Scientific, Germany

Trypsin-EDTA Solution (0.25%)	25200056	Thermo Fisher Scientific, Germany
XF96 V3 PS Cell Culture Microplates	101085004	Agilent Technologies, Germany

Table 11: Cell culture consumables

8.1.5 Commercial kits

Kit	Catalogue N	Supplier
Dual-Luciferase® Reporter Assay System	E1910	Promega, USA
KAPA HiFi PCR Kit	KK2103	Kapabiosystems, USA
L-Lactate Assay Kit (Colorimetric/Fluorometric)	ab65330	Abcam, UK
Methylated DNA Quantification Kit (Colorimetric)	ab117128	Abcam, UK
Mouse Homocysteine (Hcy) ELISA Kit	MBS260152	MyBioSource, USA
Pierce BCA Protein Assay Kit	23225	Thermo Fisher Scientific, Germany
Pierce Classic IP Kit	26146	Thermo Fisher Scientific, Germany
QIAamp DNA Mini Kit (250)	51306	Qiagen, Germany
QIAprep Spin Maxiprep Kit	12162	Qiagen, Germany
QIAprep Spin Miniprep Kit	27104	Qiagen, Germany
QIAquick Gel Extraction Kit	28704	Qiagen, Germany
QIAquick PCR Purification Kit	28104	Qiagen, Germany
Quant-iT™ PicoGreen® dsDNA Reagent and Kits	P11496	Thermo Fisher Scientific, Germany
QuikChange Lightning Site-Directed Mutagenesis Kit	210518	Agilent Technologies, USA

RNeasy plus Mini Kit	74134	Qiagen, Germany
S-Adenosylmethionine (SAM) and S-Adenosylhomocysteine (SAH) ELISA Combo Kit	STA-671-C	Cell Biolabs, USA
SuperScript® VILO cDNA Synthesis Kit	11755050	Thermo Fisher Scientific, Germany
TaqMan™ Universal PCR Master Mix 4324018		Thermo Fisher Scientific, Germany

Table 12: Commercial kits

8.1.6 Solutions and buffers

Buffer	Composition
1x XT MOPS running buffer	50ml XT MOPS running buffer 950ml H ₂ O
1x Tris/Glycine transfer buffer	200ml 10x Tris/Glycine transfer buffer 400ml Methanol 1400ml H ₂ O
10x TBS buffer	24.2g Tris base 80g NaCl H ₂ O to 1L pH 7.6
Agar plates	10g tryptone 5g yeast extract 15g agar 10g NaCl H ₂ O to 1L pH 7
Blocking solution (ICC)	1% BSA

	0.5% Triton X100
	PBS
Blocking solution (WB)	5% non-fat milk powder
	TBS-T buffer
CHIP dilution buffer	16.7mM Tris-HCl
	1.2mM EDTA
	0.01% SDS
	167mM NaCl
	1.1% Triton X100
	pH 7.6
CHIP lysis buffer	50mM Tris-HCl
	10mM EDTA
	1%SDS
	pH 7.6
Co-IP lysis buffer	25mM Tris-HCl
	1mM EDTA
	150mM NaCl
	1% CHAPS
	pH 7.4
Hand-made Laemmli (without glycerol)	32.9mM Tris-HCl
	1% SDS
	0.005% bromophenol blue
	20mM DTT
	pH 6.8
LB medium	10g tryptone
	5g yeast extract
	10g NaCl

	H2O to 1L pH 7
MS low salt buffer	20mM Tris-HCl 2mM EDTA 0.1% SDS 150mM NaCl pH 7.6
RIPA buffer	50 mM Tris-HCl 150 mM NaCl 1% Triton-X100 0.5% Sodium deoxycholate 0.1% SDS 3 mM EDTA
TBS-T buffer	100ml 10xTBS buffer 900ml H2O 1ml Tween-20
TE buffer	10mM Tris-HCl 1mM EDTA pH 8

Table 13: Solutions and buffers

8.1.7 Antibodies

8.1.7.1 Primary antibodies

Target	Host	Dilution	Catalogue N	Supplier
ATP1A3	Rabbit	1:1000 (WB)	ab150287	Abcam, UK
ATP1A3 (XVIF9-G10)	Mouse	1:1000 (WB)	MA3-915	Thermo Fisher Scientific, Germany

ATP5A (15H4C4)	Mouse	1:4000 (WB)	ab14748	Abcam, UK
Beta Actin (AC-15)	Mouse	1:5000 (WB)	GTX26276	GeneTex, USA
Catalase (D5N7V)	Rabbit	1:1000 (WB)	14097	Cell signaling technology, USA
COX IV (4D11-B3-E8)	Mouse	1:1000 (WB)	11967	Cell signaling technology, USA
Dj-1	Goat	1:1000 (WB) 10µg (IP)	AF3668	R&D Systems, USA
Dj-1	Goat	1:1000 (WB) 10µg (IP)	ab4150	Abcam, UK
Dj-1	Rabbit	1:1000 (WB) 10µg (IP)	NB100-483	Novus Biologicals, USA
Erk1/2 (137F5)	Rabbit	1:1000 (WB)	4695	Cell signaling technology, USA
GAPDH (GT239)	Mouse	1:5000 (WB)	GTX627408	GeneTex, USA
GFAP	Mouse	1:500 (ICC)	G3893	Sigma-Aldrich, Germany
HPRT (FL-218)	Rabbit	1:1000 (WB)	sc-20975	Santa Cruz, USA
Iba1	Goat	1:200 (ICC)	ab5076	Abcam, UK
IκBα (L35A5)	Mouse	1:1000 (WB)	4814	Cell signaling technology, USA
MTHFR	Goat	1:1000 (WB)	SAB2501754	Sigma-Aldrich, Germany
NDUFB8 (20E9DH10C12)	Mouse	1:1000 (WB)	459210	Thermo Fisher Scientific, Germany
NR4A2 (Nurr1)	Rabbit	1:1000 (WB)	N6413	Sigma-Aldrich, Germany
p38 MAPK	Rabbit	1:1000 (WB)	9212	Cell signaling technology, USA
Phospho-Erk1/2 (Thr202/Tyr204) (20G11)	Rabbit	1:1000 (WB)	4376	Cell signaling technology, USA

Phospho-IkBa (Ser32/36) (5A5)	Mouse	1:1000 (WB)	9246	Cell signaling technology, USA
Phospho-p38 MAPK (Thr180/Tyr182) (12F8)	Rabbit	1:1000 (WB)	4631	Cell signaling technology, USA
PLSCR4	Rabbit	1:500 (WB)	12630-1-AP	Proteintech, USA
SDHB (21A11AE7)	Mouse	1:500 (WB)	459230	Thermo Fisher Scientific, Germany
SLC25A3	Rabbit	1:500 (WB)	15855-1-AP	Proteintech, USA
Spermidine synthase	Rabbit	1:2000 (WB)	19858-1-AP	Proteintech, USA
UQCRC2 (13G12AF12BB11)	Mouse	1:2000 (WB)	ab14745	Abcam, UK

Table 14: Primary antibodies

8.1.7.2 Secondary antibodies

Target	Conjugate	Host	Dilution	Catalogue N	Supplier
Goat IgG	Peroxidase	Rabbit	1:10000 (WB)	305-035-003	Dianova, Germany
Goat IgG	Alexa 488	Donkey	1:500 (ICC)	A11055	Thermo Fisher Scientific, Germany
Mouse IgG	Peroxidase	Goat	1:10000 (WB)	115-035-003	Dianova, Germany
Mouse IgG	Alexa 594	Donkey	1:500 (ICC)	A21203	Thermo Fisher Scientific, Germany
Rabbit IgG	Peroxidase	Goat	1:10000 (WB)	111-035-003	Dianova, Germany
Sheep IgG	Peroxidase	Rabbit	1:10000 (WB)	313-035-003	Dianova, Germany

Table 15: Secondary antibodies

8.1.8 Enzymes

Enzyme	Catalogue N	Supplier
Bbs1	R0539S	New England Biolabs, USA
HindIII	R0104S	New England Biolabs, USA
Kpn1	R0142S	New England Biolabs, USA
Proteinase K	A3830	AppliChem, Germany
RNAse A	A797C	Promega, USA
T7 endonuclease I	E3321	New England Biolabs, USA

Table 16: Enzymes

8.1.9 Primers

Description	5'-3' sequence
Dj-1 guide N1 for	CACCGCATCACGGCTACTGACG (without PAM)
Dj-1 guide N1 rev	AAACCGTGCAGGTAGCCGTGATGC (without PAM)
Dj-1 guide N2 for	CACCGCATCCTGGCCAAAGGAGCAG (without PAM)
Dj-1 guide N2 rev	AAACCTGCTCCTTTGGCCAGGATGC (without PAM)
Dj-1 mut reverse	CGGTACCAGACTCTCCCATC
Dj-1 target2 seq 1for	CTGCTTGCTTCCATGGATCC
Dj-1 target2 seq 1rev	CTATGCTGTCCCAACTGTGC
Dj-1 wt forward	AGGCAGTGGAGAAGTCCATC
Dj-1 wt reverse	AACATACAGACCCGGGATGA
GLprimer2	CTTTATGTTTTTGGCGTCTTCCA
<i>Mthfr</i> prom1 for	TAGATCGGTACCCGCGGAGGTAAGCTGGAT
<i>Mthfr</i> prom1 rev	AGTTCTAAGCTTCTTTCGTCAGATCGGTG
<i>Mthfr</i> prom2 for	TAGATCGGTACCGCACGCCTTTAATCCCAACA

<i>Mthfr</i> prom2 rev	AGTTCTAAGCTTCCCGATCTGCTCAGACCC
<i>Mthfr</i> prom3 for	TAGATCGGTACCGCCTCCAGACCAAAGAGCTA
<i>Mthfr</i> prom3 mut1 for	CTGACACAGAACCCTGCGTCTTCCCCGACCCTGC
<i>Mthfr</i> prom3 mut1 rev	GCAGGGTCGGGGGAAGACGCAGGGTTCTGTGTCAG
<i>Mthfr</i> prom3 mut2 for	CTGACACAGAACCCTGGTTGGTCCCCGACCCTGC
<i>Mthfr</i> prom3 mut2 rev	GCAGGGTCGGGGGACCAACCAGGGTTCTGTGTCAG
<i>Mthfr</i> prom3 rev	AGTTCTAAGCTTACCTCCTCGCCCCATTTTAT
RVprimer3	CTAGCAAATAGGCTGTCCC
U6 promoter F	TTCACCGAGGGCCTATTTCCCATG

Table 17: Primers

8.1.10 DNA vectors

Description	Catalogue N	Supplier/reference/producer
pCCLsin.PPT.hPGK.rtTAm2 (rTTA)	N/A	Caiazza et al. 2011, [37]
pGL3 basic	E1751	Promega, USA
pLL3.7 CAG IRES GFP	N/A	Available at the IDG
pLL3.7 CAG mDj-1 IRES GFP	N/A	Available at the IDG
pMasterblaster CAS9 v.2	N/A	Available at the IDG; generated by J. Truong
pRL-SV40 Vector (Renilla)	E2231	Promega, USA
Tet-O-Nurr1	N/A	Caiazza et al. 2011, [37]
Tet-O-T2A-dsRed	N/A	Available at the IDG

Table 18: DNA vectors

8.1.11 Taqman probes

Description	Catalogue N	Supplier
<i>Actb</i>	Mm00607939_s1	Thermo Fisher Scientific, Germany
<i>Cat</i>	Mm00437992_m1	Thermo Fisher Scientific, Germany
<i>Hadha</i>	Mm00805228_m1	Thermo Fisher Scientific, Germany
<i>Il1b</i>	Mm00434228_m1	Thermo Fisher Scientific, Germany
<i>Mthfr</i>	Mm00487784_m1	Thermo Fisher Scientific, Germany
<i>Mthfr (Mthfr-001)</i>	Mm01263627_g1	Thermo Fisher Scientific, Germany
<i>Mthfr (Mthfr-003)</i>	Mm01263629_m1	Thermo Fisher Scientific, Germany
<i>iNos</i>	Mm00440502_m1	Thermo Fisher Scientific, Germany
<i>Nr4a2</i>	Mm00443060_m1	Thermo Fisher Scientific, Germany
<i>Park7</i>	Mm00498538_m1	Thermo Fisher Scientific, Germany
<i>Srm</i>	Mm00726089_s1	Thermo Fisher Scientific, Germany
<i>Tnf</i>	Mm00443258_m1	Thermo Fisher Scientific, Germany

Table 19: Taqman Probes

8.1.12 Cell lines

Description	Catalogue N	Supplier
HEK293	CRL-1573	ATCC, USA
Neuro-2a	CCL-131	ATCC, USA
MEFs	-	Available at the IDG
SIM A9	T0247	ABM, Canada

Table 20: Cell lines

8.1.13 Bacterial strains

Description	Catalogue N	Supplier
DH5 α	18265017	Thermo Fisher Scientific, Germany

Table 21: Bacterial strains

8.1.14 Mouse strains

Description	Producer
PARK7_XE726_GT	Available at the IDG

Table 22: Mouse strains

8.2 Methods

8.2.1 Cell culture

8.2.1.1 Storage and thawing of the cell lines

Storage of stable cell lines was performed as follows: after the splitting procedure and removal of the supernatant, cells were resuspended in complete medium (DMEM/F12 GlutaMAX with 10% fetal bovine serum (FBS), 5% horse serum (HS) and 1% Pen/Strep) with 10% dimethyl sulfoxide. Subsequently they were put into cryogenic tubes and placed on ice and frozen at -80°C. After one day of storage at -80°C, they were placed inside liquid nitrogen for long-term storage.

To thaw the cells, the frozen cryogenic tube was quickly warmed up in a water bath to 37°C with following addition to a falcon tube containing 5ml of complete medium. Subsequently, cells were centrifuged for 3 min at 200 x g, and the supernatant was aspirated. Afterwards, cells were resuspended in a proper volume of complete medium (normally 12ml) and plated on a T75 flask – poly-D-Lysine (PDL) pre-coated or not, dependent on the cell line.

8.2.1.2 Culture conditions

Primary cells and the SIM A9 microglial cell line were incubated at 37°C, 5% CO₂. HEK293 and N2A cell lines were kept under 37°C and 7% CO₂.

8.2.1.3 Counting of cells

To determine the amount of the cells, a Neubauer cell counting chamber was used. 10µl of medium with resuspended cells was added to the pocket of the counting chamber. Under the microscope, the number of the cells in the top- left and right, and bottom- left and right was counted. Cell number in one millilitre was determined by the following equation:

$$\text{Cell number (per ml)} = \frac{\text{total number of cells}}{4 \times 10000}$$

8.2.1.4 Coating culture plates and flask

Poly-D-Lysine (PDL) was diluted 25 times, and, according to the manufacturer's protocol an appropriate volume of PDL solution was added to a plate or flask. The plate was incubated for at least 1 hour at 37°C with two subsequent washings with sterile water. Following, the surface of the plate was allowed to dry under the laminar flow before usage of the plates. If needed, PDL coated plates were stored at 4°C up to 2 weeks.

For immunostainings experiments with primary microglia cells and the SIM A9 microglial cell line, glass cover slips were disinfected with ethanol and incorporated into the wells of 24-well plates before the coating procedure.

8.2.1.5 Isolation and culture of primary microglia cells

Newborn pups, from two to four days old, were used for primary microglia cell isolation. Pups were decapitated with sharp scissors, and the head was placed into a 50ml falcon tube filled with 10ml of Hank's Balanced Salt Solution (HBSS) and 1% Penicillin-Streptomycin (HBSS+Pen/Strep). Additionally, a part of the tail was cut and frozen for further DNA isolation and genotyping analysis. Afterwards, the head was washed in the 50ml tube, placed inside a Petri dish filled with HBSS+Pen/Strep for the further procedure. Under a stereomicroscope, the skin was removed from the head and a cut along the superior sagittal sinus of skull was performed. Subsequently, the skullcaps were removed and the brain was released to the Petri dish. Cerebellum, midbrain, hippocampus and olfactory bulbs were removed in a way that only the two hemispheres of the cerebral cortexes were left intact. In a following step, the meninges and leftovers from the blood vessels were carefully removed. Then the cortex hemispheres were washed in the Petri dish with HBSS+Pen/Strep to remove possible meninges contaminants, and afterwards the cortexes were placed to in a 50ml falcon tube with 10ml of fresh HBSS+Pen/Strep. All following steps were performed under a laminar flow.

The cortexes in their buffer were placed into a Petri dish and chopped robustly with a blade. The obtained cell suspension was collected in a 15ml tube and centrifuged for 5 min at 200 x g. The supernatant was carefully removed and the cell pellet was elaborately resuspended in 3ml of a 0.05% Trypsin solution with a 10 min incubation at 37°C. Later on, 6ml of complete microglia growth medium (DMEM/F12 GlutaMAX with 10% fetal bovine serum (FBS) and 1% Pen/Strep) were added and the tube was inverted for several times with subsequent addition of 4.5 µl of DNase and 10 minutes incubation at 37°C. After the second incubation period, cells had to be centrifuged for 10 min at 200 x g again, then the supernatant was removed and the cells were resuspended in 12ml of complete microglia growth medium with subsequent plating on a T75 PDL pre-coated flask.

Cells were incubated at 37°C, with medium changes twice a week. Three days, after the cells have grown completely confluent (normally around 15 days after the plating), microglia cells were separated from the other cell types present. To do so, the cells were washed once with DMEM/F12 GlutaMAX medium without any supplement and then 8ml of the mixture (DMEM/F12 GlutaMAX 3:1 Trypsin 0.25% dilution) were added for 20 min at 37°C. After the incubation, the upper layer was removed by aspiration and the residual attached microglia cells were supplied with complete microglia growth medium. These cells were incubated at least for 1 day before the experimental procedures.

8.2.1.6 Culture of SIM A9 microglia cell line

SIM A9 cells were cultured in DMEM/F12 GlutaMAX with 10% fetal bovine serum (FBS), 5% horse serum (HS) and 1% Pen/Strep (complete medium). They were kept on PDL coated T75 flask with medium change 2-3 times per week, until a confluency of 80-90% was reached. When the proper confluency was reached, the cells were split. To do so, they were washed once with Dulbecco's Phosphate-Buffered Saline (DPBS) and trypsin 0.25% was added for 2 min at 37°C. After that, a 5 times larger volume of complete medium was added to neutralize the trypsin and cells centrifuged for 3 min 200 x g. After removal of the supernatant, cells were diluted in complete medium and counted. For maintenance culture, 200.000 cells/ 15ml of medium were plated to a new PDL coated T75 flask.

8.2.1.7 Culture of HEK293, N2A, and primary MEFs

HEK293, N2A, and primary MEFs cells were cultured and split in the similar manner as SIM A9 cells, however using different complete medium (DMEM with 10% FBS (and 1% Pen/Strep for primary MEFs)). In addition, the T75 flasks for culturing and the plates for experiments with these cells were not PDL coated.

8.2.1.8 Lipofection

Lipofection of SIM A9, HEK293, and N2A cells was done using the Lipofectamine 2000 kit according the manufacturer's protocol. Desired amount of DNA was mixed with Opti-MEM medium, while in parallel the lipofectamine 2000 reagent was mixed with Opti-MEM medium. Diluted lipofectamine and DNA were mixed and incubated for 20 min. After the incubation period, the mixture was applied to cells and allowed to incubate for 6 hours. Afterwards, the medium was changed to the complete medium with incubation of the cells until the performance of the experiments.

8.2.1.8.1 Lipofection of HEK293 cells for luciferase assay

HEK293 cells were plated to a 24-well plate (5×10^4 cells per well in 500 μ l of complete medium). The mixture of DNA plasmids (table 23) for each condition was prepared and 50 μ l with Opti-MEM medium were added. Then, 50 μ l of Opti-MEM medium with 2 μ l of lipofectamine 2000 were added to the DNA mixture. 100 μ l of final mixture (four conditions for each promoter: control, Nurr1 overexpression, Dj-1 overexpression, Nurr1 and Dj-1 overexpression) were applied per well. In the end, five pGL3 basic plasmids were used - with promoter N1, N2, N3 cloned under the luciferase, and, in addition, two types of mutated promoter N3 (mut1 and mut2). After 6 hours, the medium was changed to 500 μ l of complete medium with 4 μ g/ml of doxycycline. 48 hours later the luciferase assay was performed.

Plasmids (μg per well)	Control	Nurr1 OE	Dj-1 OE	Nurr1 OE + Dj-1 OE
pGL3 basic with MTHFR promoter	0.2	0.2	0.2	0.2
pRL-SV40 Vector (Renilla)	0.0001	0.0001	0.0001	0.0001
Tet-O-Nurr1	0	0.2	0	0.2
pLL3.7 CAG mDj-1 IRES GFP	0	0	0.2	0.2
pLL3.7 CAG IRES GFP (control)	0.4	0.2	0.2	0
pCCLsin.PPT.hPGK.rtTAm2 (rTTA)	0.2	0.2	0.2	0.2
Σ DNA [μg]	0.8001	0.8001	0.8001	0.8001

Table 23: Plasmids combination for different conditions of HEK293 luciferase assay.

8.2.1.8.2 Lipofection of N2A cells for T7 assay

N2A cells were plated to a 24-well plate (5×10^4 cells per well in 500 μl of complete medium). pMasterblaster Cas9 plasmids with two different guide RNAs (Dj-1 guide N1 and Dj-1 guide N2) were tested with three different lipofectamine concentrations (1 μl , 1.5 μl , and 2.5 μl), 6 conditions in total. 0.5 μg of the plasmid were added to 50 μl of Opti-MEM medium, then 50 μl of Opti-MEM medium with lipofectamine was mixed with diluted plasmid and incubated for 20 min. 50 μl from 100 μl of the final mixture were applied to the cells. After 6 hours of incubation, the medium was changed to the complete medium and additional 48 hours incubation took place before the DNA isolation for T7 assay.

8.2.1.8.3 Lipofection of SIM A9 cells for Dj-1 knockout generation

SIM A9 cells were plated to a PDL-coated 24-well plate (5×10^4 cells per well in 500 μl of complete medium). The procedure of lipofection was the same as it was with N2A cells. In this experiment 0.5 μg of pMasterblaster Cas9 plasmid with Dj-1 guide N2 was used and 1.5 μl of lipofectamine per well. After 6 hours of incubation, the medium was changed to the complete medium and additional 24 hours incubation took place before the clonal selection procedure.

8.2.1.9 Transduction of primary microglia with Lentiviruses

Nurr1 overexpression in primary microglia was achieved by transduction of the cells with Lentiviruses: for Nurr1 overexpression - Tet-O-Nurr1 and Tet-O-T2A-dsRed as control. Primary microglia cells were plated to a 12-well plate (5×10^4 cells per well in 1ml of complete medium) and 24 hours later, the transduction procedure was performed with a multiplicity of infection (MOI) of 1.2, which was equal to 6×10^4 virus particles per well. When viruses with Tet-on system were used, 1 μl (was detected experimentally in laboratory) of pCCLsin.PPT.hPGK.rtTAm2 (rTTA) virus was added to each well in addition. On the next day, the medium was changed to the complete medium (for viruses with Tet-on system, medium was supplemented with 4 $\mu\text{g}/\text{ml}$ of Doxycycline). 72 hours later, the medium was exchanged to 900 μl of DMEM/F12 GlutaMAX

without any additional supplements. On the next day the LPS treatment experiment was performed.

8.2.1.10 Clonal selection of SIM A9 cells

Clonal selection of SIM A9 cells was performed by dilution. 24 hours, after the cells were lipofected with the pMasterblaster Cas9 Dj-1 guide N2 plasmid, they were detached, counted and diluted in complete media to the concentration of 5 cells per 1ml. 100µl of cell solution were placed per well in 96-well plate (plates were pre-coated with PDL in advance). After 7 days of incubation, colonies were identified under the microscope, and were transferred to the PDL pre-coated 24-well plates with 500µl of complete media. After a confluency of 90% was reached, cells were trypsinised and split in 2 parts: one part was transferred to PDL pre-coated 12 well plates with 1ml of complete media, the other one was centrifuged and the pellet was collected for the further DNA and protein isolation.

8.2.1.11 LPS treatment experiments

In all experiments with primary microglia, the final concentration of LPS used was 10ng/ml, for SIM A9 cells 100 ng/ml. The general procedure in all LPS treatment experiments was the following: cells were plated in the morning in complete medium with the desired amount. After 8 hours the medium was exchanged to the medium without any supplement (90% of the final volume). On the next day, 10% of the volume with 10X LPS was added, thus the final concentration of LPS was 1X. For controls, just 10% of medium without supplement was added. After the desired time of treatment was done, cells were used for their subsequent analyses. Table 24 describes the parameters of the experiments in detail.

Cell type	Experiment	Cell amount	Final volume (plate)	LPS concentration	Treatment duration
primary microglia	qPCR	3-5x10 ⁴	500µl (24-well)	10ng/ml *	8 hours
	Western blot	10-15x10 ⁴	2.5ml (6-well)		24 hours
	immunocytochemistry	2.5x10 ⁴	500µl (24-well)		1-48 hours
	Dj-1 immunoprecipitation for mass spectrometry	30-40x10 ⁴	10ml (T75)		4 hours
	Homocysteine ELISA	15x10 ⁴	2.5ml (6-well)		24 hours
	SAM/SAH ELISA	15x10 ⁴	2.5ml (6-well)		24 hours
	Methylated DNA ELISA	3x10 ⁴	500µl (24-well)		24 hours
SIM A9 cells	qPCR	10x10 ⁴	1ml (12-well)	100ng/ml	8 hours
	Western blot	15x10 ⁴	2.5ml (6-well)		0-120 min, 24 hours
	Dj-1 immunoprecipitation for Co-IP optimization and mass spectrometry	100x10 ⁴	15ml (T75)		1 hour

Table 24: The main parameters of LPS treatment experiments. * In experiment with PDTC (inhibitor of NFκB), 50µM PDTC was applied 1 hour prior LPS treatment.

8.2.2 Nucleic acid isolation procedure

8.2.2.1 RNA isolation

RNA isolation from primary microglia and cell lines was performed with the RNeasy plus mini kit according to manufacturer's instructions.

RNA isolation from tissue was performed as follows: tissue was placed in a 2ml Eppendorf tube with 1ml of Trizol and was homogenised with a T25 basic ULTRA-TURRAX. 0.2ml of Chloroform were added after homogenisation with subsequent mixing of the constituents by inverting the tube for 15 seconds. Then the mixture was left for 3min at RT and a centrifugation step for 10min at 18500 x g was performed. 0.5ml from the upper fraction were collected, mixed with an equal amount of 70% ethanol and incubated for 10 min at RT. The final mixture was applied to a DNA column of the RNeasy plus mini kit, and standard procedure according to the manufacturer's protocol was performed.

8.2.2.2 DNA isolation

DNA extraction from primary microglia and cell lines was performed with QIAamp DNA Mini Kit according to manufacturer's instructions.

DNA isolation from tissue was performed as follows: the tissue was placed in a 1,5ml Eppendorf tube with a lysis solution mixture (500µl of nuclei lysis solution, 120µl of 0.5M EDTA and 37.5µl of proteinase K). Tubes were incubated in a Thermomixer comfort (Eppendorf) at 55°C and 800rpm for 3 hours until the tissue was dissolved. The tubes were cooled down to RT and 3µl of RNase A was added and mixed with a subsequent incubation for 15min at 37°C. After the incubation, 200µl of protein precipitation solution were added, vortexed for 20 seconds and chilled on ice for 5 min. Following, samples were spun down for 15 min at rpm≥16000 x g, 4°C. The supernatant was collected and mixed with 600µl of isopropanol. Again, centrifugation was performed for 1min at rpm≥16000 x g at RT. The supernatant was removed and the pellet was washed with 600µl of 70% ethanol with another following centrifugation step. The supernatant again was removed and the pellet was air-dried. Afterwards, the pellet was reconstituted in an appropriate volume of sterile H₂O (100-200µl).

Polymerase chain reaction (PCR) DNA fragments were cleaned up from enzymes and salts with the QIAquick PCR Purification Kit according to manufacturer's instructions. To isolate DNA from agarose gels, a QIAquick Gel Extraction Kit was used according to manufacturer's instructions.

8.2.3 Complementary DNA (cDNA) synthesis

Complementary DNA was synthesized from previously isolated RNA using the SuperScript® VILO cDNA Synthesis Kit according to manufacturer's protocol. For cDNA preparation from primary

microglia cells, 200ng of RNA were used per sample, in all other cases 400ng of RNA. The obtained 20µl of cDNA solution normally was diluted 5 to 10 times, depending on the amount of the primer probes used in the following qPCR. If applicable, undiluted cDNA was stored at -20°C until further usage.

8.2.4 Agarose gel electrophoresis

To identify or separate DNA fragments during cloning or genotyping procedures, agarose gel electrophoresis was performed. Agarose was cooked in 1xTAE buffer, with subsequent addition of ethidium bromide (4-8µl for 100ml of agarose solution) for band identification. For an expected band size of up to 1kb 2g of agarose per 100ml of TAE buffer were used, for larger bands a 1% agarose solution was used. After the gel was cast, a proper amount of DNA was mixed with loading buffer and applied to a gel, with a subsequent electrophoresis at 120V for approximately 40 min. Analysis and images were done using E.A.S.Y Win32 Gel-Documentation system.

8.2.5 Molecular cloning

8.2.5.1 Cloning of *Mthfr* promoters under the luciferase gene reporter system

Mthfr promoters were amplified from mouse genomic (wildtype) DNA using the KAPA HiFi PCR Kit with primers, which added a restriction site for the Kpn1 enzyme to the 5 prime end of the PCR fragment and a HindIII restriction site to the 3 prime end. Three *Mthfr* promoters were amplified: promoter 1 (promoter of the *Mthfr*-003 transcript), promoter 2 (promoter of the *Mthfr*-001 transcript) and promoter 3 (promoter of the *Mthfr*-004 transcript). The vector pGL3 was used as firefly luciferase reporter plasmid. Digestion of the pGL3 plasmid as well as of all DNA fragments of the *Mthfr* promoters was done with Kpn1 and HindIII restriction enzymes.. After purification of the desired DNA fragments (in case of restricted backbone gel electrophoresis was performed with extraction of the needed fragment with the QIAquick Gel Extraction Kit; in case of the *Mthfr* promoters' fragments PCR purification was done using the QIAquick PCR Purification Kit), ligation procedure was performed for 30min at RT using a T4 ligase.

Creation of mutated versions of the *Mthfr* promoter 3 was done using the primers *Mthfr* prom3 mut1 for, *Mthfr* prom3 mut1 rev, *Mthfr* prom3 mut2 for and *Mthfr* prom3 mut2 rev and the QuikChange Lightning Site-Directed Mutagenesis Kit, according to manufacturer's instructions.

8.2.5.2 Cloning of Dj-1 guide RNAs

pMasterBlaster CAS9v.2 plasmid was used for generation of Dj-1 knockout cells. Guide RNAs were designed using the platform benchling.com. Primers for guide RNAs (Dj-1 guide N1 - Dj-1 guide N1 forward and reverse and Dj-1 guide N2 - Dj-1 guide N2 forward and reverse) were created in

a way that 5 prime ends included additional nucleotides for restriction digestion and sticky end ligation into the vector backbone. Annealing of the primers was done as follows: 1µl of 100pM of each, forward and reverse primer, were mixed and diluted in 100µl of TE buffer. Subsequently, they were heated to 99°C for 5min and cooled down very slowly to RT. In parallel, pMasterBlaster CAS9v.2 plasmid was digested with the Bbs1 restriction enzyme and purified by agarose gel electrophoresis and gel extraction. Afterwards, ligation (T4 ligase) of the guides DNA fragments with the vector backbone was performed at 16°C overnight.

8.2.5.3 Transformation of competent bacteria, plasmid multiplication and purification

DH5α chemically competent cells were used for amplification of the plasmids. 50µl of bacteria were gently thawed on ice and 4µl of the plasmid (after the ligation step) were added to the bacteria. After 30 min on ice, cells were heat-shocked for 30 seconds at 42°C and then cooled down on ice for 3 min. 1ml of pre-warmed LB medium was added to the transformed bacteria with subsequent shaking for 1 hour at 37°C. Bacteria were plated on agar plates with a corresponding selection marker and incubated at 37°C overnight.

The following day, single cell colonies were picked and placed into a plastic tube with 3ml of pre-warmed LB medium, supplemented with selection marker, for overnight shaking at 37°C. On the next day, 2ml of suspension was taken for the plasmid purification using the QIAprep Spin Miniprep Kit according to manufacturer's protocol. Isolated plasmids were sent for sequencing with corresponding primers. After sequences were verified, the remaining 1ml of the bacterial solution was added to 250ml of LB medium, supplemented with selection marker and incubated overnight shaking at 180rpm at 37°C. The following day, the plasmid was purified using the QIAprep Spin Maxiprep Kit and sent for sequencing for final validation. Concentrations of plasmids were determined using a NanoDrop-2000 system.

8.2.6 Luciferase assay

A luciferase assay was used to analyse the ability of Nurr1 and Dj-1 to regulate the expression of the luciferase gene using different types of *Mthfr* promoters. The dual-luciferase reporter system was used in these experiments. A *firefly luciferase* was expressed under the control of the different *Mthfr* promoters. *Renilla luciferase* was expressed on an independent plasmid under the constitutively active simian virus 40 (*SV40*) promoter and was used for normalisation. The procedure of lipofection of HEK293 cells for the luciferase assay was described above (see 8.2.1.8.1). 48 hours after lipofection, cells were lysed by adding 100µl of passive lysis (Dual-Luciferase® Reporter Assay System) buffer with following shaking for 15 min at RT. 10µl of lysate were used to determine firefly and renilla luciferase activities on a white 96-well plate using a

Centro LB 960 luminometer. The program of MicroWin32 luminometer software is represented in table 25.

Step	Operation	Definition
Dispense	Volume	50µl
	Speed	Middle
	Measured operation	By well
	Repeated operation	Yes
	Duration	2s
Delay	Measurement option	By well
	Name	Firefly or renilla
Firefly/Renilla	Counting time	5s
	Measurement option	By well

Table 25: MicroWin32 luminometer software settings.

Firefly activity in one well was normalized to renilla activity of the same well. At least three technical replicates were measured for each condition.

8.2.7 T7 assay

48 hours after N2A cells were lipofected (see 8.2.1.8.2), DNA was isolated and amplification of the Dj-1 target 1 and 2 was performed by PCR. After PCR fragments' purification with the QIAquick PCR Purification Kit, 400ng of DNA were taken for T7 assay performance: 17µl of DNA were mixed with 2µl of NEB buffer 2 and placed in a thermocycler. The samples were kept at 95°C for 5 min, then a gradual decrease of temperature from 95°C to 85°C (2°C per second) and from 85°C to 25°C (0.1°C per second) was performed. 1µl of T7 endonuclease was added to the samples and incubated at 37°C for 1 hour. Fragments were analysed on agarose gel using an E.A.S.Y Win32 Gel-Documentation system.

8.2.8 Homocysteine ELISA

Primary microglia cells were washed once with DPBS after 24 hours of LPS treatment. 1ml of DPBS, supplemented with 10µl of Halt™ Protease and Phosphatase Inhibitor Cocktail (100X), was added to each well with following gentle scraping of cells from the bottom. The cell suspension was then homogenised in an ultrasonic bath RK100 (twice for 2 min with 1 min cooling period in-between). Then the samples were centrifuged for 10min at 1000 x g and the supernatant was used for the homocysteine measurements. A small aliquot (50µl) was taken from each sample for further normalisation procedure using a BCA assay. Homocysteine measurements were performed with the Mouse Homocysteine (Hcy) ELISA Kit according to manufacturer's protocol. Colorimetric measurements were done with a SpectraMax M5 Microplate Reader.

8.2.9 S-Adenosylmethionine (SAM) and S-Adenosylhomocysteine (SAH) ELISA

Preparation of the samples from primary microglia cells for SAM/SAH measurements was done in the same manner as for the homocysteine ELISA. Obtained supernatants were used for SAM/SAH detection with SAM and SAH ELISA Combo Kit according to manufacturer's instructions. Colorimetric measurements were done with a SpectraMax M5 Microplate Reader.

8.2.10 Methylated DNA determination

Primary microglia cells were washed once with DPBS after 24 hours of LPS treatment. 0.2ml of DPBS were added to each well with subsequent gentle scraping of cells. The cell suspension was used for genomic DNA isolation with QIAamp DNA Mini Kit according to manufacturer's protocol. 40ng of purified genomic DNA was used for detection of methylated DNA with the Methylated DNA Quantification Kit. Colorimetric measurements were done with a SpectraMax M5 Microplate Reader.

8.2.11 Cellular DNA content quantification

SIM A9 cellular DNA content measurement was done for normalisation of seahorse and lactate measurement experiments. After the seahorse procedure, 50µl of medium were removed for lactate determination and 10µl of proteinase K were added to each well of the seahorse XF96-well plate. After shaking the plate, it was incubated at 37°C for 1 hour. After an additional shaking step, the plate was centrifuged for 5 min at 400 x g. 10µl from the supernatant fraction were used for DNA content determination using Quant-iT™ PicoGreen® dsDNA Reagent and kit. PicoGreen reagent was diluted 1:200 in 1x TE buffer, with following addition of 100µl per well, each of which contained 10µl of the supernatant from the lysed cells. Medium from four wells, which served as a background control in the seahorse experiment, was used as background control in this experiment too. Four standard control probes with genomic DNA concentrations of 0, 1, 2, and 5 µg/ml were used for the calculation of a standard curve by linear regression analysis. After PicoGreen addition, samples were incubated for 5 min in the dark. Fluorescence intensity was measured at Ex480nm/Em520nm using a SpectraMax M5 Microplate Reader. DNA concentrations were calculated using linear regression analysis.

8.2.12 L-lactate measurement

After the seahorse experiment, 50µl of medium was taken from each well for lactate content determination. L-Lactate content was measured using the L-Lactate Assay Kit (Colorimetric/Fluorometric) according to manufacturer's instructions. Fluorescence intensity was measured at Ex535nm/Em587nm using a SpectraMax M5 Microplate Reader. Lactate

concentrations were determined using linear regression analysis and were normalized to cellular DNA content (see 8.2.11).

8.2.13 Immunocytochemistry and microscopy

For immunocytochemistry experiments, primary microglia cells were seeded on PDL coated glass cover slips in 24 well format. For the pre-fixation procedure, an equal volume of 10% formalin was added to the medium, and the plate was incubated for 10 min at 37°C. Then the medium was exchanged for to 500µl of 10% formalin with a following subsequent repetition of the incubation step. Afterwards, Cells cells were washed three times afterwards with DPBS, and 200µl of the primary antibodies, diluted in the blocking buffer (1% BSA, 0.5 % Triton-X-100 in PBS), were applied. The plate was incubated overnight at 4°C on a shaker. On the following day, three subsequent washing steps with DPBS were performed, and secondary antibodies, diluted in blocking solution, were applied. Incubation of cells with the secondary antibodies was performed in the dark for 1 hour at RT on a shaker. After the incubation, 100 ng/ml of DPBS DAPI solution was applied to cells for 3min (for cells' nuclei nucleus visualization). After three additional washing steps, coverslips with containing the cells were mounted on a glass slides with using AquaPolyMount. Slides were dried overnight and were stored in the dark at 4°C before the analysis.

Images of fluorescent stained cells were taken with an Axioplan 2 microscope with an AxioCam HRc camera.

8.2.14 Quantitative real-time polymerase chain reaction (qRT-PCR)

qRT-PCR was performed in 384-well plate format. 9µl of pre-diluted cDNA (see 8.2.3) were added per well with subsequent addition of 11µl of mastermix (10µl of TaqMan universal PCR mastermix and 1µl of probe). Three technical replicates were used for all samples. After pipetting, the plate was sealed with adhesive seal foils. Following, the plate was placed into an ABI Prism 7900 HT Real-Time PCR System for the performance of the qRT-PCR measurement (table 26). The analysis of data was done using the SDS 2.4.1 software and MS Excel.

Step/cycles	Cycles	Temperature (°C)	Duration (sec)
Initial denaturation	1	95	600
Denaturation	40	95	15
Annealing and amplification		60	60

Table 26: qRT-PCR Program.

8.2.15 Western Blot

Experiments with primary microglia and cell lines were performed in a 6-well format, if the following application was western blotting analysis. First, cells were washed once with DPBS. Then 200-300µl of RIPA buffer, supplemented with Halt™ Protease and Phosphatase Inhibitor Cocktail, were added. The lysis procedure was performed on ice for 10min with periodical shaking. After that, additional scraping was done and the content of the well was placed in an Eppendorf tube. Tubes were centrifuged for 15min at 4°C at maximum speed (21000 x g) and the supernatant was collected in a separate tube.

Protein concentration was measured with the Pierce BCA protein assay kit as described by the manufacturer. Quantitation of protein concentration was done using Microsoft Excel via linear regression analysis in relation to the standard samples. Samples were stored at -80°C until the western blot analysis was performed.

Electrophoresis of protein samples was performed using a Criterion Cell System.. 5-10µg of protein per sample was used for western blot experiments. Samples were diluted with RIPA buffer to a final volume of 20µl. 6.6µl of 4x NuPAGE LDS sample buffer, containing 4% β-mercaptoethanol, were added to each of sample and heated for 5min to 95°C (samples used for the detection of mitochondrial complexes were heated to 65°C for 12min). Then, samples were cooled down slowly to RT. Afterwards, protein samples and protein marker (protein marker VI, AppliChem) were loaded to Criterion XT 4-12% Bis-Tris precast gels, inserted into a running chamber which was subsequently filled with 1x XT MOPS running buffer. Empty pockets of the gel were filled with RIPA, supplemented with NuPAGE LDS sample buffer, to prevent non-equal running of the samples. The electrophoresis procedure was performed on ice for approximately 75min at 180V. During electrophoresis 1x Tris/Glycine transfer buffer was made, as described by manufacturer and cooled down at 4°C.

After the run was completed, the gel was placed on filter paper inside the blotting cassette. The gel was covered with a pre-cut and pre-incubated (in 100% methanol for 1min) PVDF membrane. Then, an additional layer of filter paper was used and the cassette was inserted into the blotting chamber, which was filled with chilled blotting buffer. Protein transfer was done overnight at 20V and 4°C.

On the following day, the membrane was blocked using blocking solution (5% milk in TBS-T buffer) for 1 hour with slight agitation. Then, the membrane was cut, if needed, and was transferred to a 50ml falcon with 5ml of primary antibodies solution (0.5% milk in TBS-T plus appropriate amount of primary antibodies). The membrane was incubated overnight at 4°C on a roller shaker with 35rpm. The next day, the membrane was washed 3 times with TBS-T and the secondary antibodies solution (5% milk in TBS-T plus appropriate amount of secondary antibodies) was applied and incubated for 1 hour at RT on a roller shaker. Afterwards, three subsequent washing steps were done and the membrane was developed using Clarity Western

ECL Substrate and a ChemiDoc MP imaging system. Processing of the images was done with the Image Lab software and calculations were performed in Microsoft Excel.

8.2.16 Dj-1 Co-IP in primary microglia for mass spectrometry analysis

Four hours after LPS treatment (see 8.2.1.11) of primary microglia, cells were cross-linked with formaldehyde at final concentration of 1% (270 μ l of 37% formaldehyde was added to 10ml of medium with cells) for 10 min at 37°C. Then, cells were washed twice with ice cold DPBS supplemented with cOmplete™ Mini Protease Inhibitor Cocktail. Subsequently, cells were scraped and transferred into a 15ml tube containing 8ml of DPBS plus protease inhibitors and spun down for 6 min at 2000rpm centrifugation at 4°C. After the centrifugation, the cell pellet was lysed with 200 μ l of CHIP lysis buffer supplemented with Halt™ Protease and Phosphatase Inhibitor Cocktail for 10 min on ice. Using the a sonication bath, the cell lysate was sonicated as follows: two repetitions of 4 min sonication and 1min cool down followed by another 2 min sonication and 1 min cool down. Then, samples were centrifuged for 10 min at 16000 x g at 4°C. The supernatant was collected and diluted with 1.8ml of CHIP dilution buffer. 60 μ l of Pierce Control Agarose Resin (Thermo Fisher Scientific) were added to 2ml sample and incubated with slight agitation for 1 hour at 4°C to reduce non-specific binding. Then, the agarose was pelleted and the supernatant was collected. Now, 10 μ g of Dj-1 antibody (R&D) was added to the supernatant with following overnight incubation at 4°C. The next day, 30 μ l of Pierce Protein A/G Plus Agarose and salmon sperm DNA (with a final concentration 0.1 μ g/ μ l) were added to the samples with subsequent 2 hours of incubation at 4°C. After the incubation, the agarose was pelleted a by 1000 x g centrifugation step for 1 min and the supernatant was discarded. After the pellet was obtained, it was washed twice with MS low salt buffer and twice with TE buffer. The elution was done by adding 60 μ l of 2x Laemmli solution to 60 μ l of agarose beads solution, with a subsequent incubation for 5 min at 95°C. Then the samples were centrifuged for 1min at 1000 x g and the supernatant was collected and stored at -80°C until the mass spectrometry was performed.

8.2.17 Dj-1 Co-IP optimization in SIM A9 cells for mass spectrometry analysis

All the steps in Dj-1 Co-IP optimization in SIM A9 cells were the same as in the Dj-1 Co-IP in SIM A9 cells for mass spectrometry analysis (described in 8.2.18), yet with some variations. First, there were many different conditions tested (buffers, antibodies, time of precipitation and so on (presented in table 6 in results block). Second, during the optimization procedure, 700 μ l of lysis buffer were used, as 100 μ l were kept as a later input control for IP efficiency calculation. Third, the elution step was performed with commercial Laemmli containing glycerol, which opened the possibility to load the protein samples on gel for IP efficiency analysis. Dj-1 IP efficiency was calculated via western blot by comparison of Dj-1 signal in IP and control probes using the Image Lab software and Microsoft Excel.

8.2.18 Dj-1 Co-IP in SIM A9 cells for mass spectrometry analysis

1 hour after LPS treatment (see 8.2.1.11) of SIM A9 cells, they were cross-linked for 10 min at 37°C using formaldehyde at a final concentration of 1% (405µl of 37% formaldehyde were added to 15ml of medium with cells). After the incubation period, cells were washed twice with ice cold DPBS supplemented with cOmplete™ Mini Protease Inhibitor Cocktail. Then, 600µl of Co-IP lysis buffer supplemented with Halt™ Protease and Phosphatase Inhibitor Cocktail, were added and cells were lysed on ice for 5 min, with subsequent scraping and collection in a 1.5ml Eppendorf tube. The sonication step in the sonication bath was performed with two repetitions of 3 min sonication with a subsequent 1 min cool down each. Then, the lysate was centrifuged for 10 min at 16000 x g and supernatant was collected. The supernatant was added to a spin column together with 80µl of Pierce Control Agarose Resin, inverted several times to mix and was incubated for 1 hour at 4°C. The column was centrifuged for 1 min at 1000 x g and the DJ-1 antibodies (10µg of R&D and 10µg of Abcam) were added to flow-through for overnight incubation at 4°C. The following day, 20µl of Pierce Protein A/G Plus Agarose was added to the sample and incubated for 2 hours at 4°C. Then, the sample was centrifuged for 1 min at 1000 x g, the beads were washed 4 times with lysis buffer with detergent and twice with lysis buffer without detergent. The elution was done with hand-made Laemmli (without glycerol) supplemented with 20µM dithiothreitol (DTT) at 100°C for 10 min. Then the eluates were collected after a last centrifugation step (1 min at 1000 x g) and were frozen and sent for mass spectrometry.

8.2.19 Respiratory analysis (Seahorse)

Three clones from wildtype and Dj-1 knockout SIM A9 cells were plated in multiple replica (14-16) on a PDL pre-coated XF96 V3 PS cell culture plate at a density of 25.000 cells per well. Each clone was plated in three to four replica (wells) for each of the four conditions (will be described later). Several hours after the plating, the medium was changed to DMEM/F12 GlutaMAX medium without any supplement. The following day, medium for the four different conditions of experiment was prepared. Seahorse XF assay medium was used as base medium for the four different conditions and supplemented with either: 1) 25mM glucose, 2) 25mM glucose + 100ng/ml LPS, 3) 5mM pyruvate or 4) 5mM pyruvate + 100ng/ml LPS. Cells were washed once with plain Seahorse XF assay medium and 180µl of the freshly prepared assay medium was added to corresponding wells, with a subsequent equilibration period of 1 hour at 37°C. Meanwhile, the chemical solutions for the injections were prepared at desired concentrations and added into the ports of a previously hydrated cartridge: port A – 20µl of 10µg/ml oligomycin (for the final concentration in the medium – 1µg/ml), port B – 22µl of 5µM FCCP (for 0.5µM final concentration in the medium), port C – 25µl of 50µM (5µM – final concentration) rotenone and 20µM antimycin A (2µM – final concentration) and port D – 27µl of 1M 2-deoxyglucose (final concentration –

100mM). After the cartridge was prepared, the Seahorse XF96 software was programmed for the experiment (table 27). Then, the plate and cartridge were placed into a Seahorse XFe96 analyzer and the program was started.

	Action	Time
	Calibrate probes	
x10	Mix	1min
	Time delay	2min
	Measure	3min
	Inject port A	
x3	Mix	1min
	Time delay	2min
	Measure	3min
	Inject port B	
x3	Mix	1min
	Time delay	2min
	Measure	3min
	Inject port C	
x3	Mix	1min
	Time delay	2min
	Measure	3min
	Inject port D	
x3	Mix	1min
	Time delay	2min
	Measure	3min
	Program end	

Table 27: Seahorse program of experiment with SIM A9 cells.

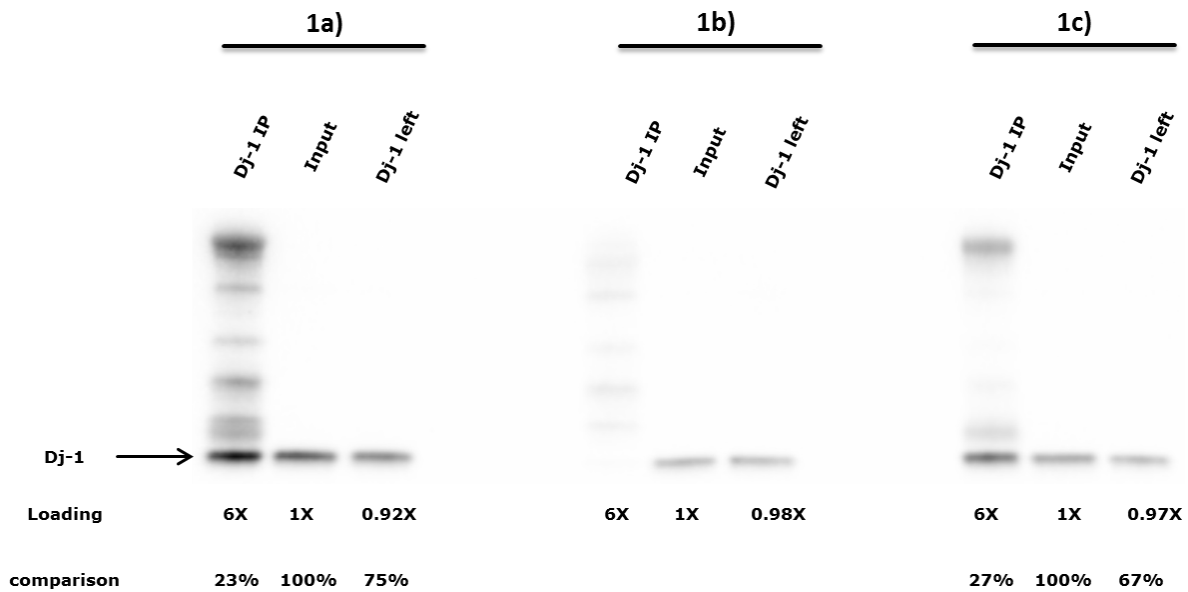
8.2.20 Statistical analysis.

Statistical analysis was performed using the GraphPad Prism 6 software. Only experiments with at least three biological replicates were used for statistical analysis. Statistical analysis was started with outliers identification test (if applicable), with subsequent normality test performance (D'Agostino and Pearson omnibus normality tests). In case of Gaussian distribution, t-test or one-way ANOVA analysis with Tukey's multiple comparison test were applied. In case of not normal distribution, Mann-Whitney or Kruskal-Wallis tests were applied respectively. When two or more factors were included in the experiment, two-way ANOVA analysis with Tukey's multiple comparison test was implemented. P-values below 0.05 were considered significant. All datasets are represented with mean \pm standard deviation (SD), with exception of the Seahorse progression measurements (mean \pm standard error of mean (SEM)).

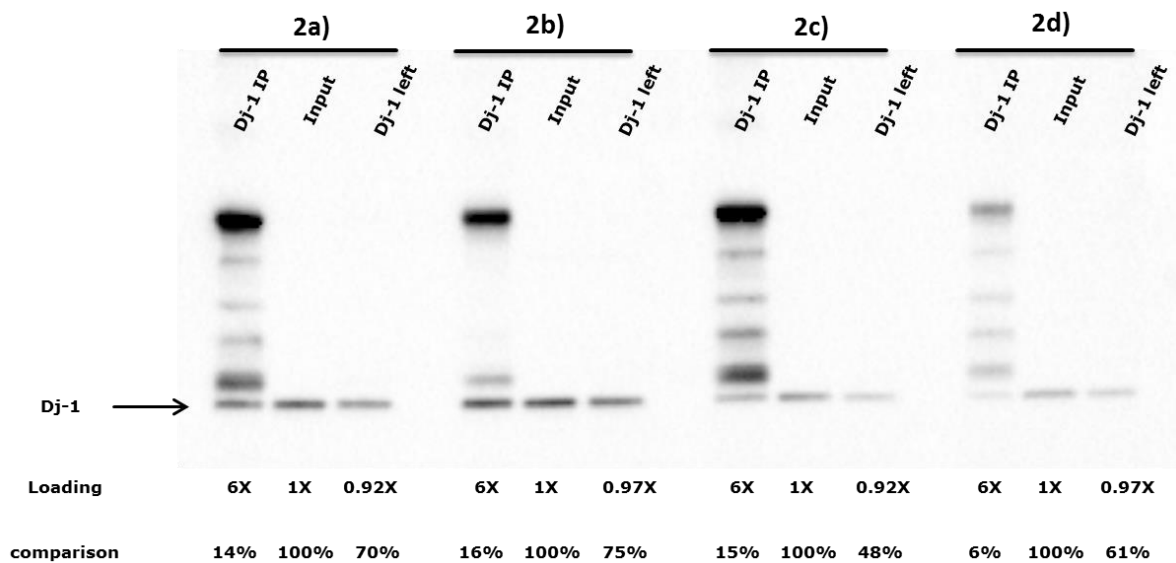
9 Appendix

9.1 Supplementary materials

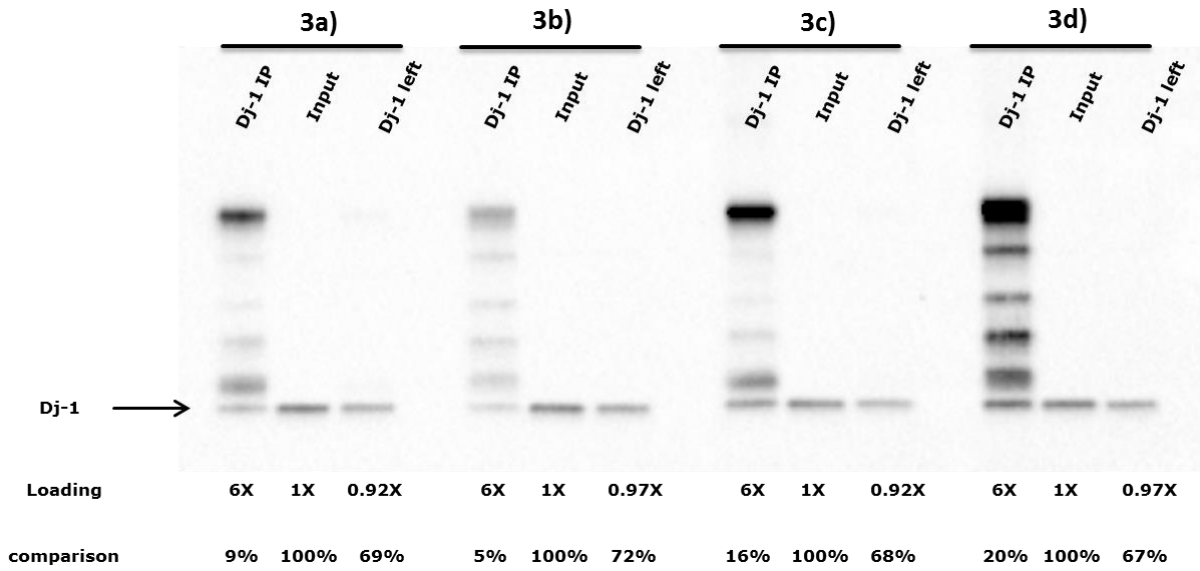
Supplementary fig. 1: Western blots of Dj-1 IP optimization experiments



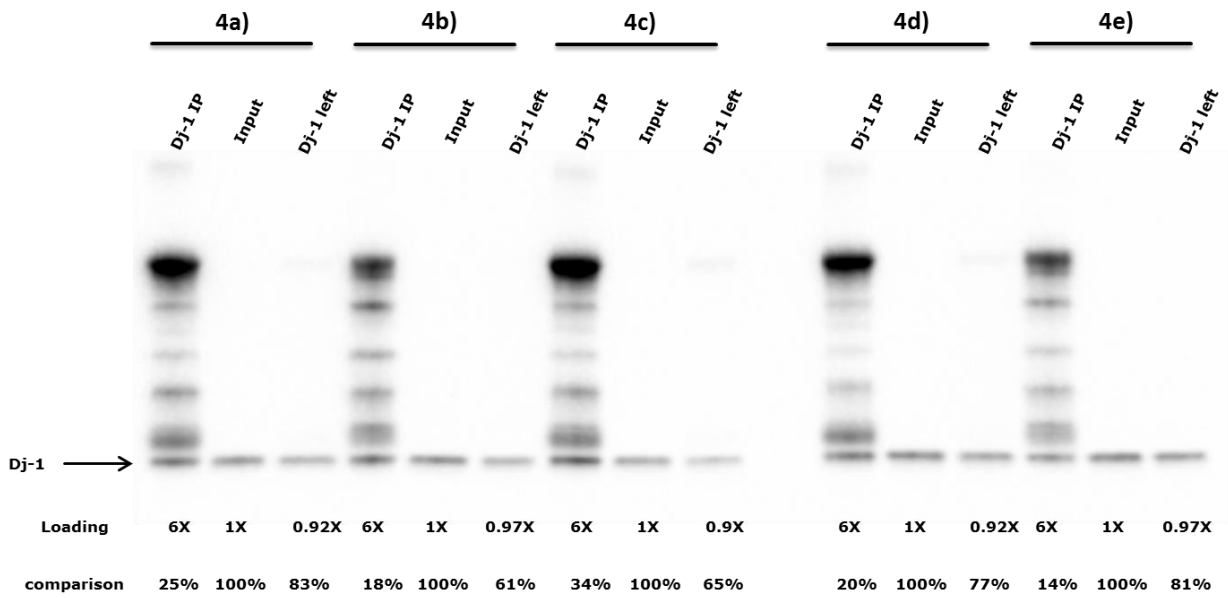
Supplementary fig. 1 (1a-1c): Western blots of Dj-1 IP optimization experiments, conditions represented in table 6.



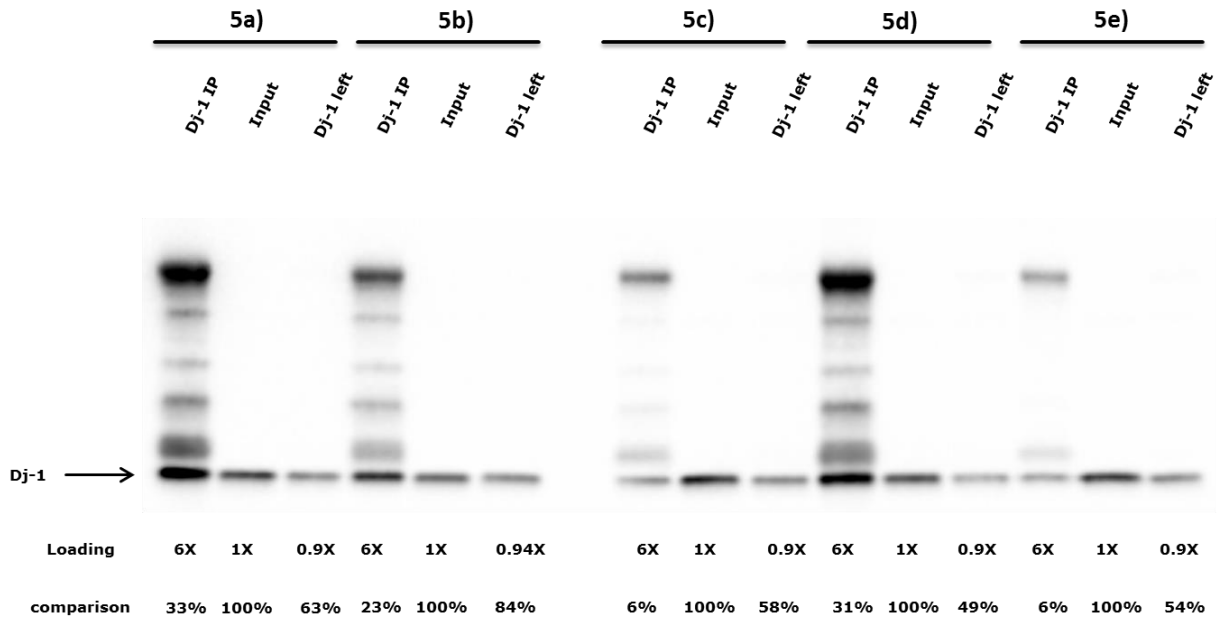
Supplementary fig. 1 (2a-2d): Western blots of Dj-1 IP optimization experiments, conditions represented in table 6.



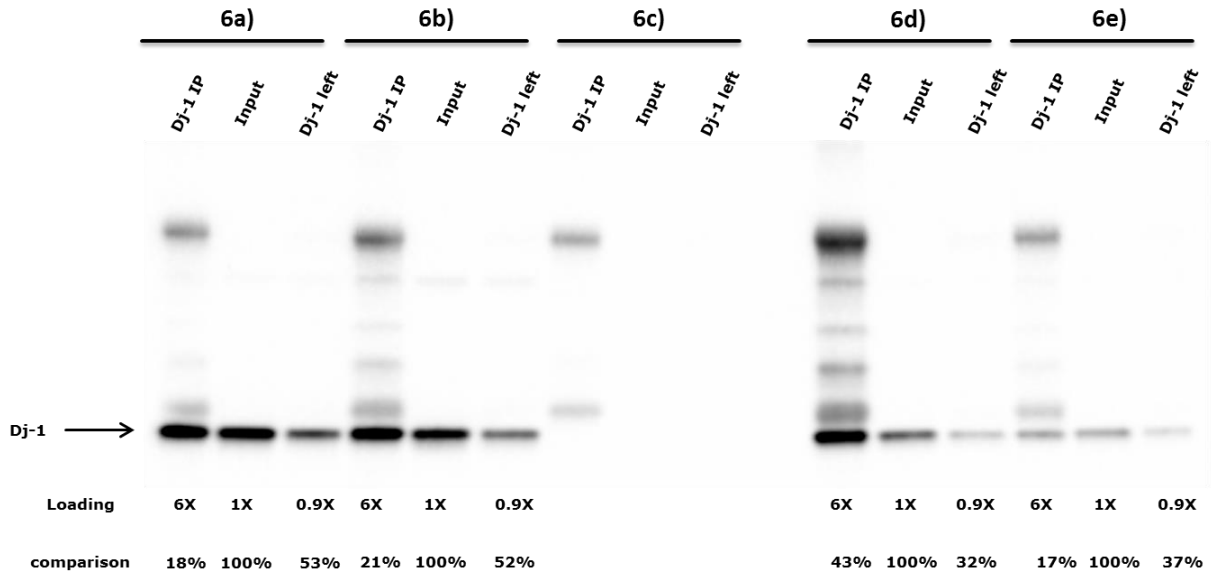
Supplementary fig. 1 (3a-3d): Western blots of Dj-1 IP optimization experiments, conditions represented in table 6.



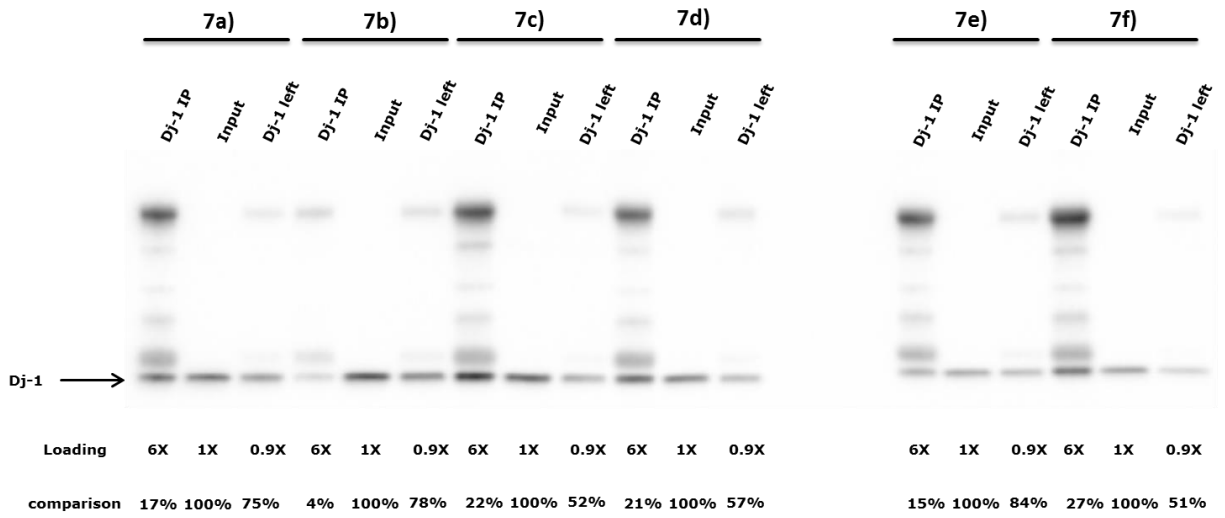
Supplementary fig. 1 (4a-4e): Western blots of Dj-1 IP optimization experiments, conditions represented in table 6.



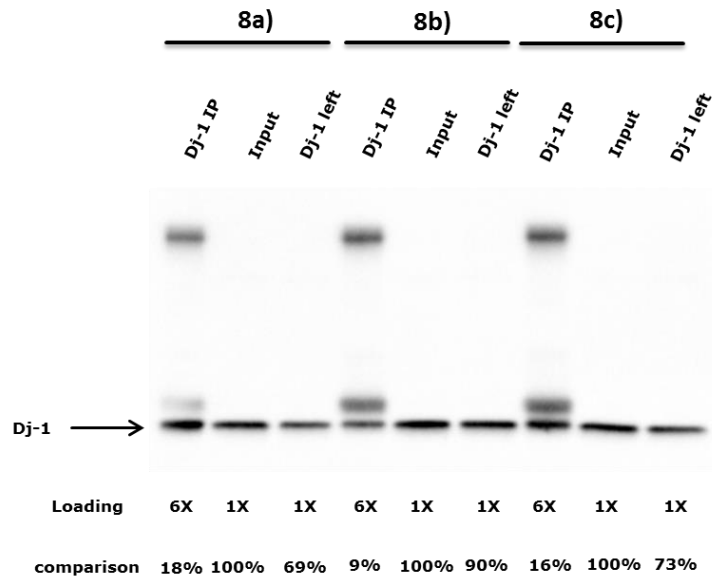
Supplementary fig. 1 (5a-5e): Western blots of Dj-1 IP optimization experiments, conditions represented in table 6.



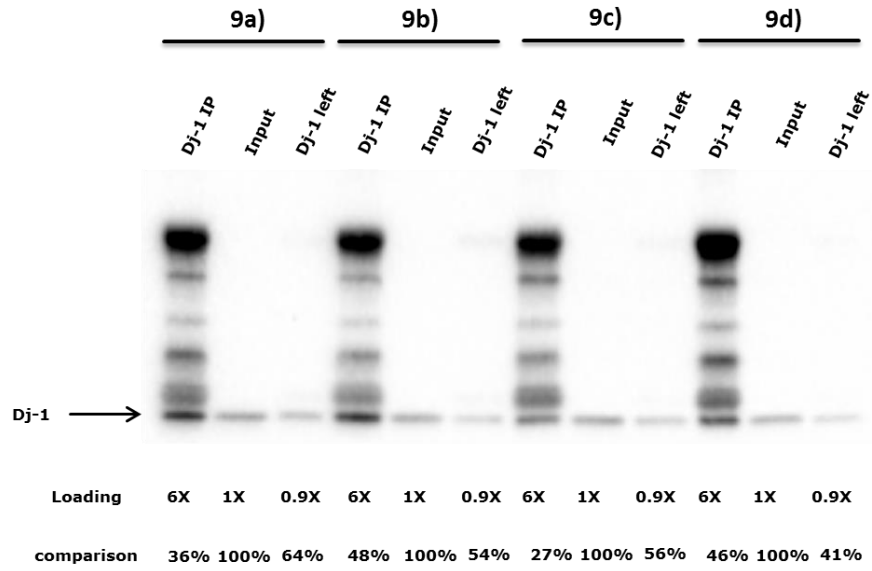
Supplementary fig. 1 (6a-6e): Western blots of Dj-1 IP optimization experiments, conditions represented in table 6.



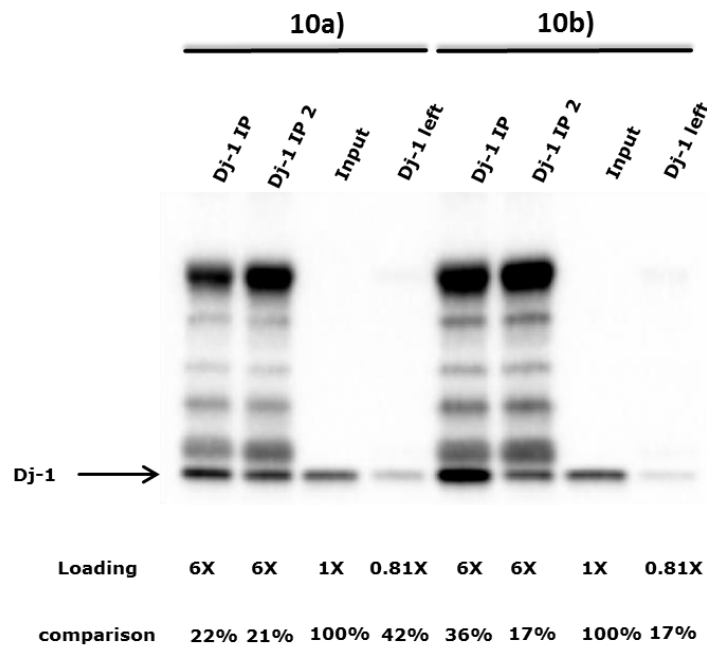
Supplementary fig. 1 (7a-7f): Western blots of Dj-1 IP optimization experiments, conditions represented in table 6.



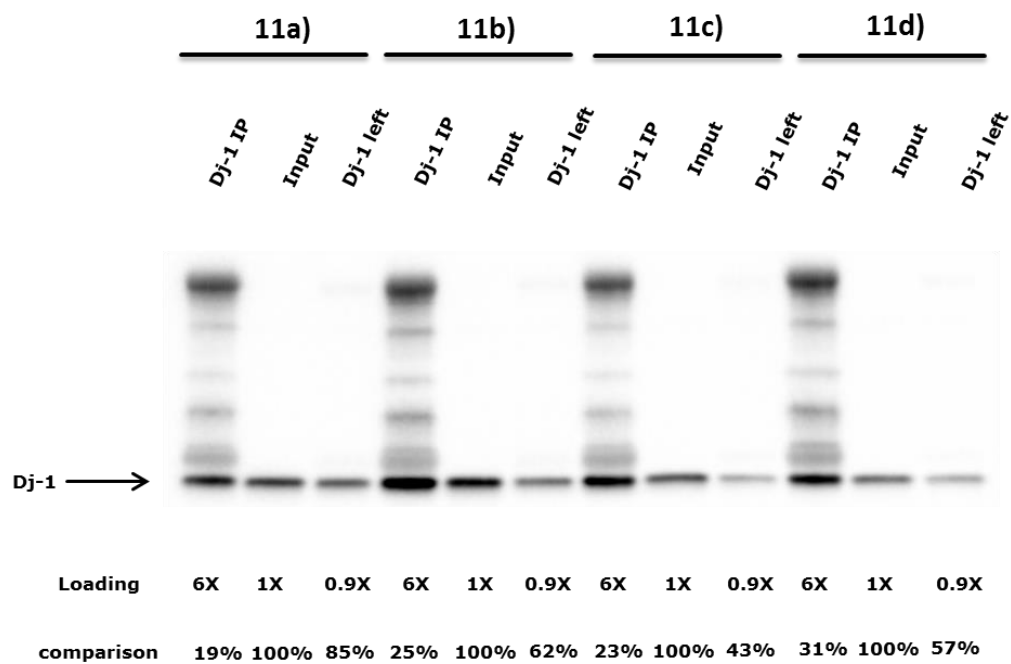
Supplementary fig. 1 (8a-8c): Western blots of Dj-1 IP optimization experiments, conditions represented in table 6.



Supplementary fig. 1 (9a-9d): Western blots of Dj-1 IP optimization experiments, conditions represented in table 6.



Supplementary fig. 1 (10a-10b): Western blots of Dj-1 IP optimization experiments, conditions represented in table 6.



Supplementary fig. 1 (11a-11d): Western blots of Dj-1 IP optimization experiments, conditions represented in table 6.

Supplementary table 1: Calculations of western blots of Dj-1 IP optimization experiments represented in supplementary figure 1

Number	Sample	Signal density	Normalized density	Protein loading difference	Ratios	Ratios in %	IP efficiency
1a	Dj-1 IP	4876875	1.39	6x	0.23	23%	23%
	Input	3519700	1	1x	1	100%	
	Left	2427275	0.69	0.92x	0.75	75%	
1b	Dj-1 IP	0		6x			
	Input			1x			
	Left			0.98x			
1c	Dj-1 IP	2935625	1.62	6x	0.27	27%	27%
	Input	1807125	1	1x	1	100%	
	Left	1150050	0.64	0.97x	0.66	67%	
2a	Dj-1 IP	1487952	0.85	6x	0.14	14%	14%
	Input	1757682	1	1x	1	100%	
	Left	1135764	0.65	0.92x	0.70	70%	
2b	Dj-1 IP	1996992	0.98	6x	0.16	16%	16%
	Input	2043306	1	1x	1	100%	
	Left	1482354	0.73	0.97x	0.75	75%	
2c	Dj-1 IP	813870	0.92	6x	0.15	15%	15%
	Input	887436	1	1x	1	100%	
	Left	381492	0.43	0.92x	0.47	48%	
2d	Dj-1 IP	225666	0.35	6x	0.06	6%	6%
	Input	642438	1	1x	1	100%	
	Left	377712	0.59	0.97x	0.61	61%	
3a	Dj-1 IP	783000	0.56	6x	0.09	9%	9%
	Input	1399770	1	1x	1	100%	
	Left	882666	0.63	0.92x	0.69	69%	
3b	Dj-1 IP	422820	0.29	6x	0.05	5%	5%
	Input	1448046	1	1x	1	100%	
	Left	1009260	0.70	0.97x	0.72	72%	
3c	Dj-1 IP	1183842	0.95	6x	0.16	16%	16%
	Input	1240182	1	1x	1	100%	
	Left	772614	0.62	0.92x	0.68	68%	
3d	Dj-1 IP	1836864	1.24	6x	0.21	20%	20%
	Input	1486170	1	1x	1	100%	
	Left	966384	0.65	0.97x	0.67	67%	
4a	Dj-1 IP	1239819	1.49	6x	0.25	25%	25%
	Input	833511	1	1x	1	100%	
	Left	636699	0.76	0.92x	0.83	83%	
4b	Dj-1 IP	1025703	1.07	6x	0.18	18%	18%

	Input	961296	1	1x	1	100%	
	Left	573384	0.60	0.97x	0.61	61%	
4c	Dj-1 IP	1414119	2.05	6x	0.34	34%	34%
	Input	690165	1	1x	1	100%	
	Left	403998	0.59	0.9x	0.65	65%	
4d	Dj-1 IP	1179332	1.17	6x	0.20	20%	20%
	Input	1006588	1	1x	1	100%	
	Left	711260	0.71	0.92x	0.77	77%	
4e	Dj-1 IP	767206	0.83	6x	0.14	14%	14%
	Input	926574	1	1x	1	100%	
	Left	723536	0.78	0.97x	0.81	81%	
5a	Dj-1 IP	3578564	1.98	6x	0.33	33%	33%
	Input	1808180	1	1x	1	100%	
	Left	1021130	0.56	0.9x	0.63	63%	
5b	Dj-1 IP	1993794	1.39	6x	0.23	23%	23%
	Input	1437216	1	1x	1	100%	
	Left	1128776	0.79	0.94x	0.84	84%	
5c	Dj-1 IP	748052	0.37	6x	0.06	6%	6%
	Input	2030463	1	1x	1	100%	
	Left	1056091	0.52	0.9x	0.58	58%	
5d	Dj-1 IP	3001408	1.86	6x	0.31	31%	31%
	Input	1617475	1	1x	1	100%	
	Left	716312	0.44	0.9x	0.49	49%	
5e	Dj-1 IP	716726	0.38	6x	0.06	6%	6%
	Input	1869003	1	1x	1	100%	
	Left	911927	0.49	0.9x	0.54	54%	
6a	Dj-1 IP	3681449	1.09	6x	0.18	18%	18%
	Input	3366832	1	1x	1	100%	
	Left	1608689	0.48	0.9x	0.53	53%	
6b	Dj-1 IP	3456256	1.28	6x	0.21	21%	21%
	Input	2701442	1	1x	1	100%	
	Left	1271532	0.47	0.9x	0.52	52%	
6c	Dj-1 IP						
	Input						
	Left						
6d	Dj-1 IP	3325409	2.57	6x	0.43	43%	43%
	Input	1292048	1	1x	1	100%	
	Left	371542	0.29	0.9x	0.32	32%	
6e	Dj-1 IP	584476	0.99	6x	0.17	17%	17%
	Input	589766	1	1x	1	100%	
	Left	193867	0.33	0.9x	0.37	37%	

7a	Dj-1 IP	1806720	1.00	6x	0.17	17%	17%
	Input	1815380	1	1x	1	100%	
	Left	1232280	0.68	0.9x	0.75	75%	
7b	Dj-1 IP	527800	0.22	6x	0.04	4%	4%
	Input	2349800	1	1x	1	100%	
	Left	1647260	0.70	0.9x	0.78	78%	
7c	Dj-1 IP	2653980	1.29	6x	0.22	22%	22%
	Input	2052640	1	1x	1	100%	
	Left	963560	0.47	0.9x	0.52	52%	
7d	Dj-1 IP	1855260	1.27	6x	0.21	21%	21%
	Input	1462120	1	1x	1	100%	
	Left	747080	0.51	0.9x	0.57	57%	
7e	Dj-1 IP	931960	0.90	6x	0.15	15%	15%
	Input	1031320	1	1x	1	100%	
	Left	779240	0.76	0.9x	0.84	84%	
7f	Dj-1 IP	1829140	1.60	6x	0.27	27%	27%
	Input	1142100	1	1x	1	100%	
	Left	526640	0.46	0.9x	0.51	51%	
8a	Dj-1 IP	5447648	1.06	6x	0.18	18%	18%
	Input	5148864	1	1x	1	100%	
	Left	3569504	0.69	1x	0.69	69%	
8b	Dj-1 IP	3298816	0.52	6x	0.09	9%	9%
	Input	6287040	1	1x	1	100%	
	Left	5636480	0.90	1x	0.90	90%	
8c	Dj-1 IP	5489440	0.97	6x	0.16	16%	16%
	Input	5644768	1	1x	1	100%	
	Left	4133056	0.73	1x	0.73	73%	
9a	Dj-1 IP	1021932	2.17	6x	0.36	36%	36%
	Input	471834	1	1x	1	100%	
	Left	269892	0.57	0.9x	0.64	64%	
9b	Dj-1 IP	1113930	2.88	6x	0.48	48%	48%
	Input	386334	1	1x	1	100%	
	Left	187542	0.49	0.9x	0.54	54%	
9c	Dj-1 IP	683676	1.61	6x	0.27	27%	27%
	Input	425934	1	1x	1	100%	
	Left	215136	0.51	0.9x	0.56	56%	
9c	Dj-1 IP	874008	2.77	6x	0.46	46%	46%
	Input	315450	1	1x	1	100%	
	Left	116946	0.37	0.9x	0.41	41%	
10a	Dj-1 IP 1	1281596	1.34	6x	0.22	22%	22%
	Dj-1 IP 2	1195202	1.25	6x	0.21	21%	21%

	Input	958868	1	1x	1	100%	
	Left	328610	0.34	0.81x	0.42	42%	
10b	Dj-1 IP 1	2365890	2.14	6x	0.36	36%	36%
	Dj-1 IP 2	1145358	1.04	6x	0.17	17%	17%
	Input	1103266	1	1x	1	100%	
	Left	153187	0.14	0.81x	0.17	17%	
11a	Dj-1 IP	2954056	1.15	6x	0.19	19%	19%
	Input	2572706	1.00	1x	1	100%	
	Left	1960487	0.76	0.9x	0.85	85%	
11b	Dj-1 IP	4847089	1.53	6x	0.25	25%	25%
	Input	3169439	1	1x	1	100%	
	Left	1775583	0.56	0.9x	0.62	62%	
11c	Dj-1 IP	3391521	1.39	6x	0.23	23%	23%
	Input	2444990	1	1x	1	100%	
	Left	946937	0.39	0.9x	0.43	43%	
11d	Dj-1 IP	3614821	1.87	6x	0.31	31%	31%
	Input	1928674	1	1x	1	100%	
	Left	989016	0.51	0.9x	0.57	57%	

Supplementary table 1: Calculations of western blots of Dj-1 IP optimization experiments represented in supplementary figure 1. Abbreviations: Dj-1 IP – amount of Dj-1 after immunoprecipitation; Input – loading control taken from sample before immunoprecipitation; Left – amount of not precipitated Dj-1.

Supplementary table 2: Mass spectrometry data

Ratio wt/ko	T-TEST wt/ko	Ratio LPS wt/ko	T-TEST LPS wt/ko	Gene symbol	Description
2.1	0.0002	2.1	0.0198	Slc25a3	Q8VEM8 MPCP_MOUSE Phosphate carrier protein, mitochondrial OS=Mus musculus GN=Slc25a3 PE=1 SV=1
0.6	0.0066	0.6	0.0897	Hadha	Q8BMS1 ECHA_MOUSE Trifunctional enzyme subunit alpha, mitochondrial OS=Mus musculus GN=Hadha PE=1 SV=1
0.2	0.0071	0.0	0.0266	Cct3	P80318 TCPG_MOUSE T-complex protein 1 subunit gamma OS=Mus musculus GN=Cct3 PE=1 SV=1
0.1	0.0084	0.1	0.1124	Ide	Q9JHR7 IDE_MOUSE Insulin-degrading enzyme OS=Mus musculus GN=Ide PE=1 SV=1
0.5	0.0115	0.9	0.6981	Phb2	O35129 PHB2_MOUSE Prohibitin-2 OS=Mus musculus GN=Phb2 PE=1 SV=1
0.5	0.0136	0.5	0.1329	Bcap29	Q61334 BAP29_MOUSE B-cell receptor-associated protein 29 OS=Mus musculus GN=Bcap29 PE=1 SV=1
0.5	0.0174	0.5	0.1351	Adsl	P54822 PUR8_MOUSE Adenylosuccinate lyase OS=Mus musculus GN=Adsl PE=1 SV=2
0.2	0.0174	0.3	0.0409	Cat	P24270 CATA_MOUSE Catalase OS=Mus musculus GN=Cat PE=1 SV=4
0.5	0.0217	1.0	0.9295	Phb	P67778 PHB_MOUSE Prohibitin OS=Mus musculus GN=Phb PE=1 SV=1
0.1	0.0222	0.1	0.1200	Clcc1	Q99LI2 CLCC1_MOUSE Chloride channel CLIC-like protein 1 OS=Mus musculus GN=Clcc1 PE=1 SV=1
0.3	0.0224	0.4	0.3073	Rpl3	P27659 RL3_MOUSE 60S ribosomal protein L3 OS=Mus musculus GN=Rpl3 PE=1 SV=3
58.2	0.0252	63.8	0.0224	Park7	Q99LX0 PARK7_MOUSE Protein deglycase DJ-1 OS=Mus musculus GN=Park7 PE=1 SV=1
0.5	0.0288	0.5	0.1432	Lrrfip1	Q3UZ39 LRRF1_MOUSE Leucine-rich repeat flightless-interacting protein 1 OS=Mus musculus GN=Lrrfip1 PE=1 SV=2
0.9	0.0331	0.9	0.5846	Slc25a4	P48962 ADT1_MOUSE ADP/ATP translocase 1 OS=Mus musculus GN=Slc25a4 PE=1 SV=4
2.3	0.0385	0.6	0.4809	Atp1a3	Q6PIC6 AT1A3_MOUSE Sodium/potassium-transporting ATPase subunit alpha-3 OS=Mus musculus GN=Atp1a3 PE=1 SV=1
0.7	0.0391	0.6	0.2719	Srm	Q64674 SPEE_MOUSE Spermidine synthase OS=Mus musculus GN=Srm PE=1 SV=1
2.5	0.0495	1.7	0.1345	Plscr4	P58196 PLS4_MOUSE Phospholipid scramblase 4 OS=Mus musculus GN=Plscr4 PE=2 SV=2

0.3	0.0505	0.4	0.1137	Atp2a1	Q8R429 AT2A1_MOUSE Sarcoplasmic/endoplasmic reticulum calcium ATPase 1 OS=Mus musculus GN=Atp2a1 PE=1 SV=1
0.7	0.0546	0.7	0.3594	Rplp0	P14869 RLA0_MOUSE 60S acidic ribosomal protein P0 OS=Mus musculus GN=Rplp0 PE=1 SV=3
0.3	0.0633	0.4	0.1766	Hsd17b4	P51660 DHB4_MOUSE Peroxisomal multifunctional enzyme type 2 OS=Mus musculus GN=Hsd17b4 PE=1 SV=3
0.6	0.0654	0.8	0.4860	Actc1	P68033 ACTC_MOUSE Actin, alpha cardiac muscle 1 OS=Mus musculus GN=Actc1 PE=1 SV=1
0.6	0.0692	0.8	0.1630	Flii	Q9JJ28 FLII_MOUSE Protein flightless-1 homolog OS=Mus musculus GN=Flii PE=1 SV=1
1.7	0.0709	1.0	0.9944	Arpc1b	Q9WV32 ARC1B_MOUSE Actin-related protein 2/3 complex subunit 1B OS=Mus musculus GN=Arpc1b PE=1 SV=4
0.7	0.0741	0.6	0.2148	Atp5d	Q9D3D9 ATPD_MOUSE ATP synthase subunit delta, mitochondrial OS=Mus musculus GN=Atp5d PE=1 SV=1
0.3	0.0789	0.3	0.3094	Gphn	Q8BUV3 GEPH_MOUSE Gephyrin OS=Mus musculus GN=Gphn PE=1 SV=2
0.4	0.0854	0.3	0.2867	Rps2	P25444 RS2_MOUSE 40S ribosomal protein S2 OS=Mus musculus GN=Rps2 PE=1 SV=3
0.2	0.0895	0.0	0.3959	Hist1h2bc	Q6ZWY9 H2B1C_MOUSE Histone H2B type 1-C/E/G OS=Mus musculus GN=Hist1h2bc PE=1 SV=3
0.2	0.0906	0.3	0.1931	Rps16	P14131 RS16_MOUSE 40S ribosomal protein S16 OS=Mus musculus GN=Rps16 PE=1 SV=4
0.7	0.0920	1.0	0.9758	Rack1	P68040 RACK1_MOUSE Receptor of activated protein C kinase 1 OS=Mus musculus GN=Rack1 PE=1 SV=3
2.1	0.0934	1.1	0.8674	Tma7	Q8K003 TMA7_MOUSE Translation machinery-associated protein 7 OS=Mus musculus GN=Tma7 PE=3 SV=1
0.5	0.0979	0.5	0.2981	Rpl7	P14148 RL7_MOUSE 60S ribosomal protein L7 OS=Mus musculus GN=Rpl7 PE=1 SV=2
0.8	0.0986	1.0	0.8413	Cct7	P80313 TCPH_MOUSE T-complex protein 1 subunit eta OS=Mus musculus GN=Cct7 PE=1 SV=1
1.4	0.0989	1.1	0.7228	Alb	P07724 ALBU_MOUSE Serum albumin OS=Mus musculus GN=Alb PE=1 SV=3
0.7	0.1017	0.9	0.2378	Hnrnpk	P61979 HNRPK_MOUSE Heterogeneous nuclear ribonucleoprotein K OS=Mus musculus GN=Hnrnpk PE=1 SV=1

0.4	0.1041	0.3	0.1676	Hspd1	P63038 CH60_MOUSE 60 kDa heat shock protein, mitochondrial OS=Mus musculus GN=Hspd1 PE=1 SV=1
0.4	0.1064	0.5	0.2963	Rps14	P62264 RS14_MOUSE 40S ribosomal protein S14 OS=Mus musculus GN=Rps14 PE=1 SV=3
0.6	0.1077	0.7	0.0426	Usmg5	Q78IK2 USMG5_MOUSE Up-regulated during skeletal muscle growth protein 5 OS=Mus musculus GN=Usmg5 PE=1 SV=1
0.8	0.1105	0.7	0.2750	Eef1d	P57776 EF1D_MOUSE Elongation factor 1-delta OS=Mus musculus GN=Eef1d PE=1 SV=3
0.7	0.1159	0.9	0.5847	Ralb	Q9JIW9 RALB_MOUSE Ras-related protein Ral-B OS=Mus musculus GN=Ralb PE=1 SV=1
2.0	0.1180	0.8	0.7062	Cnbp	P53996 CNBP_MOUSE Cellular nucleic acid-binding protein OS=Mus musculus GN=Cnbp PE=1 SV=2
0.5	0.1194	0.5	0.1262	Eif3g	Q9Z1D1 EIF3G_MOUSE Eukaryotic translation initiation factor 3 subunit G OS=Mus musculus GN=Eif3g PE=1 SV=2
0.2	0.1251	0.3	0.1543	Rpl18	P35980 RL18_MOUSE 60S ribosomal protein L18 OS=Mus musculus GN=Rpl18 PE=1 SV=3
1.6	0.1265	0.3	0.5167	Krt86	P97861 KRT86_MOUSE Keratin, type II cuticular Hb6 OS=Mus musculus GN=Krt86 PE=2 SV=2
0.3	0.1270	0.5	0.0512	Pck2	Q8BH04 PCKGM_MOUSE Phosphoenolpyruvate carboxykinase [GTP], mitochondrial OS=Mus musculus GN=Pck2 PE=1 SV=1
0.4	0.1292	0.4	0.0847	Pmpca	Q9DC61 MPPA_MOUSE Mitochondrial-processing peptidase subunit alpha OS=Mus musculus GN=Pmpca PE=1 SV=1
0.3	0.1332	0.2	0.0057	Pabpc1	P29341 PABP1_MOUSE Polyadenylate-binding protein 1 OS=Mus musculus GN=Pabpc1 PE=1 SV=2
0.7	0.1388	0.7	0.1667	Snx9	Q91VH2 SNX9_MOUSE Sorting nexin-9 OS=Mus musculus GN=Snx9 PE=1 SV=1
1.7	0.1438	1.9	0.1973	Hspa8	P63017 HSP7C_MOUSE Heat shock cognate 71 kDa protein OS=Mus musculus GN=Hspa8 PE=1 SV=1
0.6	0.1481	0.3	0.2245	Ywhae	P62259 1433E_MOUSE 14-3-3 protein epsilon OS=Mus musculus GN=Ywhae PE=1 SV=1
2.5	0.1525	0.6	0.3698	Ncl	P09405 NUCL_MOUSE Nucleolin OS=Mus musculus GN=Ncl PE=1 SV=2
0.2	0.1543	0.2	0.1400	Acaa1a	Q921H8 THIKA_MOUSE 3-ketoacyl-CoA thiolase A, peroxisomal OS=Mus musculus GN=Acaa1a PE=1 SV=1

1.5	0.1655	0.3	0.3476	Lsm8	Q6ZWM4 LSM8_MOUSE U6 snRNA-associated Sm-like protein LSm8 OS=Mus musculus GN=Lsm8 PE=1 SV=3
0.4	0.1682	0.5	0.3067	Rps17	P63276 RS17_MOUSE 40S ribosomal protein S17 OS=Mus musculus GN=Rps17 PE=1 SV=2
0.8	0.1710	0.9	0.5193	1 SV	P01631 KV2A7_MOUSE Ig kappa chain V-II region 26-10 OS=Mus musculus PE=1 SV=1
0.6	0.1713	0.7	0.3771	Rpl5	P47962 RL5_MOUSE 60S ribosomal protein L5 OS=Mus musculus GN=Rpl5 PE=1 SV=3
0.5	0.1769	0.7	0.2733	Slc25a5	P51881 ADT2_MOUSE ADP/ATP translocase 2 OS=Mus musculus GN=Slc25a5 PE=1 SV=3
1.5	0.1869	1.1	0.6485	Hspa5	P20029 GRP78_MOUSE 78 kDa glucose-regulated protein OS=Mus musculus GN=Hspa5 PE=1 SV=3
0.7	0.1901	0.5	0.2594	Fkbp3	Q62446 FKBP3_MOUSE Peptidyl-prolyl cis-trans isomerase FKBP3 OS=Mus musculus GN=Fkbp3 PE=1 SV=2
0.9	0.1952	1.0	0.9224	Actb	P60710 ACTB_MOUSE Actin, cytoplasmic 1 OS=Mus musculus GN=Actb PE=1 SV=1
0.8	0.1965	1.1	0.6801	Ighg1	P01868 IGHG1_MOUSE Ig gamma-1 chain C region secreted form OS=Mus musculus GN=Ighg1 PE=1 SV=1
0.6	0.2047	1.1	0.9255	Pycr2	Q922Q4 P5CR2_MOUSE Pyrroline-5-carboxylate reductase 2 OS=Mus musculus GN=Pycr2 PE=1 SV=1
0.5	0.2056	0.5	0.5325	Eif4b	Q8BGD9 IF4B_MOUSE Eukaryotic translation initiation factor 4B OS=Mus musculus GN=Eif4b PE=1 SV=1
2.5	0.2064	1.4	0.1556	Krt77	Q61FZ6 K2C1B_MOUSE Keratin, type II cytoskeletal 1b OS=Mus musculus GN=Krt77 PE=1 SV=1
1.9	0.2086	1.4	0.2489	Flg2	Q2VIS4 FILA2_MOUSE Filaggrin-2 OS=Mus musculus GN=Flg2 PE=1 SV=2
1.7	0.2125	1.0	0.9208	Rap1b	Q99JI6 RAP1B_MOUSE Ras-related protein Rap-1b OS=Mus musculus GN=Rap1b PE=1 SV=2
0.9	0.2138	1.0	0.7843	Phgdh	Q61753 SERA_MOUSE D-3-phosphoglycerate dehydrogenase OS=Mus musculus GN=Phgdh PE=1 SV=3
0.4	0.2141	0.5	0.2931	Pcbp1	P60335 PCBP1_MOUSE Poly(rC)-binding protein 1 OS=Mus musculus GN=Pcbp1 PE=1 SV=1
0.6	0.2182	0.4	0.0174	Fabp5	Q05816 FABP5_MOUSE Fatty acid-binding protein, epidermal OS=Mus musculus GN=Fabp5 PE=1 SV=3
0.7	0.2197	0.5	0.3645	Rpl12	P35979 RL12_MOUSE 60S ribosomal protein L12 OS=Mus musculus GN=Rpl12 PE=1 SV=2

1.7	0.2208	1.2	0.5830	Krt17	Q9QWL7 K1C17_MOUSE Keratin, type I cytoskeletal 17 OS=Mus musculus GN=Krt17 PE=1 SV=3
1.9	0.2214	1.5	0.3436	Lmna	P48678 LMNA_MOUSE Prelamin-A/C OS=Mus musculus GN=Lmna PE=1 SV=2
0.6	0.2215	0.3	0.1625	Caprin1	Q60865 CAPR1_MOUSE Caprin-1 OS=Mus musculus GN=Caprin1 PE=1 SV=2
0.6	0.2254	0.9	0.6720	Aars	Q8BGQ7 SYAC_MOUSE Alanine--tRNA ligase, cytoplasmic OS=Mus musculus GN=Aars PE=1 SV=1
0.8	0.2305	0.7	0.3256	Rpl11	Q9CXW4 RL11_MOUSE 60S ribosomal protein L11 OS=Mus musculus GN=Rpl11 PE=1 SV=4
1.5	0.2347	0.8	0.4965	Msn	P26041 MOES_MOUSE Moesin OS=Mus musculus GN=Msn PE=1 SV=3
0.9	0.2393	0.7	0.3960	Atp5b	P56480 ATPB_MOUSE ATP synthase subunit beta, mitochondrial OS=Mus musculus GN=Atp5b PE=1 SV=2
0.6	0.2430	0.3	0.2423	Rpl8	P62918 RL8_MOUSE 60S ribosomal protein L8 OS=Mus musculus GN=Rpl8 PE=1 SV=2
1.3	0.2467	1.2	0.4760	Psm2	Q8VDM4 PSMD2_MOUSE 26S proteasome non-ATPase regulatory subunit 2 OS=Mus musculus GN=Psm2 PE=1 SV=1
0.3	0.2505	0.1	0.4301	Krt85	Q9Z2T6 KRT85_MOUSE Keratin, type II cuticular Hb5 OS=Mus musculus GN=Krt85 PE=1 SV=2
0.7	0.2662	0.1	0.3869	Hist1h4a	P62806 H4_MOUSE Histone H4 OS=Mus musculus GN=Hist1h4a PE=1 SV=2
1.9	0.2762	1.2	0.6164	Pkm	P52480 KPYM_MOUSE Pyruvate kinase PKM OS=Mus musculus GN=Pkm PE=1 SV=4
0.2	0.2790	0.3	0.2876	Rpl7a	P12970 RL7A_MOUSE 60S ribosomal protein L7a OS=Mus musculus GN=Rpl7a PE=1 SV=2
0.6	0.2819	0.8	0.3323	Acaa2	Q8BWT1 THIM_MOUSE 3-ketoacyl-CoA thiolase, mitochondrial OS=Mus musculus GN=Acaa2 PE=1 SV=3
2.5	0.2820	1.3	0.3615	Krt19	P19001 K1C19_MOUSE Keratin, type I cytoskeletal 19 OS=Mus musculus GN=Krt19 PE=1 SV=1
0.8	0.2906	0.9	0.7183	Atp5a1	Q03265 ATPA_MOUSE ATP synthase subunit alpha, mitochondrial OS=Mus musculus GN=Atp5a1 PE=1 SV=1
0.8	0.2926	1.1	0.6753	1 SV	P01786 HVM17_MOUSE Ig heavy chain V region MOPC 47A OS=Mus musculus PE=1 SV=1
2.1	0.2974	1.4	0.4263	Afg3l1	Q920A7 AFG31_MOUSE AFG3-like protein 1 OS=Mus musculus GN=Afg3l1 PE=1 SV=2
0.5	0.3004	1.0	0.9328	Tubb4b	P68372 TBB4B_MOUSE Tubulin beta-4B chain OS=Mus musculus GN=Tubb4b PE=1 SV=1

2.1	0.3033	1.7	0.3400	S100a4	P07091 S10A4_MOUSE Protein S100-A4 OS=Mus musculus GN=S100a4 PE=1 SV=1
0.7	0.3048	1.3	0.1972	1 SV	P84751 HVM63_MOUSE Ig heavy chain Mem5 (Fragment) OS=Mus musculus PE=1 SV=1
2.8	0.3056	1.0	0.9411	Krt79	Q8VED5 K2C79_MOUSE Keratin, type II cytoskeletal 79 OS=Mus musculus GN=Krt79 PE=1 SV=2
1.5	0.3126	0.7	0.0971	1 SV	P01837 IGKC_MOUSE Ig kappa chain C region OS=Mus musculus PE=1 SV=1
0.7	0.3132	0.7	0.4824	Suc1g1	Q9WUM5 SUCA_MOUSE Succinate--CoA ligase [ADP/GDP-forming] subunit alpha, mitochondrial OS=Mus musculus GN=Suc1g1 PE=1 SV=4
2.5	0.3219	1.1	0.6992	Krt42	Q6IFX2 K1C42_MOUSE Keratin, type I cytoskeletal 42 OS=Mus musculus GN=Krt42 PE=1 SV=1
2.6	0.3224	1.0	0.9451	Surf4	Q64310 SURF4_MOUSE Surfeit locus protein 4 OS=Mus musculus GN=Surf4 PE=1 SV=1
0.8	0.3239	0.9	0.5654	Ubb	P0CG49 UBB_MOUSE Polyubiquitin-B OS=Mus musculus GN=Ubb PE=2 SV=1
1.9	0.3246	1.3	0.5915	Krt24	A1L317 K1C24_MOUSE Keratin, type I cytoskeletal 24 OS=Mus musculus GN=Krt24 PE=2 SV=2
0.9	0.3250	1.4	0.0985	1 SV	P01657 KV3A5_MOUSE Ig kappa chain V-III region PC 2413 OS=Mus musculus PE=1 SV=1
1.3	0.3261	0.9	0.7317	lqgap1	Q9JKF1 IQGA1_MOUSE Ras GTPase-activating-like protein IQGAP1 OS=Mus musculus GN=lqgap1 PE=1 SV=2
1.7	0.3265	1.1	0.7615	Krt2	Q3TTY5 K22E_MOUSE Keratin, type II cytoskeletal 2 epidermal OS=Mus musculus GN=Krt2 PE=1 SV=1
0.7	0.3271	0.5	0.2802	Rps3	P62908 RS3_MOUSE 40S ribosomal protein S3 OS=Mus musculus GN=Rps3 PE=1 SV=1
0.0	0.3278	0.0	0.4225	Krt84	Q99M73 KRT84_MOUSE Keratin, type II cuticular Hb4 OS=Mus musculus GN=Krt84 PE=2 SV=2
2.1	0.3283	0.8	0.7494	Cd22	P35329 CD22_MOUSE B-cell receptor CD22 OS=Mus musculus GN=Cd22 PE=1 SV=1
1.2	0.3315	1.1	0.7553	Eno1	P17182 ENOA_MOUSE Alpha-enolase OS=Mus musculus GN=Eno1 PE=1 SV=3
1.9	0.3333	1.1	0.6943	Krt5	Q922U2 K2C5_MOUSE Keratin, type II cytoskeletal 5 OS=Mus musculus GN=Krt5 PE=1 SV=1
0.8	0.3424	0.8	0.3141	Baiap2	Q8BKX1 BAIP2_MOUSE Brain-specific angiogenesis inhibitor 1-associated protein 2 OS=Mus musculus GN=Baiap2 PE=1 SV=2

0.0	0.3558	0.2	0.5185	Eif3e	P60229 EIF3E_MOUSE Eukaryotic translation initiation factor 3 subunit E OS=Mus musculus GN=Eif3e PE=1 SV=1
0.8	0.3595	1.0	0.9259	Cct6a	P80317 TCPZ_MOUSE T-complex protein 1 subunit zeta OS=Mus musculus GN=Cct6a PE=1 SV=3
0.8	0.3621	1.0	0.8901	Hsp90ab1	P11499 HS90B_MOUSE Heat shock protein HSP 90-beta OS=Mus musculus GN=Hsp90ab1 PE=1 SV=3
1.9	0.3638	0.2	0.4997	Krt82	Q99M74 KRT82_MOUSE Keratin, type II cuticular Hb2 OS=Mus musculus GN=Krt82 PE=1 SV=2
2.4	0.3640	1.2	0.7313	Krt6a	P50446 K2C6A_MOUSE Keratin, type II cytoskeletal 6A OS=Mus musculus GN=Krt6a PE=1 SV=3
1.2	0.3640	1.3	0.4665	Arf4	P61750 ARF4_MOUSE ADP-ribosylation factor 4 OS=Mus musculus GN=Arf4 PE=1 SV=2
0.7	0.3645	0.4	0.4513	Hist1h1b	P43276 H15_MOUSE Histone H1.5 OS=Mus musculus GN=Hist1h1b PE=1 SV=2
1.0	0.3672	1.0	0.7704	Set	Q9EQU5 SET_MOUSE Protein SET OS=Mus musculus GN=Set PE=1 SV=1
2.8	0.3681	1.6	0.1951	Grn	P28798 GRN_MOUSE Granulins OS=Mus musculus GN=Grn PE=1 SV=2
1.3	0.3700	1.1	0.5243	Prdx1	P35700 PRDX1_MOUSE Peroxiredoxin-1 OS=Mus musculus GN=Prdx1 PE=1 SV=1
1.4	0.3744	1.1	0.6872	Krt10	P02535 K1C10_MOUSE Keratin, type I cytoskeletal 10 OS=Mus musculus GN=Krt10 PE=1 SV=3
0.6	0.3749	0.6	0.1960	Hnrnpa2b1	O88569 ROA2_MOUSE Heterogeneous nuclear ribonucleoproteins A2/B1 OS=Mus musculus GN=Hnrnpa2b1 PE=1 SV=2
1.5	0.3791	1.1	0.4445	Txn	P10639 THIO_MOUSE Thioredoxin OS=Mus musculus GN=Txn PE=1 SV=3
0.7	0.3795	0.4	0.3835	Rps18	P62270 RS18_MOUSE 40S ribosomal protein S18 OS=Mus musculus GN=Rps18 PE=1 SV=3
3.9	0.3812	0.6	0.4039	S100a14	Q9D2Q8 S10AE_MOUSE Protein S100-A14 OS=Mus musculus GN=S100a14 PE=1 SV=1
1.2	0.3848	0.8	0.7435	Krt75	Q8BGZ7 K2C75_MOUSE Keratin, type II cytoskeletal 75 OS=Mus musculus GN=Krt75 PE=1 SV=1
1.8	0.3986	1.3	0.3630	Anxa2	P07356 ANXA2_MOUSE Annexin A2 OS=Mus musculus GN=Anxa2 PE=1 SV=2
0.6	0.3988	0.4	0.3831	Pfn1	P62962 PROF1_MOUSE Profilin-1 OS=Mus musculus GN=Pfn1 PE=1 SV=2
0.8	0.3991	0.9	0.6877	Gapdh	P16858 G3P_MOUSE Glyceraldehyde-3-phosphate dehydrogenase OS=Mus musculus GN=Gapdh PE=1 SV=2

2.0	0.4013	0.9	0.7368	Krt76	Q3UV17 K22O_MOUSE Keratin, type II cytoskeletal 2 oral OS=Mus musculus GN=Krt76 PE=1 SV=1
1.9	0.4071	0.8	0.7621	Tmed9	Q99KF1 TMED9_MOUSE Transmembrane emp24 domain-containing protein 9 OS=Mus musculus GN=Tmed9 PE=1 SV=2
1.8	0.4096	0.9	0.7231	Hmga1	P17095 HMGA1_MOUSE High mobility group protein HMG-I/HMG-Y OS=Mus musculus GN=Hmga1 PE=1 SV=4
0.8	0.4111	0.8	0.4844	Tomm20	Q9DCC8 TOM20_MOUSE Mitochondrial import receptor subunit TOM20 homolog OS=Mus musculus GN=Tomm20 PE=1 SV=1
3.2	0.4161	0.3	0.4053	Pgd	Q9DCD0 6PGD_MOUSE 6-phosphogluconate dehydrogenase, decarboxylating OS=Mus musculus GN=Pgd PE=1 SV=3
0.6	0.4172	1.1	0.8661	Actbl2	Q8BFZ3 ACTBL_MOUSE Beta-actin-like protein 2 OS=Mus musculus GN=Actbl2 PE=1 SV=1
1.9	0.4189	0.8	0.7727	Tpm3	P21107 TPM3_MOUSE Tropomyosin alpha-3 chain OS=Mus musculus GN=Tpm3 PE=1 SV=3
0.7	0.4191	0.9	0.8033	Rnh1	Q91VI7 RINI_MOUSE Ribonuclease inhibitor OS=Mus musculus GN=Rnh1 PE=1 SV=1
2.0	0.4201	1.0	0.9184	Plec	Q9QXS1 PLEC_MOUSE Plectin OS=Mus musculus GN=Plec PE=1 SV=3
1.3	0.4201	1.7	0.2986	Tpi1	P17751 TPIS_MOUSE Triosephosphate isomerase OS=Mus musculus GN=Tpi1 PE=1 SV=4
0.0	0.4207	0.2	0.4243	Hba	P01942 HBA_MOUSE Hemoglobin subunit alpha OS=Mus musculus GN=Hba PE=1 SV=2
2.9	0.4210	0.1	0.3037	Vim	P20152 VIME_MOUSE Vimentin OS=Mus musculus GN=Vim PE=1 SV=3
0.0	0.4226	0.0	0.2096	1 SV	P10404 ENV1_MOUSE MLV-related proviral Env polyprotein OS=Mus musculus PE=1 SV=3
0.0	0.4226	0.0	#DIV/0!	Pcna	P17918 PCNA_MOUSE Proliferating cell nuclear antigen OS=Mus musculus GN=Pcna PE=1 SV=2
1.4	0.4248	0.7	0.1933	Pin4	Q9CWW6 PIN4_MOUSE Peptidyl-prolyl cis-trans isomerase NIMA-interacting 4 OS=Mus musculus GN=Pin4 PE=1 SV=1
121.6	0.4250	0.0	0.4210	Krt15	Q61414 K1C15_MOUSE Keratin, type I cytoskeletal 15 OS=Mus musculus GN=Krt15 PE=1 SV=2
95.4	0.4267	0.5	0.7123	Cct8	P42932 TCPQ_MOUSE T-complex protein 1 subunit theta OS=Mus musculus GN=Cct8 PE=1 SV=3
3.1	0.4317	1.6	0.3340	Gpnmb	Q99P91 GPNMB_MOUSE Transmembrane glycoprotein NMB OS=Mus musculus GN=Gpnmb PE=1 SV=2

1.9	0.4327	1.2	0.6951	Krt16	Q9Z2K1 K1C16_MOUSE Keratin, type I cytoskeletal 16 OS=Mus musculus GN=Krt16 PE=1 SV=3
0.7	0.4372	0.7	0.4717	ldh2	P54071 IDHP_MOUSE Isocitrate dehydrogenase [NADP], mitochondrial OS=Mus musculus GN=ldh2 PE=1 SV=3
1.6	0.4377	0.9	0.7715	Rps15a	P62245 RS15A_MOUSE 40S ribosomal protein S15a OS=Mus musculus GN=Rps15a PE=1 SV=2
1.2	0.4446	0.9	0.7703	Nasp	Q99MD9 NASP_MOUSE Nuclear autoantigenic sperm protein OS=Mus musculus GN=Nasp PE=1 SV=2
2.6	0.4500	0.5	0.3456	Serpinc1	P32261 ANT3_MOUSE Antithrombin-III OS=Mus musculus GN=Serpinc1 PE=1 SV=1
1.3	0.4578	1.1	0.8531	Hsp90aa1	P07901 HS90A_MOUSE Heat shock protein HSP 90-alpha OS=Mus musculus GN=Hsp90aa1 PE=1 SV=4
0.7	0.4600	0.5	0.4041	Aldh2	P47738 ALDH2_MOUSE Aldehyde dehydrogenase, mitochondrial OS=Mus musculus GN=Aldh2 PE=1 SV=1
1.4	0.4662	0.6	0.3075	Myl6	Q60605 MYL6_MOUSE Myosin light polypeptide 6 OS=Mus musculus GN=Myl6 PE=1 SV=3
0.6	0.4685	0.7	0.5957	Rps25	P62852 RS25_MOUSE 40S ribosomal protein S25 OS=Mus musculus GN=Rps25 PE=1 SV=1
1.6	0.4722	0.5	0.6352	Krt35	Q49714 KRT35_MOUSE Keratin, type I cuticular Ha5 OS=Mus musculus GN=Krt35 PE=1 SV=1
1.5	0.4871	1.0	0.8430	Krt1	P04104 K2C1_MOUSE Keratin, type II cytoskeletal 1 OS=Mus musculus GN=Krt1 PE=1 SV=4
0.8	0.4873	0.2	0.3762	Hist1h1t	Q07133 H1T_MOUSE Histone H1t OS=Mus musculus GN=Hist1h1t PE=1 SV=4
1.3	0.4887	0.8	0.3693	Edf1	Q9JMG1 EDF1_MOUSE Endothelial differentiation-related factor 1 OS=Mus musculus GN=Edf1 PE=1 SV=1
0.3	0.4942	0.5	0.5722	Anxa1	P10107 ANXA1_MOUSE Annexin A1 OS=Mus musculus GN=Anxa1 PE=1 SV=2
1.8	0.5031	1.0	0.8884	Jup	Q02257 PLAK_MOUSE Junction plakoglobin OS=Mus musculus GN=Jup PE=1 SV=3
0.9	0.5090	1.1	0.3626	Capzb	P47757 CAPZB_MOUSE F-actin-capping protein subunit beta OS=Mus musculus GN=Capzb PE=1 SV=3
1.5	0.5103	0.5	0.2462	Eif1ax	Q8BMJ3 IF1AX_MOUSE Eukaryotic translation initiation factor 1A, X-chromosomal OS=Mus musculus GN=Eif1ax PE=2 SV=3
0.8	0.5108	0.5	0.3906	Rps5	P97461 RS5_MOUSE 40S ribosomal protein S5 OS=Mus musculus GN=Rps5 PE=1 SV=3

3.2	0.5122	0.2	0.2663	Ppid	Q9CR16 PPID_MOUSE Peptidyl-prolyl cis-trans isomerase D OS=Mus musculus GN=Ppid PE=1 SV=3
2.1	0.5129	0.6	0.3179	Rps4x	P62702 RS4X_MOUSE 40S ribosomal protein S4, X isoform OS=Mus musculus GN=Rps4x PE=1 SV=2
0.8	0.5151	1.1	0.8843	Tubb5	P99024 TBB5_MOUSE Tubulin beta-5 chain OS=Mus musculus GN=Tubb5 PE=1 SV=1
1.9	0.5227	0.9	0.8192	Dsp	E9Q557 DESP_MOUSE Desmoplakin OS=Mus musculus GN=Dsp PE=1 SV=1
2.4	0.5233	0.1	0.4644	Krt33a	Q8K0Y2 KT33A_MOUSE Keratin, type I cuticular Ha3-I OS=Mus musculus GN=Krt33a PE=1 SV=1
0.6	0.5234	5.0	0.2244	Ppia	P17742 PPIA_MOUSE Peptidyl-prolyl cis-trans isomerase A OS=Mus musculus GN=Ppia PE=1 SV=2
0.6	0.5245	0.5	0.2535	Tfrc	Q62351 TFR1_MOUSE Transferrin receptor protein 1 OS=Mus musculus GN=Tfrc PE=1 SV=1
0.6	0.5357	0.6	0.5519	Gart	Q64737 PUR2_MOUSE Trifunctional purine biosynthetic protein adenosine-3 OS=Mus musculus GN=Gart PE=1 SV=3
0.8	0.5372	0.9	0.6470	Kbtbd4	Q8R179 KBTB4_MOUSE Kelch repeat and BTB domain-containing protein 4 OS=Mus musculus GN=Kbtbd4 PE=2 SV=1
0.9	0.5560	0.9	0.7244	Igk-V19-17	P01633 KV5A1_MOUSE Ig kappa chain V19-17 OS=Mus musculus GN=Igk-V19-17 PE=1 SV=1
1.3	0.5658	1.1	0.9014	Ptpn6	P29351 PTN6_MOUSE Tyrosine-protein phosphatase non-receptor type 6 OS=Mus musculus GN=Ptpn6 PE=1 SV=2
0.7	0.5662	0.5	0.2255	Apex1	P28352 APEX1_MOUSE DNA-(apurinic or apyrimidinic site) lyase OS=Mus musculus GN=Apex1 PE=1 SV=2
0.4	0.5670	1.8	0.6237	Krt73	Q6NXH9 K2C73_MOUSE Keratin, type II cytoskeletal 73 OS=Mus musculus GN=Krt73 PE=1 SV=1
0.9	0.5724	0.4	0.0908	Stip1	Q60864 STIP1_MOUSE Stress-induced-phosphoprotein 1 OS=Mus musculus GN=Stip1 PE=1 SV=1
1.1	0.5794	1.0	0.9563	Rpl22	P67984 RL22_MOUSE 60S ribosomal protein L22 OS=Mus musculus GN=Rpl22 PE=1 SV=2
0.9	0.5980	0.7	0.2393	Rps20	P60867 RS20_MOUSE 40S ribosomal protein S20 OS=Mus musculus GN=Rps20 PE=1 SV=1
0.9	0.5983	0.7	0.3769	Calml3	Q9D6P8 CALL3_MOUSE Calmodulin-like protein 3 OS=Mus musculus GN=Calml3 PE=2 SV=1

0.9	0.6001	0.8	0.4613	Sprr2b	O70554 SPR2B_MOUSE Small proline-rich protein 2B OS=Mus musculus GN=Sprr2b PE=2 SV=1
0.8	0.6008	0.9	0.8427	Ipo5	Q8BK55 IPO5_MOUSE Importin-5 OS=Mus musculus GN=Ipo5 PE=1 SV=3
1.1	0.6030	0.7	0.5023	Cct4	P80315 TCPD_MOUSE T-complex protein 1 subunit delta OS=Mus musculus GN=Cct4 PE=1 SV=3
1.7	0.6075	3.9	0.4787	Cct2	P80314 TCPB_MOUSE T-complex protein 1 subunit beta OS=Mus musculus GN=Cct2 PE=1 SV=4
1.5	0.6080	0.9	0.7814	Krt14	Q61781 K1C14_MOUSE Keratin, type I cytoskeletal 14 OS=Mus musculus GN=Krt14 PE=1 SV=2
1.3	0.6125	0.7	0.3664	Naca	Q60817 NACA_MOUSE Nascent polypeptide-associated complex subunit alpha OS=Mus musculus GN=Naca PE=1 SV=1
0.8	0.6251	1.0	0.9150	Hspa9	P38647 GRP75_MOUSE Stress-70 protein, mitochondrial OS=Mus musculus GN=Hspa9 PE=1 SV=3
1.3	0.6370	0.5	0.3415	Eif4a1	P60843 IF4A1_MOUSE Eukaryotic initiation factor 4A-I OS=Mus musculus GN=Eif4a1 PE=1 SV=1
1.1	0.6438	1.0	0.9063	Eef2	P58252 EF2_MOUSE Elongation factor 2 OS=Mus musculus GN=Eef2 PE=1 SV=2
1.2	0.6489	0.7	0.4805	Rps7	P62082 RS7_MOUSE 40S ribosomal protein S7 OS=Mus musculus GN=Rps7 PE=2 SV=1
1.1	0.6539	0.9	0.7410	Ddx3x	Q62167 DDX3X_MOUSE ATP-dependent RNA helicase DDX3X OS=Mus musculus GN=Ddx3x PE=1 SV=3
0.8	0.6553	0.5	0.3184	Vdac2	Q60930 VDAC2_MOUSE Voltage-dependent anion-selective channel protein 2 OS=Mus musculus GN=Vdac2 PE=1 SV=2
1.2	0.6604	0.8	0.2053	Atpif1	O35143 ATIF1_MOUSE ATPase inhibitor, mitochondrial OS=Mus musculus GN=Atpif1 PE=1 SV=2
1.3	0.6765	1.1	0.8975	Hadhb	Q99JY0 ECHB_MOUSE Trifunctional enzyme subunit beta, mitochondrial OS=Mus musculus GN=Hadhb PE=1 SV=1
0.9	0.6779	0.5	0.2725	Rps12	P63323 RS12_MOUSE 40S ribosomal protein S12 OS=Mus musculus GN=Rps12 PE=1 SV=2
0.9	0.6849	1.0	0.7934	Acadl	P51174 ACADL_MOUSE Long-chain specific acyl-CoA dehydrogenase, mitochondrial OS=Mus musculus GN=Acadl PE=1 SV=2
2.0	0.6875	0.0	0.2685	Rpn1	Q91YQ5 RPN1_MOUSE Dolichyl-diphosphooligosaccharide--protein

					glycosyltransferase subunit 1 OS=Mus musculus GN=Rpn1 PE=1 SV=1
0.9	0.6887	0.7	0.4601	1 SV	P01823 HVM47_MOUSE Ig heavy chain V region 36-60 OS=Mus musculus PE=1 SV=1
0.9	0.6968	0.8	0.5367	Ran	P62827 RAN_MOUSE GTP-binding nuclear protein Ran OS=Mus musculus GN=Ran PE=1 SV=3
0.8	0.6974	0.4	0.3323	Eif3b	Q8JZQ9 EIF3B_MOUSE Eukaryotic translation initiation factor 3 subunit B OS=Mus musculus GN=Eif3b PE=1 SV=1
0.9	0.7093	1.1	0.6266	Psma5	Q9Z2U1 PSA5_MOUSE Proteasome subunit alpha type-5 OS=Mus musculus GN=Psma5 PE=1 SV=1
0.7	0.7185	0.4	0.5613	Lyz1	P17897 LYZ1_MOUSE Lysozyme C-1 OS=Mus musculus GN=Lyz1 PE=1 SV=1
1.4	0.7252	0.5	0.1602	Cycs	P62897 CYC_MOUSE Cytochrome c, somatic OS=Mus musculus GN=Cycs PE=1 SV=2
0.9	0.7257	0.7	0.6251	Sord	Q64442 DHSO_MOUSE Sorbitol dehydrogenase OS=Mus musculus GN=Sord PE=1 SV=3
1.3	0.7384	0.8	0.7254	Ubap2l	Q80X50 UBP2L_MOUSE Ubiquitin-associated protein 2-like OS=Mus musculus GN=Ubap2l PE=1 SV=1
1.1	0.7393	0.8	0.6353	Eif2s3x	Q9Z0N1 IF2G_MOUSE Eukaryotic translation initiation factor 2 subunit 3, X-linked OS=Mus musculus GN=Eif2s3x PE=1 SV=2
1.1	0.7406	0.8	0.5626	Rpl9	P51410 RL9_MOUSE 60S ribosomal protein L9 OS=Mus musculus GN=Rpl9 PE=2 SV=2
0.9	0.7429	1.6	0.0324	Tuba1c	P68373 TBA1C_MOUSE Tubulin alpha-1C chain OS=Mus musculus GN=Tuba1c PE=1 SV=1
0.9	0.7469	1.0	0.9013	Dnaja2	Q9QYJ0 DNJA2_MOUSE DnaJ homolog subfamily A member 2 OS=Mus musculus GN=Dnaja2 PE=1 SV=1
0.9	0.7665	0.6	0.2755	Serbp1	Q9CY58 PAIRB_MOUSE Plasminogen activator inhibitor 1 RNA-binding protein OS=Mus musculus GN=Serbp1 PE=1 SV=2
1.1	0.7800	1.1	0.5363	Eef1a1	P10126 EF1A1_MOUSE Elongation factor 1-alpha 1 OS=Mus musculus GN=Eef1a1 PE=1 SV=3
0.8	0.7800	30.6	0.4113	Spata16	Q8C636 SPT16_MOUSE Spermatogenesis-associated protein 16 OS=Mus musculus GN=Spata16 PE=2 SV=1
1.2	0.8142	0.2	0.2900	Myl12b	Q3THE2 ML12B_MOUSE Myosin regulatory light chain 12B OS=Mus musculus GN=Myl12b PE=1 SV=2
1.0	0.8228	0.7	0.4363	Ces1	Q8VCC2 EST1_MOUSE Liver carboxylesterase 1 OS=Mus musculus GN=Ces1 PE=1 SV=1

1.0	0.8268	0.8	0.6279	Pgk1	P09411 PGK1_MOUSE Phosphoglycerate kinase 1 OS=Mus musculus GN=Pgk1 PE=1 SV=4
0.9	0.8269	0.7	0.4323	Rps10	P63325 RS10_MOUSE 40S ribosomal protein S10 OS=Mus musculus GN=Rps10 PE=1 SV=1
0.9	0.8287	0.8	0.5267	Nono	Q99K48 NONO_MOUSE Non-POU domain-containing octamer-binding protein OS=Mus musculus GN=Nono PE=1 SV=3
0.7	0.8329	0.0	0.2210	Rps13	P62301 RS13_MOUSE 40S ribosomal protein S13 OS=Mus musculus GN=Rps13 PE=1 SV=2
0.9	0.8340	1.0	0.9855	Klk14	Q8CGR5 KLK14_MOUSE Kallikrein-14 OS=Mus musculus GN=Klk14 PE=2 SV=1
1.0	0.8398	0.7	0.5268	Aldoa	P05064 ALDOA_MOUSE Fructose-bisphosphate aldolase A OS=Mus musculus GN=Aldoa PE=1 SV=2
1.0	0.8523	1.3	0.0897	Ptma	P26350 PTMA_MOUSE Prothymosin alpha OS=Mus musculus GN=Ptma PE=1 SV=2
1.1	0.8525	3.9	0.2709	Acadm	P45952 ACADM_MOUSE Medium-chain specific acyl-CoA dehydrogenase, mitochondrial OS=Mus musculus GN=Acadm PE=1 SV=1
1.1	0.8557	0.8	0.7475	Pfkl	P12382 PFKAL_MOUSE ATP-dependent 6-phosphofructokinase, liver type OS=Mus musculus GN=Pfkl PE=1 SV=4
1.0	0.8574	1.1	0.4995	Itih1	Q61702 ITIH1_MOUSE Inter-alpha-trypsin inhibitor heavy chain H1 OS=Mus musculus GN=Itih1 PE=1 SV=2
0.9	0.8633	1.0	0.9196	Csn1s1	P19228 CASA1_MOUSE Alpha-S1-casein OS=Mus musculus GN=Csn1s1 PE=2 SV=1
1.0	0.8734	1.0	0.9169	Tcp1	P11983 TCPA_MOUSE T-complex protein 1 subunit alpha OS=Mus musculus GN=Tcp1 PE=1 SV=3
1.0	0.8748	0.5	0.2290	Fus	P56959 FUS_MOUSE RNA-binding protein FUS OS=Mus musculus GN=Fus PE=1 SV=1
1.0	0.8943	0.4	0.4760	Lcp1	Q61233 PLSL_MOUSE Plastin-2 OS=Mus musculus GN=Lcp1 PE=1 SV=4
1.0	0.8944	0.9	0.7717	Sec61b	Q9CQS8 SC61B_MOUSE Protein transport protein Sec61 subunit beta OS=Mus musculus GN=Sec61b PE=1 SV=3
1.0	0.8965	0.7	0.3001	Rps19	Q9CZX8 RS19_MOUSE 40S ribosomal protein S19 OS=Mus musculus GN=Rps19 PE=1 SV=3
1.0	0.9065	0.7	0.3168	Npm1	Q61937 NPM_MOUSE Nucleophosmin OS=Mus musculus GN=Npm1 PE=1 SV=1
0.9	0.9107	2.2	0.2121	Krt13	P08730 K1C13_MOUSE Keratin, type I cytoskeletal 13 OS=Mus musculus GN=Krt13 PE=1 SV=2

0.9	0.9145	0.1	0.1329	Sars	P26638 SYSC_MOUSE Serine--tRNA ligase, cytoplasmic OS=Mus musculus GN=Sars PE=1 SV=3
0.9	0.9184	0.7	0.5583	Slc22a21	Q9WTN6 S22AL_MOUSE Solute carrier family 22 member 21 OS=Mus musculus GN=Slc22a21 PE=2 SV=1
1.0	0.9345	0.8	0.6946	Ranbp1	P34022 RANG_MOUSE Ran-specific GTPase-activating protein OS=Mus musculus GN=Ranbp1 PE=1 SV=2
1.0	0.9482	1.4	0.5298	Ndufa4	Q62425 NDUA4_MOUSE Cytochrome c oxidase subunit NDUFA4 OS=Mus musculus GN=Ndufa4 PE=1 SV=2
1.0	0.9510	0.7	0.3792	Eif2s1	Q6ZWX6 IF2A_MOUSE Eukaryotic translation initiation factor 2 subunit 1 OS=Mus musculus GN=Eif2s1 PE=1 SV=3
1.0	0.9589	1.0	0.9402	Eif5a	P63242 IF5A1_MOUSE Eukaryotic translation initiation factor 5A-1 OS=Mus musculus GN=Eif5a PE=1 SV=2
1.0	0.9659	1.0	0.9524	Farsa	Q8C0C7 SYFA_MOUSE Phenylalanine--tRNA ligase alpha subunit OS=Mus musculus GN=Farsa PE=1 SV=1
1.0	0.9821	0.9	0.4229	Cfl1	P18760 COF1_MOUSE Cofilin-1 OS=Mus musculus GN=Cfl1 PE=1 SV=3
1.0	0.9838	0.3	0.2818	Ywhaz	P63101 1433Z_MOUSE 14-3-3 protein zeta/delta OS=Mus musculus GN=Ywhaz PE=1 SV=1
1.0	0.9896	1.1	0.7859	Rtn4	Q99P72 RTN4_MOUSE Reticulon-4 OS=Mus musculus GN=Rtn4 PE=1 SV=2
1.0	0.9914	0.9	0.7611	Rab1b	Q9D1G1 RAB1B_MOUSE Ras-related protein Rab-1B OS=Mus musculus GN=Rab1b PE=1 SV=1
0.0	#DIV/0!	4.0	0.5358	Eef1g	Q9D8N0 EF1G_MOUSE Elongation factor 1-gamma OS=Mus musculus GN=Eef1g PE=1 SV=3

Supplementary table 2: Mass spectrometry data.

9.2 List of figures

Fig. 1: Simplified scheme of basal ganglia system	18
Fig. 2: ICC of primary microglial culture isolated from 2-4 days old wildtype (a) and Dj-1 knockout (b) littermates using the microglial marker ionized calcium-binding adapter molecule 1 (IBA-1)	41
Fig. 3: ICC of primary microglia during the course of LPS treatment	43
Fig. 4: mRNA expression analysis of <i>Mthfr</i> in wildtype and Dj-1 knockout primary microglia under basal condition	44
Fig. 5: mRNA expression analysis of <i>Mthfr</i> in wildtype and Dj-1 knockout primary microglia .	45
Fig. 6: Shown are the different transcripts of <i>Mthfr</i>	46
Fig. 7: Detection of MTHFR in wildtype and Dj-1 knockout primary microglia under basal conditions and after LPS treatment (24hours) using Western blot	47
Fig. 8: Metabolic map of several cycles with connection to MTHFR. Modified from Bistulfi ..	49
Fig. 9: ELISA for methylated DNA in wildtype and Dj-1 knockout primary microglia	49
Fig. 10: mRNA expression analysis of <i>Mthfr</i> (a) and <i>iNos</i> (b) in wildtype and Dj-1 knockout primary microglia under different conditions	52
Fig. 11: <i>Mthfr</i> transcripts map, green bars indicate predicted Nurr1 binding sites; (b) Validation of Nurr1 and Dj-1 overexpression constructs in HEK293 cells by Western Blot; (c), (d), (e) Luciferase activity assay with different <i>Mthfr</i> promoters cloned under luciferase gene	54
Fig. 12: (a) Core of the Nurr1 binding sequence in the promoter of the <i>Mthfr</i> -004 transcript (from MatBase 9.1(c) Genomatix); Luciferase activity assay with (b) wildtype promoter <i>Mthfr</i> -004 and (c) the mutated sequence: AGGC substituted by GACG, (d) mutated sequence: AGGC substituted by CCAA	55
Fig. 13: mRNA expression analysis in primary microglia (a) <i>Nurr1</i> , (b) <i>Mthfr</i> and (c) <i>iNos</i>	56
Fig. 14: mRNA expression analysis of selected inflammatory genes in the SIM A9 cell line upon LPS treatment	59
Fig. 15: Fragments of Dj-1 murine genomic sequences represent in blue, (a) first coding exon of Dj-1 and (b) second coding exon of Dj-1	60
Fig. 16: Visualization of the performed T7 assay on an agarose gel	61
Fig. 17: Alignments of clone sequences with the genomic target region of Dj-1 (from Benchling.com)	62

Fig. 18: Alignments of sub clone N2 clone N10 sequences with a genomic target region of Dj-1	63
Fig. 19: Protein expression analysis for Dj-1 in Dj-1 knockout candidates sub clones and wildtype sub clones	63
Fig. 20: Western blot for NFkB pathway activation during course of LPS treatment in SIM A9 wildtype and Dj-1 knockout cells	65
Fig. 21: Western blot for ERK pathway activation during course of LPS treatment in SIM A9 wildtype and Dj-1 knockout cells	66
Fig. 22: Western blot for P38 pathway activation during course of LPS treatment in SIM A9 wildtype and Dj-1 knockout cells	67
Fig. 23: mRNA expression analysis for <i>Mthfr</i> and <i>iNos</i> in SIM A9 cells under basal conditions and after LPS treatment (8 hours)	68
Fig. 24: mRNA expression analysis for <i>Mthfr</i> in (a) MEFs from wildtype and Dj-1 knockout embryos, (b) liver lysates from 2-4 days old pups and (c) primary microglia from 2-4 days old pups	69
Fig. 25: Western blot for testing the conditions in Dj-1 Co-IP	70
Fig. 26: Western blots of validation of Dj-1 possible interaction with Scl25a3, ATP1a3 and Plscr4 under basal and LPS treatment conditions	73
Fig. 27: Western blots of validation of Dj-1 possible interaction with Scl25a3, ATP1a3 and Plscr4 under basal and LPS treatment conditions	73
Fig. 28: mRNA expression analysis for Hadha, Catalase and Srm in (a) SIM A9 wildtype clone N38-1 and Dj-1 knockout clone N10-2 and (b) SIM A9 wildtype clones N57, 60, 61 and Dj-1 knockout clones N50, 78, 79	74
Fig. 29: Western blot analysis for Catalase and Srm in (a) SIM A9 wildtype clone N38-1 and Dj-1 knockout clone N10-2, (b) SIM A9 wildtype clones N57, 60, 61 and Dj-1 knockout clones N50, 78, 79	75
Fig. 30: Western blot analysis for Slc25a3, Plscr4 and ATP1a3 in (a) SIM A9 wildtype clone N38-1 and Dj-1 knockout clone N10-2, (b) SIM A9 wildtype clones N57, 60, 61 and Dj-1 knockout clones N50, 78, 79	76
Fig. 31: Examples of (a) the oxygen consumption rate (OCR) and (b) the extracellular acidification rate (ECAR) in a routine run on a Seahorse XF96 analyzer	78
Fig. 32: Respiratory analysis using a Seahorse XF96 analyzer with three wildtype and three Dj-1 knockout SIM A9 clones with 25mM glucose only during the time frame of the experiment	79

Fig. 33: ECAR values from the seahorse experiment with three wildtype and three Dj-1 knockout SIM A9 clones with only 25mM glucose supplemented during the time frame of the experiment	80
Fig. 34: Respiratory analysis using a Seahorse XF96 analyzer with three wildtype and three Dj-1 knockout SIM A9 clones with only 25mM glucose supplemented plus LPS treatment during the time frame of the experiment	81
Fig. 35: ECAR values from seahorse experiment with three wildtype and three Dj-1 knockout SIM A9 clones with only 25mM glucose supplemented plus LPS treatment during the time frame of the experiment	82
Fig. 36: OCR and ECAR values from seahorse experiment with three wildtype and three Dj-1 knockout SIM A9 clones with only 25mM glucose supplemented under basal and LPS treatment conditions	83
Fig. 37: Respiratory analysis using a Seahorse XF96 analyzer with three wildtype and three Dj-1 knockout SIM A9 clones with only 5mM pyruvate supplemented under basal and LPS treatment conditions	85
Fig. 38: Lactate content normalized to μg of DNA in SIM A9 wildtype and Dj-1 knockout cells	86
Fig. 39: Western blot results represent mitochondrial complexes abundance in wildtype and Dj-1 knockout SIM A9 cells	87
Supplementary fig. 1: Western blots of Dj-1 IP optimization experiments	140

9.3 List of tables

Table 1: Braak stages of idiopathic Parkinson's disease	21
Table 2: Genes involved in monogenic forms of Parkinson's disease	23
Table 3: Metabolites differences in the ventral midbrain of wildtype and Dj-1 knockout mice discovered by targeted metabolomic analysis	50
Table 4: Transcription factors known to interact with Dj-1 or to regulate common pathways	53
Table 5: Table represents the results obtained by a first test mass spectrometry experiment with n=1 of wildtype and Dj-1 knockout primary microglia under control conditions and n=2 of wildtype and Dj-1 knockout primary microglia after LPS treatment (4 hours)	58
Table 6: Table represents IP conditions which were used during Dj-1 IP optimization procedure	71

Table 7: Table represents part of mass spectrometry results of Dj-1 interactome in SIM A9 cells	72
Table 8: Equipment	109
Table 9: Chemicals	110
Table 10: General consumables	112
Table 11: Cell culture consumables	113
Table 12: Commercial kits	115
Table 13: Solutions and buffers	116
Table 14: Primary antibodies	118
Table 15: Secondary antibodies	120
Table 16: Enzymes	121
Table 17: Primers	121
Table 18: DNA vectors	122
Table 19: Taqman Probes	123
Table 20: Cell lines	123
Table 21: Bacterial strains	124
Table 22: Mouse strains	124
Table 23: Plasmids combination for different conditions of HEK293 luciferase assay	128
Table 24: The main parameters of LPS treatment experiments	129
Table 25: MicroWin32 luminometer software settings	133
Table 26: qRT-PCR Program	135
Table 27: Seahorse program of experiment with SIM A9 cells	139
Supplementary table 1: Calculations of western blots of Dj-1 IP optimization experiments represented in supplementary figure 1	146
Supplementary table 2: Mass spectrometry data	150

9.4 List of abbreviations

2-DG	2-deoxyglucose
6-OHDA	6-hydroxy dopamine
AAV	Adeno-associated virus
AB	Antibody
AD	Autosomal dominant
AGEs	Advance glycated end products
AKT	Protein kinase B
AR	Autosomal recessive
ARE	Adenylate-uridylate-rich elements
ASK1	Apoptosis signal-regulating kinase 1
ATP13A2	Probable cation-transporting ATPase 13A2
ATP1A3	Sodium/potassium-transporting ATPase subunit alpha-3
ATXN	Ataxin
BAX	Bcl-2-associated X protein
BG	Basal ganglia
BM	Bowel movement
BS	Brain stem
CCK	Cholecystokinin
CCL2	CC-motif ligand 2
CHCHD2	Coiled-coil-helix-coiled-coil-helix domain containing 2
CNS	Central nervous system
COREST	REST corepressor 1
CSF	Cerebrospinal fluid
Cu(II)ATSM	Copper(II)-diacetyl-di(N4-methylthiosemicarbazone)
CXCL10	C-X-C motif chemokine 10
DAPI	4',6-diamidino-2-phenylindole
DAT	Dopamine transporter
DAXX	Death domain-associated protein 6
dcSAM	Decarboxylated S-Adenosylmethionine
DCTN1	Dynactin subunit 1
DDC	4-dihydroxy-l-phenylalanine decarboxylase
DNAJC6	Putative tyrosine-protein phosphatase auxilin
DOPAL	3,4-dihydroxyphenyl-acetaldehyde
DRD1	Dopamine receptor D1
DRD2	Dopamine receptor D2
DUSP1	Dual-specificity phosphate 1
ECAR	Extracellular acidification rate
EGF	Epidermal growth factor
EIF4G1	Eukaryotic translation initiation factor 4 gamma

eIF5A	Eukaryotic initiation factor 5A
Elk	ETS-domain containing protein transcription factor
ERK	Extracellular signal regulated kinase
ES cells	Embryonic stem cells
ETC	Electron transport chain
FBX07	F-box only protein 7
FCCP	Carbonyl cyanide 4-(trifluoromethoxy) phenylhydrazone
FDR	False discovery rate
FIZZ1	Found in inflammatory zone 1
FMR1	Fragile X mental retardation 1
GABA	Gamma-Aminobutyric acid
GAPDH	Glyceraldehyde 3-phosphate dehydrogenase
GFAP	Glial fibrillary acidic protein
Glu	Glutamine
GO	Glyoxal
GPe	Globus pallidus external
GPi	Globus pallidus internal
GWAS	Genome-wide association study
Hadha	Mitochondrial trifunctional enzyme subunit alpha
HER3	Human epidermal growth factor receptor 3
HPRT	Hypoxanthine-guanine phosphoribosyltransferase
HSC70	Lysosomal 70 kDa heat-shock cognate protein
Hsp70	Heat shock protein, 70kDa
Hz	Hertz
IBA-1	Ionized calcium-binding adapter molecule 1
ICAM-1	Intercellular adhesion molecule 1
IFN- γ	Interferon gamma
IL	Interleukin
IL-1RA	IL-1 receptor antagonist
IRF3	Interferon regulatory factor 3
JNK	c-Jun N-terminal kinase
Keap1	Kelch-like ECH-associated protein 1
LAMP2A	Lysosome-associated membrane protein 2a
LB	Lewy bodies
LC	Locus ceruleus
LDLR	Low-density lipoprotein receptor
L-Dopa	L-3,4-dihydroxyphenylalanine
LPS	Lipopolysaccharide
LRRK2	Leucine rich repeat kinase 2
MED7	Mediator of RNA polymerase II transcription subunit 7
MEF	Mouse embryonic fibroblasts

MG	Methylglyoxal
MHC	Major histocompatibility complex
Mib2	Mind bomb-2 protein
MPP+	1-methyl-4-phenylpyridinium
MPTP	1-methyl-4-phenyl-1,2,3,6-tetrahydropyridine
MS	Mass spectrometry
MTA	5-methylthioadenosine
MTHFR	Methylene tetrahydrofolate reductase
NADPH	Nicotinamide adenine dinucleotide
NFkB	Nuclear factor kappa-light-chain-enhancer of activated B-cells
NMDA	N-Methyl-D-aspartic acid
NO	Nitric oxide
NOS	Nitric oxide synthases
Nrf2	Nuclear factor (erythroid-derived 2)-like 2
NRG-1	Neuregulin 1
Nurr1	Nuclear receptor related 1 protein
OCR	Oxygen consumption rate
OMM	Outer mitochondrial membrane
OR	Odds ratio
p38	p38 mitogen-activated protein kinase
p53	Tumor protein p53
PAK4	p21-activated kinase 4
PAMPs	Pathogen associated molecular patterns
PANK2	Pantothenate kinase 2, mitochondrial
PD	Parkinson's disease
PDTC	Ammonium pyrrolidinedithiocarbamate
PET	Positron emission tomography
PI3K	Phosphoinositide 3-kinase
PIASx α	Protein inhibitor of activated STAT x-alpha
PINK-1	PTEN-induced putative kinase 1
PLA2G6	Calcium-independent phospholipase A2
Plscr4	Phospholipid scramblase 4
pNPA	4-nitrophenyl acetate
POLG1	DNA polymerase subunit gamma
PPAR γ	Peroxisome proliferator-activated receptor gamma
PPP	Pentose phosphate pathway
PRAK	p38 regulated/activated kinase
PSF	Pyrimidine tract-binding protein-associated splicing factor
PTEN	Phosphatase and tensin homolog
rAAV	Recombinant adeno-associated virus
RAB39B	Ras-related protein Rab-39B

RDP	Rapid-onset dystonia parkinsonism
REM	Rapid eye movement
Ret	Receptor tyrosine kinase
ROS	Reactive oxygen species
RREBP1	Ras-responsive element binding protein 1
SAH	S-Adenosylhomocysteine
SAM	S-Adenosylmethionine
SETD6	N-lysine methyltransferase SET-domain containing 6 protein
SHP-1	Src-homology region 2 domain-containing phosphatase-1
SIRT1	Sirtuin-1
Slc25a3	Mitochondrial phosphate carrier
Sms	Spermine synthase
SN	Substantia nigra
SNCA	α -synuclein
SNP	Single-nucleotide polymorphism
SNpc	Substantia nigra pars compacta
SNpr	Substantia nigra pars reticulate
SOD	Superoxide dismutase
SPECT	Single-photon emission computed tomography
SRE	Sterol regulatory element
SREBP	Sterol regulatory element binding protein
Srm	Spermidine synthase
STAT1	Signal transducer and activator of transcription 1
STN	Subthalamic nucleus
TCA	Tricarboxylic acid
TF	Transcription factor
TGF- β	Transforming growth factor β
TH	Tyrosine hydroxylase
TLR	Toll-like receptor
TNF- α	Tumor necrosis factor- α
Trx1	Thioredoxin 1
TSS	Transcription starting site
UCP	Uncoupling protein
VMAT2	Vesicular monoamine transporter 2
VPS35	Vacuolar protein sorting-associated protein 35
YM1	Mouse homolog chitinase 3 like 1

10 Bibliography

Aarsland, D., Andersen, K., Larsen, J.P., Perry, R., Wentzel-Larsen, T., Lolk, A., and Kragh-Sørensen, P. (2004). The rate of cognitive decline in Parkinson disease. *Arch. Neurol.* *61*, 1906–1911.

Aarsland, D., Zaccai, J., and Brayne, C. (2005). A systematic review of prevalence studies of dementia in Parkinson's disease. *Mov. Disord.* *20*, 1255–1263.

Abbott, R.D., Petrovitch, H., White, L.R., Masaki, K.H., Tanner, C.M., Curb, J.D., Grandinetti, A., Blanchette, P.L., Popper, J.S., and Ross, G.W. (2001). Frequency of bowel movements and the future risk of Parkinson's disease. *Neurology* *57*, 456–462.

Abou-Sleiman, P.M., Healy, D.G., Quinn, N., Lees, A.J., and Wood, N.W. (2003). The role of pathogenic DJ-1 mutations in Parkinson's disease. *Ann. Neurol.* *54*, 283–286.

Agnati, L.F., Ferré, S., Genedani, S., Leo, G., Guidolin, D., Filaferro, M., Carriba, P., Casadó, V., Lluís, C., Franco, R., et al. (2006). Allosteric modulation of dopamine D2 receptors by homocysteine. *J. Proteome Res.* *5*, 3077–3083.

Akundi, R.S., Huang, Z., Eason, J., Pandya, J.D., Zhi, L., Cass, W.A., Sullivan, P.G., and Büeler, H. (2011). Increased mitochondrial calcium sensitivity and abnormal expression of innate immunity genes precede dopaminergic defects in Pink1-deficient mice. *PLoS ONE* *6*, e16038.

Aleyasin, H., Rousseaux, M.W.C., Phillips, M., Kim, R.H., Bland, R.J., Callaghan, S., Slack, R.S., During, M.J., Mak, T.W., and Park, D.S. (2007). The Parkinson's disease gene DJ-1 is also a key regulator of stroke-induced damage. *Proc Natl Acad Sci U S A* *104*, 18748–18753.

Aleyasin, H., Rousseaux, M.W.C., Marcogliese, P.C., Hewitt, S.J., Irrcher, I., Joselin, A.P., Parsanejad, M., Kim, R.H., Rizzu, P., Callaghan, S.M., et al. (2010). DJ-1 protects the nigrostriatal axis from the neurotoxin MPTP by modulation of the AKT pathway. *Proc Natl Acad Sci U S A* *107*, 3186–3191.

Andersen, A.D., Binzer, M., Stenager, E., and Gramsbergen, J.B. (2017). Cerebrospinal fluid biomarkers for Parkinson's disease - a systematic review. *Acta Neurol. Scand.* *135*, 34–56.

Andres-Mateos, E., Perier, C., Zhang, L., Blanchard-Fillion, B., Greco, T.M., Thomas, B., Ko, H.S., Sasaki, M., Ischiropoulos, H., Przedborski, S., et al. (2007). DJ-1 gene deletion reveals that DJ-1 is an atypical peroxiredoxin-like peroxidase. *Proc. Natl. Acad. Sci. U.S.A.* *104*, 14807–14812.

Anselm, I.A., Sweadner, K.J., Gollamudi, S., Ozelius, L.J., and Darras, B.T. (2009). RAPID-ONSET DYSTONIA-PARKINSONISM IN A CHILD WITH A NOVEL ATP1A3 GENE MUTATION. *Neurology* *73*, 400–401.

- Ariga, H., Takahashi-Niki, K., Kato, I., Maita, H., Niki, T., and Iguchi-Ariga, S.M.M. (2013). Neuroprotective Function of DJ-1 in Parkinson's Disease. *Oxidative Medicine and Cellular Longevity* 2013, 1–9.
- Aron, L., Klein, P., Pham, T.-T., Kramer, E.R., Wurst, W., and Klein, R. (2010). Pro-Survival Role for Parkinson's Associated Gene DJ-1 Revealed in Trophically Impaired Dopaminergic Neurons. *PLOS Biology* 8, e1000349.
- Atiya Ali, M., Poortvliet, E., Strömberg, R., and Yngve, A. (2011). Polyamines in foods: development of a food database. *Food Nutr Res* 55.
- Barkholt, P., Sanchez-Guajardo, V., Kirik, D., and Romero-Ramos, M. (2012). Long-term polarization of microglia upon α -synuclein overexpression in nonhuman primates. *Neuroscience* 208, 85–96.
- Batelli, S., Invernizzi, R.W., Negro, A., Calcagno, E., Rodilossi, S., Forloni, G., and Albani, D. (2015). The Parkinson's disease-related protein DJ-1 protects dopaminergic neurons in vivo and cultured cells from alpha-synuclein and 6-hydroxydopamine toxicity. *Neurodegener Dis* 15, 13–23.
- Benamer, H.T., Patterson, J., Wyper, D.J., Hadley, D.M., Macphee, G.J., and Grosset, D.G. (2000). Correlation of Parkinson's disease severity and duration with 123I-FP-CIT SPECT striatal uptake. *Mov. Disord.* 15, 692–698.
- Benamer, H.T.S., de Silva, R., Siddiqui, K.A., and Grosset, D.G. (2008). Parkinson's disease in Arabs: a systematic review. *Mov. Disord.* 23, 1205–1210.
- Benjamini, Y., and Hochberg, Y. (1995). Controlling the False Discovery Rate: A Practical and Powerful Approach to Multiple Testing. *Journal of the Royal Statistical Society. Series B (Methodological)* 57, 289–300.
- Bhidayasiri, R. (2005). Differential diagnosis of common tremor syndromes. *Postgraduate Medical Journal* 81, 756–762.
- Billia, F., Hauck, L., Grothe, D., Konecny, F., Rao, V., Kim, R.H., and Mak, T.W. (2013). Parkinson-susceptibility gene DJ-1/PARK7 protects the murine heart from oxidative damage in vivo. *Proc Natl Acad Sci U S A* 110, 6085–6090.
- Bistulfi, G., Diegelman, P., Foster, B.A., Kramer, D.L., Porter, C.W., and Smiraglia, D.J. (2009). Polyamine biosynthesis impacts cellular folate requirements necessary to maintain S-adenosylmethionine and nucleotide pools. *FASEB J.* 23, 2888–2897.
- Blandini, F. (2013). Neural and immune mechanisms in the pathogenesis of Parkinson's disease. *J Neuroimmune Pharmacol* 8, 189–201.

Block, M.L., Zecca, L., and Hong, J.-S. (2007). Microglia-mediated neurotoxicity: uncovering the molecular mechanisms. *Nat. Rev. Neurosci.* *8*, 57–69.

Boche, D., Perry, V.H., and Nicoll, J. a. R. (2013). Review: activation patterns of microglia and their identification in the human brain. *Neuropathol. Appl. Neurobiol.* *39*, 3–18.

Bohnen, N.I., Studenski, S.A., Constantine, G.M., and Moore, R.Y. (2008). Diagnostic performance of clinical motor and non-motor tests of Parkinson disease: a matched case-control study. *Eur. J. Neurol.* *15*, 685–691.

Boka, G., Anglade, P., Wallach, D., Javoy-Agid, F., Agid, Y., and Hirsch, E.C. (1994). Immunocytochemical analysis of tumor necrosis factor and its receptors in Parkinson's disease. *Neuroscience Letters* *172*, 151–154.

Bolaños, J.P., Delgado-Esteban, M., Herrero-Mendez, A., Fernandez-Fernandez, S., and Almeida, A. (2008). Regulation of glycolysis and pentose–phosphate pathway by nitric oxide: Impact on neuronal survival. *Biochimica et Biophysica Acta (BBA) - Bioenergetics* *1777*, 789–793.

Boldyrev, A.A. (2009). Molecular mechanisms of homocysteine toxicity. *Biochemistry Mosc.* *74*, 589–598.

Bonifati, V. (2003). Mutations in the DJ-1 Gene Associated with Autosomal Recessive Early-Onset Parkinsonism. *Science* *299*, 256–259.

Bonifati, V. (2012). Autosomal recessive parkinsonism. *Parkinsonism Relat. Disord.* *18 Suppl 1*, S4-6.

Braak, H., Del Tredici, K., Rüb, U., De Vos, R.A., Steur, E.N.J., and Braak, E. (2003). Staging of brain pathology related to sporadic Parkinson's disease. *Neurobiology of Aging* *24*, 197–211.

Brashear, A., Sweadner, K.J., Cook, J.F., Swoboda, K.J., and Ozelius, L. (1993). ATP1A3- Related Neurologic Disorders. In *GeneReviews®*, M.P. Adam, H.H. Ardinger, R.A. Pagon, S.E. Wallace, L.J. Bean, K. Stephens, and A. Amemiya, eds. (Seattle (WA): University of Washington, Seattle), p.

Brooks, D.J., Playford, E.D., Ibanez, V., Sawle, G.V., Thompson, P.D., Findley, L.J., and Marsden, C.D. (1992). Isolated tremor and disruption of the nigrostriatal dopaminergic system: an 18F-dopa PET study. *Neurology* *42*, 1554–1560.

Broussolle, E., Krack, P., Thobois, S., Xie-Brustolin, J., Pollak, P., and Goetz, C.G. (2007). Contribution of Jules Froment to the study of parkinsonian rigidity. *Mov. Disord.* *22*, 909–914.

Burn, D.J. (2002). Beyond the iron mask: towards better recognition and treatment of depression associated with Parkinson's disease. *Mov. Disord.* *17*, 445–454.

Burré, J., Sharma, M., Tsetsenis, T., Buchman, V., Etherton, M.R., and Südhof, T.C. (2010). Alpha-synuclein promotes SNARE-complex assembly in vivo and in vitro. *Science* 329, 1663–1667.

Byrne, K.G., Pfeiffer, R., and Quigley, E.M. (1994). Gastrointestinal dysfunction in Parkinson's disease. A report of clinical experience at a single center. *J. Clin. Gastroenterol.* 19, 11–16.

Calabresi, P., Picconi, B., Tozzi, A., Ghiglieri, V., and Di Filippo, M. (2014). Direct and indirect pathways of basal ganglia: a critical reappraisal. *Nat. Neurosci.* 17, 1022–1030.

von Campenhausen, S., Bornschein, B., Wick, R., Bötzel, K., Sampaio, C., Poewe, W., Oertel, W., Siebert, U., Berger, K., and Dodel, R. (2005). Prevalence and incidence of Parkinson's disease in Europe. *European Neuropsychopharmacology* 15, 473–490.

Canet-Avilés, R.M., Wilson, M.A., Miller, D.W., Ahmad, R., McLendon, C., Bandyopadhyay, S., Baptista, M.J., Ringe, D., Petsko, G.A., and Cookson, M.R. (2004). The Parkinson's disease protein DJ-1 is neuroprotective due to cysteine-sulfenic acid-driven mitochondrial localization. *Proc Natl Acad Sci U S A* 101, 9103–9108.

Cao, J., Ying, M., Xie, N., Lin, G., Dong, R., Zhang, J., Yan, H., Yang, X., He, Q., and Yang, B. (2014). The oxidation states of DJ-1 dictate the cell fate in response to oxidative stress triggered by 4-hpr: autophagy or apoptosis? *Antioxid. Redox Signal.* 21, 1443–1459.

de Carvalho Aguiar, P., Sweadner, K.J., Penniston, J.T., Zaremba, J., Liu, L., Caton, M., Linzasoro, G., Borg, M., Tijssen, M.A.J., Bressman, S.B., et al. (2004). Mutations in the Na⁺/K⁺ -ATPase alpha3 gene ATP1A3 are associated with rapid-onset dystonia parkinsonism. *Neuron* 43, 169–175.

Chang, R.C., Hudson, P., Wilson, B., Liu, B., Abel, H., Hemperly, J., and Hong, J.S. (2000b). Immune modulatory effects of neural cell adhesion molecules on lipopolysaccharide-induced nitric oxide production by cultured glia. *Brain Res. Mol. Brain Res.* 81, 197–201.

Chang, R.C., Hudson, P., Wilson, B., Haddon, L., and Hong, J.S. (2000a). Influence of neurons on lipopolysaccharide-stimulated production of nitric oxide and tumor necrosis factor-alpha by cultured glia. *Brain Res.* 853, 236–244.

Chattopadhyay, M.K., Tabor, C.W., and Tabor, H. (2003). Polyamines protect *Escherichia coli* cells from the toxic effect of oxygen. *Proc. Natl. Acad. Sci. U.S.A.* 100, 2261–2265.

Chaudhuri, K.R., and Naidu, Y. (2008). Early Parkinson's disease and non-motor issues. *J. Neurol.* 255 Suppl 5, 33–38.

Chaudhuri, K.R., Healy, D.G., and Schapira, A.H. (2006). Non-motor symptoms of Parkinson's disease: diagnosis and management. *The Lancet Neurology* 5, 235–245.

- Chen, A., Feldman, M., Vershinin, Z., and Levy, D. (2016). SETD6 is a negative regulator of oxidative stress response. *Biochimica et Biophysica Acta (BBA) - Gene Regulatory Mechanisms* 1859, 420–427.
- Chen, J., Li, L., and Chin, L.-S. (2010). Parkinson disease protein DJ-1 converts from a zymogen to a protease by carboxyl-terminal cleavage. *Hum. Mol. Genet.* 19, 2395–2408.
- Chien, C.-H., Lee, M.-J., Liou, H.-C., Liou, H.-H., and Fu, W.-M. (2016). Microglia-Derived Cytokines/Chemokines Are Involved in the Enhancement of LPS-Induced Loss of Nigrostriatal Dopaminergic Neurons in DJ-1 Knockout Mice. *PLoS ONE* 11, e0151569.
- Choi, Y.H., and Park, H.Y. (2012). Anti-inflammatory effects of spermidine in lipopolysaccharide-stimulated BV2 microglial cells. *J. Biomed. Sci.* 19, 31.
- Choi, M.S., Nakamura, T., Cho, S.-J., Han, X., Holland, E.A., Qu, J., Petsko, G.A., Yates, J.R., Liddington, R.C., and Lipton, S.A. (2014). Transnitrosylation from DJ-1 to PTEN attenuates neuronal cell death in parkinson's disease models. *J. Neurosci.* 34, 15123–15131.
- Choudhury, S., and Borah, A. (2015). Activation of NMDA receptor by elevated homocysteine in chronic liver disease contributes to encephalopathy. *Med. Hypotheses* 85, 64–67.
- Clausen, M.V., Hilbers, F., and Poulsen, H. (2017). The Structure and Function of the Na,K-ATPase Isoforms in Health and Disease. *Front Physiol* 8.
- Clements, C.M., McNally, R.S., Conti, B.J., Mak, T.W., and Ting, J.P.-Y. (2006). DJ-1, a cancer- and Parkinson's disease-associated protein, stabilizes the antioxidant transcriptional master regulator Nrf2. *Proc Natl Acad Sci U S A* 103, 15091–15096.
- Coleman, C.S., Hu, G., and Pegg, A.E. (2004). Putrescine biosynthesis in mammalian tissues. *Biochemical Journal* 379, 849–855.
- Colton, C.A., and Wilcock, D.M. (2010). Assessing activation states in microglia. *CNS Neurol Disord Drug Targets* 9, 174–191.
- Crusio, W.E. (2004). Flanking gene and genetic background problems in genetically manipulated mice. *Biological Psychiatry* 56, 381–385.
- Członkowska, A., Kohutnicka, M., Kurkowska-Jastrzebska, I., and Członkowski, A. (1996). Microglial reaction in MPTP (1-methyl-4-phenyl-1,2,3,6-tetrahydropyridine) induced Parkinson's disease mice model. *Neurodegeneration* 5, 137–143.
- Daher, J.P.L., Volpicelli-Daley, L.A., Blackburn, J.P., Moehle, M.S., and West, A.B. (2014). Abrogation of α -synuclein-mediated dopaminergic neurodegeneration in LRRK2-deficient rats. *Proc. Natl. Acad. Sci. U.S.A.* 111, 9289–9294.

Davalos, D., Grutzendler, J., Yang, G., Kim, J.V., Zuo, Y., Jung, S., Littman, D.R., Dustin, M.L., and Gan, W.-B. (2005). ATP mediates rapid microglial response to local brain injury in vivo. *Nat. Neurosci.* *8*, 752–758.

Davison, E.J., Pennington, K., Hung, C.-C., Peng, J., Rafiq, R., Ostareck-Lederer, A., Ostareck, D.H., Ardley, H.C., Banks, R.E., and Robinson, P.A. (2009). Proteomic analysis of increased Parkin expression and its interactants provides evidence for a role in modulation of mitochondrial function. *Proteomics* *9*, 4284–4297.

Dickson, D.W., Braak, H., Duda, J.E., Duyckaerts, C., Gasser, T., Halliday, G.M., Hardy, J., Leverenz, J.B., Del Tredici, K., and Wszolek, Z.K. (2009). Neuropathological assessment of Parkinson's disease: refining the diagnostic criteria. *The Lancet Neurology* *8*, 1150–1157.

Divakaruni, A.S., Paradyse, A., Ferrick, D.A., Murphy, A.N., and Jastroch, M. (2014). Analysis and Interpretation of Microplate-Based Oxygen Consumption and pH Data. In *Methods in Enzymology*, (Elsevier), pp. 309–354.

Dluzen, D.E., and McDermott, J.L. (2000). Gender differences in neurotoxicity of the nigrostriatal dopaminergic system: implications for Parkinson's disease. *J Gend Specif Med* *3*, 36–42.

Dorsey, E.R., Constantinescu, R., Thompson, J.P., Biglan, K.M., Holloway, R.G., Kieburtz, K., Marshall, F.J., Ravina, B.M., Schifitto, G., Siderowf, A., et al. (2007). Projected number of people with Parkinson disease in the most populous nations, 2005 through 2030. *Neurology* *68*, 384–386.

Doty, R.L. (2012). Olfactory dysfunction in Parkinson disease. *Nat Rev Neurol* *8*, 329–339.

Du, Y., Ma, Z., Lin, S., Dodel, R.C., Gao, F., Bales, K.R., Triarhou, L.C., Chernet, E., Perry, K.W., Nelson, D.L., et al. (2001). Minocycline prevents nigrostriatal dopaminergic neurodegeneration in the MPTP model of Parkinson's disease. *Proc. Natl. Acad. Sci. U.S.A.* *98*, 14669–14674.

Dubois, B., and Pillon, B. (1997). Cognitive deficits in Parkinson's disease. *J. Neurol.* *244*, 2–8.

Edwards, J.P., Zhang, X., Frauwirth, K.A., and Mosser, D.M. (2006). Biochemical and functional characterization of three activated macrophage populations. *J. Leukoc. Biol.* *80*, 1298–1307.

Emre, M. (2003). Dementia associated with Parkinson's disease. *Lancet Neurol* *2*, 229–237.

Fan, J., Ren, H., Jia, N., Fei, E., Zhou, T., Jiang, P., Wu, M., and Wang, G. (2008). DJ-1 decreases Bax expression through repressing p53 transcriptional activity. *J. Biol. Chem.* *283*, 4022–4030.

Fearnley, J.M., and Lees, A.J. (1991). Ageing and Parkinson's disease: substantia nigra regional selectivity. *Brain* *114 (Pt 5)*, 2283–2301.

Ferreira, M., and Massano, J. (2017). An updated review of Parkinson's disease genetics and clinicopathological correlations. *Acta Neurologica Scandinavica* 135, 273–284.

Francis, V.G., and Gummadi, S.N. (2012). Biochemical and functional characterization of human phospholipid scramblase 4 (hPLSCR4). *Biol. Chem.* 393, 1173–1181.

Frank-Cannon, T.C., Tran, T., Ruhn, K.A., Martinez, T.N., Hong, J., Marvin, M., Hartley, M., Treviño, I., O'Brien, D.E., Casey, B., et al. (2008). Parkin deficiency increases vulnerability to inflammation-related nigral degeneration. *J. Neurosci.* 28, 10825–10834.

Frosst, P., Blom, H.J., Milos, R., Goyette, P., Sheppard, C.A., Matthews, R.G., Boers, G.J.H., Heijer, M. den, Kluijtmans, L. a. J., Heuve, L.P. van den, et al. (1995). A candidate genetic risk factor for vascular disease: a common mutation in methylenetetrahydrofolate reductase. *Nature Genetics* 10, 111.

Gagnon, J.F., Bédard, M.A., Fantini, M.L., Petit, D., Panisset, M., Rompré, S., Carrier, J., and Montplaisir, J. (2002). REM sleep behavior disorder and REM sleep without atonia in Parkinson's disease. *Neurology* 59, 585–589.

Gao, H., Yang, W., Qi, Z., Lu, L., Duan, C., Zhao, C., and Yang, H. (2012). DJ-1 protects dopaminergic neurons against rotenone-induced apoptosis by enhancing ERK-dependent mitophagy. *J. Mol. Biol.* 423, 232–248.

Garcia Ruiz, P.J., Muñoz de Iñeson, J., Ayerbe, J., Frech, F., Sánchez Bernardos, V., Lopez Ferro, O., and Gudin, R. (2005). Evaluation of timed tests in advanced Parkinsonian patients who were candidates for subthalamic stimulation. *Clin Neuropharmacol* 28, 15–17.

George, J.M. (2002). The synucleins. *Genome Biol.* 3, REVIEWS3002.

George, J., Gonçalves, F.Q., Cristóvão, G., Rodrigues, L., Meyer Fernandes, J.R., Gonçalves, T., Cunha, R.A., and Gomes, C.A. (2015). Different danger signals differently impact on microglial proliferation through alterations of ATP release and extracellular metabolism. *Glia* 63, 1636–1645.

Gerfen, C.R., Engber, T.M., Mahan, L.C., Susel, Z., Chase, T.N., Monsma, F.J., and Sibley, D.R. (1990). D1 and D2 dopamine receptor-regulated gene expression of striatonigral and striatopallidal neurons. *Science* 250, 1429–1432.

Gerhard, A., Pavese, N., Hotton, G., Turkheimer, F., Es, M., Hammers, A., Eggert, K., Oertel, W., Banati, R.B., and Brooks, D.J. (2006). In vivo imaging of microglial activation with [11C](R)-PK11195 PET in idiopathic Parkinson's disease. *Neurobiol. Dis.* 21, 404–412.

Gerlai, R. (1996). Gene-targeting studies of mammalian behavior: is it the mutation or the background genotype? *Trends Neurosci.* 19, 177–181.

Gimeno-Bayón, J., López-López, A., Rodríguez, M.J., and Mahy, N. (2014). Glucose pathways adaptation supports acquisition of activated microglia phenotype: Activated Microglia Metabolic Reprogramming. *Journal of Neuroscience Research* 92, 723–731.

Gironell, A., Kulisevsky, J., Pascual-Sedano, B., and Pagonabarraga, X. (2007). “Prodromic” tremor: Prevalence and clinical correlates. *Mov. Disord.* 22, 1203–1204.

Giroto, S., Cendron, L., Bisaglia, M., Tessari, I., Mammi, S., Zanotti, G., and Bubacco, L. (2014). DJ-1 is a copper chaperone acting on SOD1 activation. *J. Biol. Chem.* 289, 10887–10899.

Glasl, L., Kloos, K., Giesert, F., Roethig, A., Di Benedetto, B., Kühn, R., Zhang, J., Hafen, U., Zerle, J., Hofmann, A., et al. (2012). Pink1-deficiency in mice impairs gait, olfaction and serotonergic innervation of the olfactory bulb. *Exp. Neurol.* 235, 214–227.

Gomes-Trolin, C., Nygren, I., Aquilonius, S.-M., and Askmark, H. (2002). Increased red blood cell polyamines in ALS and Parkinson’s disease. *Exp. Neurol.* 177, 515–520.

Gordon, A.M., Ingvarsson, P.E., and Forssberg, H. (1997). Anticipatory Control of Manipulative Forces in Parkinson’s Disease. *Experimental Neurology* 145, 477–488.

Grimbergen, Y.A.M., Langston, J.W., Roos, R.A.C., and Bloem, B.R. (2009). Postural instability in Parkinson’s disease: the adrenergic hypothesis and the locus coeruleus. *Expert Rev Neurother* 9, 279–290.

Gu, L., Cui, T., Fan, C., Zhao, H., Zhao, C., Lu, L., and Yang, H. (2009). Involvement of ERK1/2 signaling pathway in DJ-1-induced neuroprotection against oxidative stress. *Biochem. Biophys. Res. Commun.* 383, 469–474.

Guzman, J.N., Sanchez-Padilla, J., Wokosin, D., Kondapalli, J., Ilijic, E., Schumacker, P.T., and Surmeier, D.J. (2010). Oxidant stress evoked by pacemaking in dopaminergic neurons is attenuated by DJ-1. *Nature* 468, 696–700.

Hallett, M. (2003). Parkinson revisited: pathophysiology of motor signs. *Adv Neurol* 91, 19–28.

Hauser, D.N., Mamais, A., Conti, M.M., Primiani, C.T., Kumaran, R., Dillman, A.A., Langston, R.G., Beilina, A., Garcia, J.H., Diaz-Ruiz, A., et al. (2017). Hexokinases link DJ-1 to the PINK1/parkin pathway. *Mol Neurodegener* 12, 70.

Hawkes, C.H., Shephard, B.C., and Daniel, S.E. (1997). Olfactory dysfunction in Parkinson’s disease. *J. Neurol. Neurosurg. Psychiatr.* 62, 436–446.

Hayashi, T., Ishimori, C., Takahashi-Niki, K., Taira, T., Kim, Y., Maita, H., Maita, C., Ariga, H., and Iguchi-Ariga, S.M.M. (2009). DJ-1 binds to mitochondrial complex I and maintains its activity. *Biochem. Biophys. Res. Commun.* 390, 667–672.

He, Y., Appel, S., and Le, W. (2001). Minocycline inhibits microglial activation and protects nigral cells after 6-hydroxydopamine injection into mouse striatum. *Brain Res.* 909, 187–193.

Helene Doherty, G. (2013). Homocysteine and Parkinson's Disease: A Complex Relationship. *Journal of Neurological Disorders* 01.

Helmich, R.C., Hallett, M., Deuschl, G., Toni, I., and Bloem, B.R. (2012). Cerebral causes and consequences of parkinsonian resting tremor: a tale of two circuits? *Brain* 135, 3206–3226.

Hermanson, E., Joseph, B., Castro, D., Lindqvist, E., Aarnisalo, P., Wallén, A., Benoit, G., Hengerer, B., Olson, L., and Perlmann, T. (2003). Nurr1 regulates dopamine synthesis and storage in MN9D dopamine cells. *Exp. Cell Res.* 288, 324–334.

Hirsch, E.C., and Hunot, S. (2009). Neuroinflammation in Parkinson's disease: a target for neuroprotection? *The Lancet Neurology* 8, 382–397.

Hirsch, E.C., Vyas, S., and Hunot, S. (2012). Neuroinflammation in Parkinson's disease. *Parkinsonism & Related Disorders* 18, S210–S212.

Ho, A.K., Iansek, R., Marigliani, C., Bradshaw, J.L., and Gates, S. (1998). Speech impairment in a large sample of patients with Parkinson's disease. *Behav Neurol* 11, 131–137.

Honbou, K., Suzuki, N.N., Horiuchi, M., Niki, T., Taira, T., Ariga, H., and Inagaki, F. (2003). The Crystal Structure of DJ-1, a Protein Related to Male Fertility and Parkinson's Disease. *J. Biol. Chem.* 278, 31380–31384.

Hornykiewicz, O. (2008). Basic research on dopamine in Parkinson's disease and the discovery of the nigrostriatal dopamine pathway: the view of an eyewitness. *Neurodegener Dis* 5, 114–117.

Howarth, C., Gleeson, P., and Attwell, D. (2012). Updated energy budgets for neural computation in the neocortex and cerebellum. *J. Cereb. Blood Flow Metab.* 32, 1222–1232.

Hu, Q., and Wang, G. (2016). Mitochondrial dysfunction in Parkinson's disease. *Transl Neurodegener* 5.

Hu, X., and Ivashkiv, L.B. (2009). Cross-regulation of signaling pathways by interferon-gamma: implications for immune responses and autoimmune diseases. *Immunity* 31, 539–550.

Im, J.-Y., Lee, K.-W., Junn, E., and Mouradian, M.M. (2010). DJ-1 protects against oxidative damage by regulating the thioredoxin/ASK1 complex. *Neurosci. Res.* 67, 203–208.

Im, J.-Y., Lee, K.-W., Woo, J.-M., Junn, E., and Mouradian, M.M. (2012). DJ-1 induces thioredoxin 1 expression through the Nrf2 pathway. *Hum. Mol. Genet.* 21, 3013–3024.

Imamura, K., Hishikawa, N., Sawada, M., Nagatsu, T., Yoshida, M., and Hashizume, Y. (2003). Distribution of major histocompatibility complex class II-positive microglia and cytokine profile of Parkinson's disease brains. *Acta Neuropathol.* *106*, 518–526.

Irrcher, I., Aleyasin, H., Seifert, E.L., Hewitt, S.J., Chhabra, S., Phillips, M., Lutz, A.K., Rousseaux, M.W.C., Bevilacqua, L., Jahani-Asl, A., et al. (2010). Loss of the Parkinson's disease-linked gene DJ-1 perturbs mitochondrial dynamics. *Hum. Mol. Genet.* *19*, 3734–3746.

Ishikawa, S., Taira, T., Niki, T., Takahashi-Niki, K., Maita, C., Maita, H., Ariga, H., and Iguchi-Ariga, S.M.M. (2009). Oxidative Status of DJ-1-dependent Activation of Dopamine Synthesis through Interaction of Tyrosine Hydroxylase and 4-Dihydroxy-l-phenylalanine (l-DOPA) Decarboxylase with DJ-1. *J Biol Chem* *284*, 28832–28844.

Ishikawa, S., Taira, T., Takahashi-Niki, K., Niki, T., Ariga, H., and Iguchi-Ariga, S.M.M. (2010). Human DJ-1-specific transcriptional activation of tyrosine hydroxylase gene. *J. Biol. Chem.* *285*, 39718–39731.

Ishikawa, S., Tanaka, Y., Takahashi-Niki, K., Niki, T., Ariga, H., and Iguchi-Ariga, S.M.M. (2012). Stimulation of vesicular monoamine transporter 2 activity by DJ-1 in SH-SY5Y cells. *Biochem. Biophys. Res. Commun.* *421*, 813–818.

Isobe, C., Murata, T., Sato, C., and Terayama, Y. (2005). Increase of total homocysteine concentration in cerebrospinal fluid in patients with Alzheimer's disease and Parkinson's disease. *Life Sciences* *77*, 1836–1843.

Ito, G., Ariga, H., Nakagawa, Y., and Iwatsubo, T. (2006). Roles of distinct cysteine residues in S-nitrosylation and dimerization of DJ-1. *Biochemical and Biophysical Research Communications* *339*, 667–672.

Iwawaki, T., Kohno, K., and Kobayashi, K. (2000). Identification of a potential nurr1 response element that activates the tyrosine hydroxylase gene promoter in cultured cells. *Biochem. Biophys. Res. Commun.* *274*, 590–595.

Jacobson, S., and Marcus, E.M. (2011). *Neuroanatomy for the Neuroscientist* (Boston, MA: Springer US).

Jankovic, J. (2008). Parkinson's disease: clinical features and diagnosis. *J. Neurol. Neurosurg. Psychiatr.* *79*, 368–376.

Jeffrey, K.L., Camps, M., Rommel, C., and Mackay, C.R. (2007). Targeting dual-specificity phosphatases: manipulating MAP kinase signalling and immune responses. *Nat Rev Drug Discov* *6*, 391–403.

Jellinger, K.A. (1999). Post mortem studies in Parkinson's disease--is it possible to detect brain areas for specific symptoms? *J. Neural Transm. Suppl.* *56*, 1–29.

- Johnson, K.A., Conn, P.J., and Niswender, C.M. (2009). Glutamate receptors as therapeutic targets for Parkinson's disease. *CNS Neurol Disord Drug Targets* 8, 475–491.
- Joksimovic, M., and Awatramani, R. (2014). Wnt/ β -catenin signaling in midbrain dopaminergic neuron specification and neurogenesis. *J Mol Cell Biol* 6, 27–33.
- Junn, E., Taniguchi, H., Jeong, B.S., Zhao, X., Ichijo, H., and Mouradian, M.M. (2005). Interaction of DJ-1 with Daxx inhibits apoptosis signal-regulating kinase 1 activity and cell death. *Proc. Natl. Acad. Sci. U.S.A.* 102, 9691–9696.
- Kahle, P.J., Waak, J., and Gasser, T. (2009). DJ-1 and prevention of oxidative stress in Parkinson's disease and other age-related disorders. *Free Radic. Biol. Med.* 47, 1354–1361.
- Kalia, L.V., and Lang, A.E. (2015). Parkinson's disease. *The Lancet* 386, 896–912.
- Kato, I., Maita, H., Takahashi-Niki, K., Saito, Y., Noguchi, N., Iguchi-Arigo, S.M.M., and Ariga, H. (2013). Oxidized DJ-1 inhibits p53 by sequestering p53 from promoters in a DNA-binding affinity-dependent manner. *Mol. Cell. Biol.* 33, 340–359.
- Kaye, J., Gage, H., Kimber, A., Storey, L., and Trend, P. (2006). Excess burden of constipation in Parkinson's disease: a pilot study. *Mov. Disord.* 21, 1270–1273.
- Keshet, Y., and Seger, R. (2010). The MAP kinase signaling cascades: a system of hundreds of components regulates a diverse array of physiological functions. *Methods Mol. Biol.* 661, 3–38.
- Khandelwal, P.J., Herman, A.M., and Moussa, C.E.-H. (2011). Inflammation in the early stages of neurodegenerative pathology. *J. Neuroimmunol.* 238, 1–11.
- Kielian, T. (2006). Toll-Like Receptors in Central Nervous System Glial Inflammation and Homeostasis. *J Neurosci Res* 83, 711–730.
- Kim, B., Yang, M.-S., Choi, D., Kim, J.-H., Kim, H.-S., Seol, W., Choi, S., Jou, I., Kim, E.-Y., and Joe, E. (2012). Impaired Inflammatory Responses in Murine Lrrk2-Knockdown Brain Microglia. *PLOS ONE* 7, e34693.
- Kim, C.C., Nakamura, M.C., and Hsieh, C.L. (2016). Brain trauma elicits non-canonical macrophage activation states. *J Neuroinflammation* 13, 117.
- Kim, D., Paik, J.H., Shin, D.-W., Kim, H.-S., Park, C.-S., and Kang, J.-H. (2014). What is the Clinical Significance of Cerebrospinal Fluid Biomarkers in Parkinson's disease? Is the Significance Diagnostic or Prognostic? *Exp Neurobiol* 23, 352–364.
- Kim, J., Byun, J.-W., Choi, I., Kim, B., Jeong, H.-K., Jou, I., and Joe, E. (2013a). PINK1 Deficiency Enhances Inflammatory Cytokine Release from Acutely Prepared Brain Slices. *Exp Neurobiol* 22, 38–44.

- Kim, J., Choi, D., Jeong, H., Kim, J., Kim, D.W., Choi, S.Y., Park, S.-M., Suh, Y.H., Jou, I., and Joe, E.-H. (2013b). DJ-1 facilitates the interaction between STAT1 and its phosphatase, SHP-1, in brain microglia and astrocytes: A novel anti-inflammatory function of DJ-1. *Neurobiol. Dis.* *60*, 1–10.
- Kim, R.H., Smith, P.D., Aleyasin, H., Hayley, S., Mount, M.P., Pownall, S., Wakeham, A., You-Ten, A.J., Kalia, S.K., Horne, P., et al. (2005a). Hypersensitivity of DJ-1-deficient mice to 1-methyl-4-phenyl-1,2,3,6-tetrahydropyridine (MPTP) and oxidative stress. *Proc. Natl. Acad. Sci. U.S.A.* *102*, 5215–5220.
- Kim, R.H., Peters, M., Jang, Y., Shi, W., Pintilie, M., Fletcher, G.C., DeLuca, C., Liepa, J., Zhou, L., Snow, B., et al. (2005b). DJ-1, a novel regulator of the tumor suppressor PTEN. *Cancer Cell* *7*, 263–273.
- Kim, S.D., Allen, N.E., Canning, C.G., and Fung, V.S.C. (2013c). Postural instability in patients with Parkinson's disease. *Epidemiology, pathophysiology and management. CNS Drugs* *27*, 97–112.
- Kim, W.G., Mohny, R.P., Wilson, B., Jeohn, G.H., Liu, B., and Hong, J.S. (2000). Regional difference in susceptibility to lipopolysaccharide-induced neurotoxicity in the rat brain: role of microglia. *J. Neurosci.* *20*, 6309–6316.
- Kim, Y.-C., Kitaura, H., Taira, T., Iguchi-Arigo, S.M.M., and Ariga, H. (2009). Oxidation of DJ-1-dependent cell transformation through direct binding of DJ-1 to PTEN. *Int. J. Oncol.* *35*, 1331–1341.
- Kinumi, T., Kimata, J., Taira, T., Ariga, H., and Niki, E. (2004). Cysteine-106 of DJ-1 is the most sensitive cysteine residue to hydrogen peroxide-mediated oxidation in vivo in human umbilical vein endothelial cells. *Biochem. Biophys. Res. Commun.* *317*, 722–728.
- Klinefelter, G.R., Laskey, J.W., Ferrell, J., Suarez, J.D., and Roberts, N.L. (1997). Discriminant analysis indicates a single sperm protein (SP22) is predictive of fertility following exposure to epididymal toxicants. *J. Androl.* *18*, 139–150.
- Kobayashi, A., Kang, M.-I., Okawa, H., Ohtsuji, M., Zenke, Y., Chiba, T., Igarashi, K., and Yamamoto, M. (2004). Oxidative stress sensor Keap1 functions as an adaptor for Cul3-based E3 ligase to regulate proteasomal degradation of Nrf2. *Mol. Cell. Biol.* *24*, 7130–7139.
- Kobayashi, K., Imagama, S., Ohgomori, T., Hirano, K., Uchimura, K., Sakamoto, K., Hirakawa, A., Takeuchi, H., Suzumura, A., Ishiguro, N., et al. (2013). Minocycline selectively inhibits M1 polarization of microglia. *Cell Death Dis* *4*, e525.
- Kordower, J.H., Olanow, C.W., Dodiya, H.B., Chu, Y., Beach, T.G., Adler, C.H., Halliday, G.M., and Bartus, R.T. (2013). Disease duration and the integrity of the nigrostriatal system in Parkinson's disease. *Brain* *136*, 2419–2431.

- Kravitz, A.V., Freeze, B.S., Parker, P.R.L., Kay, K., Thwin, M.T., Deisseroth, K., and Kreitzer, A.C. (2010). Regulation of parkinsonian motor behaviors by optogenetic control of basal ganglia circuitry. *Nature* 466, 622–626.
- Krebiehl, G., Ruckerbauer, S., Burbulla, L.F., Kieper, N., Maurer, B., Waak, J., Wolburg, H., Gizatullina, Z., Gellerich, F.N., Voitalla, D., et al. (2010). Reduced Basal Autophagy and Impaired Mitochondrial Dynamics Due to Loss of Parkinson's Disease-Associated Protein DJ-1. *PLoS One* 5.
- Lamberti, P., Zoccolella, S., Armenise, E., Lamberti, S.V., Fraddosio, A., de Mari, M., Iliceto, G., and Livrea, P. (2005). Hyperhomocysteinemia in l-dopa treated Parkinson's disease patients: effect of cobalamin and folate administration. *European Journal of Neurology* 12, 365–368.
- Lanciego, J.L., Luquin, N., and Obeso, J.A. (2012). Functional Neuroanatomy of the Basal Ganglia. *Cold Spring Harb Perspect Med* 2.
- de Lau, L.M.L., Koudstaal, P.J., Hofman, A., and Breteler, M.M.B. (2006). Subjective complaints precede Parkinson disease: the rotterdam study. *Arch. Neurol.* 63, 362–365.
- Lazarewicz, J.W., Ziembowicz, A., Matyja, E., Stafiej, A., and Zieminska, E. (2003). Homocysteine-evoked ^{45}Ca release in the rabbit hippocampus is mediated by both NMDA and group I metabotropic glutamate receptors: in vivo microdialysis study. *Neurochem. Res.* 28, 259–269.
- Lee, J., Song, J., Kwon, K., Jang, S., Kim, C., Baek, K., Kim, J., and Park, C. (2012). Human DJ-1 and its homologs are novel glyoxalases. *Human Molecular Genetics* 21, 3215–3225.
- Lees, A.J. (2007). Unresolved issues relating to the Shaking Palsy on the celebration of James Parkinson's 250th birthday. *Movement Disorders* 22, S327–S334.
- Lees, A.J., and Smith, E. (1983). Cognitive deficits in the early stages of Parkinson's disease. *Brain* 106 (Pt 2), 257–270.
- Lees, A.J., Hardy, J., and Revesz, T. (2009). Parkinson's disease. *Lancet* 373, 2055–2066.
- L'Episcopo, F., Tirolo, C., Testa, N., Caniglia, S., Morale, M.C., Serapide, M.F., Pluchino, S., and Marchetti, B. (2014). Wnt/ β -catenin signaling is required to rescue midbrain dopaminergic progenitors and promote neurorepair in ageing mouse model of Parkinson's disease. *Stem Cells* 32, 2147–2163.
- Levine, A.J., and Harris, S.L. (2005). The p53 pathway: positive and negative feedback loops. *Oncogene* 24, 2899.
- Levy, D., Kuo, A.J., Chang, Y., Schaefer, U., Kitson, C., Cheung, P., Espejo, A., Zee, B.M., Liu, C.L., Tansombatvisit, S., et al. (2011). Lysine methylation of the NF- κ B subunit RelA by SETD6

couples activity of the histone methyltransferase GLP at chromatin to tonic repression of NF- κ B signaling. *Nat. Immunol.* *12*, 29–36.

Lewis, S.J.G., and Barker, R.A. (2009). A pathophysiological model of freezing of gait in Parkinson's disease. *Parkinsonism Relat. Disord.* *15*, 333–338.

Li, H.M., Niki, T., Taira, T., Iguchi-Arigo, S.M.M., and Ariga, H. (2005). Association of DJ-1 with chaperones and enhanced association and colocalization with mitochondrial Hsp70 by oxidative stress. *Free Radic. Res.* *39*, 1091–1099.

Liew, S.-C., and Gupta, E.D. (2015). Methylenetetrahydrofolate reductase (MTHFR) C677T polymorphism: epidemiology, metabolism and the associated diseases. *Eur J Med Genet* *58*, 1–10.

Lipton, S.A., Kim, W.-K., Choi, Y.-B., Kumar, S., D'Emilia, D.M., Rayudu, P.V., Arnette, D.R., and Stamler, J.S. (1997). Neurotoxicity associated with dual actions of homocysteine at the N-methyl-d-aspartate receptor. *Proc Natl Acad Sci U S A* *94*, 5923–5928.

Liu, D.-H., Yuan, F.-G., Hu, S.-Q., Diao, F., Wu, Y.-P., Zong, Y.-Y., Song, T., Li, C., and Zhang, G.-Y. (2013). Endogenous nitric oxide induces activation of apoptosis signal-regulating kinase 1 via S-nitrosylation in rat hippocampus during cerebral ischemia-reperfusion. *Neuroscience* *229*, 36–48.

Liu, L., Zhang, L., Guo, L., Yu, Q., Li, H., Teng, J., and Xie, A. (2018). MTHFR C677T and A1298C polymorphisms may contribute to the risk of Parkinson's disease: A meta-analysis of 19 studies. *Neuroscience Letters* *662*, 339–345.

Livingstone, S.R., Vezer, E., McGarry, L.M., Lang, A.E., and Russo, F.A. (2016). Deficits in the Mimicry of Facial Expressions in Parkinson's Disease. *Front Psychol* *7*.

Lo, R.Y., Tanner, C.M., Albers, K.B., Leimpeter, A.D., Fross, R.D., Bernstein, A.L., McGuire, V., Quesenberry, C.P., Nelson, L.M., and Van Den Eeden, S.K. (2009). Clinical features in early Parkinson disease and survival. *Arch. Neurol.* *66*, 1353–1358.

Lofrumento, D.D., Saponaro, C., Cianciulli, A., De Nuccio, F., Mitolo, V., Nicolardi, G., and Panaro, M.A. (2011). MPTP-induced neuroinflammation increases the expression of pro-inflammatory cytokines and their receptors in mouse brain. *Neuroimmunomodulation* *18*, 79–88.

Lu, J., Cao, Q., Zheng, D., Sun, Y., Wang, C., Yu, X., Wang, Y., Lee, V.W.S., Zheng, G., Tan, T.K., et al. (2013). Discrete functions of M2a and M2c macrophage subsets determine their relative efficacy in treating chronic kidney disease. *Kidney Int.* *84*, 745–755.

Lu, L., Sun, X., Liu, Y., Zhao, H., Zhao, S., and Yang, H. (2012). DJ-1 upregulates tyrosine hydroxylase gene expression by activating its transcriptional factor Nurr1 via the ERK1/2 pathway. *Int. J. Biochem. Cell Biol.* *44*, 65–71.

- Lu, L., Zhao, S., Gao, G., Sun, X., Zhao, H., and Yang, H. (2016). DJ-1/PARK7, But Not Its L166P Mutant Linked to Autosomal Recessive Parkinsonism, Modulates the Transcriptional Activity of the Orphan Nuclear Receptor Nurr1 In Vitro and In Vivo. *Mol. Neurobiol.* *53*, 7363–7374.
- Lucas, J.I., and Marín, I. (2007). A new evolutionary paradigm for the Parkinson disease gene DJ-1. *Mol. Biol. Evol.* *24*, 551–561.
- Luchtman, D.W., Shao, D., and Song, C. (2009). Behavior, neurotransmitters and inflammation in three regimens of the MPTP mouse model of Parkinson's disease. *Physiol. Behav.* *98*, 130–138.
- Luk, B., Mohammed, M., Liu, F., and Lee, F.J.S. (2015). A Physical Interaction between the Dopamine Transporter and DJ-1 Facilitates Increased Dopamine Reuptake. *PLoS One* *10*.
- Luo, Y. (2012). The function and mechanisms of Nurr1 action in midbrain dopaminergic neurons, from development and maintenance to survival. *Int. Rev. Neurobiol.* *102*, 1–22.
- Ma, Q. (2013). Role of nrf2 in oxidative stress and toxicity. *Annu. Rev. Pharmacol. Toxicol.* *53*, 401–426.
- Madeo, F., Eisenberg, T., Pietrocola, F., and Kroemer, G. (2018). Spermidine in health and disease. *Science* *359*, eaan2788.
- Maita, C., Maita, H., Iguchi-Arigo, S.M.M., and Ariga, H. (2013). Monomer DJ-1 and its N-terminal sequence are necessary for mitochondrial localization of DJ-1 mutants. *PLoS ONE* *8*, e54087.
- Majláth, Z., and Vécsei, L. (2014). NMDA antagonists as Parkinson's disease therapy: disseminating the evidence. *Neurodegener Dis Manag* *4*, 23–30.
- Marchitti, S.A., Deitrich, R.A., and Vasiliou, V. (2007). Neurotoxicity and metabolism of the catecholamine-derived 3,4-dihydroxyphenylacetaldehyde and 3,4-dihydroxyphenylglycolaldehyde: the role of aldehyde dehydrogenase. *Pharmacol. Rev.* *59*, 125–150.
- Marinova-Mutafchieva, L., Sadeghian, M., Broom, L., Davis, J.B., Medhurst, A.D., and Dexter, D.T. (2009). Relationship between microglial activation and dopaminergic neuronal loss in the substantia nigra: a time course study in a 6-hydroxydopamine model of Parkinson's disease. *J. Neurochem.* *110*, 966–975.
- Martinez, F.O., and Gordon, S. (2014). The M1 and M2 paradigm of macrophage activation: time for reassessment. *F1000Prime Rep* *6*.
- Martínez-Martín, P., Gil-Nagel, A., Gracia, L.M., Gómez, J.B., Martínez-Sarriés, J., and Bermejo, F. (1994). Unified Parkinson's Disease Rating Scale characteristics and structure. The Cooperative Multicentric Group. *Mov. Disord.* *9*, 76–83.

- Martini, M., De Santis, M.C., Braccini, L., Gulluni, F., and Hirsch, E. (2014). PI3K/AKT signaling pathway and cancer: an updated review. *Ann. Med.* *46*, 372–383.
- Mayr, J.A., Merkel, O., Kohlwein, S.D., Gebhardt, B.R., Böhles, H., Fötschl, U., Koch, J., Jaksch, M., Lochmüller, H., Horváth, R., et al. (2007). Mitochondrial phosphate-carrier deficiency: a novel disorder of oxidative phosphorylation. *Am. J. Hum. Genet.* *80*, 478–484.
- Mayr, J.A., Zimmermann, F.A., Horváth, R., Schneider, H.-C., Schoser, B., Holinski-Feder, E., Czermin, B., Freisinger, P., and Sperl, W. (2011). Deficiency of the mitochondrial phosphate carrier presenting as myopathy and cardiomyopathy in a family with three affected children. *Neuromuscul. Disord.* *21*, 803–808.
- McCubrey, J.A., Steelman, L.S., Chappell, W.H., Abrams, S.L., Wong, E.W.T., Chang, F., Lehmann, B., Terrian, D.M., Milella, M., Tafuri, A., et al. (2007). Roles of the Raf/MEK/ERK pathway in cell growth, malignant transformation and drug resistance. *Biochim. Biophys. Acta* *1773*, 1263–1284.
- McGeer, P.L., Itagaki, S., Boyes, B.E., and McGeer, E.G. (1988). Reactive microglia are positive for HLA-DR in the substantia nigra of Parkinson's and Alzheimer's disease brains. *Neurology* *38*, 1285–1291.
- McLennan, J.E., Nakano, K., Tyler, H.R., and Schwab, R.S. (1972). Micrographia in Parkinson's disease. *J. Neurol. Sci.* *15*, 141–152.
- McNally, R.S., Davis, B.K., Clements, C.M., Accavitti-Loper, M.A., Mak, T.W., and Ting, J.P.-Y. (2011). DJ-1 enhances cell survival through the binding of Cezanne, a negative regulator of NF-kappaB. *J. Biol. Chem.* *286*, 4098–4106.
- Meiser, J., Delcambre, S., Wegner, A., Jäger, C., Ghelfi, J., d'Herouel, A.F., Dong, X., Weindl, D., Stautner, C., Nonnenmacher, Y., et al. (2016). Loss of DJ-1 impairs antioxidant response by altered glutamine and serine metabolism. *Neurobiol. Dis.* *89*, 112–125.
- Melki, R. (2015). Role of Different Alpha-Synuclein Strains in Synucleinopathies, Similarities with other Neurodegenerative Diseases. *J Parkinsons Dis* *5*, 217–227.
- Mena, L.D., Coto, E., Sánchez-Ferrero, E., Ribacoba, R., Guisasola, L.M., Salvador, C., Blázquez, M., and Alvarez, V. (2009). Mutational screening of the mortalin gene (HSPA9) in Parkinson's disease. *J Neural Transm* *116*, 1289–1293.
- Menendez, D., Inga, A., and Resnick, M.A. (2009). The expanding universe of p53 targets. *Nat. Rev. Cancer* *9*, 724–737.
- Menza, M.A., Robertson-Hoffman, D.E., and Bonapace, A.S. (1993). Parkinson's disease and anxiety: comorbidity with depression. *Biol. Psychiatry* *34*, 465–470.

- Meulener, M.C., Xu, K., Thomson, L., Thompson, L., Ischiropoulos, H., and Bonini, N.M. (2006). Mutational analysis of DJ-1 in *Drosophila* implicates functional inactivation by oxidative damage and aging. *Proc. Natl. Acad. Sci. U.S.A.* *103*, 12517–12522.
- Miller, D.W., Ahmad, R., Hague, S., Baptista, M.J., Canet-Aviles, R., McLendon, C., Carter, D.M., Zhu, P.-P., Stadler, J., Chandran, J., et al. (2003a). L166P mutant DJ-1, causative for recessive Parkinson's disease, is degraded through the ubiquitin-proteasome system. *J. Biol. Chem.* *278*, 36588–36595.
- Miller, J.W., Selhub, J., Nadeau, M.R., Thomas, C.A., Feldman, R.G., and Wolf, P.A. (2003b). Effect of L-dopa on plasma homocysteine in PD patients: relationship to B-vitamin status. *Neurology* *60*, 1125–1129.
- Mitsugi, H., Niki, T., Takahashi-Niki, K., Tanimura, K., Yoshizawa-Kumagaye, K., Tsunemi, M., Iguchi-Ariga, S.M.M., and Ariga, H. (2013). Identification of the recognition sequence and target proteins for DJ-1 protease. *FEBS Lett.* *587*, 2493–2499.
- Mo, J.-S., Jung, J., Yoon, J.-H., Hong, J.-A., Kim, M.-Y., Ann, E.-J., Seo, M.-S., Choi, Y.-H., and Park, H.-S. (2010). DJ-1 modulates the p38 mitogen-activated protein kinase pathway through physical interaction with apoptosis signal-regulating kinase 1. *J. Cell. Biochem.* *110*, 229–237.
- Moehle, M.S., Webber, P.J., Tse, T., Sukar, N., Standaert, D.G., DeSilva, T.M., Cowell, R.M., and West, A.B. (2012). LRRK2 inhibition attenuates microglial inflammatory responses. *J. Neurosci.* *32*, 1602–1611.
- Mogi, M., Togari, A., Tanaka, K., Ogawa, N., Ichinose, H., and Nagatsu, T. (2000). Increase in level of tumor necrosis factor- α in 6-hydroxydopamine-lesioned striatum in rats is suppressed by immunosuppressant FK506. *Neurosci. Lett.* *289*, 165–168.
- Mookerjee, S.A., Nicholls, D.G., and Brand, M.D. (2016). Determining Maximum Glycolytic Capacity Using Extracellular Flux Measurements. *PLOS ONE* *11*, e0152016.
- Moon, H.E., and Paek, S.H. (2015). Mitochondrial Dysfunction in Parkinson's Disease. *Exp Neurobiol* *24*, 103–116.
- Moore, D.J., Zhang, L., Troncoso, J., Lee, M.K., Hattori, N., Mizuno, Y., Dawson, T.M., and Dawson, V.L. (2005). Association of DJ-1 and parkin mediated by pathogenic DJ-1 mutations and oxidative stress. *Hum Mol Genet* *14*, 71–84.
- Morais, V.A., Haddad, D., Craessaerts, K., De Bock, P.-J., Swerts, J., Vilain, S., Aerts, L., Overbergh, L., Grünwald, A., Seibler, P., et al. (2014). PINK1 loss-of-function mutations affect mitochondrial complex I activity via Ndufa10 ubiquinone uncoupling. *Science* *344*, 203–207.
- Morganti, J.M., Riparip, L.-K., and Rosi, S. (2016). Call Off the Dog(ma): M1/M2 Polarization Is Concurrent following Traumatic Brain Injury. *PLoS One* *11*.

- Mørkeberg Nilsson, F. (2012). Parkinson's disease and affective disorder: The temporal relationship. *Open Journal of Psychiatry* 02, 96–109.
- Morris, M.E., Huxham, F., McGinley, J., Dodd, K., and Iansek, R. (2001). The biomechanics and motor control of gait in Parkinson disease. *Clin Biomech (Bristol, Avon)* 16, 459–470.
- Mosser, D.M., and Edwards, J.P. (2008). Exploring the full spectrum of macrophage activation. *Nat. Rev. Immunol.* 8, 958–969.
- Mott, R.T., Ait-Ghezala, G., Town, T., Mori, T., Vendrame, M., Zeng, J., Ehrhart, J., Mullan, M., and Tan, J. (2004). Neuronal expression of CD22: novel mechanism for inhibiting microglial proinflammatory cytokine production. *Glia* 46, 369–379.
- Muñoz, P., Huenchuguala, S., Paris, I., and Segura-Aguilar, J. (2012). Dopamine oxidation and autophagy. *Parkinsons Dis* 2012, 920953.
- Murphy, M.P. (2009). How mitochondria produce reactive oxygen species. *Biochem J* 417, 1–13.
- Nagakubo, D., Taira, T., Kitaura, H., Ikeda, M., Tamai, K., Iguchi-Arigo, S.M., and Ariga, H. (1997). DJ-1, a novel oncogene which transforms mouse NIH3T3 cells in cooperation with ras. *Biochem. Biophys. Res. Commun.* 231, 509–513.
- Nagamoto-Combs, K., Kulas, J., and Combs, C.K. (2014). A novel cell line from spontaneously immortalized murine microglia. *Journal of Neuroscience Methods* 233, 187–198.
- Nalls, M.A., Pankratz, N., Lill, C.M., Do, C.B., Hernandez, D.G., Saad, M., DeStefano, A.L., Kara, E., Bras, J., Sharma, M., et al. (2014). Large-scale meta-analysis of genome-wide association data identifies six new risk loci for Parkinson's disease. *Nat. Genet.* 46, 989–993.
- Napolitano, A., Manini, P., and d'Ischia, M. (2011). Oxidation chemistry of catecholamines and neuronal degeneration: an update. *Curr. Med. Chem.* 18, 1832–1845.
- Nash, Y., Schmukler, E., Trudler, D., Pinkas-Kramarski, R., and Frenkel, D. (2017). DJ-1 deficiency impairs autophagy and reduces alpha-synuclein phagocytosis by microglia. *J. Neurochem.* 143, 584–594.
- Nimmerjahn, A., Kirchhoff, F., and Helmchen, F. (2005). Resting microglial cells are highly dynamic surveillants of brain parenchyma in vivo. *Science* 308, 1314–1318.
- Noyce, A.J., Bestwick, J.P., Silveira-Moriyama, L., Hawkes, C.H., Giovannoni, G., Lees, A.J., and Schrag, A. (2012). Meta-Analysis of Early Nonmotor Features and Risk Factors for Parkinson Disease. *Ann Neurol* 72, 893–901.
- Obeso, J.A., Rodríguez-Oroz, M.C., Rodríguez, M., Lanciego, J.L., Artieda, J., Gonzalo, N., and Olanow, C.W. (2000). Pathophysiology of the basal ganglia in Parkinson's disease. *Trends Neurosci.* 23, S8-19.

- Odekerken, V.J.J., Boel, J.A., Schmand, B.A., de Haan, R.J., Figuee, M., van den Munckhof, P., Schuurman, P.R., de Bie, R.M.A., and NSTAPS study group (2016). GPI vs STN deep brain stimulation for Parkinson disease: Three-year follow-up. *Neurology* *86*, 755–761.
- Okubadejo, N.U., Bower, J.H., Rocca, W.A., and Maraganore, D.M. (2006). Parkinson's disease in Africa: A systematic review of epidemiologic and genetic studies. *Mov. Disord.* *21*, 2150–2156.
- Olivares, D., Deshpande, V.K., Shi, Y., Lahiri, D.K., Greig, N.H., Rogers, J.T., and Huang, X. (2012). N-Methyl D-Aspartate (NMDA) Receptor Antagonists and Memantine Treatment for Alzheimer's Disease, Vascular Dementia and Parkinson's Disease. *Curr Alzheimer Res* *9*, 746–758.
- Olson, E.J., Boeve, B.F., and Silber, M.H. (2000). Rapid eye movement sleep behaviour disorder: demographic, clinical and laboratory findings in 93 cases. *Brain* *123* (Pt 2), 331–339.
- Ooe, H., Taira, T., Iguchi-Ariga, S.M.M., and Ariga, H. (2005). Induction of reactive oxygen species by bisphenol A and abrogation of bisphenol A-induced cell injury by DJ-1. *Toxicol. Sci.* *88*, 114–126.
- Orihuela, R., McPherson, C.A., and Harry, G.J. (2016). Microglial M1/M2 polarization and metabolic states: Microglia bioenergetics with acute polarization. *British Journal of Pharmacology* *173*, 649–665.
- Orth, M., and Schapira, A.H.V. (2002). Mitochondrial involvement in Parkinson's disease. *Neurochem. Int.* *40*, 533–541.
- Otsuka, M., Ichiya, Y., Kuwabara, Y., Hosokawa, S., Sasaki, M., Yoshida, T., Fukumura, T., Masuda, K., and Kato, M. (1996). Differences in the reduced 18F-Dopa uptakes of the caudate and the putamen in Parkinson's disease: correlations with the three main symptoms. *J. Neurol. Sci.* *136*, 169–173.
- Ouchi, Y., Yoshikawa, E., Sekine, Y., Futatsubashi, M., Kanno, T., Ogusu, T., and Torizuka, T. (2005). Microglial activation and dopamine terminal loss in early Parkinson's disease. *Ann. Neurol.* *57*, 168–175.
- Paik, M.-J., Ahn, Y.-H., Lee, P.H., Kang, H., Park, C.B., Choi, S., and Lee, G. (2010). Polyamine patterns in the cerebrospinal fluid of patients with Parkinson's disease and multiple system atrophy. *Clin. Chim. Acta* *411*, 1532–1535.
- Pallmann, N., Braig, M., Sievert, H., Preukschas, M., Hermans-Borgmeyer, I., Schweizer, M., Nagel, C.H., Neumann, M., Wild, P., Haralambieva, E., et al. (2015). Biological Relevance and Therapeutic Potential of the Hypusine Modification System. *J. Biol. Chem.* jbc.M115.664490.
- Park, H.K., Yoo, J.Y., Kwon, M., Lee, J.-H., Lee, S.J., Kim, S.R., Kim, M.J., Lee, M.C., Lee, S.M., and Chung, S.J. (2014). Gait freezing and speech disturbance in Parkinson's disease. *Neurol. Sci.* *35*, 357–363.

- Parnetti, L., Castrioto, A., Chiasserini, D., Persichetti, E., Tambasco, N., El-Agnaf, O., and Calabresi, P. (2013). Cerebrospinal fluid biomarkers in Parkinson disease. *Nat Rev Neurol* 9, 131–140.
- Paterna, J.-C., Leng, A., Weber, E., Feldon, J., and Büeler, H. (2007). DJ-1 and Parkin modulate dopamine-dependent behavior and inhibit MPTP-induced nigral dopamine neuron loss in mice. *Mol. Ther.* 15, 698–704.
- Pegg, A.E. (2009). Mammalian polyamine metabolism and function. *IUBMB Life* 61, 880–894.
- Pegg, A.E., and Casero, R.A. (2011). Current status of the polyamine research field. *Methods Mol. Biol.* 720, 3–35.
- Peřa-Kaján, J., Twardowski, T., and Jakubowski, H. (2007). Mechanisms of homocysteine toxicity in humans. *Amino Acids* 32, 561–572.
- Perlmann, T., and Wallén-Mackenzie, A. (2004). Nurr1, an orphan nuclear receptor with essential functions in developing dopamine cells. *Cell Tissue Res.* 318, 45–52.
- Pickell, L., Tran, P., Leclerc, D., Hiscott, J., and Rozen, R. (2005). Regulatory studies of murine methylenetetrahydrofolate reductase reveal two major promoters and NF-κB sensitivity. *Biochimica et Biophysica Acta (BBA) - Gene Structure and Expression* 1731, 104–114.
- Pisanu, A., Lecca, D., Mulas, G., Wardas, J., Simbula, G., Spiga, S., and Carta, A.R. (2014). Dynamic changes in pro- and anti-inflammatory cytokines in microglia after PPAR-γ agonist neuroprotective treatment in the MPTPp mouse model of progressive Parkinson's disease. *Neurobiol. Dis.* 71, 280–291.
- Poddar, R., and Paul, S. (2009). Homocysteine-NMDA receptor-mediated activation of extracellular signal-regulated kinase leads to neuronal cell death. *J. Neurochem.* 110, 1095–1106.
- Polymeropoulos, M.H., Lavedan, C., Leroy, E., Ide, S.E., Dehejia, A., Dutra, A., Pike, B., Root, H., Rubenstein, J., Boyer, R., et al. (1997). Mutation in the alpha-synuclein gene identified in families with Parkinson's disease. *Science* 276, 2045–2047.
- Ponsen, M.M., Stoffers, D., Booij, J., van Eck-Smit, B.L.F., Wolters, E.C., and Berendse, H.W. (2004). Idiopathic hyposmia as a preclinical sign of Parkinson's disease. *Ann. Neurol.* 56, 173–181.
- Pontone, G.M., Williams, J.R., Anderson, K.E., Chase, G., Goldstein, S.R., Grill, S., Hirsch, E.S., Lehmann, S., Little, J.T., Margolis, R.L., et al. (2011). Anxiety and self-perceived health status in Parkinson's disease. *Parkinsonism Relat Disord* 17, 249–254.

- Postuma, R.B., Lang, A.E., Massicotte-Marquez, J., and Montplaisir, J. (2006). Potential early markers of Parkinson disease in idiopathic REM sleep behavior disorder. *Neurology* 66, 845–851.
- Postuma, R.B., Gagnon, J.F., and Montplaisir, J. (2010). Clinical prediction of Parkinson's disease: planning for the age of neuroprotection. *Journal of Neurology, Neurosurgery & Psychiatry* 81, 1008–1013.
- Pringsheim, T., Jette, N., Frolkis, A., and Steeves, T.D.L. (2014). The prevalence of Parkinson's disease: a systematic review and meta-analysis. *Mov. Disord.* 29, 1583–1590.
- Purisai, M.G., McCormack, A.L., Cumine, S., Li, J., Isla, M.Z., and Di Monte, D.A. (2007). Microglial activation as a priming event leading to paraquat-induced dopaminergic cell degeneration. *Neurobiol Dis* 25, 392–400.
- Put, N.M.J. van der, Gabreëls, F., Stevens, E.M.B., Smeitink, J.A.M., Trijbels, F.J.M., Eskes, T.K.A.B., Heuvel, L.P. van den, and Blom, H.J. (1998). A Second Common Mutation in the Methylene tetrahydrofolate Reductase Gene: An Additional Risk Factor for Neural-Tube Defects? *The American Journal of Human Genetics* 62, 1044–1051.
- Py, B., Basmaciogullari, S., Bouchet, J., Zarka, M., Moura, I.C., Benhamou, M., Monteiro, R.C., Hocini, H., Madrid, R., and Benichou, S. (2009). The Phospholipid Scramblases 1 and 4 Are Cellular Receptors for the Secretory Leukocyte Protease Inhibitor and Interact with CD4 at the Plasma Membrane. *PLoS ONE* 4.
- Rabbani, N., and Thornalley, P.J. (2015). Dicarbonyl stress in cell and tissue dysfunction contributing to ageing and disease. *Biochem. Biophys. Res. Commun.* 458, 221–226.
- Rahman-Roblick, R., Hellman, U., Becker, S., Bader, F.G., Auer, G., Wiman, K.G., and Roblick, U.J. (2008). Proteomic identification of p53-dependent protein phosphorylation. *Oncogene* 27, 4854–4859.
- Rajput, A.H., Sitte, H.H., Rajput, A., Fenton, M.E., Pifl, C., and Hornykiewicz, O. (2008). Globus pallidus dopamine and Parkinson motor subtypes: clinical and brain biochemical correlation. *Neurology* 70, 1403–1410.
- Rakovic, A., Grünewald, A., Voges, L., Hofmann, S., Orolicki, S., Lohmann, K., and Klein, C. (2011). PINK1-Interacting Proteins: Proteomic Analysis of Overexpressed PINK1. *Parkinsons Dis* 2011.
- Ramani, D., De Bandt, J.P., and Cynober, L. (2014). Aliphatic polyamines in physiology and diseases. *Clin Nutr* 33, 14–22.
- Ransohoff, R.M., and Perry, V.H. (2009). Microglial physiology: unique stimuli, specialized responses. *Annu. Rev. Immunol.* 27, 119–145.

- Richard, I.H., Schiffer, R.B., and Kurlan, R. (1996). Anxiety and Parkinson's disease. *J Neuropsychiatry Clin Neurosci* 8, 383–392.
- Richarme, G., Mihoub, M., Dairou, J., Bui, L.C., Leger, T., and Lamouri, A. (2015). Parkinsonism-associated protein DJ-1/Park7 is a major protein deglycase that repairs methylglyoxal- and glyoxal-glycated cysteine, arginine, and lysine residues. *J. Biol. Chem.* 290, 1885–1897.
- Richarme, G., Liu, C., Mihoub, M., Abdallah, J., Leger, T., Joly, N., Liebart, J.-C., Jurkunas, U.V., Nadal, M., Bouloc, P., et al. (2017). Guanine glycation repair by DJ-1/Park7 and its bacterial homologs. *Science* 357, 208–211.
- Rippon, G.A., and Marder, K.S. (2005). Dementia in Parkinson's disease. *Adv Neurol* 96, 95–113.
- Rodríguez-Navarro, J.A., Casarejos, M.J., Menéndez, J., Solano, R.M., Rodal, I., Gómez, A., Yébenes, J.G. de, and Mena, M.A. (2007). Mortality, oxidative stress and tau accumulation during ageing in parkin null mice. *Journal of Neurochemistry* 103, 98–114.
- Rosenblum, S., Samuel, M., Zlotnik, S., Erikh, I., and Schlesinger, I. (2013). Handwriting as an objective tool for Parkinson's disease diagnosis. *J. Neurol.* 260, 2357–2361.
- Rossi, C., Frosini, D., Volterrani, D., De Feo, P., Unti, E., Nicoletti, V., Kiferle, L., Bonuccelli, U., and Ceravolo, R. (2010). Differences in nigro-striatal impairment in clinical variants of early Parkinson's disease: evidence from a FP-CIT SPECT study. *Eur. J. Neurol.* 17, 626–630.
- Rousseaux, M.W.C., Marcogliese, P.C., Qu, D., Hewitt, S.J., Seang, S., Kim, R.H., Slack, R.S., Schlossmacher, M.G., Lagace, D.C., Mak, T.W., et al. (2012). Progressive dopaminergic cell loss with unilateral-to-bilateral progression in a genetic model of Parkinson disease. *Proceedings of the National Academy of Sciences* 109, 15918–15923.
- Rudzińska, M., Bukowczan, S., Stożek, J., Zajdel, K., Mirek, E., Chwała, W., Wójcik-Pędziwiatr, M., Banaszkiwicz, K., and Szczudlik, A. (2013). Causes and consequences of falls in Parkinson disease patients in a prospective study. *Neurol. Neurochir. Pol.* 47, 423–430.
- Sahu, S.K., Gummadi, S.N., Manoj, N., and Aradhyam, G.K. (2007). Phospholipid scramblases: an overview. *Arch. Biochem. Biophys.* 462, 103–114.
- Saijo, K., Winner, B., Carson, C.T., Collier, J.G., Boyer, L., Rosenfeld, M.G., Gage, F.H., and Glass, C.K. (2009). A Nurr1/CoREST pathway in microglia and astrocytes protects dopaminergic neurons from inflammation-induced death. *Cell* 137, 47–59.
- Saijo, K., Crotti, A., and Glass, C.K. (2013). Regulation of microglia activation and deactivation by nuclear receptors. *Glia* 61, 104–111.
- Saitoh, M., Nishitoh, H., Fujii, M., Takeda, K., Tobiume, K., Sawada, Y., Kawabata, M., Miyazono, K., and Ichijo, H. (1998). Mammalian thioredoxin is a direct inhibitor of apoptosis signal-regulating kinase (ASK) 1. *EMBO J.* 17, 2596–2606.

- Salarian, A., Zampieri, C., Horak, F.B., Carlson-Kuhta, P., Nutt, J.G., and Aminian, K. (2009). Analyzing 180 degrees turns using an inertial system reveals early signs of progression of Parkinson's disease. *Conf Proc IEEE Eng Med Biol Soc 2009*, 224–227.
- Salmena, L., Carracedo, A., and Pandolfi, P.P. (2008). Tenets of PTEN tumor suppression. *Cell* 133, 403–414.
- Schapira, A.H., Cooper, J.M., Dexter, D., Clark, J.B., Jenner, P., and Marsden, C.D. (1990). Mitochondrial complex I deficiency in Parkinson's disease. *J. Neurochem.* 54, 823–827.
- Schapira, A.H.V., Chaudhuri, K.R., and Jenner, P. (2017). Non-motor features of Parkinson disease. *Nature Reviews Neuroscience* 18, 435–450.
- Schenck, C.H., Bundlie, S.R., and Mahowald, M.W. (1996). Delayed emergence of a parkinsonian disorder in 38% of 29 older men initially diagnosed with idiopathic rapid eye movement sleep behaviour disorder. *Neurology* 46, 388–393.
- Schillaci, O., Chiaravalloti, A., Pierantozzi, M., Di Pietro, B., Koch, G., Bruni, C., Stanzione, P., and Stefani, A. (2011). Different patterns of nigrostriatal degeneration in tremor type versus the akinetic-rigid and mixed types of Parkinson's disease at the early stages: molecular imaging with 123I-FP-CIT SPECT. *Int. J. Mol. Med.* 28, 881–886.
- Schrag, A., Jahanshahi, M., and Quinn, N. (2000). What contributes to quality of life in patients with Parkinson's disease? *J. Neurol. Neurosurg. Psychiatr.* 69, 308–312.
- Schrag, A., Jahanshahi, M., and Quinn, N.P. (2001). What contributes to depression in Parkinson's disease? *Psychological Medicine* 31, 65–73.
- Schuller, A.P., Wu, C.C.-C., Dever, T.E., Buskirk, A.R., and Green, R. (2017). eIF5A Functions Globally in Translation Elongation and Termination. *Mol. Cell* 66, 194-205.e5.
- Schulte, C., and Gasser, T. (2011). Genetic basis of Parkinson's disease: inheritance, penetrance, and expression. *Appl Clin Genet* 4, 67–80.
- Schulz-Schaeffer, W.J. (2010). The synaptic pathology of α -synuclein aggregation in dementia with Lewy bodies, Parkinson's disease and Parkinson's disease dementia. *Acta Neuropathol* 120, 131–143.
- Schüpbach, W.M.M., Corvol, J.-C., Czernecki, V., Djebara, M.B., Golmard, J.-L., Agid, Y., and Hartmann, A. (2010). Segmental progression of early untreated Parkinson's disease: a novel approach to clinical rating. *Journal of Neurology, Neurosurgery & Psychiatry* 81, 20–25.
- Segura-Aguilar, J., Paris, I., Muñoz, P., Ferrari, E., Zecca, L., and Zucca, F.A. (2014). Protective and toxic roles of dopamine in Parkinson's disease. *J. Neurochem.* 129, 898–915.

Seifert, E.L., Ligeti, E., Mayr, J.A., Sondheimer, N., and Hajnóczy, G. (2015). The mitochondrial phosphate carrier: Role in oxidative metabolism, calcium handling and mitochondrial disease. *Biochemical and Biophysical Research Communications* 464, 369–375.

Shahed, J., and Jankovic, J. (2007). Motor symptoms in Parkinson's disease. *Handbook of Clinical Neurology* 83, 329–342.

Shendelman, S., Jonason, A., Martinat, C., Leete, T., and Abeliovich, A. (2004). DJ-1 is a redox-dependent molecular chaperone that inhibits alpha-synuclein aggregate formation. *PLoS Biol.* 2, e362.

Sherer, T.B., Betarbet, R., Kim, J.H., and Greenamyre, J.T. (2003). Selective microglial activation in the rat rotenone model of Parkinson's disease. *Neurosci. Lett.* 341, 87–90.

Sheridan, G.K., and Murphy, K.J. (2013). Neuron–glia crosstalk in health and disease: fractalkine and CX3CR1 take centre stage. *Open Biol* 3.

Shulman, L.M., Taback, R.L., Bean, J., and Weiner, W.J. (2001). Comorbidity of the nonmotor symptoms of Parkinson's disease. *Mov. Disord.* 16, 507–510.

Sigmund, C.D. (2000). Viewpoint: are studies in genetically altered mice out of control? *Arterioscler. Thromb. Vasc. Biol.* 20, 1425–1429.

Singer, C., Weiner, W.J., and Sanchez-Ramos, J.R. (1992). Autonomic dysfunction in men with Parkinson's disease. *Eur. Neurol.* 32, 134–140.

Singleton, A.B., Farrer, M.J., and Bonifati, V. (2013). The genetics of Parkinson's disease: progress and therapeutic implications. *Mov Disord* 28, 14–23.

Soda, K., Kano, Y., Sakuragi, M., Takao, K., Lefor, A., and Konishi, F. (2009). Long-term oral polyamine intake increases blood polyamine concentrations. *J. Nutr. Sci. Vitaminol.* 55, 361–366.

Spillantini, M.G., Schmidt, M.L., Lee, V.M., Trojanowski, J.Q., Jakes, R., and Goedert, M. (1997). Alpha-synuclein in Lewy bodies. *Nature* 388, 839–840.

Srivastava, S., Blower, P.J., Aubdool, A.A., Hider, R.C., Mann, G.E., and Siow, R.C. (2016). Cardioprotective effects of Cu(II)ATSM in human vascular smooth muscle cells and cardiomyocytes mediated by Nrf2 and DJ-1. *Sci Rep* 6, 7.

Starkstein, S.E., Petracca, G., Chmerinski, E., Tesón, A., Sabe, L., Merello, M., and Leiguarda, R. (1998). Depression in classic versus akinetic-rigid Parkinson's disease. *Mov. Disord.* 13, 29–33.

Streit, W.J. (2002). Microglia as neuroprotective, immunocompetent cells of the CNS. *Glia* 40, 133–139.

- Su, X., Maguire-Zeiss, K.A., Giuliano, R., Prifti, L., Venkatesh, K., and Federoff, H.J. (2008). Synuclein activates microglia in a model of Parkinson's disease. *Neurobiol. Aging* 29, 1690–1701.
- Sun, S.-Y., An, C.-N., and Pu, X.-P. (2012). DJ-1 protein protects dopaminergic neurons against 6-OHDA/MG-132-induced neurotoxicity in rats. *Brain Res. Bull.* 88, 609–616.
- Tai, L.-H., Lee, A.M., Benavidez, N., Bonci, A., and Wilbrecht, L. (2012). Transient stimulation of distinct subpopulations of striatal neurons mimics changes in action value. *Nat. Neurosci.* 15, 1281–1289.
- Taipa, R., Pereira, C., Reis, I., Alonso, I., Bastos-Lima, A., Melo-Pires, M., and Magalhães, M. (2016). DJ-1 linked parkinsonism (PARK7) is associated with Lewy body pathology. *Brain* 139, 1680–1687.
- Taira, T., Saito, Y., Niki, T., Iguchi-Ariga, S.M.M., Takahashi, K., and Ariga, H. (2004). DJ-1 has a role in antioxidative stress to prevent cell death. *EMBO Rep.* 5, 213–218.
- Takahashi, K., Taira, T., Niki, T., Seino, C., Iguchi-Ariga, S.M.M., and Ariga, H. (2001). DJ-1 Positively Regulates the Androgen Receptor by Impairing the Binding of PIAS α to the Receptor. *J. Biol. Chem.* 276, 37556–37563.
- Takahashi-Niki, K., Niki, T., Taira, T., Iguchi-Ariga, S.M.M., and Ariga, H. (2004). Reduced anti-oxidative stress activities of DJ-1 mutants found in Parkinson's disease patients. *Biochem. Biophys. Res. Commun.* 320, 389–397.
- Takahashi-Niki, K., Kato-Ose, I., Murata, H., Maita, H., Iguchi-Ariga, S.M.M., and Ariga, H. (2015). Epidermal Growth Factor-dependent Activation of the Extracellular Signal-regulated Kinase Pathway by DJ-1 Protein through Its Direct Binding to c-Raf Protein. *J. Biol. Chem.* 290, 17838–17847.
- Takahashi-Niki, K., Ganaha, Y., Niki, T., Nakagawa, S., Kato-Ose, I., Iguchi-Ariga, S.M.M., and Ariga, H. (2016). DJ-1 activates SIRT1 through its direct binding to SIRT1. *Biochem. Biophys. Res. Commun.* 474, 131–136.
- Tang, B., Xiong, H., Sun, P., Zhang, Y., Wang, D., Hu, Z., Zhu, Z., Ma, H., Pan, Q., Xia, J.-H., et al. (2006). Association of PINK1 and DJ-1 confers digenic inheritance of early-onset Parkinson's disease. *Hum. Mol. Genet.* 15, 1816–1825.
- Tang, J., Liu, J., Li, X., Zhong, Y., Zhong, T., Liu, Y., Wang, J.H., and Jiang, Y. (2014). PRAK Interacts with DJ-1 and Prevents Oxidative Stress-Induced Cell Death.
- Tansey, M.G., and Goldberg, M.S. (2010). Neuroinflammation in Parkinson's disease: its role in neuronal death and implications for therapeutic intervention. *Neurobiol. Dis.* 37, 510–518.

- Thenganatt, M.A., and Louis, E.D. (2012). Distinguishing essential tremor from Parkinson's disease: bedside tests and laboratory evaluations. *Expert Review of Neurotherapeutics* 12, 687–696.
- Theodore, S., Cao, S., McLean, P.J., and Standaert, D.G. (2008). Targeted Overexpression of Human Alpha-Synuclein Triggers Microglial Activation and an Adaptive Immune Response in a Mouse Model of Parkinson Disease. *J Neuropathol Exp Neurol* 67, 1149–1158.
- Thomas, K.J., McCoy, M.K., Blackinton, J., Beilina, A., van der Brug, M., Sandebring, A., Miller, D., Maric, D., Cedazo-Minguez, A., and Cookson, M.R. (2011). DJ-1 acts in parallel to the PINK1/parkin pathway to control mitochondrial function and autophagy. *Hum. Mol. Genet.* 20, 40–50.
- Tissingh, G., Booij, J., Bergmans, P., Winogrodzka, A., Janssen, A.G., van Royen, E.A., Stoof, J.C., and Wolters, E.C. (1998). Iodine-123-N-omega-fluoropropyl-2beta-carbomethoxy-3beta-(4-iodophenyl)tropine SPECT in healthy controls and early-stage, drug-naive Parkinson's disease. *J. Nucl. Med.* 39, 1143–1148.
- Tobiume, K., Matsuzawa, A., Takahashi, T., Nishitoh, H., Morita, K., Takeda, K., Minowa, O., Miyazono, K., Noda, T., and Ichijo, H. (2001). ASK1 is required for sustained activations of JNK/p38 MAP kinases and apoptosis. *EMBO Rep.* 2, 222–228.
- Toro-Funes, N., Bosch-Fusté, J., Veciana-Nogués, M.T., Izquierdo-Pulido, M., and Vidal-Carou, M.C. (2013). In vitro antioxidant activity of dietary polyamines. *Food Research International* 51, 141–147.
- Toyoda, Y., Erkut, C., Pan-Montojo, F., Boland, S., Stewart, M.P., Müller, D.J., Wurst, W., Hyman, A.A., and Kurzchalia, T.V. (2014). Products of the Parkinson's disease-related glyoxalase DJ-1, D-lactate and glycolate, support mitochondrial membrane potential and neuronal survival. *Biol Open* 3, 777–784.
- Tran, T.A., Nguyen, A.D., Chang, J., Goldberg, M.S., Lee, J.-K., and Tansey, M.G. (2011). Lipopolysaccharide and Tumor Necrosis Factor Regulate Parkin Expression via Nuclear Factor-Kappa B. *PLoS One* 6.
- Trinh, J., and Farrer, M. (2013). Advances in the genetics of Parkinson disease. *Nat Rev Neurol* 9, 445–454.
- Trudler, D., Weinreb, O., Mandel, S.A., Youdim, M.B.H., and Frenkel, D. (2014). DJ-1 deficiency triggers microglia sensitivity to dopamine toward a pro-inflammatory phenotype that is attenuated by rasagiline. *J. Neurochem.* 129, 434–447.
- Tufekci, K.U., Meuwissen, R., Genc, S., and Genc, K. (2012). Inflammation in Parkinson's disease. *Adv Protein Chem Struct Biol* 88, 69–132.

Uchiki, T., Weikel, K.A., Jiao, W., Shang, F., Caceres, A., Pawlak, D., Handa, J.T., Brownlee, M., Nagaraj, R., and Taylor, A. (2012). Glycation-altered proteolysis as a pathobiologic mechanism that links dietary glycemic index, aging, and age-related disease (in nondiabetics). *Aging Cell* *11*, 1–13.

Van Den Eeden, S.K., Tanner, C.M., Bernstein, A.L., Fross, R.D., Leimpeter, A., Bloch, D.A., and Nelson, L.M. (2003). Incidence of Parkinson's disease: variation by age, gender, and race/ethnicity. *Am. J. Epidemiol.* *157*, 1015–1022.

Vázquez-Mayorga, E., Díaz-Sánchez, Á.G., Dagda, R.K., Domínguez-Solís, C.A., Dagda, R.Y., Coronado-Ramírez, C.K., and Martínez-Martínez, A. (2016). Novel Redox-Dependent Esterase Activity (EC 3.1.1.2) for DJ-1: Implications for Parkinson's Disease. *Int J Mol Sci* *17*.

Verstraeten, A., Theuns, J., and Van Broeckhoven, C. (2015). Progress in unraveling the genetic etiology of Parkinson disease in a genomic era. *Trends in Genetics* *31*, 140–149.

Vivekanantham, S., Shah, S., Dewji, R., Dewji, A., Khatri, C., and Ologunde, R. (2015). Neuroinflammation in Parkinson's disease: role in neurodegeneration and tissue repair. *Int. J. Neurosci.* *125*, 717–725.

Vogel, D.Y.S., Vereyken, E.J.F., Glim, J.E., Heijnen, P.D.A.M., Moeton, M., van der Valk, P., Amor, S., Teunissen, C.E., van Horsen, J., and Dijkstra, C.D. (2013). Macrophages in inflammatory multiple sclerosis lesions have an intermediate activation status. *J Neuroinflammation* *10*, 35.

Voloboueva, L.A., Emery, J.F., Sun, X., and Giffard, R.G. (2013). Inflammatory response of microglial BV-2 cells includes a glycolytic shift and is modulated by mitochondrial glucose-regulated protein 75/mortalin. *FEBS Letters* *587*, 756–762.

Waak, J., Weber, S.S., Görner, K., Schall, C., Ichijo, H., Stehle, T., and Kahle, P.J. (2009). Oxidizable residues mediating protein stability and cytoprotective interaction of DJ-1 with apoptosis signal-regulating kinase 1. *J. Biol. Chem.* *284*, 14245–14257.

Wagenfeld, A., Gromoll, J., and Cooper, T.G. (1998). Molecular cloning and expression of rat contraception associated protein 1 (CAP1), a protein putatively involved in fertilization. *Biochem. Biophys. Res. Commun.* *251*, 545–549.

Wakabayashi, N., Itoh, K., Wakabayashi, J., Motohashi, H., Noda, S., Takahashi, S., Imakado, S., Kotsuji, T., Otsuka, F., Roop, D.R., et al. (2003). Keap1-null mutation leads to postnatal lethality due to constitutive Nrf2 activation. *Nat. Genet.* *35*, 238–245.

Wang, Z., Liu, J., Chen, S., Wang, Y., Cao, L., Zhang, Y., Kang, W., Li, H., Gui, Y., Chen, S., et al. (2011). DJ-1 modulates the expression of Cu/Zn-superoxide dismutase-1 through the Erk1/2-Elk1 pathway in neuroprotection. *Ann. Neurol.* *70*, 591–599.

- Watson, M.B., Richter, F., Lee, S.K., Gabby, L., Wu, J., Masliah, E., Effros, R.B., and Chesselet, M.-F. (2012). Regionally-specific microglial activation in young mice over-expressing human wildtype alpha-synuclein. *Exp. Neurol.* *237*, 318–334.
- Weisskopf, M.G., Chen, H., Schwarzschild, M.A., Kawachi, I., and Ascherio, A. (2003). Prospective study of phobic anxiety and risk of Parkinson's disease. *Mov. Disord.* *18*, 646–651.
- Wilcock, D.M. (2012). A Changing Perspective on the Role of Neuroinflammation in Alzheimer's Disease. *International Journal of Alzheimer's Disease* *2012*, 1–7.
- Wilson, M.A. (2011). The Role of Cysteine Oxidation in DJ-1 Function and Dysfunction. *Antioxid Redox Signal* *15*, 111–122.
- Wolff, E.C., and Park, M.H. (2015). Role of the Polyamine Spermidine as a Precursor for Hypusine Modification in eIF5A. In *Polyamines*, (Springer, Tokyo), pp. 121–129.
- Wu, D.C., Jackson-Lewis, V., Vila, M., Tieu, K., Teismann, P., Vadseth, C., Choi, D.-K., Ischiropoulos, H., and Przedborski, S. (2002). Blockade of microglial activation is neuroprotective in the 1-methyl-4-phenyl-1,2,3,6-tetrahydropyridine mouse model of Parkinson disease. *J. Neurosci.* *22*, 1763–1771.
- Wu, R., Liu, X., Sun, J., Chen, H., Ma, J., Dong, M., Peng, S., Wang, J., Ding, J., Li, D., et al. (2017). DJ-1 maintains energy and glucose homeostasis by regulating the function of brown adipose tissue. *Cell Discovery* *3*, 16054.
- Xilouri, M., Brekk, O.R., and Stefanis, L. (2013). α -Synuclein and protein degradation systems: a reciprocal relationship. *Mol. Neurobiol.* *47*, 537–551.
- Xiong, H., Wang, D., Chen, L., Choo, Y.S., Ma, H., Tang, C., Xia, K., Jiang, W., Ronai, Z., Zhuang, X., et al. (2009). Parkin, PINK1, and DJ-1 form a ubiquitin E3 ligase complex promoting unfolded protein degradation. *J. Clin. Invest.* *119*, 650–660.
- Xu, C.-Y., Kang, W.-Y., Chen, Y.-M., Jiang, T.-F., Zhang, J., Zhang, L.-N., Ding, J.-Q., Liu, J., and Chen, S.-D. (2017). DJ-1 Inhibits α -Synuclein Aggregation by Regulating Chaperone-Mediated Autophagy. *Front. Aging Neurosci.* *9*.
- Xu, J., Zhong, N., Wang, H., Elias, J.E., Kim, C.Y., Woldman, I., Pifl, C., Gygi, S.P., Geula, C., and Yankner, B.A. (2005). The Parkinson's disease-associated DJ-1 protein is a transcriptional co-activator that protects against neuronal apoptosis. *Hum. Mol. Genet.* *14*, 1231–1241.
- Xu, X.M., Lin, H., Maple, J., Björkblom, B., Alves, G., Larsen, J.P., and Møller, S.G. (2010). The Arabidopsis DJ-1a protein confers stress protection through cytosolic SOD activation. *J. Cell. Sci.* *123*, 1644–1651.

- Yadav, S., Gupta, S.P., Srivastava, G., Srivastava, P.K., and Singh, M.P. (2012). Role of secondary mediators in caffeine-mediated neuroprotection in maneb- and paraquat-induced Parkinson's disease phenotype in the mouse. *Neurochem. Res.* *37*, 875–884.
- Yamaguchi, S., Yamane, T., Takahashi-Niki, K., Kato, I., Niki, T., Goldberg, M.S., Shen, J., Ishimoto, K., Doi, T., Iguchi-Ariga, S.M.M., et al. (2012). Transcriptional activation of low-density lipoprotein receptor gene by DJ-1 and effect of DJ-1 on cholesterol homeostasis. *PLoS ONE* *7*, e38144.
- Yamane, T., Suzui, S., Kitaura, H., Takahashi-Niki, K., Iguchi-Ariga, S.M.M., and Ariga, H. (2013). Transcriptional Activation of the Cholecystokinin Gene by DJ-1 through Interaction of DJ-1 with RREB1 and the Effect of DJ-1 on the Cholecystokinin Level in Mice. *PLoS One* *8*.
- Yan, Y.-F., Yang, W.-J., Xu, Q., Chen, H.-P., Huang, X.-S., Qiu, L.-Y., Liao, Z.-P., and Huang, Q.-R. (2015). DJ-1 upregulates anti-oxidant enzymes and attenuates hypoxia/re-oxygenation-induced oxidative stress by activation of the nuclear factor erythroid 2-like 2 signaling pathway. *Mol Med Rep* *12*, 4734–4742.
- Yanagisawa, D., Kitamura, Y., Inden, M., Takata, K., Taniguchi, T., Morikawa, S., Morita, M., Inubushi, T., Tooyama, I., Taira, T., et al. (2008). DJ-1 protects against neurodegeneration caused by focal cerebral ischemia and reperfusion in rats. *J. Cereb. Blood Flow Metab.* *28*, 563–578.
- Yokota, T., Sugawara, K., Ito, K., Takahashi, R., Ariga, H., and Mizusawa, H. (2003). Down regulation of DJ-1 enhances cell death by oxidative stress, ER stress, and proteasome inhibition. *Biochem. Biophys. Res. Commun.* *312*, 1342–1348.
- Zhang, J. (2013). Autophagy and mitophagy in cellular damage control. *Redox Biology* *1*, 19–23.
- Zhang, L., Shimoji, M., Thomas, B., Moore, D.J., Yu, S.-W., Marupudi, N.I., Torp, R., Torgner, I.A., Ottersen, O.P., Dawson, T.M., et al. (2005). Mitochondrial localization of the Parkinson's disease related protein DJ-1: implications for pathogenesis. *Hum. Mol. Genet.* *14*, 2063–2073.
- Zhang, M., Wang, H., and Tracey, K.J. (2000). Regulation of macrophage activation and inflammation by spermine: a new chapter in an old story. *Crit. Care Med.* *28*, N60-66.
- Zhang, S., Mukherjee, S., Fan, X., Salameh, A., Mujoo, K., Huang, Z., Li, L., To'a Salazar, G., Zhang, N., and An, Z. (2016). Novel association of DJ-1 with HER3 potentiates HER3 activation and signaling in cancer. *Oncotarget* *7*, 65758–65769.
- Zhong, N., Kim, C.Y., Rizzu, P., Geula, C., Porter, D.R., Pothos, E.N., Squitieri, F., Heutink, P., and Xu, J. (2006). DJ-1 transcriptionally up-regulates the human tyrosine hydroxylase by inhibiting the sumoylation of pyrimidine tract-binding protein-associated splicing factor. *J. Biol. Chem.* *281*, 20940–20948.

Zhou, W., Zhu, M., Wilson, M.A., Petsko, G.A., and Fink, A.L. (2006). The oxidation state of DJ-1 regulates its chaperone activity toward alpha-synuclein. *J. Mol. Biol.* 356, 1036–1048.

Zhu, Y., Zhu, R.-X., He, Z.-Y., Liu, X., and Liu, H.-N. (2015). Association of *MTHFR* C677T with total homocysteine plasma levels and susceptibility to Parkinson's disease: a meta-analysis. *Neurol Sci* 36, 945–951.

Zhu, Z., Ai, Q., Wang, W., and Xiao, Z. (2013). Meta-analysis supports association of a functional SNP (rs1801133) in the *MTHFR* gene with Parkinson's disease. *Gene* 531, 78–83.

Zondler, L., Miller-Fleming, L., Repici, M., Gonçalves, S., Tenreiro, S., Rosado-Ramos, R., Betzer, C., Straatman, K.R., Jensen, P.H., Giorgini, F., et al. (2014). DJ-1 interactions with α -synuclein attenuate aggregation and cellular toxicity in models of Parkinson's disease. *Cell Death Dis* 5, e1350.

Zoumas-Morse, C., Rock, C.L., Quintana, E.L., Neuhouser, M.L., Gerner, E.W., and Meyskens, F.L. (2007). Development of a polyamine database for assessing dietary intake. *J Am Diet Assoc* 107, 1024–1027.

(2008). *Fundamental neuroscience* (Amsterdam ; Boston: Elsevier / Academic Press).

(2009). *Encyclopedia of neuroscience* (Berlin ; [New York]: Springer).

11 Eidesstattliche Erklärung

Ich erkläre an Eides statt, dass ich die bei der Fakultät Wissenschaftszentrum Weihenstephan für Ernährung, Landnutzung und Umwelt (promotionsführende Einrichtung) der Technischen Universität München zur Promotionsprüfung vorgelegte Arbeit mit dem Titel: „Function of Dj-1 in the pathoetiology of Parkinson’s disease“ / „Die Funktion von Dj-1 in der Patho-Äthiologie von Morbus Parkinson“ unter der Anleitung und Betreuung durch Professor Dr. Wolfgang Wurst ohne sonstige Hilfe erstellt und bei der Abfassung nur die gemäß § 6 Abs. 6 und 7 Satz 2 angegebenen Hilfsmittel benutzt habe.

Ich habe keine Organisation eingeschaltet, die gegen Entgelt Betreuerinnen und Betreuer für die Anfertigung von Dissertationen sucht, oder die mir obliegenden Pflichten hinsichtlich der Prüfungsleistungen für mich ganz oder teilweise erledigt. Weder ich noch andere haben diese Dissertation in dieser oder ähnlicher Form in einem anderen Prüfungsverfahren als Prüfungsleistung vorgelegt. Ich habe den angestrebten Doktorgrad noch nicht erworben und bin nicht in einem früheren Promotionsverfahren für den angestrebten Doktorgrad endgültig gescheitert. Die öffentlich zugängliche Promotionsordnung der TUM ist mir bekannt, insbesondere habe ich die Bedeutung von § 28 (Nichtigkeit der Promotion) und § 29 (Entzug des Doktorgrades) zur Kenntnis genommen. Ich bin mir der Konsequenzen einer falschen Eidesstattlichen Erklärung bewusst.

Ort / Datum

Artem Romanov
Engasserbogen 16
80639 München

12 Acknowledgements

First of all I would like to thank Prof. Dr. Wolfgang Wurst, Dr. Daniela Vogt Weisenhorn and HELENA Graduate School for giving me the great opportunity for performing my PhD work. Particularly, I would like to thank you Daniela for the nice supervision of my project as well as for the great support and help which you provided to me during all this time. I also would like to thank the members of my thesis committee Prof. Dr. Wolfgang Wurst, Dr. Daniela Vogt Weisenhorn, Dr. Florian Giesert, Dr. Nilima Prakash and Dr. Giovanni Piccoli for all the discussions, which were very important and helpful for me. I also thank the members of my examination committee Prof. Dr. Angelika Schnieke, Prof. Dr. Wolfgang Wurst and Prof. Dr. Aphrodite Kapurniotu.

I gratefully acknowledge Dr. Florian Giesert for all our fruitful discussions and the generation of new ideas and scientific hypotheses together. Thanks a lot, Florian, you were always there to discuss the problem and to give proper advice. I am also indebted to Annerose Kurz-Drexler for all this time which we spent together working at one bench. Your advice concerning methodological issues were very supportive during the daily laboratory work. I also want to thank Dr. Stefanie Hauck for performance of mass spectrometry experiments.

My deepest appreciation goes to my friends and outstanding colleagues who made my life during the PhD time unforgettable. Many thanks to Valentin Evsyukov, Constantin Stautner, Petra Dirscherl, Benedict Rauser, Jeffery Truong, Dietrich Truembach, Oscar Ortiz, Angelika Hummel, Luise Ernst, Natalia Pino, Anke Wittman, Marie Wertz, Jessica Schwab, Annemarie Zimprich, Lillian Garret, Anja Folchert, Susanne Badeke, Irina Rodionova, Julia Zarle, Ulrich Haffen, Elisabeth Findeiss, Michaela Bosch and Clara Zoe Wende.

I also owe my deepest gratitude to my former supervisors from Saint-Petersburg – Prof. Dr. Natalia Eschenko, Dr. Sergey Dagaev and Larissa Kubarskaya for introducing me to the exciting field of neurodegenerative research and for your inspiration.

And of course I would particularly like to thank my family – my father Andrey, my mother Galina and my sister Anastasia. During my entire life you have been sharing with me the joy of my triumphs and the bitterness of failures, you always support me - no matter what. Thank you so much for your love!